

A STABLE SULFUR ISOTOPE STUDY OF GEORGIA KAOLIN AND IMPLICATIONS  
FOR BACTERIAL SULFATE REDUCTION

by

JOSEPH RUSSELL BOREMAN

(under the direction of Douglas Crowe)

ABSTRACT

The clays of the industrially important kaolin district in central Georgia contain measurable pyrite, an iron sulfide mineral that can provide a window into the early diagenetic history of the deposits. Measuring  $\delta^{34}\text{S}$  of this pyrite yields fractionations caused by bacterial influence ranging from 6.4 – 48.9‰. These fractionation values demonstrate depositional environments ranging from open sulfate supplies (high fractionation) to closed sulfate supplies (low fractionation) indicating four different depositional regimes within the Huber Formation and Twiggs Clay of central Georgia: 1. The lower Huber Dissimilatory Sulfate Reducing Bacteria (SRB) dominated Open System (~363 – 375 feet) 2. The upper Huber Disproportionate SRB dominated Open System (375 – 401 feet) 3. The Top of the Huber Closed System (~400 – 404 feet) 4. The Twiggs Dissimilatory SRB dominated Open System (401 – 409 feet). This data, in conjunction with powder X-Ray diffraction data, shows that these clays have undergone two periods of post depositional oxidation.

INDEX WORDS: diagenesis, disproportionate sulfate reducing bacteria, dissimilatory sulfate reducing bacteria, geochemistry, Georgia, isotopes, kaolin, pyrite, sulfur, X-ray diffraction,  $\delta^{34}\text{S}$

A STABLE SULFUR ISOTOPE STUDY OF GEORGIA KAOLIN AND IMPLICATIONS  
FOR BACTERIAL SULFATE REDUCTION

by

JOSEPH RUSSELL BOREMAN

B.S., Denison University, 2009

A Thesis Submitted to the Graduate Faculty of The University of Georgia in Partial Fulfillment  
of the Requirements for the Degree

MASTER OF SCIENCE

ATHENS, GEORGIA

2013

© 2013

Joseph Russell Boreman

All Rights Reserved

A STABLE SULFUR ISOTOPE STUDY OF GEORGIA KAOLIN AND IMPLICATIONS  
FOR BACTERIAL SULFATE REDUCTION

by

JOSEPH RUSSELL BOREMAN

Major Professor: Douglas Crowe

Committee: Paul Schroeder  
Steven Holland

Electronic Version Approved:

Maureen Grasso  
Dean of the Graduate School  
The University of Georgia  
August 2013

DEDICATION

To

Mom, Dad, Melissa, and Megan

For supporting me through this adventure.

## ACKNOWLEDGEMENTS

This project would not have been possible without the financial and intellectual assistance of KaMin LLC and Gil Rowland. Gil's importance in acquiring samples and guiding the initial stages of the project cannot be overstated.

I would like to thank all the faculty, staff, and students at the University of Georgia for their expertise, mentorship, and patience through this process. There are several individuals who deserve recognition here. Dr. Paul Schroeder, brought me up to speed and supported me amidst many XRD questions. Dr. Steven Holland always had an open door for my questions, whether related to geology or not. Julia Cox, for answering all my questions during my many hours in your lab and taking some late night phone calls; Chris Fleisher assistance in prepping samples for the SEM; Stephanie Fochtman, for lending experience on the sulfur extraction line; and to Christopher Ginn for taking this wild ride with me.

I'd like to thank my adviser, Dr. Doug Crowe, for his countless hours of sacrifice, assistance, and discussion to make this thesis possible, he proved that every Fight can have one more round.

I'd finally like to thank my family for their loving support and patience as I navigated the process of graduate school.

## TABLE OF CONTENTS

	Page
ACKNOWLEDGEMENTS.....	v
LIST OF TABLES .....	viii
LIST OF FIGURES .....	ix
LIST OF EQUATIONS.....	xi
CHAPTER	
1 INTRODUCTION .....	1
2 PREVIOUS WORK.....	4
Deposition and Diagenesis .....	4
Sedimentology and Stratigraphy.....	7
3 METHODS.....	10
Scanning Electron Microscope .....	10
Sample Collection.....	11
X-Ray Diffraction .....	15
Sulfur Extraction and Mass Spectrometry.....	15
4 RESULTS .....	17
Scanning Electron Microscope .....	17
Sample Collection.....	21
X-Ray Diffraction .....	22

SO <sub>2</sub> Extraction .....	34
δ <sup>34</sup> S Signature .....	40
5 DISCUSSION.....	46
Early Pyrite Diagenesis .....	46
Post Depositional Oxidation.....	53
6 CONCLUSIONS .....	56
REFERENCES .....	57
APPENDICES	
A Drill Core Photos .....	62
B X-Ray Diffraction Plots .....	82
C Data Tables.....	134

## LIST OF TABLES

	Page
Table 1: Driller's summarized log data.....	21
Table 2: Average XRD counts and average SO <sub>2</sub> yield of Twiggs Clay .....	33
Table 3: SO <sub>2</sub> yield data for core X2100 Y2400.....	35
Table 4: SO <sub>2</sub> yield data for core X2250 Y2650.....	36
Table 5: SO <sub>2</sub> yield data for core X2400 Y2800.....	37
Table 6: SO <sub>2</sub> yield data for core X2500 Y2700.....	38
Table 7: SO <sub>2</sub> yield data for all samples .....	39
Table 8: δ <sup>34</sup> S for core X2100 Y2400 .....	41
Table 9: δ <sup>34</sup> S for core X2250 Y2650 .....	42
Table 10: δ <sup>34</sup> S for core X2400 Y2800 .....	43
Table 11: δ <sup>34</sup> S for core X2500 Y2700 .....	44
Table 12: δ <sup>34</sup> S for all data.....	45
Table 13: Iron mineral reactions with dissolved sulfide .....	49

## LIST OF FIGURES

	Page
Figure 1: Map of the South Carolina-Georgia-Alabama kaolin belt .....	2
Figure 2: Stratigraphic columns of the four cores drilled for this study .....	9
Figure 3: Using the SEM at the University of Georgia to photograph pyrite .....	11
Figure 4: Map of drilling area with locations of four cores indicated .....	13
Figure 5: Truck mounted rig and crew drilling through Huber Formation near the intersection of Georgia Highway 17 and Purvis Schoolhouse Road.....	14
Figure 6: Login Drilling Company crew washing off newly collected core of the Jeffersonville Member of the Huber Formation.....	15
Figure 7: Small crystal of pyrite in preliminary cream clay, PM-1 .....	18
Figure 8: Large crystal of pyrite in preliminary gray clay, CS-1 .....	19
Figure 9: Large euhedral pyrite crystal in preliminary gray clay CS-2 .....	20
Figure 10: Small crystal of pyrite in preliminary cream clay, GR-1 .....	21
Figure 11: An example of a XRD plot from the upper part of the Huber Formation within the X2100 Y2400 core .....	22
Figure 12: 3D XRD plot of X2250 Y2650.....	23
Figure 13: 3D XRD plot of X2100 Y2400.....	27
Figure 14: 3D XRD plot of X2400 Y2800.....	29
Figure 15: 3D XRD plot of X2500 Y2700.....	32

Figure 16: Pyrite XRD counts and SO <sub>2</sub> data in the Twiggs clay, showing an exponential relationship.....	33
Figure 17: SO <sub>2</sub> yield in the Huber Formation and Twiggs Clay in core X2100 Y2400 .....	35
Figure 18: SO <sub>2</sub> yield in the Huber Formation and Twiggs Clay in core X2250 Y2650 .....	36
Figure 19: SO <sub>2</sub> yield in the Huber Formation and Twiggs Clay in core X2400 Y2800 .....	37
Figure 20: SO <sub>2</sub> yield in the Huber Formation and Twiggs Clay in core X2500 Y2700 .....	38
Figure 21: SO <sub>2</sub> yield in the Huber Formation and Twiggs Clay for all data .....	39
Figure 22: δ <sup>34</sup> S as related to SO <sub>2</sub> yield for all data .....	40
Figure 23: Stratigraphic variation in δ <sup>34</sup> S in the Huber Formation and Twiggs Clay for core X2100 Y2400 .....	41
Figure 24: Stratigraphic variation of δ <sup>34</sup> S in the Huber Formation and Twiggs Clay for core X2250 Y2650 .....	42
Figure 25: Stratigraphic variation of δ <sup>34</sup> S in the Huber Formation and Twiggs Clay for core X2400 Y2800 .....	43
Figure 26: Stratigraphic variation of δ <sup>34</sup> S in the Huber Formation and Twiggs Clay for core X2500 Y2700 .....	44
Figure 27: Stratigraphic variation of δ <sup>34</sup> S in the Huber Formation and Twiggs Clay for all data.	45
Figure 28: δ <sup>34</sup> S variations in open v. closed conditions of early pyrite diagenesis .....	48
Figure 29: δ <sup>34</sup> S results organized into four depositional groups. ....	50
Figure 30: Fractionation values for Dissimilatory SRB, Disproportionate SRB, and Oxidation processes in Georgia kaolin. ....	52
Figure 31: SO <sub>2</sub> yield and δ <sup>34</sup> S among red (oxidized) and gray (reduced) Twiggs Clay .....	55

## LIST OF EQUATIONS

Equations 1: Definition of $\delta^{34}\text{S}$ .....	16
Equations 2: Bacterial reduction of sulfate .....	46
Equations 3: Reaction of Hydrogen sulfide with iron oxides.....	46
Equations 4: Reaction of Iron(II) sulfide with elemental sulfur.....	46
Equations 5: Simplified reaction of disproportionate sulfur-reducing bacteria .....	51

## CHAPTER 1

### INTRODUCTION

The kaolin group is a collection of vital industrial minerals. Its uses, among others, include white pigmentation of paper and paint, ceramics, and as a primary ingredient in refractory, brick, and fiberglass products. Kaolinite [ $\text{Al}_2\text{Si}_2\text{O}_5(\text{OH})_4$ ] is the most common and industrially important of the kaolin minerals (Murray and Keller, 1993). Although kaolin minerals are extremely common, large deposits of highly pure kaolin that can be used in industrial processing facilities with access to global transportation infrastructures are uncommon (Patterson and Murray 1984).

In the United States, the largest deposits are found in the South Carolina-Georgia-Alabama kaolin belt (Fig.1). This region contains an estimated seven to ten billion tons of kaolin, making it the world's primary supply of sedimentary kaolin (Patterson and Murray, 1984). In Georgia, the kaolin belt is located in the coastal plain just south of the fall line, a geologic boundary separating Piedmont crystalline rocks to the north from Mesozoic to Cenozoic sedimentary rocks to the south. Because of kaolin's commercial uses, as well as its importance as a geologic indicator of diagenesis, this kaolin belt has been extensively studied (Hurst and Pickering 1997; Schroeder et al. 2004; and others). Much of this research has focused on mineralogy and petrology to determine the depositional environment and diagenesis of these kaolins. Some studies have used stable isotopes to interpret the original sediments, the depositional environment, and the amount of alteration (Over et al., 1987; Sprague et al., 1988; Cheshire et al, 2012).

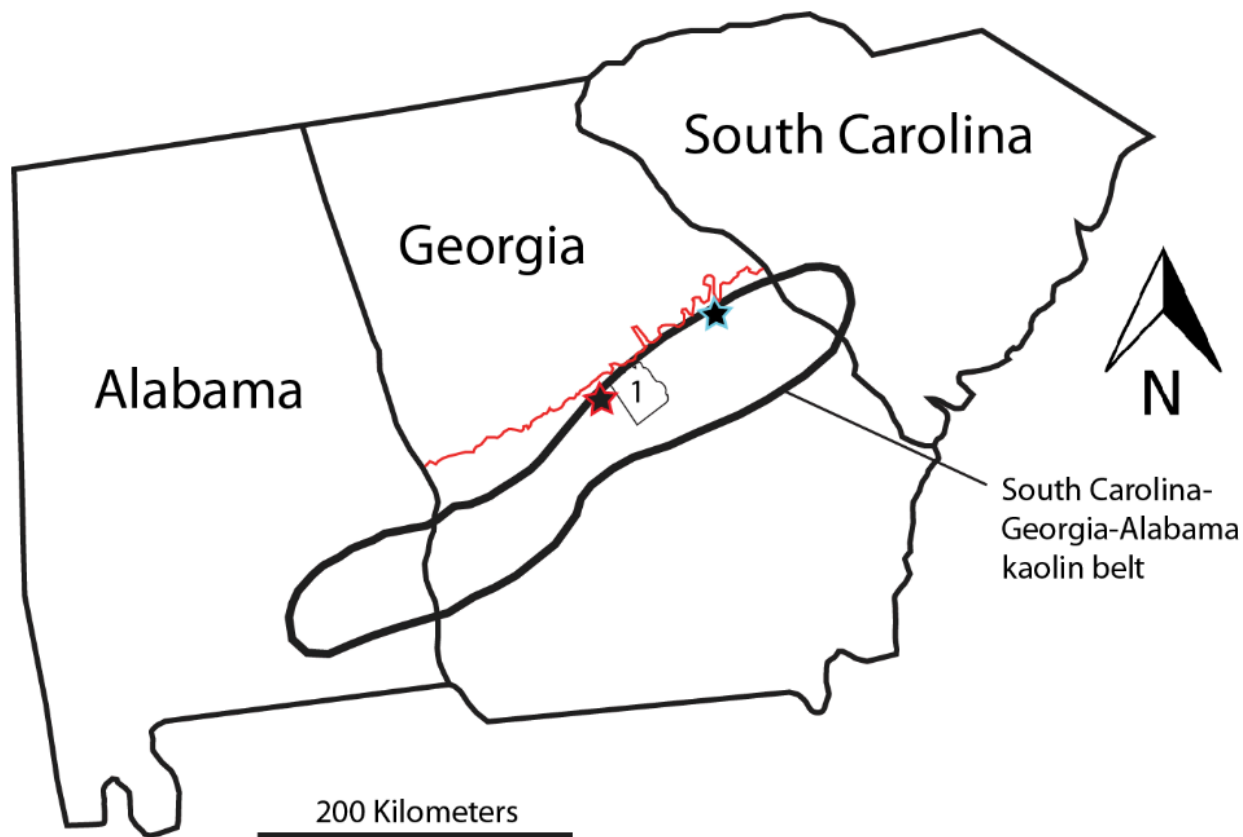


Figure 1. Map of the South Carolina-Georgia-Alabama kaolin belt. The red line indicates the location of the fall line. The blue star indicates the location of sampling for this study. The red star indicates the location of Dry Branch, Georgia. The county labeled 1 is Wilkinson County, Georgia. Modified from Patterson and Murray, 1984.

The purpose of this investigation is to use powder X-ray diffraction (XRD) and  $\delta^{34}\text{S}$  analysis to determine whether the depositional conditions of the Huber Formation and Twiggs Clays in Georgia were open or closed to sulfate supply and the degree of post depositional oxidation. The reduced iron phase (gray clays) of Georgia kaolin represent the least altered and least oxidized deposits (Schroeder et al. 2004). These deposits, with a measureable sulfur component sequestered in  $\text{FeS}_2$  by sulfate-reducing bacteria, may provide insight into the original depositional conditions of the Georgia kaolin (Canfield and Thamdrup, 1994; Habicht and Canfield, 1996, 2001a, 2001b). Sulfur isotopes can provide a tool for understanding the depositional environment because the ocean mixes rapidly ( $\sim 2 \times 10^3$

years) relative to the residence time of sulfate in seawater ( $\sim 2 \times 10^7$  years). This disparity in rates demonstrates that the  $\delta^{34}\text{S}$  value of the ancient ocean would be ubiquitous and confirms that variation in  $\delta^{34}\text{S}$  among Georgia kaolin deposits is the result of forces other than global seawater chemistry (Claypool, 1980).

## CHAPTER 2

### PREVIOUS WORK

#### Deposition and Diagenesis

For more than a century, studies have focused on the depositional environments and alteration conditions of the commercially important kaolin clays in central Georgia. For much of that time, workers have concluded the source of sediments for the Cretaceous and Tertiary kaolins were intensely weathered granites and gneisses of the Piedmont (Stull and Bole, 1926; Keller, 1977; Hurst and Pickering, 1989). When weathered, these crystalline rocks formed saprolites containing kaolinite, which were eroded off the Piedmont and transported fluvially to the Cretaceous and Tertiary shorelines where they were deposited (Hurst and Pickering, 1989).

Stull and Bole (1926) developed six descriptive categories for Georgia's clay, including the current distinctions between "hard" and "soft" kaolins. These distinctions are qualitative and differentiate between kaolins that may have been formed in different ways. Soft kaolins are the result of erosion of saprolite detritus from the Piedmont, which was transported by fluvial processes to the coast, where they underwent diagenesis after deposition of the original kaolin. Hard kaolins formed as the result of *in situ* alteration of the Piedmont, forming saprolites containing kaolinite, which were eroded and transported to coastal waters and deposited as kaolin. Using this classification, Stull and Bole (1926) argued that Georgia kaolin formation occurred in two distinct episodes. In the Mesozoic, hard kaolins were deposited and diagenetically altered to soft kaolin. In the Tertiary, hard kaolin was deposited but was not altered (Stull and Bole, 1926). These theories of sedimentation from piedmont saprolite

continued to gain support throughout the mid 20<sup>th</sup> century based on studies of large-scale features observed within the kaolin (Smith, 1929; LeGrand and Furcron, 1956; Kesler, 1956).

In the 1960s, studies focused on the chemistry, mineralogy, and petrology of the Georgia kaolins began to contradict the direct sedimentary origin of these formations. The first such study was conducted on the kaolin deposits of Dry Branch, Georgia (Fig. 1). The study examined the orientation of muscovite grains in relation to the kaolinite grains using oriented thin section, X-ray diffraction, and disaggregated sand-sized grains. It was found that the large muscovite grains showed a preferred horizontal orientation, while the kaolinite grains showed no preferred orientation. This suggested that the mica platelets were deposited sedimentologically and then post-depositionally altered to kaolin (Jonas, 1964). With the proliferation of modern electron microscopy, numerous studies focused on the mineralogy and petrology of Georgia kaolins helped to substantiate this secondary alteration interpretation (Buie and Fountain, 1967; Bohor and Randall, 1971; Austin, 1972; Tschudy and Patterson, 1975; Buie et al., 1979; Barker and Hurst, 1992).

Hurst and Pickering (1997) also concluded that the formation of pure Georgian kaolins is not possible by sedimentary processes alone. The original sediments deposited in the coastal zone (micaceous to arkosic sands; impure kaolinitic and metahalloysitic fine sands and clays; and smectitic clays, marls, and carbonates) underwent compositional and textural alteration, removal of organic matter, iron, and manganese, and recrystallization of kaolinite and metahalloysite (Hurst and Pickering, 1997). The existence of erosional unconformities separated by coastal sediments lead to the further conclusion that kaolins were produced, at different rates, by dyoxic and oxic weathering in saturated and unsaturated ground water zones, respectively, and that kaolinization of the host rock was generally not completed by the time of deposition

(Hurst and Pickering, 1997). Hurst and Pickering (1997) concisely summarize their conclusions regarding the sedimentary nature of the Georgia kaolins by stating: “Since accumulated data now show that [Georgia kaolins] did not originate by sedimentary processes (Hurst, 1997), calling them ‘sedimentary’ is unjustified, even in allusion to their occurrence in sedimentary rocks, unless Cornwall kaolins (England) derived from granitic rocks are called ‘igneous’ and Shaoping kaolins (China) derived from rhyolitic tuffs are called ‘volcanic’.” They suggested that the term ‘Coastal Plain’ kaolins replace ‘sedimentary’ kaolins.

Further research concluded that oxic weathering contributed significantly to the development of the Eocene Huber Formation in Wilkinson County, Georgia (Fig. 1). Using chemical, crystallographic, and Raman spectroscopic analysis techniques, Schroeder et al. (2004) determined that color variations within the Huber Formation formed from oxidative weathering fronts. These color variations are important to the current study and include variations from gray (caused by pyrite, marcasite, ferrous silicates, and kerogen), to pink (hematite), to cream (goethite and anatase) clays. Gray clays were interpreted to be the most reduced, and the pyrite, biotite, and ilmenite they included were a precursor to the iron (pink) and titanium (cream) bearing phases before the gray clay underwent oxidation (Schroeder et al. 2004).

Cheshire et al. (2012) used organic  $\delta^{13}\text{C}$  and biomarker analysis to determine the origin and nature of the Georgia kaolin’s original sediments, depositional environment, and degree of alteration. Categorizing the kaolin into “organic-lean” and “lignitic”, bulk organic  $\delta^{13}\text{C}$  ranged from -26 to -19‰. A relationship was observed between enrichment in  $^{13}\text{C}$  and lack of organic content in the kaolin. This enrichment is interpreted as the result of microbial decomposition of the organic matter in the kaolins that preferentially broke weaker  $^{12}\text{C}$ - $^{12}\text{C}$  bonds, opposed to stronger  $^{13}\text{C}$ - $^{13}\text{C}$  or  $^{12}\text{C}$ - $^{13}\text{C}$  bonds, as well as the presence of different

organic carbon reservoirs with varying  $\delta^{13}\text{C}$ . The data suggests that microbial lipids are the current dominant organic matter in the lean kaolins, while terrestrial plant matter dominated during deposition of the lignitic kaolin (Cheshire et al., 2012).

### Sedimentology and Stratigraphy

The Huber Formation and Twiggs Clay are Paleocene to Eocene clays deposited down dip of the central Georgian fall line (Fig. 1). The Huber Formation is a Paleocene to Eocene deposit of upward-fining sand to clay, deposited in a marginal marine environment (Buie and Fountain, 1967). The Huber Formation is divided into two members, the lower Marion Member and the upper Jeffersonville Member. The Marion Member is characterized by soft kaolin suggested to be deposited in freshwater environments, while the Jeffersonville Member contains the distinctive, and economically important, hard kaolins suggested to be deposited in marginal marine environments (Huddleston and Hetrick, 1991). The Huber Formation is capped by an unconformity above which there are no economically significant kaolin deposits, making the Huber an important stratigraphic target for kaolin exploration (Kogel et al. 2002; Allen et al. 2009).

The Twiggs Clay is the first member of the Barnwell Group, which overlies the Huber Formation (Fig. 2). The Twiggs Clay was deposited as discontinuous lenses that interfinger with sands, muds, and limestones of the overlying second member of the Barnwell Group, the Irwinton Sand Formation (Kogel et al. 2002, Eversull, 2005). The Twiggs is a hard clay deposited in a marine environment, and it contains no economically important kaolin deposits (Al-Sanabani, 1991). Much of the overburden drilled in the study area was composed of the Irwinton Sand Formation (Table 1).

Age relations between the Twiggs Clay and the Huber Formation are constrained by geochronology and paleontological data. Concordant K-Ar data from glaucony within the Twiggs Clay reports an age of about 34 Ma (Wampier et al., 2001). The Clinchfield Sand, a sand unit that sometimes occurs between the Twiggs Clay and Huber Formation, includes fossils from Nannofossil Zone NP 19-20 correlating to an age of 34.2 to 36.0 Ma (Parmley and Holman, 2003). Nanofossils in the Jeffersonville Member of the Huber Formation, from the biochronozone CP 14, are associated with the Ypresian and Lutetian stages of the middle Eocene (Kogel et al, 2002). These data indicate that the period of deposition between the Jeffersonville Member of the Huber Formation and the Twiggs Clay is between 7.2 and 22 Ma.

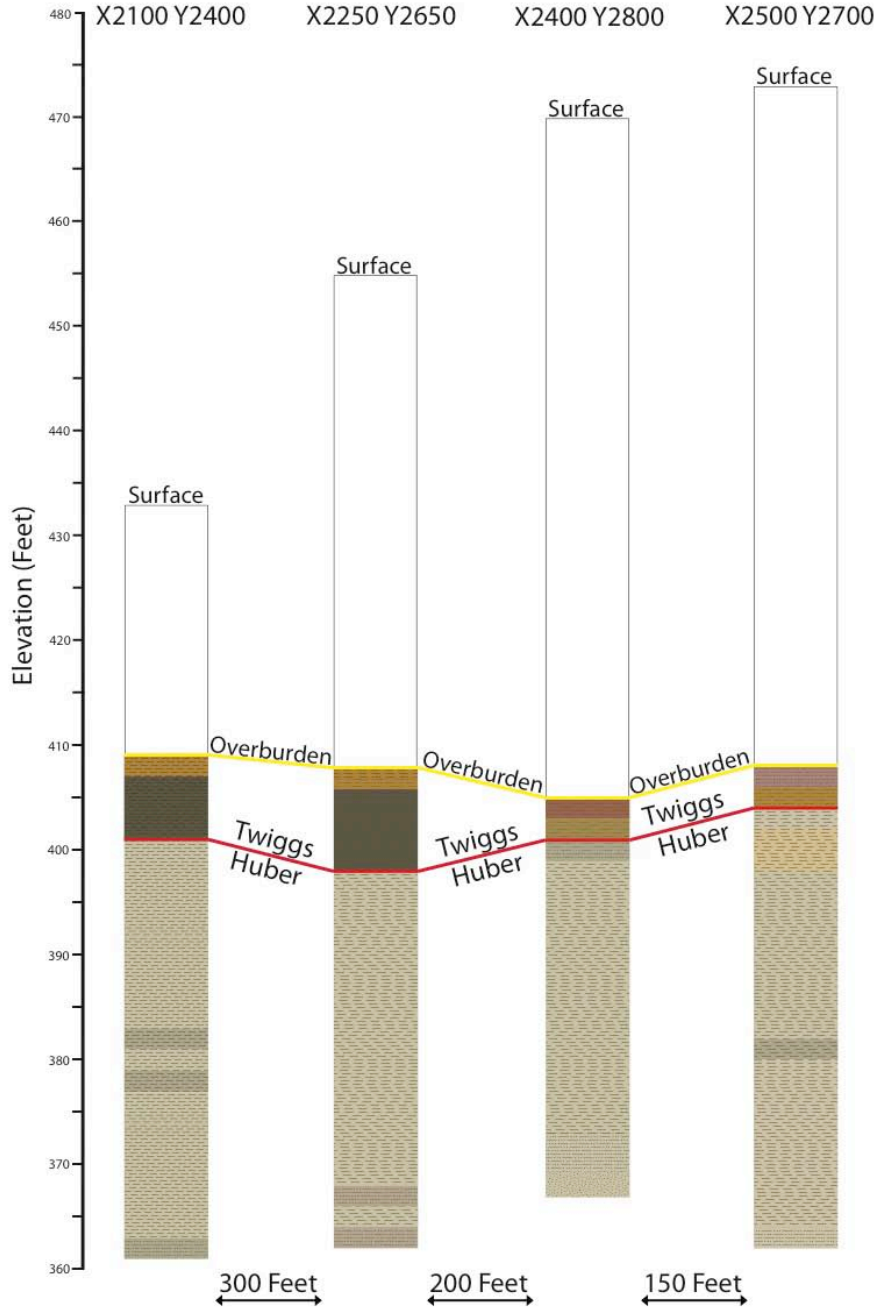


Figure 2. Stratigraphic columns of the four cores drilled for this study. Colors are coordinate with Munsell Soil Color system. The textures on the columns represent the three qualitative textures used in this study: 1. Dashes (clay) 2. Dashes and dots (sandy clay) 3. Dots (sand)

## CHAPTER 3

### METHODS

#### Scanning Electron Microscope

KaMin LLC sent four preliminary clay samples from nearby private properties to test the methods of this study. The samples included 3 reduced gray clays and 1 oxidized cream clay. Electron backscatter images of these samples were taken using a Zeiss 1450EP Scanning Electron Microscope at the University of Georgia Center for Advanced Ultrastructural Research (Fig. 3) in order to establish the existence of significant pyrite within the Huber clay. The survey of these clays was merely cursory with no intention of analysis beyond observation. Once the presence of pyrite was established, trials of modified versions of the  $V_2O_5$  sulfur extraction methodology (Ueda and Krouse, 1986) were tested to determine how to best extract a measureable amount of  $SO_2$  gas.



Figure 3. Using the SEM at the University of Georgia to photograph pyrite.

### Sample Collection

Four cores through the Huber and Twiggs were drilled on March 20-21, 2013 from private property near the crossing of Purvis School House Road and Georgia Highway 17 (Fig. 4), approximately halfway between Wrens, Georgia and Thomson, Georgia (Fig. 1) by the Login Drilling Company (Fig. 5), contracted by KaMin LLC. Each core was named for its location on an X-Y coordinate system used by KaMin LLC. The minimum distance between cores is 150 feet and the maximum distance is 300 feet.

The cores were boxed after drilling and brought to the University of Georgia, where samples of a few grams were collected every two feet in the Jeffersonville Member of the Huber

Formation and every foot in the Twiggs Clay. The Twiggs Clay and Huber Formations were distinguished by a sudden color transition within each core. In two of the cores (X2100 Y2400 and X2250 Y2650), this color change is a stark contrast between the gray Huber Formation and the dark gray/black Twiggs Formation. In the other two cores (X2400 Y2800 and X2500 Y2700), the color change appears as sharp contact between the gray Huber Formation and orange overlying Twiggs Clay. Samples were named by the coordinates for the core they were collected from with the elevation in feet of the sample in parentheses (e.g., X2100 Y2400 (363)). Sample color was described using the Munsell color system, and sample textures were described qualitatively as 'clay', 'sandy clay', or 'sand'. Once samples were collected, they were stored in a vacuum. Photographs of all cores before sampling are included in Appendix A.

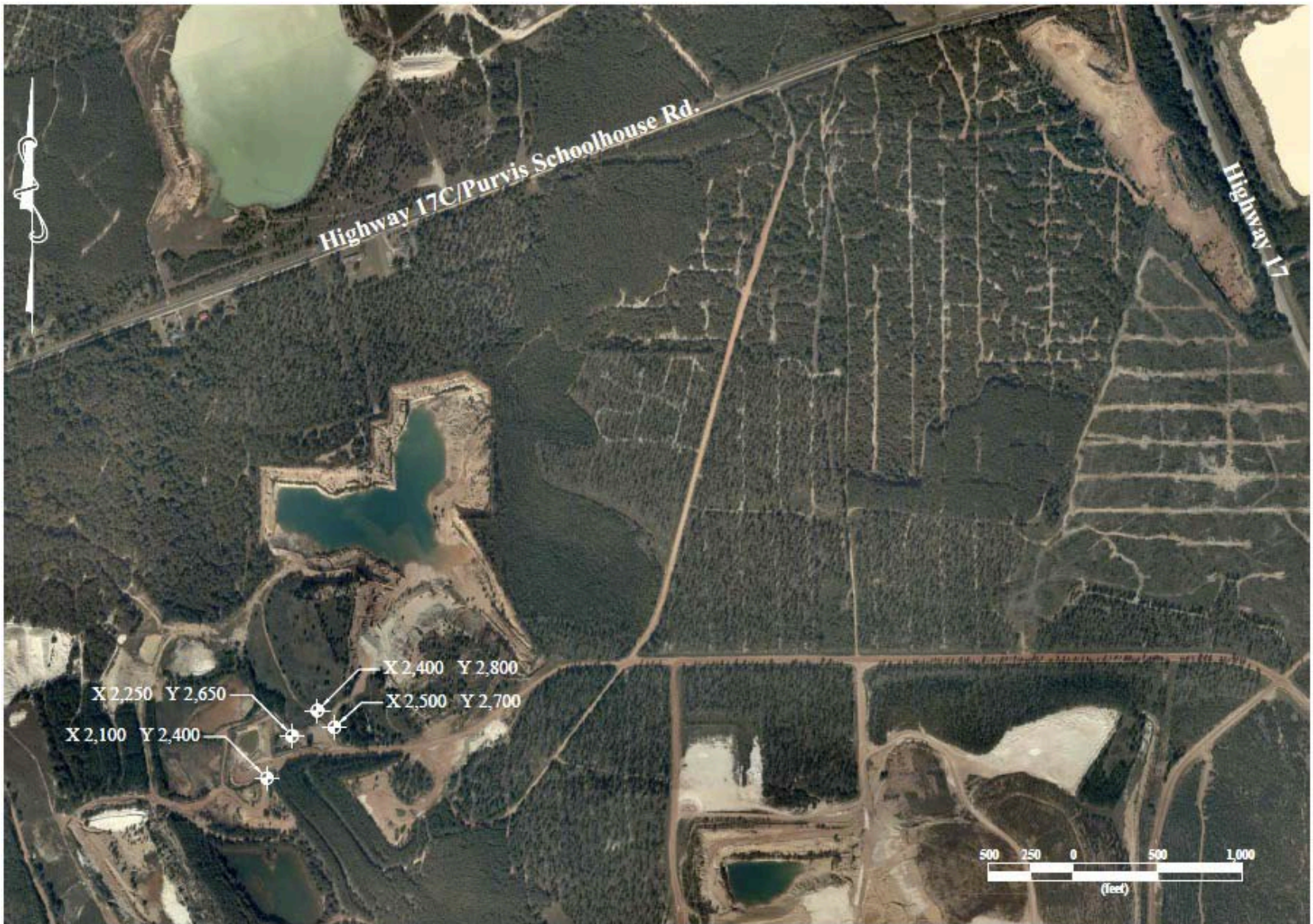


Figure 4. Map of drilling area with locations of four cores indicated. This map corresponds to the star on Fig. 1.



Figure 5. Truck mounted rig and crew drilling through Huber Formation near the intersection of Georgia Highway 17 and Purvis Schoolhouse Road.

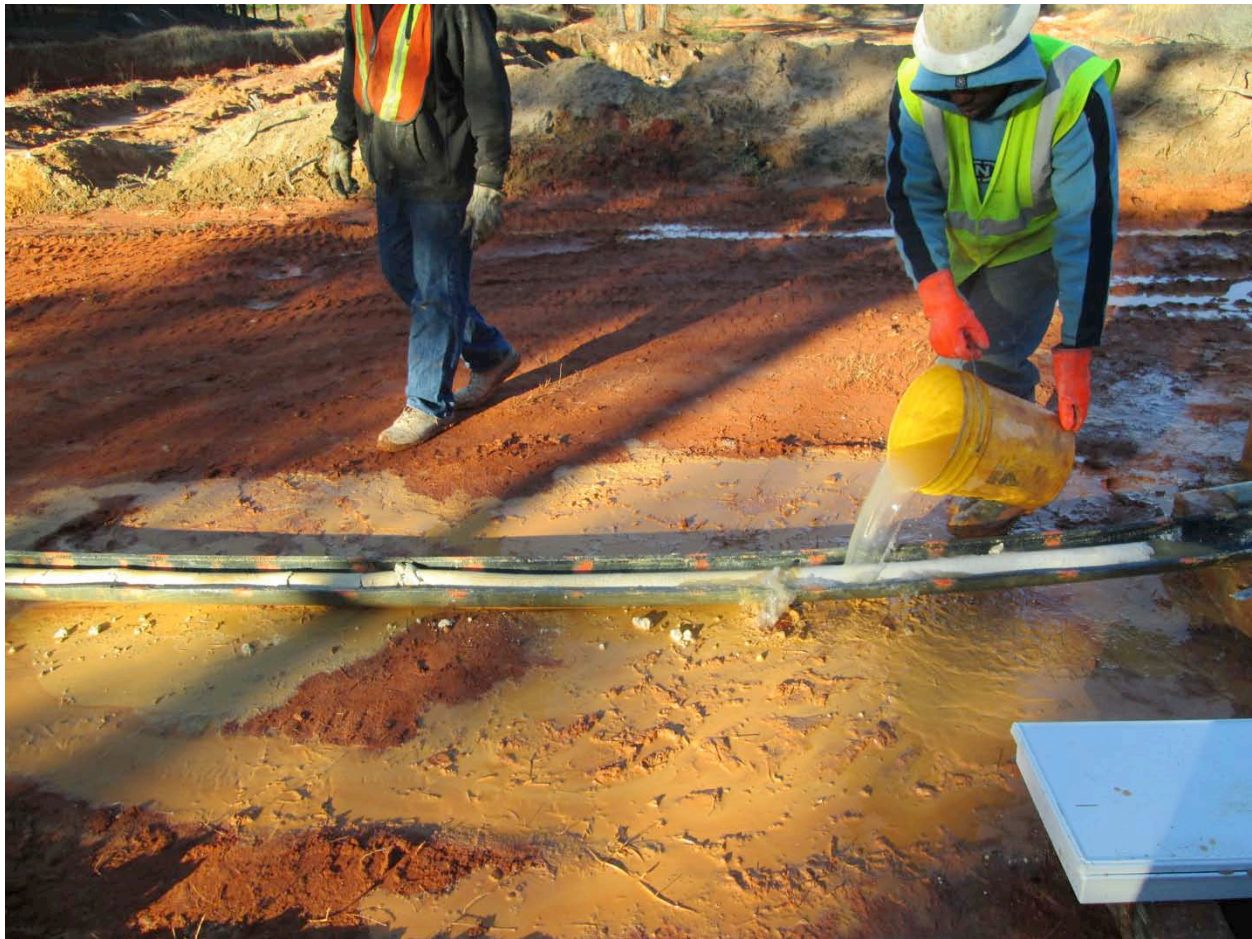


Figure 6. Login Drilling Company crew washing off newly collected core of the Jeffersonville Member of the Huber Formation.

### X-Ray Diffraction

XRD data were obtained with the Bruker D8 X-ray diffractometer at the University of Georgia. Samples were dewatered by baking overnight at 100°C. The samples were ground into a powder using a mortar and pestle, and approximately 2 grams of ground sample was mounted on a slide by pressing at 400 P.S.I. for approximately one minute. Parameters of the XRD analysis and XRD data are provided in Appendix B.

### Sulfur Extraction and Mass Spectrometry

Samples were prepared and analyzed at the University of Georgia Department of Geology Stable Isotope Laboratory using the sulfur cryogenic extraction line using a modified

V<sub>2</sub>O<sub>5</sub> extraction method (Ueda and Krouse, 1986). To remove the high organic content of these clays, samples were baked for 12 – 18 hours at 450°C in a muffle furnace. After baking, 2.00 g of clay was measured and mixed with 50 mg each of V<sub>2</sub>O<sub>5</sub>, copper metal powder, and quartz powder. The V<sub>2</sub>O<sub>5</sub> acts as a donor of the necessary oxygen to produce SO<sub>2</sub> gas, the metal copper is a buffer that represses the formation of SO and SO<sub>3</sub>, and the quartz powder is an abrasive agent during grinding. Once mixed, the sample was ground in a mortar and pestle and loaded into a quartz sample tube.

The sample was placed into the sulfur extraction line and combusted for fifteen minutes at a temperature of 1050°C. The line cryogenically isolates the SO<sub>2</sub> gas from non-condensable gasses, CO<sub>2</sub>, and H<sub>2</sub>O using a dry ice and ethanol slush and a variable temperature trap. The SO<sub>2</sub> gas was measured using a calibrated mercury manometer, converted, and reported as actual SO<sub>2</sub> yield. SO<sub>2</sub> was collected in a Pyrex breakseal and analyzed using a Finnigan MAT 252 mass spectrometer. An error of ±0.6 2σ was determined based upon replicate analysis of Esperanza and ZS495 standards. The data are reported relative to the Canyon Diablo Troilite Standard (CDT) defining δ<sup>34</sup>S as:

$$\delta^{34}\text{S} = \left( \frac{\left( \frac{{}^{34}\text{S}}{{}^{32}\text{S}} \right)_{\text{sample}} - \left( \frac{{}^{34}\text{S}}{{}^{32}\text{S}} \right)_{\text{reference}}}{\left( \frac{{}^{34}\text{S}}{{}^{32}\text{S}} \right)_{\text{reference}}} \right) \times 1000 \quad (1)$$

## CHAPTER 4

### RESULTS

#### Scanning Electron Microscope

SEM analysis of the samples was necessary to determine the plausibility of this study. Four clay samples were observed and described by KaMin LLC as the following: one cream sample (PM-1, assumed to be least reduced), two gray samples (CS-1 and CS-2, assumed to be moderately reduced), and one dark gray sample (GR-1, assumed to be most reduced). SEM electron backscatter images show the presence of pyrite in all four samples. PM-1 has small crystals of pyrite; the largest observed are no larger than 5  $\mu\text{m}$  (Fig. 7). CS-1 and CS-2 not only have the largest pyrite crystals found in these initial samples, with some exceeding 20  $\mu\text{m}$  (Fig. 8), but they have the most perfectly euhedral specimens as well (Fig. 9). The pyrite within the very gray sample, GR-1, is very similar to that of PM-1: large pyrite crystals are rare and no larger than 5  $\mu\text{m}$ . The kaolin constituent of all samples has the very fine texture associated with 'hard' kaolins (Pruett et al. 2009).

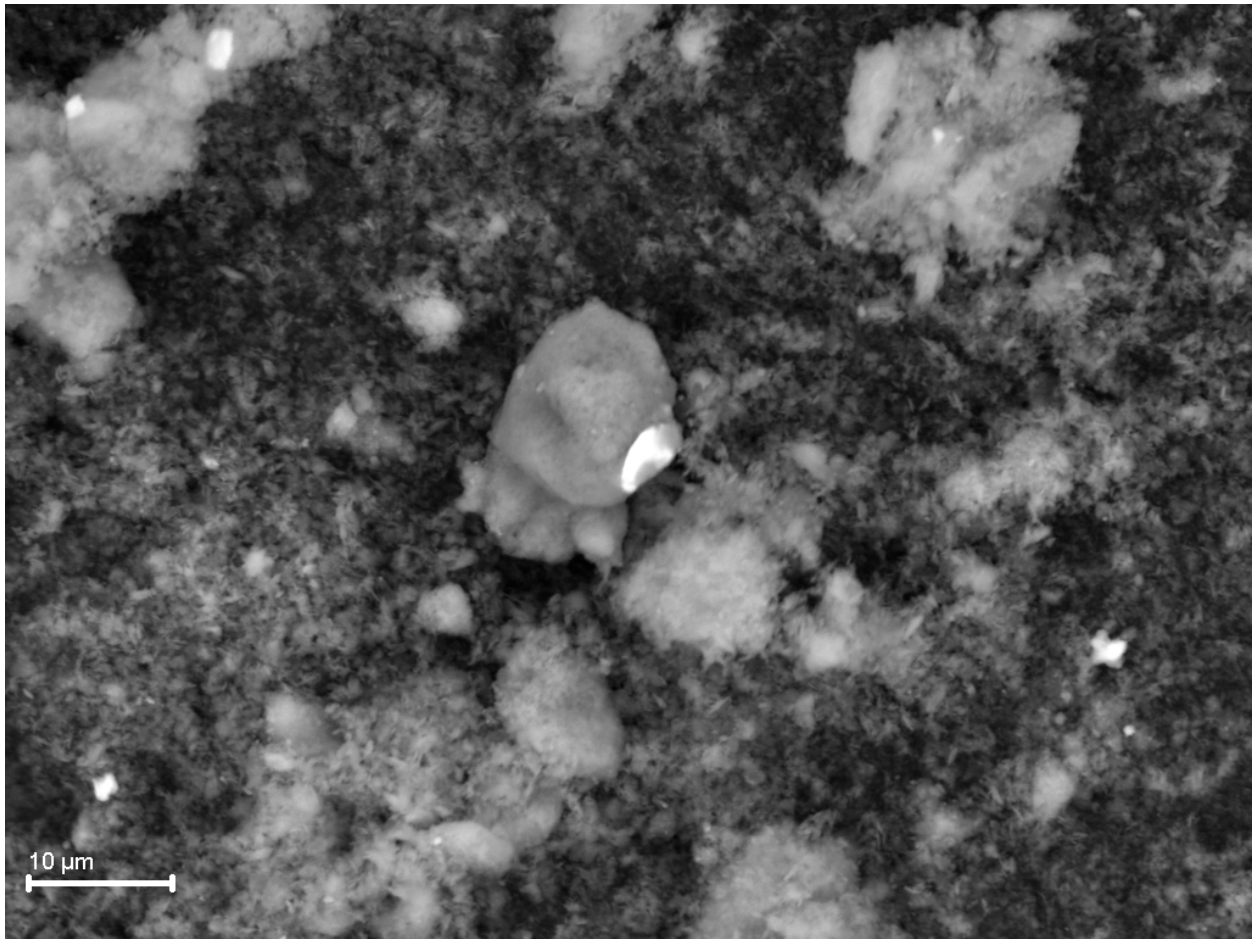


Figure 7. Small crystal of pyrite in preliminary cream clay, PM-1.

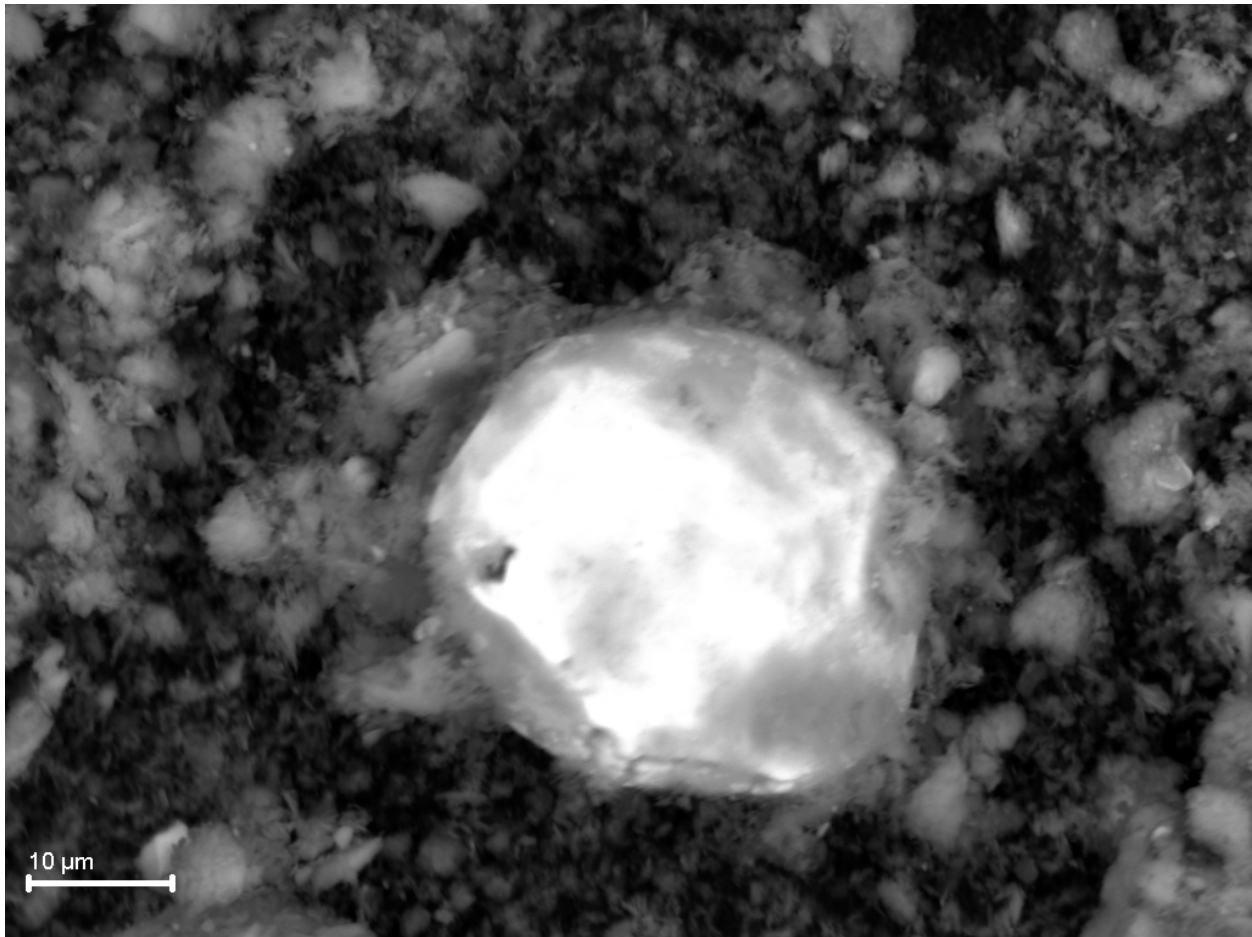


Figure 8. Large crystal of pyrite in preliminary gray clay, CS-1. The fineness of clay particles is typical of Tertiary “hard” kaolins.

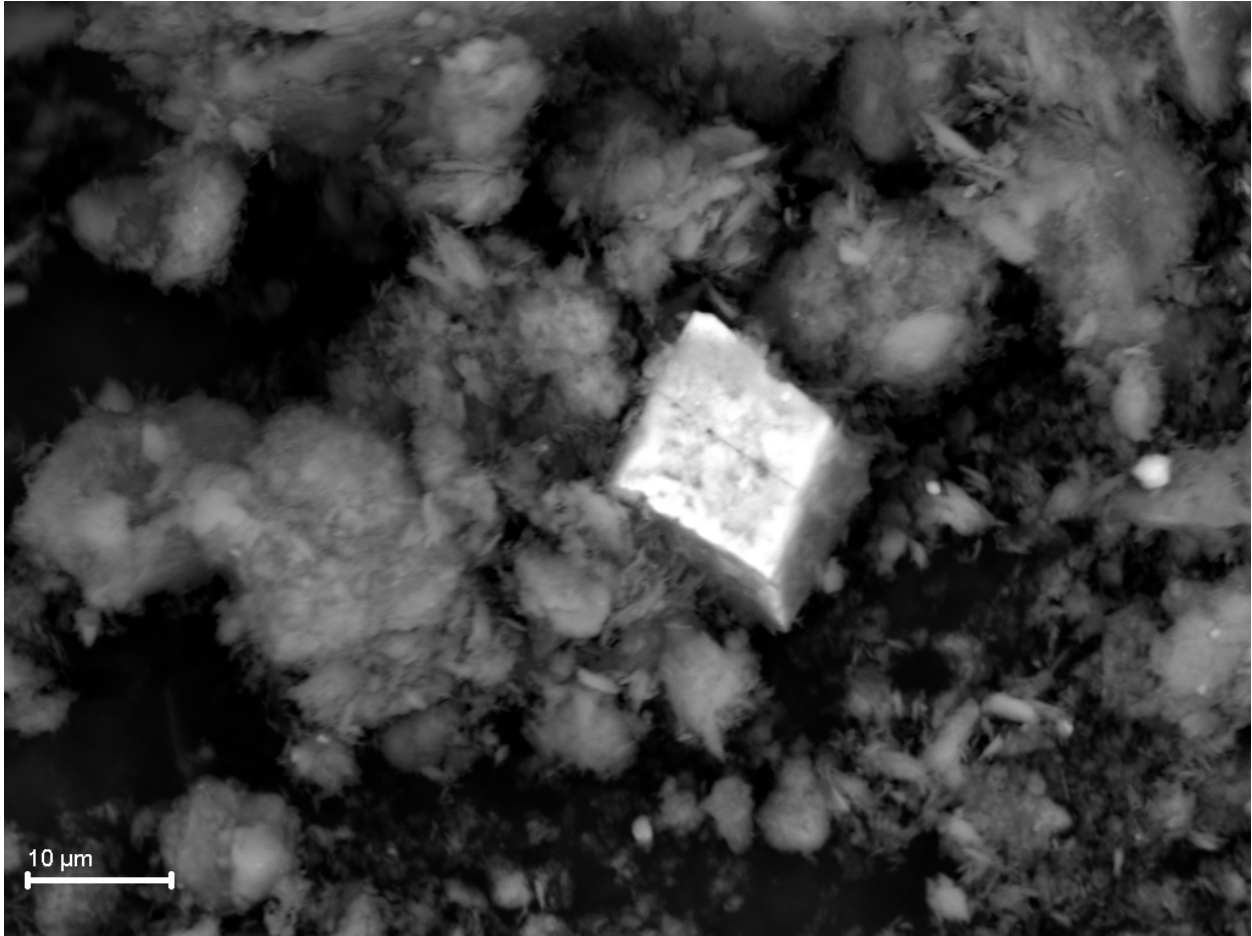


Figure 9. Large euhedral pyrite crystal in preliminary gray clay CS-2.

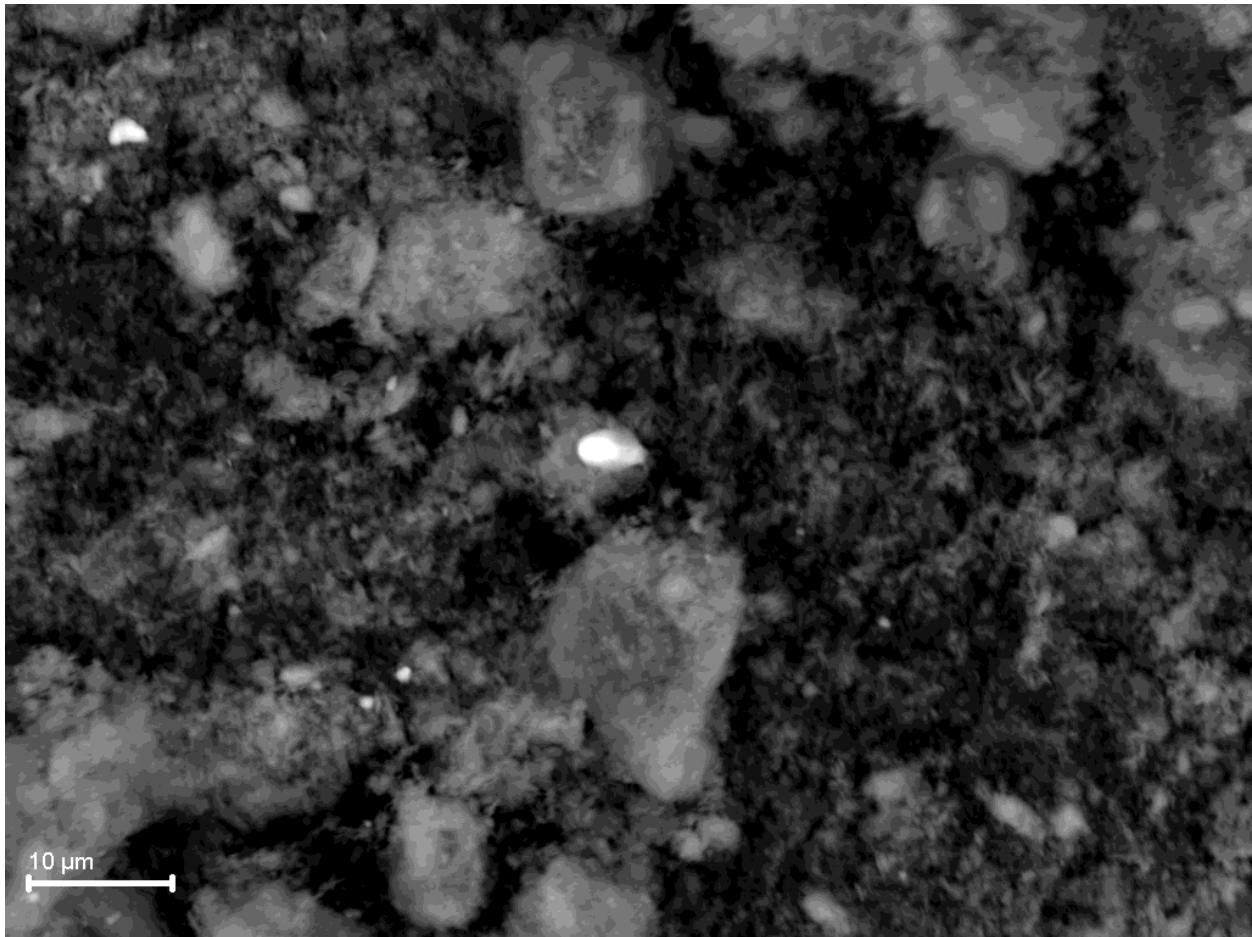


Figure 10. Small crystal of pyrite in preliminary cream clay, GR-1.

### Sample Collection

Driller's summarized log data is summarized in Table 1 with sample colors and textures summarized in appendix C.

TABLE 1. DRILLER'S SUMMARIZED LOG DATA

Core coordinates	Top elevation (ft)*	Overburden (ft)	Collected thickness (ft)†	Samples bagged
X2500 Y2700	473	65	44	25
X2400 Y2800	470	65	37	21
X2250 Y2650	455	47	45	28
X2100 Y2400	433	24	47	28

\*Elevation of drill collar at time of collection

†Total thickness of both Twiggs Clay and Huber Formation collected

## X-Ray Diffraction

XRD analysis was used to determine the bulk mineralogical composition of the Twiggs and Huber Formations within each core. The four cores are all presented in the same manner: 3D graphs have been constructed to better demonstrate the mineralogical transitions that exist stratigraphically

It is important to understand the axes of these graphs to appreciate the results presented below. A single sample, two-dimension plot shows a relationship between 2-Theta, the measurement of the angle between X-ray incident beam and diffracted beam, and the X-ray counts, or intensity of the reflected beam (Fig. 11). The 3D graphs show these same data on the X and Y-axes while stacking all the data by elevation in on a Z-axis. Owing to hand grinding these samples for analysis, approximately 10% error can be accounted for among the XRD counts. Complete Figures of individual sample XRD results can be found in appendix B.

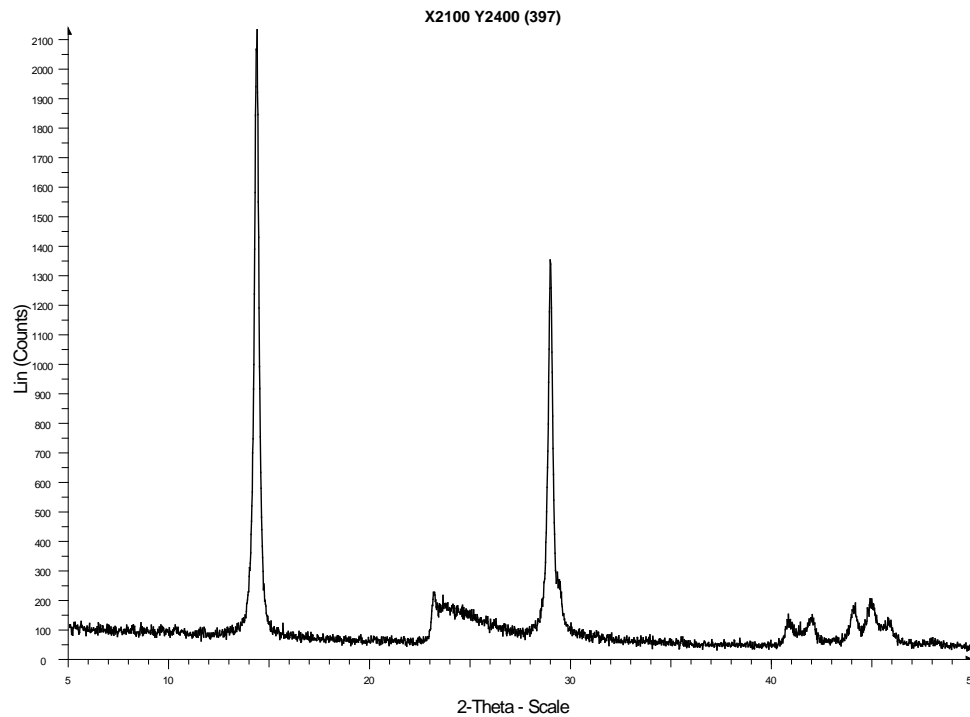


Figure 11. An example of a XRD plot from the upper part of the Huber Formation within the X2100 Y2400 core.

# X2250 Y2650 X-Ray Diffraction

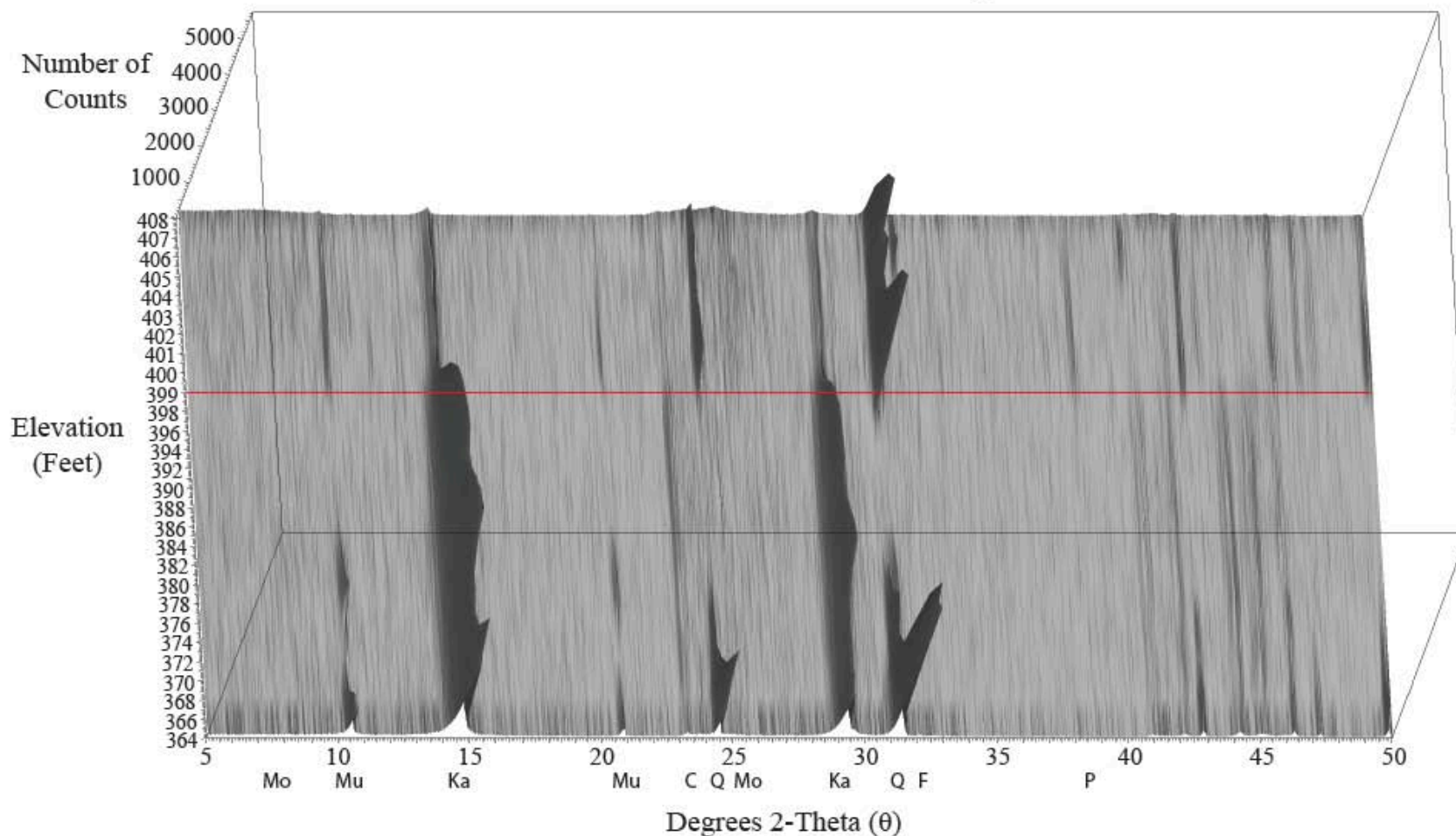


Figure 12. 3D XRD plot of X2250 Y2650. Red line indicates the Twiggs Clay/Huber Formation boundary. Mineral abbreviations indicate the location of the 2-Theta signature for a particular mineral; Montmorillonite (Mo), Muscovite (Mu), Kaolinite (Ka), Various Clays (C), Quartz (Q), Potassium Feldspar (F), Pyrite (P)

X2250 Y2650

At the base of the Huber in X2250 Y2650 (Fig. 12), the most prominent phyllosilicate peaks occur at  $14.4^\circ$  two-theta ( $7.17 \text{ \AA}$ ) and  $29.1^\circ$  ( $3.58 \text{ \AA}$ ) two-theta, indicating a high abundance of kaolinite that continues upsection to the Huber/Twiggs boundary. Large peaks at  $24.3^\circ$  two-theta ( $4.26 \text{ \AA}$ ) and  $31.1^\circ$  two-theta ( $3.34 \text{ \AA}$ ) indicate large quantities of quartz. This is consistent with textural observations at the base of the Huber, which becomes sandier with depth. Less prominent peaks at  $10.4^\circ$  two-theta ( $9.95 \text{ \AA}$ ) (muscovite),  $20.8^\circ$  two-theta ( $4.32 \text{ \AA}$ ) (muscovite), and  $23.2^\circ$  two-theta ( $3.88 \text{ \AA}$ ) (various clays) demonstrate other sheet silicates within the Huber Formation. The presence of muscovite appears to be restricted to the lower half of the Huber section while kaolinite and various clays appear consistently up section. Among the phyllosilicates, recession occurs between elevations of 372 and 376 feet, where counts are lower in all cases and nearly disappear for muscovite. At 386 feet, kaolin and various clays rebound and peaks are present up to the Twiggs/Huber boundary.

An abrupt transition occurs at 399 feet, corresponding to the Twiggs/Huber boundary. The most prominent peak at  $31.1^\circ$  two-theta ( $3.34 \text{ \AA}$ ) and another peak at  $24.3^\circ$  two-theta ( $4.26 \text{ \AA}$ ) show the return of quartz in the Twiggs, confirming textural observations that the Twiggs is much sandier than the Huber Formation. The Kaolin counts ( $14.4^\circ$  two-theta ( $7.17 \text{ \AA}$ ) and  $29.1^\circ$  two-theta ( $3.58 \text{ \AA}$ )) decrease while muscovite ( $10.4^\circ$  two-theta ( $9.95 \text{ \AA}$ ) and  $20.8^\circ$  two-theta ( $4.32 \text{ \AA}$ )) counts return after reduction within the upper Huber. Small peaks of other minerals not present within the Huber Formation appear at the boundary, starting with small bulges at  $7.7^\circ$  two-theta ( $11.60 \text{ \AA}$ ) and  $25.2^\circ$  two-theta ( $3.58 \text{ \AA}$ ) (montmorillonite) and a small peak at  $32.0^\circ$  two-theta ( $2.80 \text{ \AA}$ ) (potassium feldspar).

One of the small abundances that appear above the Twiggs/Huber boundary is the peak at 38.6° two-theta (2.36 Å), indicating the presence of pyrite. Pyrite is much more common in the Twiggs Clay than the Huber Formation. This observation is also supported by the sulfur extraction data discussed below.

#### *X2100 Y2400*

The most prominent peaks at the base of the Huber in X2100 Y2400 (Fig. 13) occur at 14.4° two-theta (7.17 Å) and 29.1° two-theta (3.58 Å) (kaolinite) and 24.3° two-theta (4.26) and 31.1° two-theta (3.34 Å) (quartz). The base of the Huber Formation in this core becomes sandier with depth, and the XRD confirms this textural observation. The other phyllosilicates, muscovite (10.4° two-theta (9.95 Å) and 20.8° two-theta (4.32 Å)), and various clays (23.2° two-theta (3.88 Å)) also occur at the base of the Huber. Muscovite peaks at the base of the section, but counts of it decrease to nearly zero around 373 feet, form a small prominent peak near 383 feet, then decrease to near zero again until the Twiggs/Huber boundary. The various clays produce a small peak continuously through the section to the Twiggs/Huber boundary.

There is a sharp mineralogical change at 402 feet, the Twiggs/Huber boundary. At the upper portion of the Huber, kaolin (14.4° two-theta (7.17 Å) and 29.1° two-theta (3.58 Å)) and various clays (23.2° two-theta (3.88 Å)) peaks drop sharply while quartz (24.3° two-theta (4.26) and 31.1° two-theta (3.34 Å)) peaks rise abruptly, confirming textural observations. Muscovite (10.4° two-theta (9.95 Å) and 20.8° two-theta (4.32 Å)) is prominent above the Twiggs/Huber boundary, along with a small rise in montmorillonite (7.7° two-theta (11.60 Å) and 25.2° two-theta (3.58 Å)) and potassium feldspar (32.0° two-theta (2.80 Å)).

Most important to the current study a small peak of pyrite (38.6° two-theta (2.36 Å)) occurs within the Twiggs Clay. The pyrite peak rises at the Twiggs/Huber boundary and

decreases near the top of the section. This variation in pyrite content between the Huber and Twiggs and within the Twiggs is supported by the sulfur extraction data discussed below.

# X2100 Y2400 X-Ray Diffraction

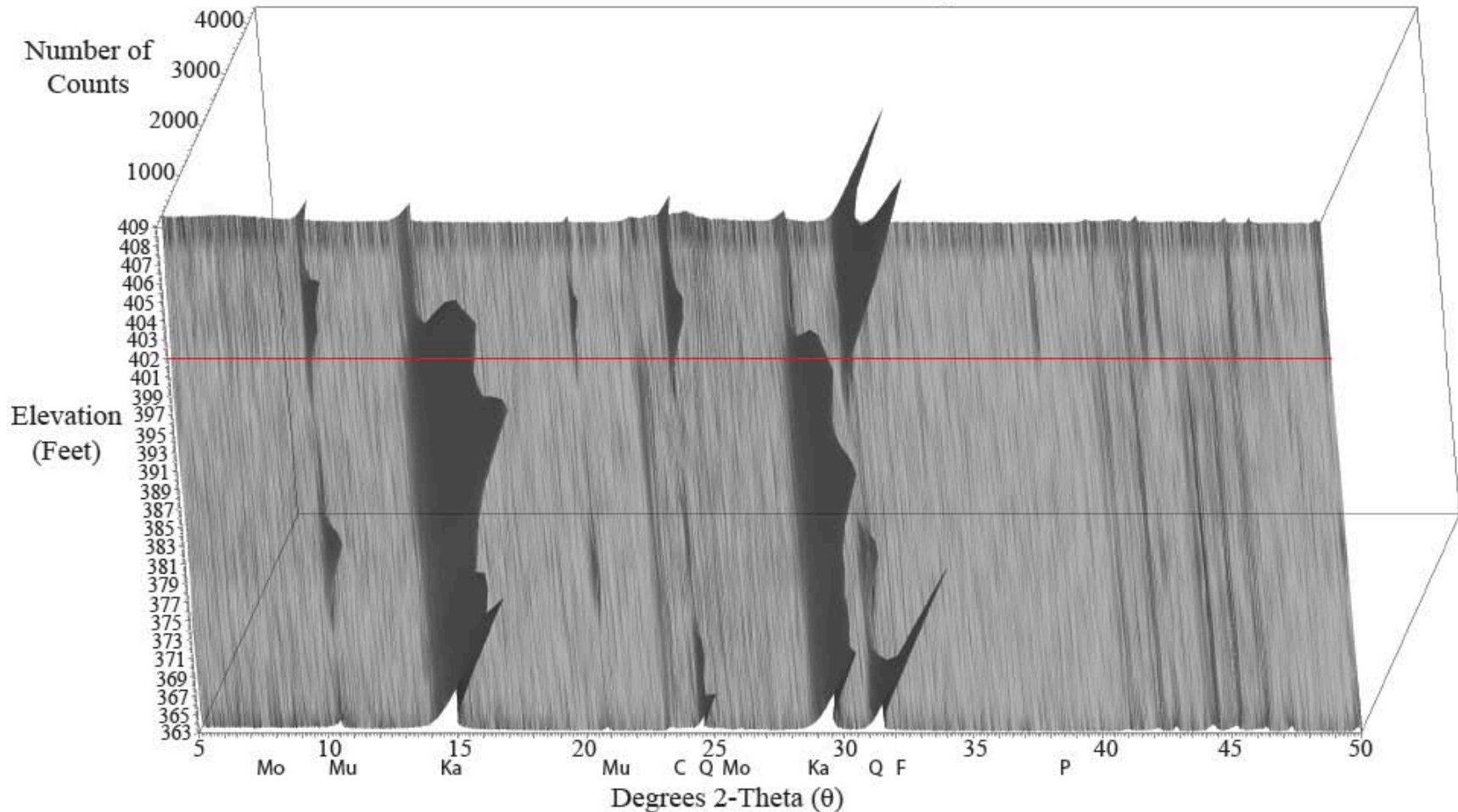


Figure 13. 3D XRD plot of X2100 Y2400. Red line indicates the Twiggs Clay/Huber Formation boundary. Mineral abbreviations indicate the location of the 2-Theta signature for a particular mineral; Montmorillonite (Mo), Muscovite (Mu), Kaolinite (Ka), Various Clays (C), Quartz (Q), Potassium Feldspar (F), Pyrite (P)

X2400 Y2800

At the base of the Huber Formation in X2400 Y2800 (Fig. 14), the most prominent peak is the quartz peak ( $31.1^\circ$  two-theta ( $3.34 \text{ \AA}$ )) along with a second significant quartz peak ( $23.3^\circ$  two-theta). In this core, as in the others, the base of the Huber becomes sandier down core and the bottom sample of this core is almost pure sand, which is confirmed by these XRD data. Large peaks at  $14.4^\circ$  two-theta ( $7.17 \text{ \AA}$ ) and  $29.1^\circ$  two-theta ( $3.58 \text{ \AA}$ ) indicate substantial kaolin throughout the Huber. The kaolin counts in this core remain more consistent than the other cores with less variation ( $\pm 800$  counts at  $14.4^\circ$  two-theta ( $7.17 \text{ \AA}$ ) two-theta and  $\pm 500$  counts at  $29.1^\circ$  two-theta). Less prominent peaks at  $10.4^\circ$  two-theta ( $9.95 \text{ \AA}$ ) (muscovite),  $20.8^\circ$  two-theta ( $4.32 \text{ \AA}$ ) (muscovite),  $23.2^\circ$  two-theta ( $3.88 \text{ \AA}$ ) (various clays), and  $32.0^\circ$  two-theta ( $2.80 \text{ \AA}$ ) (potassium feldspar) also occur in this section. Muscovite and potassium feldspar are restricted to the lower half of the section and have lower counts between 373 and 377 feet. In the Huber,  $23.2^\circ$  two-theta ( $3.88 \text{ \AA}$ ) (various clays) appears up section consistently.

The transition at the Twiggs/Huber boundary at 405 feet is more subdued than in the previous cores, but there is still a decrease in kaolin ( $14.4^\circ$  two-theta ( $7.17 \text{ \AA}$ ) and  $29.1^\circ$  two-theta) and an increase in quartz ( $23.3^\circ$  and  $31.1^\circ$  two-theta ( $3.34 \text{ \AA}$ )), consistent with textural observations of the Twiggs Clay. Muscovite ( $10.4^\circ$  two-theta ( $9.95 \text{ \AA}$ ) and  $20.8^\circ$  two-theta ( $4.32 \text{ \AA}$ )) and montmorillonite ( $7.7^\circ$  two-theta ( $11.60 \text{ \AA}$ ) and  $25.2^\circ$  two-theta ( $3.58 \text{ \AA}$ )) counts rise in the Twiggs as well.

Unlike the two previous cores discussed, there is no significant peak of pyrite at  $38.6^\circ$ . This lack of a significant count increase is supported by a lower  $\text{SO}_2$  extraction yield.

# X2400 Y2800 X-Ray Diffraction

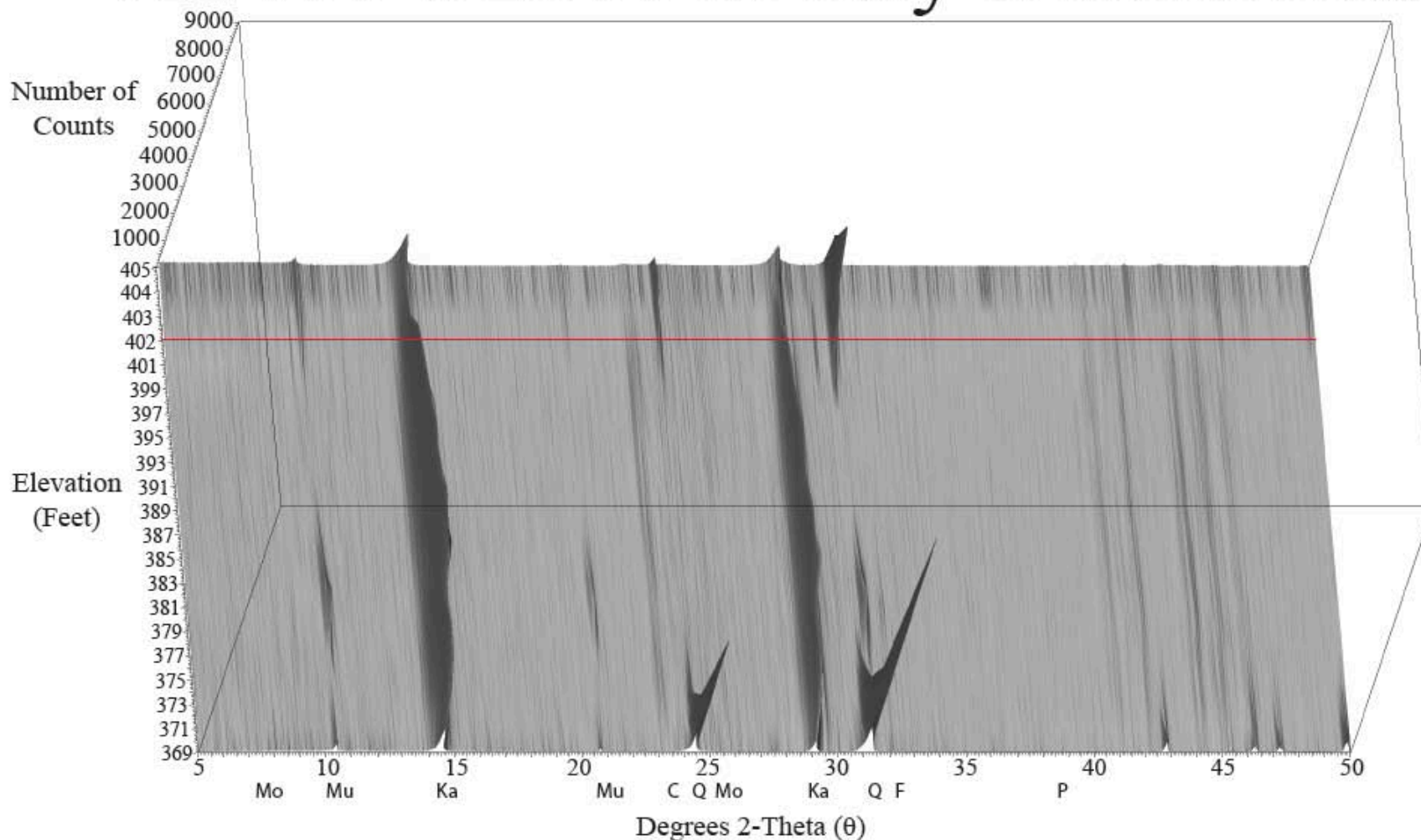


Figure 14. 3D XRD plot of X2400 Y2800. Red line indicates the Twigg's Clay/Huber Formation boundary. Mineral abbreviations indicate the location of the 2-Theta signature for a particular mineral; Montmorillonite (Mo), Muscovite (Mu), Kaolinite (Ka), Various Clays (C), Quartz (Q), Potassium Feldspar (F), Pyrite (P)

### *X2500 Y2700*

The base of the Huber in X2500 Y2700 (Fig. 15) has significant quartz peaks ( $23.3^\circ$  and  $31.1^\circ$  two-theta ( $3.34 \text{ \AA}$ )), confirming textural observation of increasing sand down core. Significant peaks at  $14.4^\circ$  two-theta ( $7.17 \text{ \AA}$ ) and  $29.1^\circ$  two-theta ( $3.58 \text{ \AA}$ ) indicate substantial kaolin throughout the Huber. The kaolin peaks show some variation, but remain steady up to the Twiggs/Huber boundary. Less prominent peaks at  $10.4^\circ$  two-theta ( $9.95 \text{ \AA}$ ) (muscovite),  $20.8^\circ$  two-theta ( $4.32 \text{ \AA}$ ) (muscovite), and  $23.2^\circ$  two-theta ( $3.88 \text{ \AA}$ ) (various clays) occur at the bottom of the section as well. The muscovite peak disappears near 370 feet but returns between 378 and 388 feet, along with a small peak at  $32.0^\circ$  two-theta ( $2.80 \text{ \AA}$ ) (potassium feldspar) at the same interval. The peak at  $23.2^\circ$  two-theta ( $3.88 \text{ \AA}$ ) (various clays) is consistently observed throughout the section.

The Twiggs/Huber boundary at 405 feet is a sharp contact, marked by an abrupt decrease in kaolin ( $14.4^\circ$  two-theta ( $7.17 \text{ \AA}$ ) and  $29.1^\circ$  two-theta ( $3.58 \text{ \AA}$ )) counts and a sharp rise in quartz ( $23.3^\circ$  and  $31.1^\circ$  two-theta ( $3.34 \text{ \AA}$ )), consistent with the textural observations. Muscovite ( $10.4^\circ$  two-theta ( $9.95 \text{ \AA}$ ) and  $20.8^\circ$  two-theta ( $4.32 \text{ \AA}$ )) and montmorillonite ( $7.7^\circ$  two-theta ( $11.60 \text{ \AA}$ ) and  $25.2^\circ$  two-theta ( $3.58 \text{ \AA}$ )) have higher counts above the Twiggs/Huber boundary as well.

There is no significant peak of pyrite at  $38.6^\circ$ , and the low count is supported by a low  $\text{SO}_2$  extraction yield.

### *Sulfur in XRD Data confirming extraction methodology*

The number of counts, or intensity, of the XRD signature at  $38.6^\circ$  (pyrite) varies systematically with the  $\text{SO}_2$  extraction in the Twiggs Clay among the four cores. The average

count and the average SO<sub>2</sub> extracted appear to be related exponentially in the Twiggs Clay (Fig. 16). Average XRD counts and average SO<sub>2</sub> yield of Twiggs Clay are summarized in Table 2:

# X2500 Y2700 X-Ray Diffraction

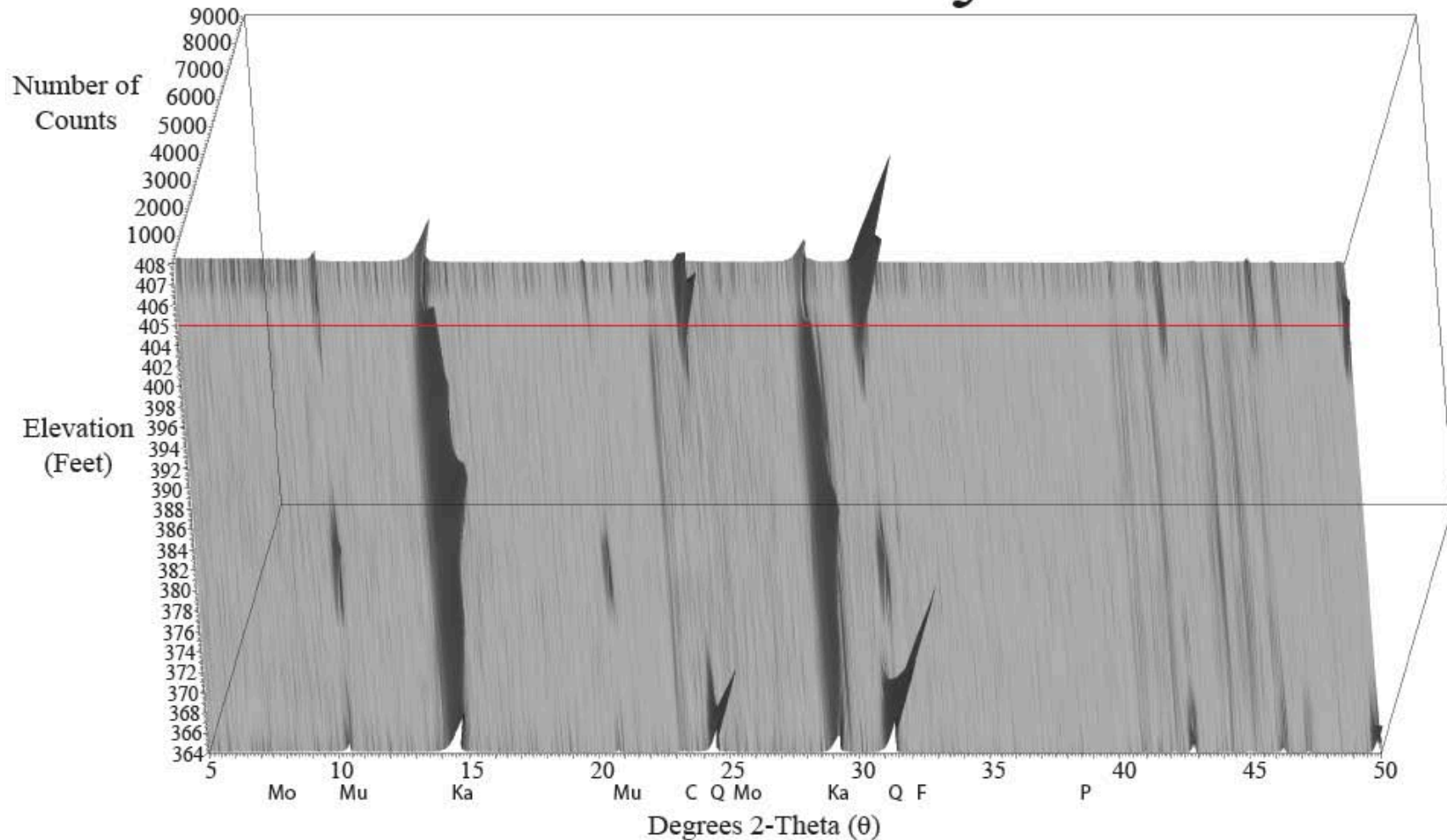


Figure 15. 3D XRD plot of X2500 Y2700. Red line indicates the Twiggs Clay/Huber Formation boundary. Mineral abbreviations indicate the location of the 2-Theta signature for a particular mineral; Montmorillonite (Mo), Muscovite (Mu), Kaolinite (Ka), Various Clays (C), Quartz (Q), Potassium Feldspar (F), Pyrite (P)

TABLE 2. AVERAGE XRD COUNTS AND AVERAGE SO<sub>2</sub> EXTRACTION OF TWIGGS CLAY

Core	Twiggs Samples	Average 38.6° (pyrite) Count	SO <sub>2</sub> Extraction
X2100 Y2400	7	129.9	229.6
X2250 Y2650	10	112.3	166.3
X2400 Y2800	4	80.5	19.6
X2500 Y2700	4	61.5	8.8

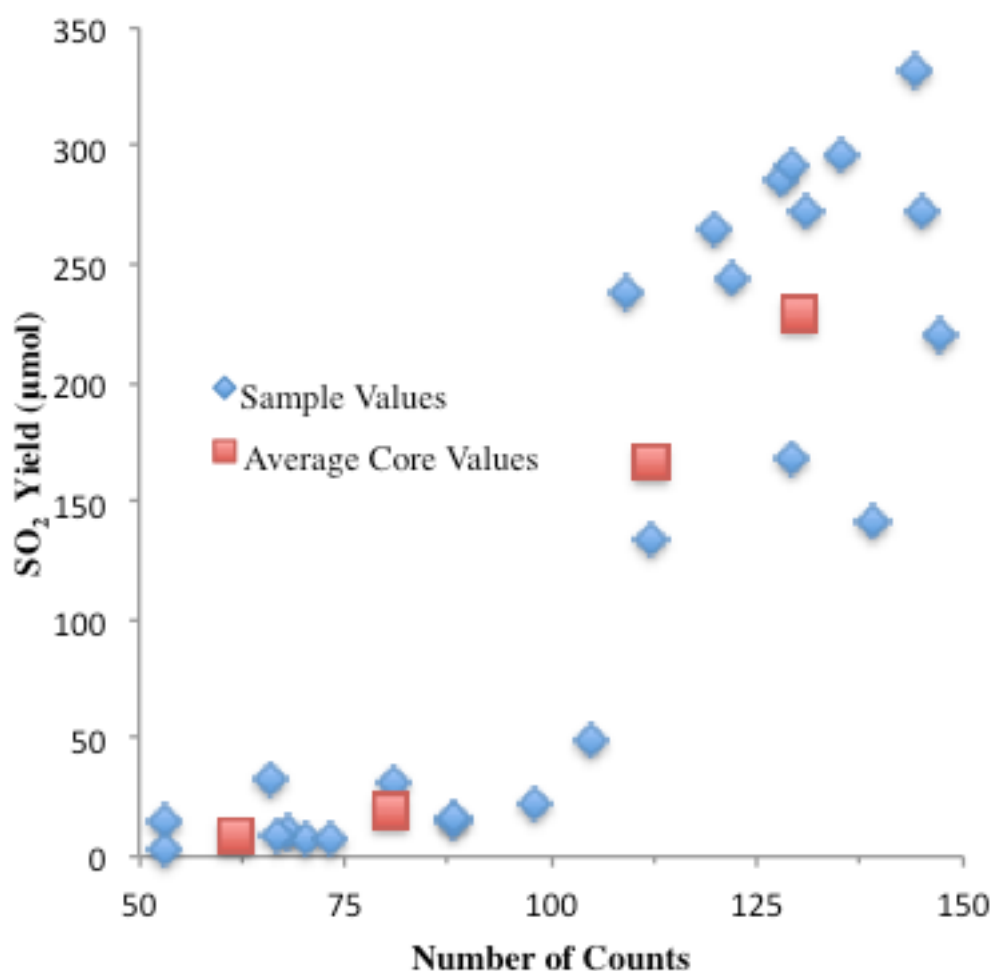


Figure 16. Pyrite XRD counts and SO<sub>2</sub> data in the Twiggs clay, showing an exponential relationship.

XRD and SO<sub>2</sub> data is plotted to show the consistency of SO<sub>2</sub> yield in relation to a measure of pyrite within the each sample. Not knowing the exact sulfur-bearing mineral of these

samples, this apparent exponential relationship supports the experimental assumption that pyrite is the dominant sulfur-bearing mineral, because SO<sub>2</sub> increases along with abundance of pyrite. There also appears to be a spatial relationship between the high and low sulfur yield Twiggs Clay. The low yield Twiggs samples are all from the cores drilled in the northeast portion of the field area and the high yield samples originate from the southwest. It is possible that this variation in sulfur yield indicates a facies change or variable oxidation in the area. Finding a similar relationship in the Huber Formation was not attempted owing to the low sulfur yields and low counts of pyrite in the XRD data. The XRD pyrite counts found in the Huber are low enough that there is no distinguishable difference between actual pyrite variation and error.

#### SO<sub>2</sub> Extraction

Two types of stratigraphic patterns in SO<sub>2</sub> yield are present. First, some drill cores show low SO<sub>2</sub> yield, with little variation within the Huber Formation and have much greater yield in the Twiggs Clay. Second, other cores have a low SO<sub>2</sub> yield in the Huber Formation and in the Twiggs Clay.

#### *X2100 Y2400*

SO<sub>2</sub> yields at the base of the Huber Formation are consistent, with an average of 15.0 mol. Notably the largest yields in the Huber occur within the upper part, with a range of 19.4 – 34.1 μmol, approaching the values in the Twiggs Clay (Fig. 17). At the Twiggs/Huber contact, SO<sub>2</sub> extraction increases markedly, with an average yield of 229.6 μmol. The minimum yield within the Twiggs Clay (31.3 μmol) occurs in the uppermost part of the section. SO<sub>2</sub> yield data for core X2100 Y2400 summarized in Table 3.

TABLE 3. SO<sub>2</sub> YIELD DATA FOR CORE X2100 Y2400

Formation	Average SO <sub>2</sub> Yield (μmol)	Max Yield (μmol)	Min Yield (μmol)	n*
Twiggs	229.6	331.9	31.3	7
Huber	15.0	34.1	6.5	18
Total	75.1	331.9	6.5	25

\*Number of samples

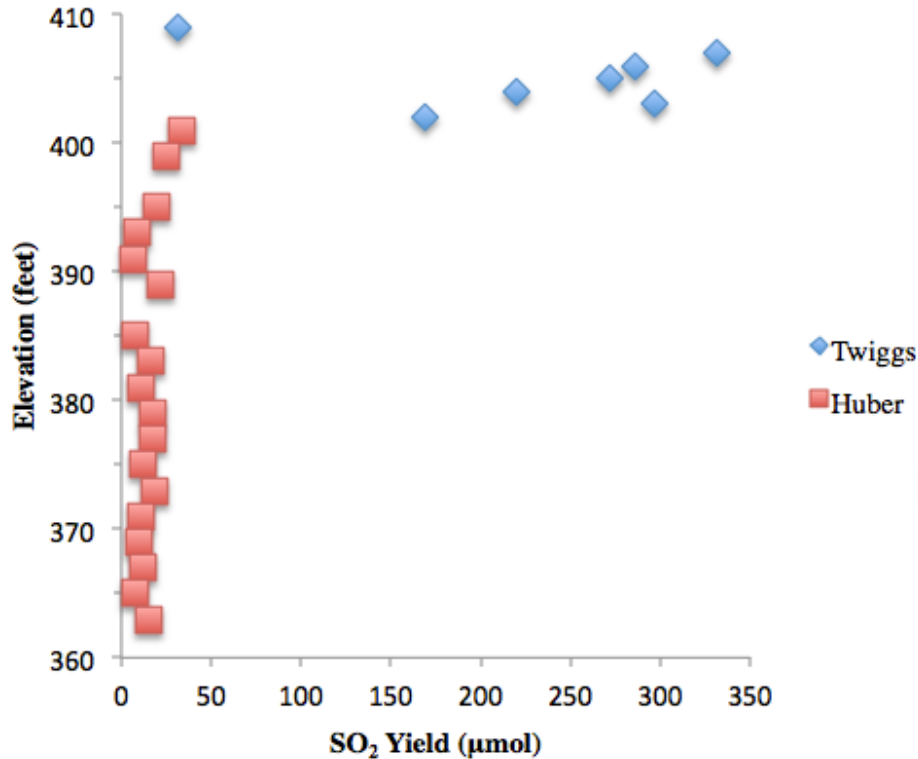


Figure 17. SO<sub>2</sub> yield in the Huber Formation and Twiggs Clay in core X2100 Y2400.

*X2250 Y2650*

In core X2250 Y2650, the lower portion of the Huber Formation produces relatively low SO<sub>2</sub> yields, with an average yield of 20.7 μmol. Yields increase near the top of the Huber Formation with a range of 20.3 – 43.3 μmol, and a large increase in yield occur across the Huber/Twiggs contact with the Twiggs yielding an average of 272.9 μmol (Fig. 18). Again, the lowest yields within the Twiggs Clay occur at the top of the formation with yield range of 11.1 – 14.8 μmol. This and the previous core have the first SO<sub>2</sub> extraction pattern discussed previously:

a relatively consistent, low yield in the Huber Formation with a large increase in SO<sub>2</sub> yield across the Twiggs/Huber contact. SO<sub>2</sub> yield data for core X2250 Y2650 is summarized in Table 4.

TABLE 4. SO<sub>2</sub> YIELD DATA FOR CORE X2250 Y2650

Formation	Average SO <sub>2</sub> Yield (μmol)	Max Yield (μmol)	Min Yield (μmol)	n*
Twiggs	272.9	291.4	11.1	10
Huber	20.7	44.3	2.8	17
Total	72.7	291.4	2.8	27

\*Number of samples

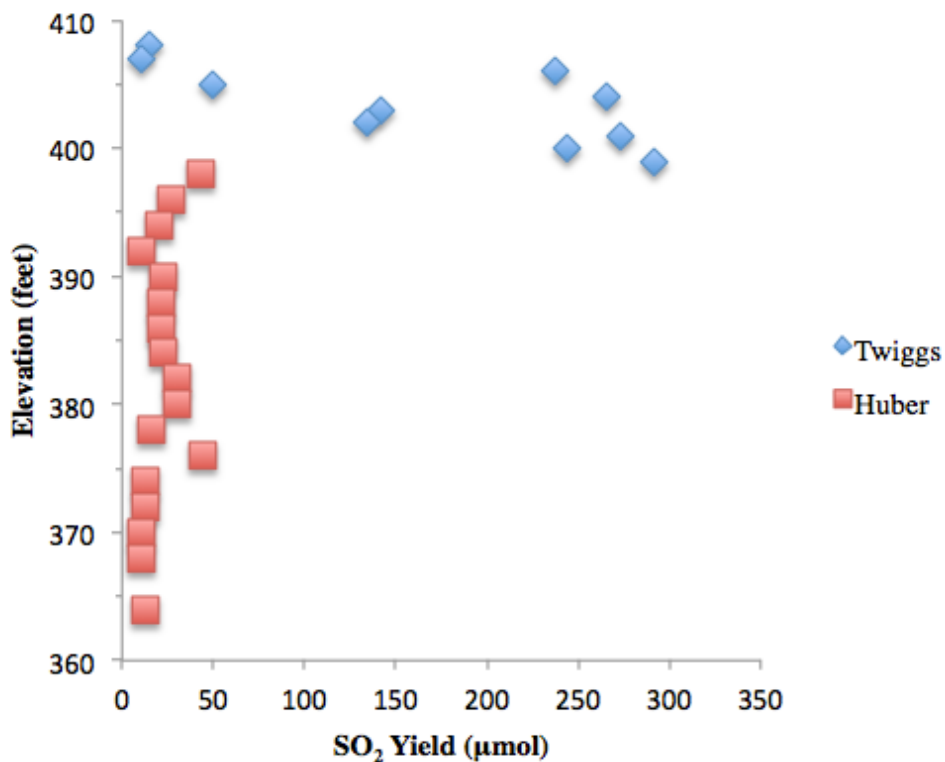


Figure 18. SO<sub>2</sub> yield in the Huber Formation and Twiggs Clay in core X2250 Y2650.

*X2400 Y2800*

In core X2400 Y2800, the lower section of the Huber Formation produced low yields of SO<sub>2</sub>, with an outlier at 383 feet. As in the other cores, the low yield average of 31.7 μmol gives way to an increase in SO<sub>2</sub> yield at the upper Huber Formation, just before the Huber/Twiggs contact, yielding 45.2 – 47.0 μmol. At the Huber/Twiggs boundary, there is little change in SO<sub>2</sub>

yield, the average yield drops and is more similar to values in the lower Huber Formation in the this core than is true for the Twiggs SO<sub>2</sub> yields in the two previous cores (Fig. 19). SO<sub>2</sub> yield data for core X2400 Y2800 is summarized in table 5.

TABLE 5. SO<sub>2</sub> YIELD DATA FOR CORE X2400 Y2800

Formation	Average SO <sub>2</sub> Yield (μmol)	Max Yield (μmol)	Min Yield (μmol)	n*
Twiggs	19.6	32.3	7.4	4
Huber	31.7	204.7	8.3	15
Total	29.2	204.7	7.4	19

\*Number of samples

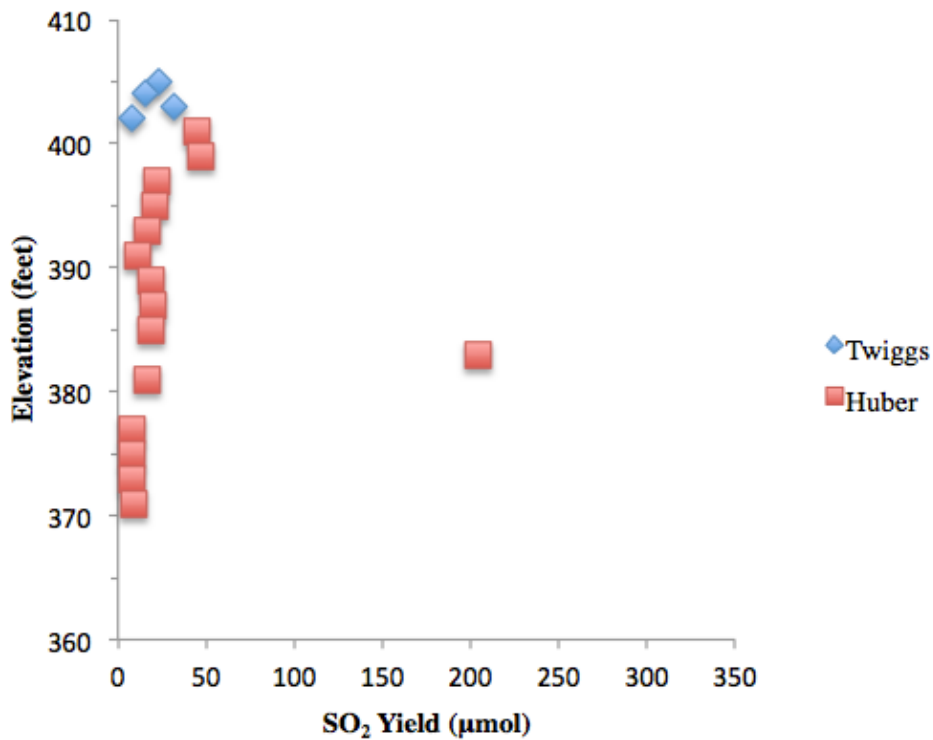


Figure 19. SO<sub>2</sub> yield in the Huber Formation and Twiggs Clay in core X2400 Y2800.

X2500 Y2700

In core X2500 Y2700 (Fig. 20), the lower Huber Formation produces low SO<sub>2</sub> yields similar to the base of other cores from 364 – 378 feet. Above this interval, SO<sub>2</sub> yields in the Huber become more chaotic, with a few high-yield outliers (383 and 388 feet) and a peak of

higher yield between 380 – 394 feet, 154.9  $\mu\text{mol}$  at 388 feet. The top of the Huber Formation produces higher yields that range from 55.3 – 96.8  $\mu\text{mol}$ . This rise in  $\text{SO}_2$  occurs in all the cores, but not to the extent seen here. Above the Twiggs/Huber contact,  $\text{SO}_2$  yields drop substantially (3.7 – 14.8  $\mu\text{mol}$ ).  $\text{SO}_2$  yield data for core X2500 Y2700 is summarized in Table 6.

TABLE 6.  $\text{SO}_2$  YIELD DATA FOR CORE X2500 Y2700

Formation	Average $\text{SO}_2$ Yield ( $\mu\text{mol}$ )	Max Yield ( $\mu\text{mol}$ )	Min Yield ( $\mu\text{mol}$ )	n*
Twiggs	8.8	14.8	3.7	3
Huber	36.8	154.9	5.5	20
Total	32.3	154.9	3.7	23

\*Number of samples

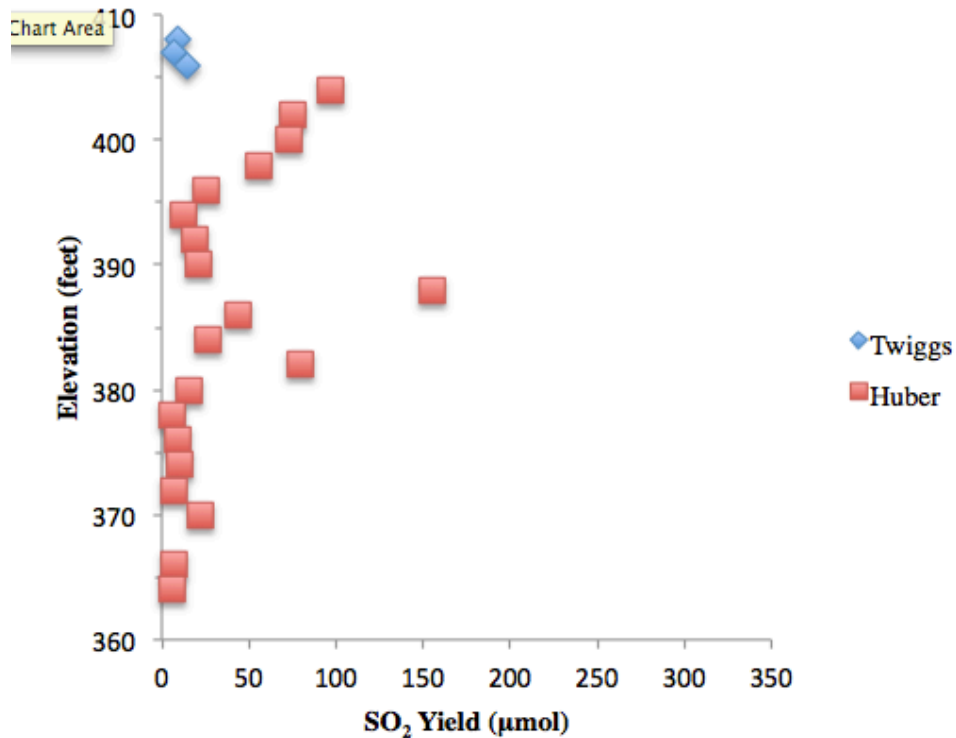


Figure 20.  $\text{SO}_2$  yield in the Huber Formation and Twiggs Clay in core X2500 Y2700.

*All Data*

Plotting all of the  $\text{SO}_2$  yield data from this study produces a composite picture of the four individual cores (Fig. 21). The Huber produces low quantities of  $\text{SO}_2$  with yields increasing dramatically near the top of the section.  $\text{SO}_2$  Yields in the Twiggs Clay can be divided into two

categories: the low-yield Twiggs and the high-yield Twiggs. In all cores, the top of the Twiggs produces low-yields of SO<sub>2</sub>. However two cores (X2400 Y2800 and X2500 Y2700), which showed only low-yield Twiggs, have thin (<4 feet) sections of the clay. Perhaps the clay formed under reducing conditions, but owing to its thinness, was more thoroughly oxidized following deposition. An F-Test was conducted on these data and within 99% confidence the variances in SO<sub>2</sub> yield we can reject the null hypothesis that the variances between the Huber and Twiggs values are the same (F=14.5, n<sub>1</sub>=70, n<sub>2</sub>=24, p=2.56x10<sup>-18</sup>). SO<sub>2</sub> yield data for all samples is summarized in Table 7.

TABLE 7. SO<sub>2</sub> YIELD DATA FOR ALL SAMPLES

Formation	Average SO <sub>2</sub> Yield (μmol)	Max Yield (μmol)	Min Yield (μmol)	n*
Twiggs	140.8	331.9	7.4	24
Huber	26.9	204.7	5.5	70
Total	56.0	331.9	5.5	94

\*Number of samples

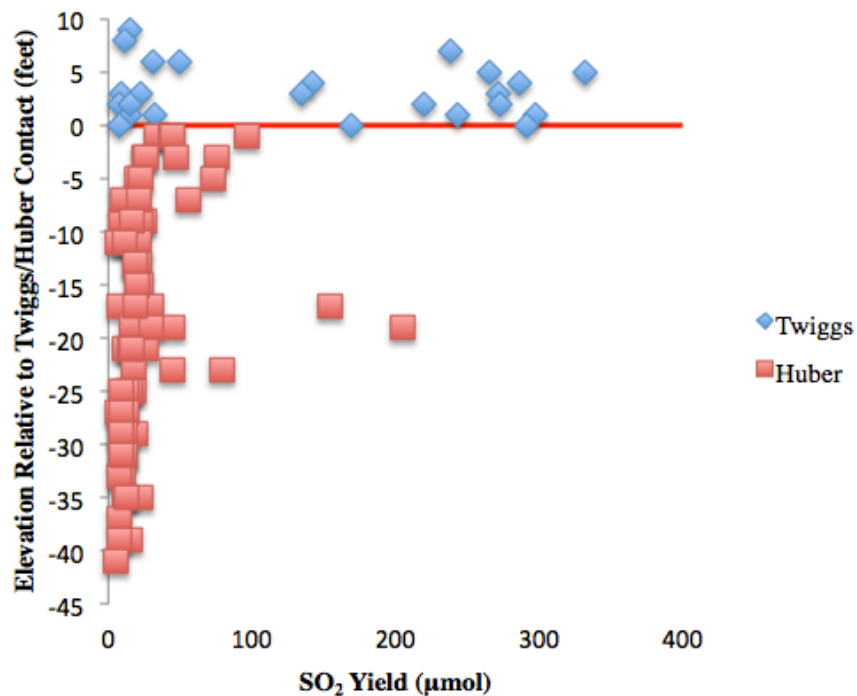


Figure 21. SO<sub>2</sub> yield in the Huber Formation and Twiggs Clay for all data. The Huber/Huber contact is the datum. The red line is the Huber/Huber contact.

## $\delta^{34}\text{S}$ Signature

$\delta^{34}\text{S}$  composition varies greatly among and between the cores with a range of -26.9‰ – 13.6‰. Values of  $\delta^{34}\text{S}$  for all samples are contained in Appendix A. No obvious correlation exists between  $\text{SO}_2$  yield and  $\delta^{34}\text{S}$  composition (Fig. 22).

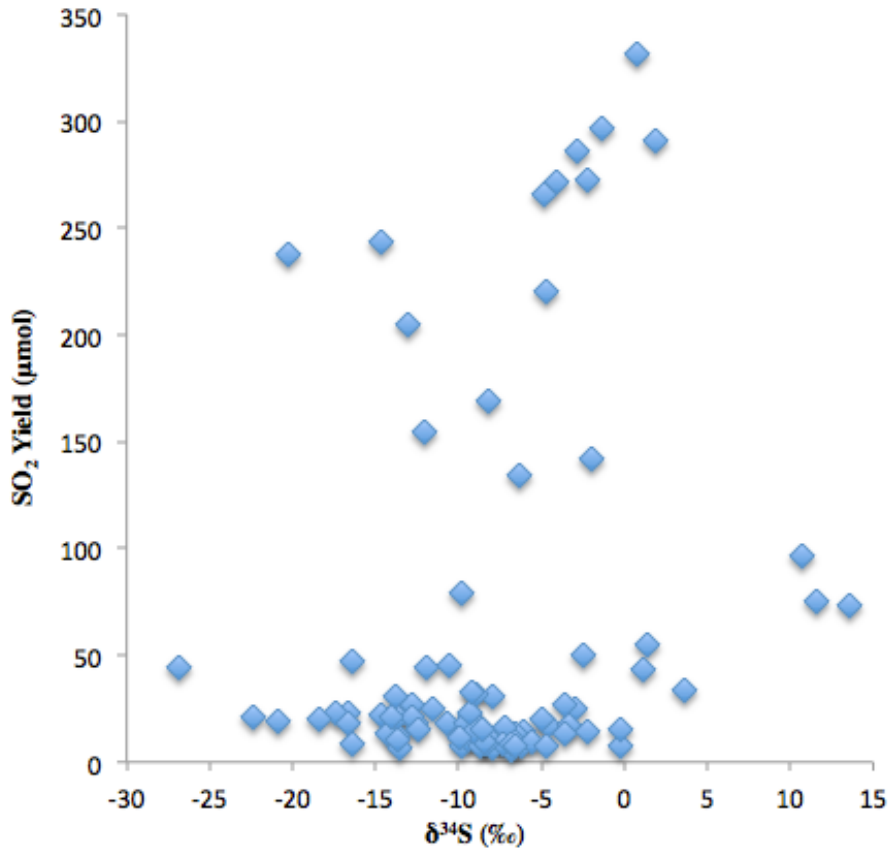


Figure 22.  $\delta^{34}\text{S}$  as related to  $\text{SO}_2$  yield for all data.

### *X2100 Y2400*

At the base of the Huber,  $\delta^{34}\text{S}$  composition within core X2100 Y2400 (Fig. 22) centers around -8‰ before dropping steadily to a minimum of -20.8‰ (395 feet) and rising sharply to a maximum of 3.6‰ (401 feet). Above the Twiggs/Huber contact, the  $\delta^{34}\text{S}$  composition of the Twiggs shows little variation around -4‰.  $\delta^{34}\text{S}$  for core X2100 Y2400 is summarized in Table 8.

TABLE 8.  $\delta^{34}\text{S}$  FOR CORE X2100 Y2400

Formation	Average $\delta^{34}\text{S}$ (‰)	Max $\delta^{34}\text{S}$ (‰)	Min $\delta^{34}\text{S}$ (‰)	n*
Twiggs	-3.4	0.7	-8.9	7
Huber	-8.4	3.6	-20.8	18
Total	-7.2	3.6	-20.8	25

\*Number of samples

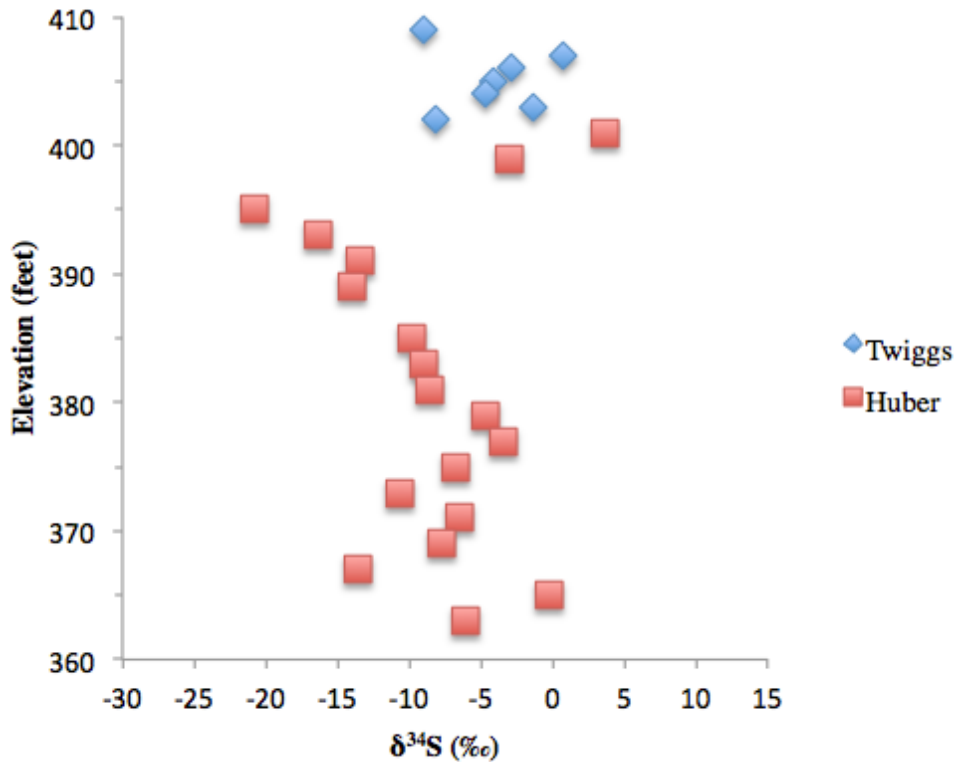


Figure 23. Stratigraphic variation in  $\delta^{34}\text{S}$  in the Huber Formation and Twiggs Clay for core X2100 Y2400.

*X2250 Y2650*

Values of  $\delta^{34}\text{S}$  in the Huber Formation in core X2250 Y2650 (Fig. 23) show significant stratigraphic variation. The base of the Huber has a maximum  $\delta^{34}\text{S}$  composition of -3.6‰, which drops steadily to a minimum -17.4‰ (384 feet). Approaching the Twiggs/Huber contact,  $\delta^{34}\text{S}$  rises to a formation maximum of 1.1‰ (398 feet). Across the formation contact, the  $\delta^{34}\text{S}$  composition of the Twiggs clusters around -4‰, with the exception of a few low outliers.  $\delta^{34}\text{S}$  for core X2250 Y2650 is summarized in Table 9.

TABLE 9.  $\delta^{34}\text{S}$  FOR CORE X2250 Y2650

Formation	Average $\delta^{34}\text{S}$ (‰)	Max $\delta^{34}\text{S}$ (‰)	Min $\delta^{34}\text{S}$ (‰)	n*
Twiggs	-6.3	1.8	-20.3	10
Huber	-10.4	1.1	-26.9	17
Total	-8.9	1.8	-26.9	27

\*Number of samples

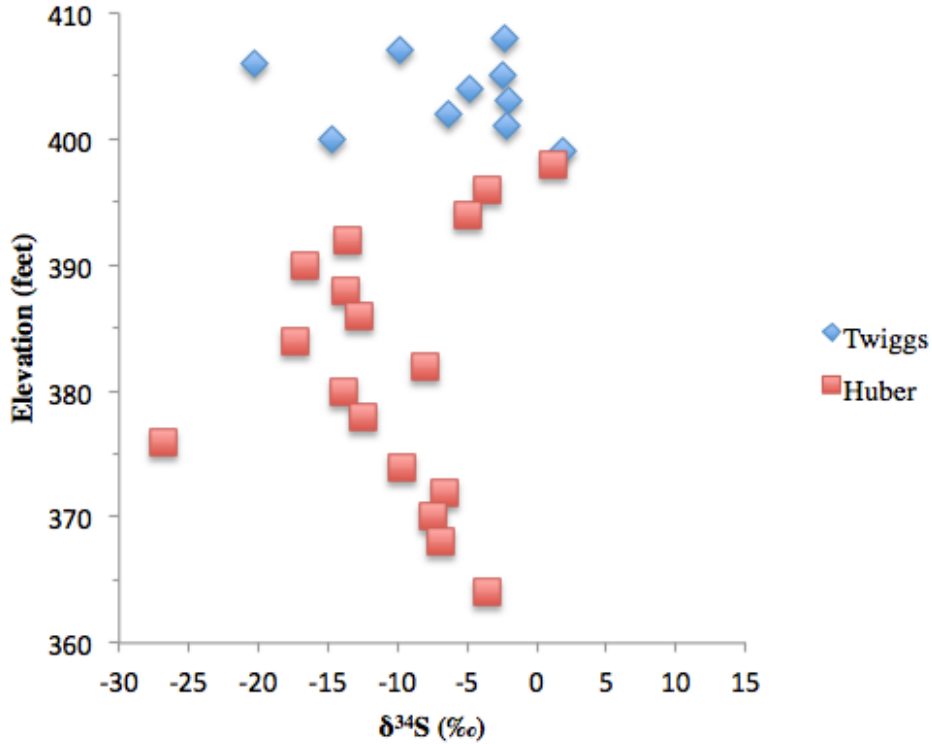


Figure 24. Stratigraphic variation of  $\delta^{34}\text{S}$  in the Huber Formation and Twiggs Clay for core X2250 Y2650.

*X2400 Y2800*

The  $\delta^{34}\text{S}$  composition of the Huber formation in core X2400 Y2800 (Fig. 24) remains relatively consistent at -9‰ to -10‰ with the exception of two negative excursions of -18.4‰ (383 – 387 feet) and -16.4‰ (395-399 feet). The Twiggs Clay  $\delta^{34}\text{S}$  composition steadily clusters at -8.4‰.  $\delta^{34}\text{S}$  for core X2400 Y2800 is summarized in Table 10.

TABLE 10.  $\delta^{34}\text{S}$  FOR CORE X2400 Y2800

Formation	Average $\delta^{34}\text{S}$ (‰)	Max $\delta^{34}\text{S}$ (‰)	Min $\delta^{34}\text{S}$ (‰)	n*
Twiggs	-8.4	-6.5	-9.3	4
Huber	-11.2	-6.9	-18.4	15
Total	-10.6	-6.5	-18.4	19

\*Number of samples

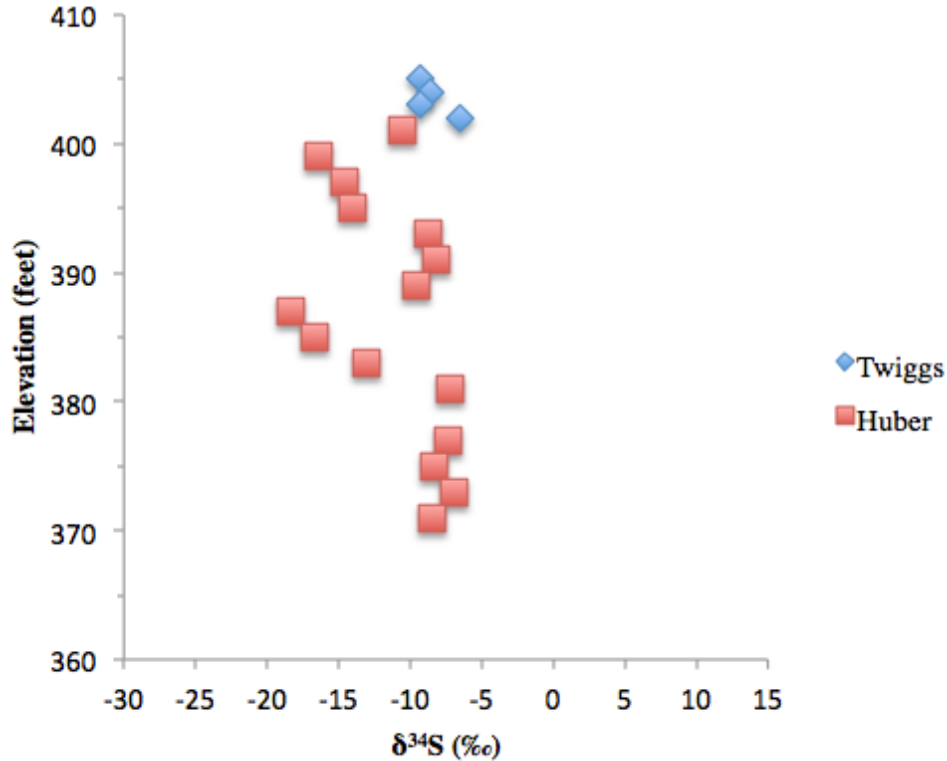


Figure 25. Stratigraphic variation of  $\delta^{34}\text{S}$  in the Huber Formation and Twiggs Clay for core X2400 Y2800.

X2500 Y2700

The  $\delta^{34}\text{S}$  composition from the base of the Huber formation in core X2500 Y2700 (Fig. 25) becomes isotopically lighter starting at -6.9‰ and decreasing to -14.3‰ (394 feet). Above this, the Huber becomes relatively enriched in  $^{34}\text{S}$  with a sharp increase in  $\delta^{34}\text{S}$  composition to a peak ratio of 13.6‰ (400 feet). At the Twiggs/Huber contact, the Twiggs Clay shows little variation and averages around -6.4‰.  $\delta^{34}\text{S}$  for core X2500 Y2700 is summarized in Table 11.

TABLE 11.  $\delta^{34}\text{S}$  FOR CORE X2500 Y2700

Formation	Average $\delta^{34}\text{S}$ (‰)	Max $\delta^{34}\text{S}$ (‰)	Min $\delta^{34}\text{S}$ (‰)	n*
Twiggs	-6.4	-4.7	-9.0	3
Huber	-6.4	13.6	-22.4	20
Total	-6.4	13.6	-22.4	23

\*Number of samples

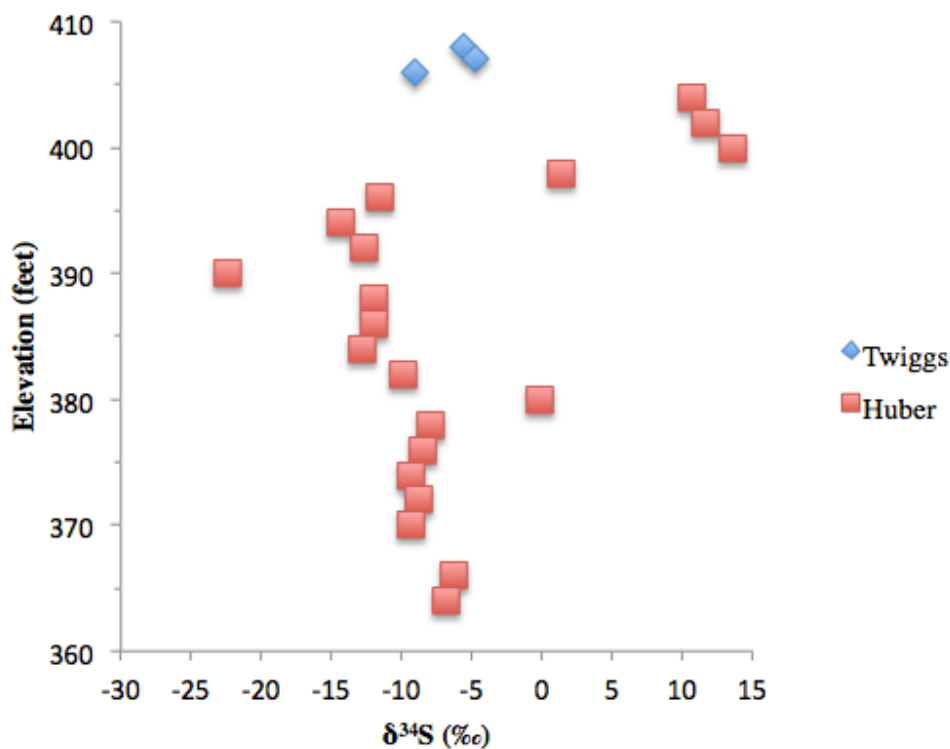


Figure 26. Stratigraphic variation of  $\delta^{34}\text{S}$  in the Huber Formation and Twiggs Clay for core X2500 Y2700.

*All Data*

By combining all  $\delta^{34}\text{S}$  data four intervals can be recognized: 1. The lower Huber Formation, characterized by isotope ratios that are tightly clustered between -6.1‰ and -10.7‰, with three outliers. 2. The middle Huber Formation, characterized by isotope ratios become increasingly scattered ranging from -8.0‰ and -22.4‰. 3. The top of the Huber Formation, characterized by  $\delta^{34}\text{S}$  ratios become sharply and increasingly heavy to a peak of 13.6‰. 4. The Twiggs Clay, characterized by stable ratios with a range of -1.3‰ to -9.0‰ (Fig. 26).

An F-Test comparing the variance in  $\delta^{34}\text{S}$  data between the Huber and Twiggs indicated a significant difference ( $F=2.07$ ,  $n_1=69$ ,  $n_2=23$ ,  $p=0.027$ ) with the Huber showing greater variation than the Twiggs.  $\delta^{34}\text{S}$  for all data is summarized in Table 12.

TABLE 12.  $\delta^{34}\text{S}$  FOR ALL DATA

Formation	Average $\delta^{34}\text{S}$ (‰)	Max $\delta^{34}\text{S}$ (‰)	Min $\delta^{34}\text{S}$ (‰)	n*
Twiggs	-6.1	1.8	-20.3	24
Huber	-8.9	13.6	-26.9	70
Total	-8.2	13.6	-26.9	94

\*Number of samples

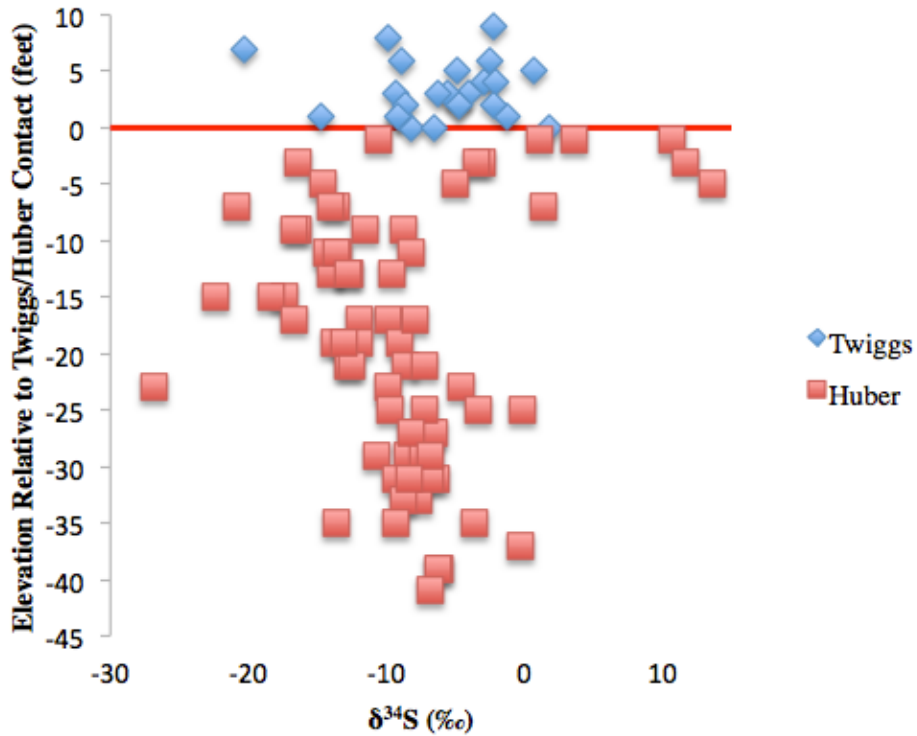


Figure 27. Stratigraphic variation of  $\delta^{34}\text{S}$  in the Huber Formation and Twiggs Clay for all data.

## CHAPTER 5

### DISCUSSION

#### Early Pyrite Diagenesis

The diagenetic sulfate reduction that ultimately forms the pyrite in these kaolins resulted from the metabolic processes of sulfate reducing bacteria (Skyring, 1987). Through oxidation of organic matter, marine sediments contain enough carbon (as little as a few tenths of a percent) to create the necessary anoxic environment for these bacteria to thrive (Raiswell, 1997). These microorganisms played a significant role in the diagenesis that produced the kaolin found in east-central Georgia. Sulfate reducing bacteria and iron reducing and iron oxidizing bacteria, flourish in the kaolin environments (Hurst and Pickering, 1997; Shelobolina et al, 2005).

The chemical reaction that produces pyrite in these anoxic environments requires the microbially reduced  $\text{SO}_4^{2-}$  to produce  $\text{H}_2\text{S}$ , which reacts with iron to form pyrite (Berner, 1964; Raiswell, 1997; Raiswell and Canfield, 2012). The reaction occurs rapidly in the uppermost section of marine sediments (Canfield, 1989). This reduction process, completed by dissimilatory sulfate reducing bacteria, is simplified below:



Over 100 species of sulfate reducing bacteria exist, and while most previous work has focused on *Desulfovibrio desulfuricans*, laboratory tests and theoretical models demonstrate that dissimilatory sulfate reducing bacteria (SRB) typically produce depletions in  $^{34}\text{S}$  ( $\delta^{34}_{\text{sulfate-}}$

$\delta^{34}_{\text{sulfide}}$  of 0 – 46 ‰ (Rees, 1973; Canfield and Thamdrup, 1994; Canfield and Teske, 1996; Habicht and Canfield, 1996, 2001; Canfield, 2001a; Detmers et al. 2001; Brabec et al., 2008).

These fractionations occur because molecules bearing the two most common sulfur isotopes,  $^{32}\text{S}$  and  $^{34}\text{S}$ , react at different rates, with the lighter of the two,  $^{32}\text{S}$ , reacting faster. In the case of the above equations  $^{32}\text{SO}_4^{2-} \rightarrow \text{H}_2^{32}\text{S} \rightarrow \text{Fe}^{32}\text{S}_2$  occurs more readily than  $^{34}\text{SO}_4^{2-} \rightarrow \text{H}_2^{34}\text{S} \rightarrow \text{Fe}^{34}\text{S}_2$  ( $K=1.074$  at  $25^\circ\text{C}$ ) (Raiswell, 1997).

The Jeffersonville Member of the Huber Formation and the Twigg's Clay were deposited in oceanic environments, where seawater acted as the source of sulfate for bacterial metabolism.  $\delta^{34}_{\text{sulfate}}$  values for the Tertiary ocean were  $\sim 22\text{‰}$  (Claypool, 1980). Given laboratory sulfate depletions ( $\sim 0\text{--}46\text{‰}$ ), this should produce resultant  $\delta^{34}_{\text{sulfide}}$  in the Georgia kaolin ranging between  $22\text{‰}$  (initial sulfate, closed system) and  $-24\text{‰}$  (depleted sulfate, open system). This range of values agrees with most of the current study's results with the exception of one Huber sample with a  $\delta^{34}_{\text{sulfide}}$  value of  $-26.9\text{‰}$  (fractionation value of  $48.9\text{‰}$ ).

The degree of fractionation depends greatly on whether the sulfate system is open or closed. The biogenic reduction of sulfate occurs below the sediment/seawater interface and, as such, its degree of burial and interaction with the ocean is variable. In an open system, sulfate is replaced at the same rate that reduction occurs. In the ocean, this would mean that seawater sulfate is able, through sediment porosity, to replace the sulfate supply at the same rate that diagenetic reduction occurs (Fig. 27). Owing to the replacement of sulfate creating a continuous supply of the more readily reacted  $^{32}\text{SO}_4^{2-}$ , open systems produce large fractionations ( $\sim 30\text{--}40\text{‰}$ ) (Canfield, 2001a,b). In a closed system, where sulfate is not replenished during reduction owing to restricted sulfate supply, fractionations will be smaller and the  $\delta^{34}_{\text{sulfide}}$  composition will approach the composition of the sulfate source (Raiswell, 1997). Between these two extremes, an

intermediate stage exists, a partially closed system, where sulfate is replaced at a slower rate than it is removed by reduction. This would produce intermediate  $\delta^{34}_{\text{sulfide}}$  fractionation. The open vs. closed system seems simple and should lend itself to easy interpretation, but there is no way to know the exact proportions of open, closed, or semi-closed systems and reduction products which have been mixed together in a final pyrite deposit.

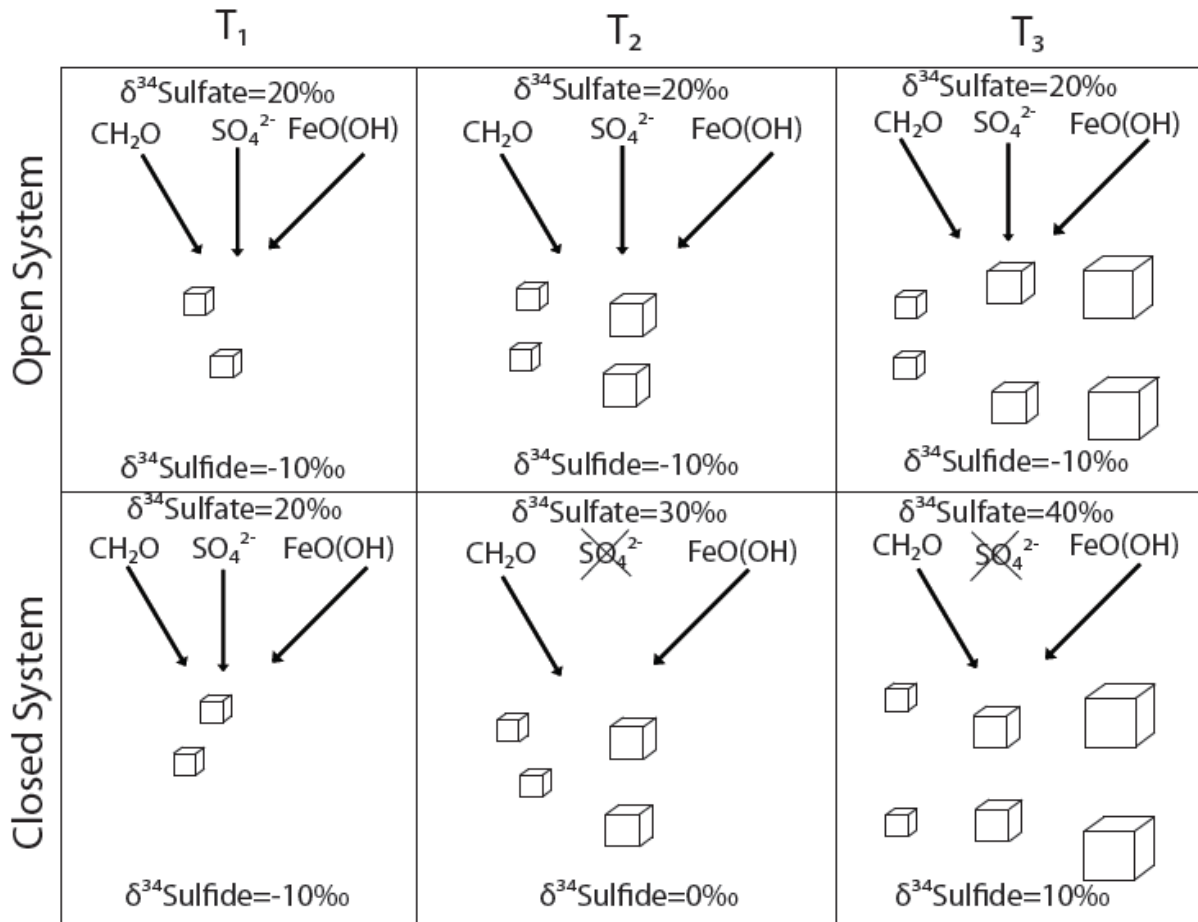


Figure 28.  $\delta^{34}\text{S}$  variations in open v. closed conditions of early pyrite diagenesis.  $\delta^{34}_{\text{sulfate}}$  refers to the sulfate composition within the pyrite producing conditions below the sediment/water interface. The  $\delta^{34}_{\text{sulfate}}$  in the open system remains constant because the system continually receives sulfate from the seawater. In the closed system, the pyrite becomes isotopically heavy and the sulfate follows suit as the SRB favorably reduces  $^{32}\text{S}$ , enriching the source sulfate in  $^{34}\text{S}$ . CH<sub>2</sub>O is a simple carbohydrate that represents SRB; SO<sub>4</sub><sup>2-</sup> represents the sulfate within the pyrite producing system; FeO(OH) represents the iron necessary to complete the reaction after sulfate reduction to produce pyrite. The increasing size and number of pyrite cubes represents the increased formation of pyrite through time.

In addition to the open or closed nature of a depositional system, the limitations upon sulfide reduction can play an important part in formation of marine pyrite. Sulfide reduction and pyrite genesis is controlled by microbial reduction of sulfate or the supply of reactive iron minerals (Canfield and Raiswell, 1991). The supply of reactive iron is especially important, owing differing reaction rates of iron minerals (Table 13).

TABLE 13. IRON MINERAL REACTIONS WITH DISSOLVED SULFIDE

Iron mineral	Rate constant (yr <sup>-1</sup> )	Half-life
Ferrihydrite	2200	2.8 hours
Lepidocrocite	85	< 3 days
Goethite	22	11.5 days
Hematite	12	31 days
Magnetite (uncoated)	6.6x10 <sup>-3</sup>	105 years
Reactive silicates	3.0x10 <sup>-3</sup>	230 years
Sheet silicates	8.2x10 <sup>-6</sup>	84000 years
Ilmenite, garnet, augite, amphibole	8.2x10 <sup>-6</sup>	>84000 years

*Note:* Values from Canfield, Raiswell, and Bottrell, 1992

Iron oxides react rapidly with dissolved sulfides, and where these minerals are present, sulfide is the limiting reactant toward the formation of pyrite. However, once iron oxides are consumed, the much slower reacting iron bearing silicates remain, allowing any type of open to partially open system to accumulate pore water sulfate (Canfield, 1989; Canfield et al. 1992). As the type and abundance of iron minerals effects the distribution of sulfate in the ocean sediments, this may also regulate  $\delta^{34}_{\text{sulfide}}$  fractionation. For example, a system in which ocean sulfate cycles through sediments on the order of 1 year would act as a closed system in the presences of iron oxides that react with sulfide on the order of days to months. In this situation, small fractionations would be expected and  $\delta^{34}_{\text{sulfide}}$  would be expected to approach the  $\delta^{34}_{\text{sulfate}}$  as in a closed system. However, if iron was sourced from sheet silicates, the ocean's recharge rate of sulfate into the marine sediments would work at a much brisker pace relative to iron reactivity. It

is possible this same system could see higher  $\delta^{34}_{\text{sulfide}}$  fractionations simply by variation in the Fe minerals present during sulfate reduction.

The  $\delta^{34}_{\text{sulfide}}$  composition of the Huber and Twigg can be divided into four groups previously discussed. Each group's  $\delta^{34}_{\text{S}}$  signature indicates variable depositional conditions in the Huber Formation and Twigg Clay (Fig. 29). Unless otherwise noted, these interpretations assume infinite supply of organic matter and iron.

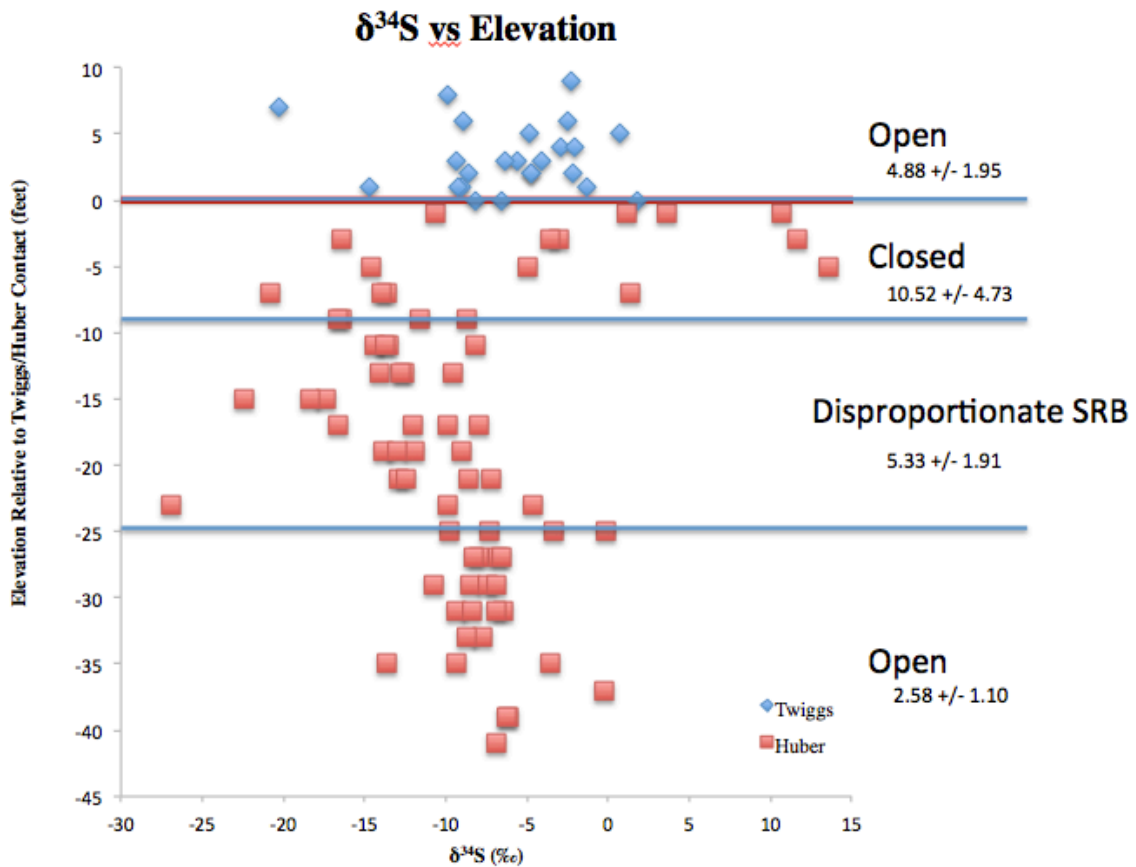


Figure 29.  $\delta^{34}_{\text{S}}$  results organized into four depositional groups. Standard deviations and 95% confidence intervals are included.

The tight grouping of the  $\delta^{34}_{\text{sulfide}}$  within the lower Huber is indicative of an open system with Dissimilatory SRB reducing the seawater sulfate. The consistent supply of  $\text{SO}_4^{2-}$  from the seawater limited isotopic variation among the pyrite produced (Canfield, 2001a,b). The open system most likely formed as a result of deposition under normal marine conditions.

The upper Huber system is characterized by decreased  $\delta^{34}_{\text{sulfide}}$  composition along with increased variation in  $\delta^{34}_{\text{sulfide}}$  values. The decrease in  $\delta^{34}_{\text{sulfide}}$  values most indicates a system open to sulfate supply with large fractionations. Dissimilatory SRB can produce, depending on varying laboratory conditions fractionations between 0 – 46‰ and many of the  $\delta^{34}_{\text{sulfide}}$  values in the upper Huber approach or exceed this range. SRB are anaerobic and begin to thrive and reduce sulfate once all the oxygen in the system has been removed by the oxidation of present organic matter (Cheshire et al. 2012). As such, it is not possible to oxidize the pyrite produced by Dissimilatory SRB and still maintain an easy mechanism to the sediments to facilitate a ‘second round’ of reduction.

There are two mechanisms that could produce the large  $\delta^{34}_{\text{sulfide}}$  fractionation seen in the upper Huber Formation. The first is outlined in a model produced by Brunner and Bernasconi (2005). They propose that under hypersulfidic conditions and when electron acceptor concentrations are limited, fractionations as high as 70‰ could be reached by dissimilatory SRB alone. The second mechanism is the work of disproportionating sulfur-reducing bacteria (Canfield, 2001a):



The process of disproportionating SRB works in two stages (Fig. 30). First, ocean sulfate must undergo reduction by Dissimilatory SRB and then reoxidation by microbial means into elemental sulfur to be metabolized by disproportionating SRB (Canfield and Thamdrup, 1994; Canfield et al, 1998b; Canfield, 2001a,b). Disproportionating SRB becomes the primary driver of  $\delta^{34}\text{S}$  fractionation later in the diagenesis process when nutrients become scarce (Canfield 2001 a,b).

The oxidation of sulfide to elemental sulfur produces a  $\delta^{34}\text{S}$  fractionation of  $\sim 4 - 5\text{‰}$  (Canfield et al, 1998b; Canfield, 2001a). During the metabolism of elemental sulfur, the disproportionate SRB form both sulfate and sulfide (equation 5). The sulfide produced during metabolism sees a  $\delta^{34}\text{S}$  fractionation of  $\sim 6 - 8\text{‰}$ , producing a net  $\delta^{34}\text{S}$  fractionation of  $\sim 10 - 13\text{‰}$  (Canfield et al, 1998b; Canfield, 2001a). This process can repeat as long as sulfide continues to be oxidized into elemental sulfur, producing  $\delta^{34}\text{S}$  fractionations of  $\sim 10 - 13\text{‰}$  (Canfield, 2001a). Evidence of disproportionate SRB may emerge in the  $\delta^{34}\text{S}_{\text{sulfide}}$  as variations in the upper Huber appear to step by values of  $\sim 9 - 12\text{‰}$  (Fig. 27). Disproportionate SRB likely produced the variations in the  $\delta^{34}\text{S}_{\text{sulfide}}$  composition of the upper Huber Formation.

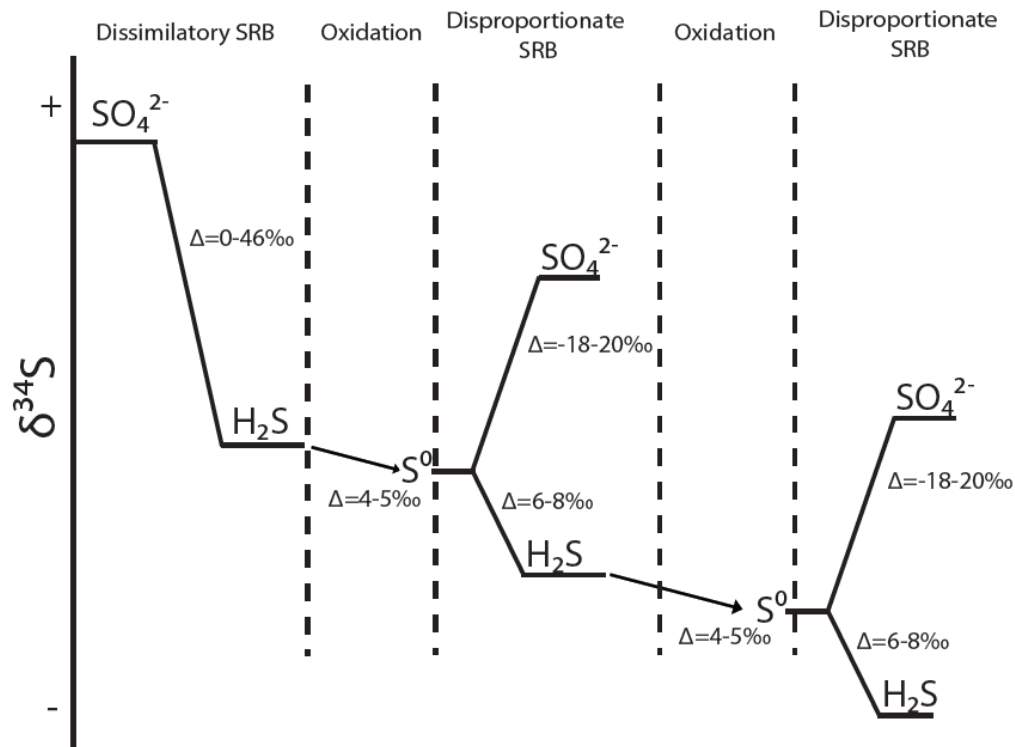


Figure 30. Fractionation values for Dissimilatory SRB, Disproportionate SRB, and Oxidation processes in Georgia kaolin. Figure modified from Canfield and Thamdrup, 1994.  $\delta^{34}\text{S}$  values and diffractions from Canfield, 2001a.

The top of the Huber Formation sees a sharp rise in  $\delta^{34}\text{S}$ , leading to isotopically heavy pyrite. Extremely low fractionations below 4‰ could result from environments with low sulfate concentrations (<1mM) (Canfield, 2001a). More likely, these isotopically heavy pyrites are the result of a closed system of limited sulfate supply. It is possible that these deposits at the top of the Huber were deposited in a system more landward with brackish to fresh water. Freshening of depositional waters would have greatly decreased the sulfate available for reduction to sulfide.

The Twiggs Clay, like the lower Huber Formation, has relatively closely packed  $\delta^{34}\text{S}_{\text{Sulfide}}$  values indicative of an open depositional system dominated by Dissimilatory SRB (Canfield et al, 1998b; Canfield, 2001a). There is more  $\delta^{34}\text{S}_{\text{Sulfide}}$  variation in the Twiggs than the lower Huber, but the variation falls well within the values expected and accepted as commonly produced by Dissimilatory SRB (Brunner and Bernasconi, 2005).

#### Post-depositional Oxidation

Interpretation of early pyrite diagenesis in the Huber Formation and Twiggs Clay assume that the samples have undergone little to no post-depositional oxidation. Using the criteria established by Schroeder et al. (2004) regarding the existence of oxidative weathering fronts propagating through Georgia kaolins, little post-depositional oxidation has occurred in the samples collected for this study.

The Twiggs Clay has undergone less oxidation than the Huber Formation and portions remain reduced similar to its state shortly after early diagenesis. The lower portion of the Twiggs Clay in the southwestern cores (X2100 Y2400; X2250 Y2650) is the most reduced clay studied. It is colored by iron-sulfide mineralization and yields high  $\text{SO}_2$  content, indicating a reduced state (White et al., 1991; Schroeder et al., 2004). This portion of the Twiggs Clay is most analogous to clay after deposition and early diagenesis. The upper portion of these two cores and the Twiggs

in the remaining two northeastern cores (X2400 Y2800; X2500 Y2700) have undergone some post-depositional oxidation. These clays have lost the sulfide gray that characterizes the rest of the Twiggs and are colors ranging from pink to red, indicating some oxidation. These portions of the Twiggs are thin, and it is likely they have undergone some oxidation after deposition, possibly from flowing groundwater in overburden layers (Schroeder et al., 2004). Overall, the Twiggs has only undergone slight post-depositional oxidation. XRD data does not produce signatures of anatase, a titanium-bearing mineral indicative of most the oxidative state found in Georgia kaolins (Schroeder and Shiflet, 2000; Schroeder et al, 2004).

The Huber Formation is more oxidized than the overlying Twiggs. Unlike the Twiggs, oxidation of the Huber appears to remain relatively consistent throughout. The color of the Huber ranges from light gray to cream to light brown. XRD data indicates a very small amount of anatase throughout the Huber, specifying oxidation (Schroeder et al, 2004). Both of these signs point to some level of post depositional oxidation in the Huber Formation. However, XRD data and SO<sub>2</sub> yield both indicate a small amount of pyrite, a remnant of the Huber's reduced past. Visual inspection of the full width and half max values in the XRD data shows consistent ranges of coherent scattering domain size, meaning little to no Ostwald ripening, or recrystallization, has occurred (Lowe, 1991). The Huber has clearly undergone more post-depositional oxidation than the Twiggs Clay, but the limited anatase signature, lack of significant Ostwald ripening, and remaining pyrite signify oxidation levels low enough to allow this kaolin to reveal its early diagenetic history.

Oxidation does not appear to effect pyrite's ability to retain its  $\delta^{34}\text{S}$  signature.  $\delta^{34}\text{S}$  difference between the red (oxidized) and gray (reduced) Twiggs Clay supports the assertion that oxidation has little to no effect on pyrite's ability to maintain its original depositional signature.

As noted previously, there is a significant drop in SO<sub>2</sub> yield, but the yield drop does not appear to effect  $\delta^{34}\text{S}$  (Fig. 31).

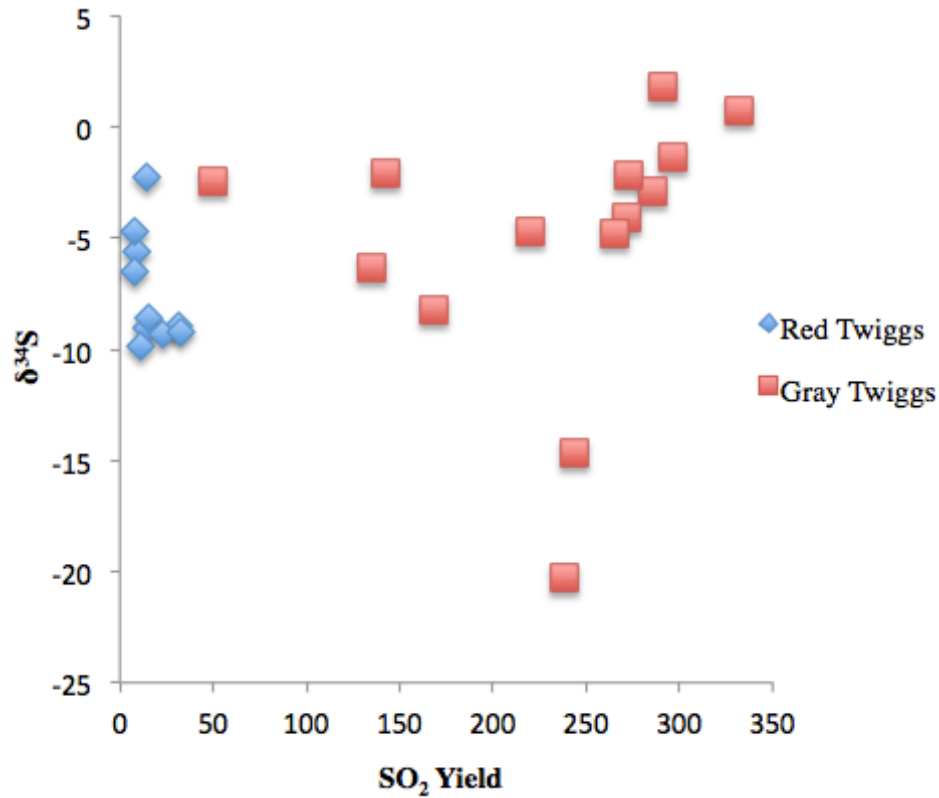


Figure 31. SO<sub>2</sub> yield and  $\delta^{34}\text{S}$  among red (oxidized) and gray (reduced) Twigg Clay.

Given the evidence within these kaolins, their oxidation history can be deduced as follows: First, the Huber Formation was deposited, kaolinized, and reduced. Second, the Huber underwent sub aerial erosion, forming the sequence boundary that caps the formation. It is likely that an oxidation front, facilitated by groundwater, moved through at this time. Third, the Twigg Clay was deposited, kaolinized, and reduced. Last, the upper portions of the Twigg was oxidized, however, lower portions saw little effect of these oxidation fronts. These oxidation reactions occur on the order of thousands of years and, with the short distances between these cores, these reactions could have occurred during the millions of years between the deposition of the Huber Formation and the Twigg Clay (Weibel, 1998)

## CHAPTER 6

### CONCLUSIONS

1. The XRD signature at  $38.6^\circ$  two-theta ( $2.36 \text{ \AA}$ ) in conjunction with  $\text{SO}_2$  yield data supports the conclusion that the primary sulfur-bearing mineral in the Huber Formation and Twiggs Clay is pyrite.
2.  $\delta^{34}\text{S}$  values suggest that there are 4 regimes of early pyrite diagenesis: 1. The lower Huber Dissimilatory SRB dominated Open System (~363 – 375 feet) 2. The upper Huber Disproportionate SRB dominated Open System (375 – 401 feet) 3. The Top of the Huber Closed System (~400 – 404 feet) 4. The Twiggs Dissimilatory SRB dominated Open System (401 – 409 feet).
3. The study area has undergone two periods of post depositional oxidation, once after the deposition of the Huber Formation, producing trace amounts of anatase, and once after the deposition of the Twiggs Clay, effecting the upper portion of the Formation and thin sections of the Twiggs Clay.
4. Pyrite is present in two distinct morphologies: euhedral and framboidal. It has been suggested that euhedral crystals form in the presence of lower organic matter leading to lower sulfide production while framboidal crystals form with high sulfide production rates (Taylor and Macquaker, 2000). A future study could include extensive SEM imaging of these kaolins to better understand the rate of sulfide production and organic content during diagenesis.

## REFERENCES

- Allen, J.A., Duncan, M.S., and Holland, S.M., 2009, late Eocene sequence stratigraphy of the upper coastal plain, east Georgia: Georgia Geological Society Guidebook, v. 29, p. 17 – 24.
- Austin, R. S., 1972, The origin of the kaolin and bauxite deposits of Twiggs, Wilkinson, And Washington counties, Georgia [Ph.D. thesis]: University of Georgia, 185 p.
- Barker, W.W., and Hurst, V.J., 1992, Bacterial trace fossils in Eocene kaolin of the Huber Formation of Georgia; *Phylloderma microsphaeroide*, n. ichnogen., n. ichnosp.: *Ichnos*, v. 2, p. 55 – 60.
- Berner, R.A., 1964, An idealized model of dissolved sulfate distribution in recent sediments: *Geochimica et Cosmochimica Acta*, v. 28, p. 1497 – 1503.
- Bohor B.F., and Randall E.H., 1971, Scanning electron microscopy of clays and clay minerals: *Clays and Clay Minerals*, v. 19, p. 49 – 54.
- Brabec, M., Lyons, T., and Mandernack, K., 2008, Fractionation of sulfur and oxygen isotopes in sulfate produced by anaerobic photosynthetic sulfur bacterium: Geochemical Society: The 18<sup>th</sup> V.M. Goldschmidt Conference Conference, Abstracts, p. A108.
- Brunner, B., and Bernasconi, S.M., 2005, A revised isotope fractionation model for dissimilatory sulfate reduction in sulfate reducing bacteria: *Geochimica et Cosmochimica Acta*, v. 69, no. 20, pp. 4759 – 4771.
- Buie, B.F., and Fountain, R.C., 1967, Tertiary and Cretaceous age of kaolin deposits in Georgia and South Carolina: Geological Society of America, Southeastern Section Program: Tallahassee, Fla., p. 465.
- Buie, B.F., Hetrick, J.H., Patterson, S.H., and Neeley, C.L., 1979, Geology and industrial mineral resources of the Macon-Gordon kaolin district, Georgia: United States Geological Survey-Open-File Report 79-526, 36 p.
- Canfield, D.E., 1989, Reactive iron in marine sediments: *Geochimica et Cosmochimica Acta*, v. 53, p. 619 – 632.
- Canfield, D.E., 2001a, Biogeochemistry of sulfur isotopes: *Stable Isotope Geochemistry*, v. 43, p. 607 – 636.

- Canfield, D.E., 2001b, Isotope fractionation by natural populations of sulfate-reducing bacteria: *Geochimica et Cosmochimica Acta*, v. 65, p. 1117 – 11224.
- Canfield, D.E., 2004, The evolution of the Earth surface sulfur reservoir: *American Journal of Science*, v. 304, p. 839 – 861.
- Canfield, D.E., and Boudreau, B.P., Mucci, A., and Gundersen, J.K., 1998a, The early diagenetic formation of organic sulfur in the sediments of Mangrove Lake, Bermuda: *Geochimica et Cosmochimica Acta*, v. 62, p. 767 – 781.
- Canfield, D.E., Raiswell, R., and Bottrell, S., 1992, The reactivity of sedimentary iron minerals toward sulfide: *American Journal of Science*, v. 292, p. 659 – 683.
- Canfield, D.E., and Teske, A., 1996, Late Proterozoic rise in atmospheric oxygen concentration inferred from phylogenetic and sulphur-isotope studies: *Nature*, v. 382, p. 127 – 132.
- Canfield, D.E., and Thamdrup, B. 1994, The production of <sup>34</sup>S-depleted sulfide during bacterial disproportionation of elemental sulfur: *Science*, v. 266, p. 1973 – 1975.
- Canfield, D.E., Thamdrup, B., and Fleisher, S. 1998b, Isotope fractionation and sulfur metabolism by pure and enrichment cultures of elemental sulfur-disproportionating bacteria: *Limnology and Oceanography*, v. 43, p. 253 – 264.
- Cheshire, M.C., Bish, D.L., and Brassell, S.C., 2012, Organic geochemical composition of the Georgia kaolins: Insights into formation and diagenetic conditions: *Clays and Clay Minerals*, v. 60, no. 4, p. 420 – 439.
- Claypool, G.E., Holser, W.T., Kaplan, I.R., Sakai, H, and Zak, I., 1980, The age curves of sulfur and oxygen isotopes in marine sulfate and their mutual interpretation: *Chemical Geology*, v. 28, p. 199 – 260.
- Detmers, J., Brüchert, V., Habicht, K.S., and Kuever, J., 2001, Diversity of sulfur isotope fractionations by sulfate-reducing prokaryotes: *Applied and Environmental Microbiology*, v. 67, n. 2, p. 888 – 894.
- Eversull, L.G., 2005, The Twiggs Clay: mineralogy, origin, and industrial properties of an upper Eocene opaline claystone in the coastal plain province of Georgia, U.S. [Ph.D. thesis]: Louisiana State University, 167 p.
- Habicht, K.S., and Canfield, D.E., 1996, Sulphur isotope fractionation in modern microbial mats and the evolution of the sulphur cycle: *Nature*, v. 382, p. 342 – 343.
- Habicht, K.S., and Canfield, D.E., 2001, Isotope fractionation by sulfate-reducing natural populations and the isotopic composition of sulfide in marine sediments: *Geology*, v. 29, p. 555 – 558.

- Holser, W.T., and Kaplan, I.R., 1966, Isotope geochemistry of sedimentary sulfates: *Chemical Geology*, v. 1, p. 93 – 135.
- Huddleston, P.F., and Hetrick, J.H., 1991, The stratigraphic framework of the Fort Valley plateau and the central Georgia kaolin district: *Georgia Geological Society Guidebook*, v. 11, p. 1 – 19.
- Hurst, V.J., and Pickering, S.M., 1997, Origin and classification of coastal plain kaolins, southeastern USA, and the role of groundwater and microbial action: *Clays and Clay Minerals*, v. 45, no. 2, p. 274 – 285.
- Jonas, E.C., 1964, Petrology of the Dry Branch, Georgia, kaolin deposits: *Clay and Clay Minerals Society*, 12<sup>th</sup> National Conference on Clays and Clay Minerals, p. 199 – 205.
- Keller, W.D., 1977, Scan electron micrographs of kaolins collected from diverse environments of origin – IV Georgia kaolin and kaolinizing source rocks: *Clays and Clay Minerals*, v. 25, p. 311 – 345.
- Kesler, T.L., 1956, Environment and origin of the Cretaceous kaolin deposits of Georgia and South Carolina: *Economic Geology*, v. 51, p. 541 – 554.
- Kogel, J.E., Pickering, S.M., Shelobolina, E., Chowns, T., Yuan, J., and Avant, D.M., 2002, The Georgia kaolins: Geology and utilization: Littleton, Colorado, Society for Mining, Metallurgy, and Exploration, Inc. (SME), p. 84.
- LeGrand, H.E., and Furcron, A.S., 1956, Geology and ground-water resources of central-east Georgia: *Georgia Geological Survey Bulletin*, no. 64, 174 p.
- Lowe, R.A., 1991, Microtextural and mineralogic differences of Georgia's kaolins and the search for ostwald ripening [M.S. Thesis]: The University of Georgia, 81 p.
- Murray, H.H., and Keller, W.D., 1993, Kaolins, kaolins, and kaolins: *The Clay Minerals Society Special Publication*, no. 1., p. 1 – 24.
- Over, J.D., Sprague, E.K., Culp, R.A., Pickering, S.M., and Wenner, D.B., 1987, Deposition of Georgia commercial kaolins in upper estuaries; indicated by organic carbon <sup>13</sup>C/<sup>12</sup>C: *Geological Society of America, Abstracts*, v. 19, i. 2, p. 122.
- Parmley, D. and Holman, J.A., 2003, *Nebrakophis* HOLMAN from the Late Eocene of Georgia (USA), the oldest known North American colubrid snake: *Acta zoologica cracoviensia*, v. 46, p. 1-8.
- Patterson, S.H., and Murray, H.H., 1984, Kaolin, refractory clay, ball clay and halloysite in North America, Hawaii and the Caribbean region: *US Geological Survey Professional Paper*, v. 1036, p. 56.

- Pruett, R.J., Davis, J., and Everett, B.C., 2009, The microtexture of Georgia kaolin: Georgia Geological Society Guidebook, v. 29, p. 59 – 64.
- Raiswell, R., 1997, A geochemical framework for the application of stable sulphur isotopes to fossil pyritization: *Journal of the Geological Society, London*, v. 154, p.343 – 356.
- Raiswell, R., Canfield, D.E., 1998, Sources of iron for pyrite formation in marine sediments: *American Journal of Science*, v. 298, p. 219 – 245.
- Raiswell, R., Canfield, D.E., 2012, The iron biogeochemical cycle past and present: *Geochemical Perspectives*, v. 1, no. 1, 2012.
- Rees, C.E., 1973, A steady-state model for sulphur isotope fractionation in bacterial reduction processes: *Geochimica et Cosmochimica Acta*, v. 37, p. 1141 – 1162.
- Schroeder, P.A., Pruett, R.J., and Melear, N.D., 2004, Crystal-chemical changes in an oxidative weathering front in a Georgia kaolin deposit: *Clays and Clay Minerals*, v. 52, n. 2, p. 211 – 220.
- Schroeder, P.A., and Shiflet, J., 2000, Ti-bearing phases in an east Georgia kaolin deposit: *Clays and Clay Minerals*, v. 48, p. 151 – 158.
- Shelobolina, E.S, Pickering, S.M., and Lovley, D.R., 2005, Fe-cycle bacteria from industrial clays mined in Georgia, USA: *Clays and Clay Minerals*, v. 53, n. 6, p. 580 – 586.
- Skyring, G.W., 1987, Sulfate reduction in coastal ecosystems: *Geomicrobiology Journal*, v. 5, 295 – 375.
- Smith R.W., 1929, Sedimentary kaolins of the coastal plain of Georgia: *Georgia Geological Survey Bulletin*, v. 44, 474 p.
- Sprague, E.K., Over, D.J., Gize, A.P., Pickering, S.M., and Wenner, D.B., 1988, Apparent salinity of depositional environments of commercial sedimentary kaolinites, Georgia, by carbon isotope analysis ( $\delta^{13}\text{C}/^{12}\text{C}$ ): Abstracts from the Annual Meeting of Geological Society of America, v. 20, i. 7, A174.
- Stull, R.T. and Bole, G.A., 1926, Beneficiation and utilization of Georgia clays: U.S. Bureau of Mines Bulletin, v. 252, 72 pp.
- Taylor, G.K., and Macquaker, J.H.S., 2000, Early diagenetic pyrite morphology in a mudstone dominated succession: the lower Jurassic Cleveland ironstone formation, eastern England: *Sedimentary Geology*, v. 131: 77 – 86.
- Tschudy, R.H., and Patterson, S.H., 1975, Palynological evidence for late Cretaceous, Paleocene, and early and middle Eocene age for strata in the kaolin belt, central Georgia: *U.S. Geological Survey Journal of Research*, v. 3, n. 4, p. 437 – 445.

Ueda, A., and Krouse, H.R., 1986, Direct conversion of sulfide and sulfate minerals to SO<sub>2</sub> for isotope analyses: *Geochemical Journal*, v. 20, p. 209 – 212.

Wampler, J.M., Elliott, C.W., White, B.W., and Pajewski, K.A., 2001, The character of glauconite in the Twiggs Clay Member along Elko Road, Houston County, Georgia (abstract): *Geological Society of America Abstracts*, no. 99.

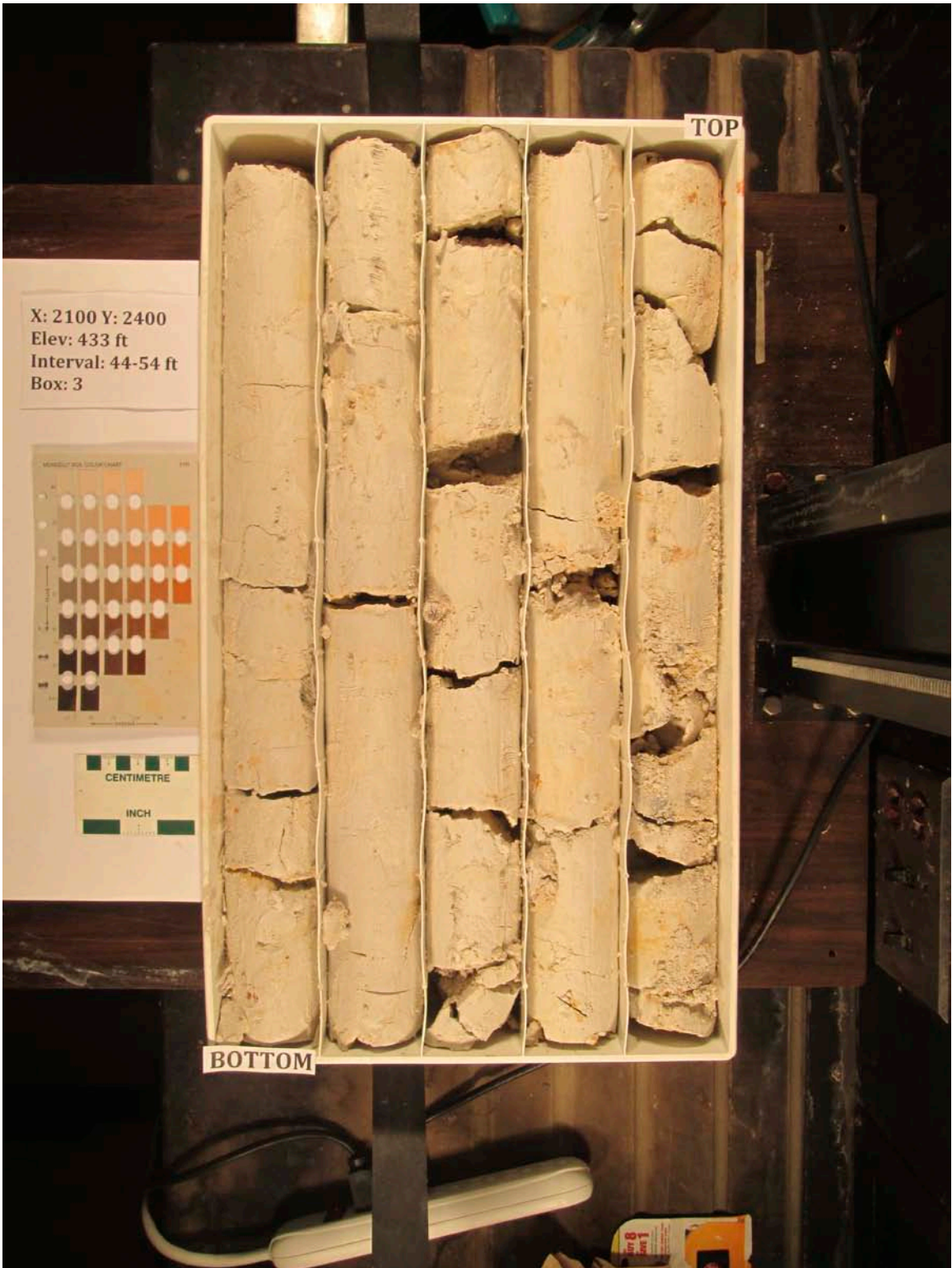
Weibel, R., 1998, Diagenesis in oxidizing and locally reducing conditions; an example from the Triassic Skagerrak Formation, Denmark: *Sedimentary Geology*, vol. 121, i. 3-4, p. 259 – 276.

White, N.G, Dixon, J.B., Weaver, R.M. and Kunkle, A.C., 1991, Genesis and morphology of iron sulfides in gray kaolins: *Clays and Clay Minerals*, v. 39, p. 70 – 76.

**APPENDIX A**  
**DRILL CORE PHOTOS**









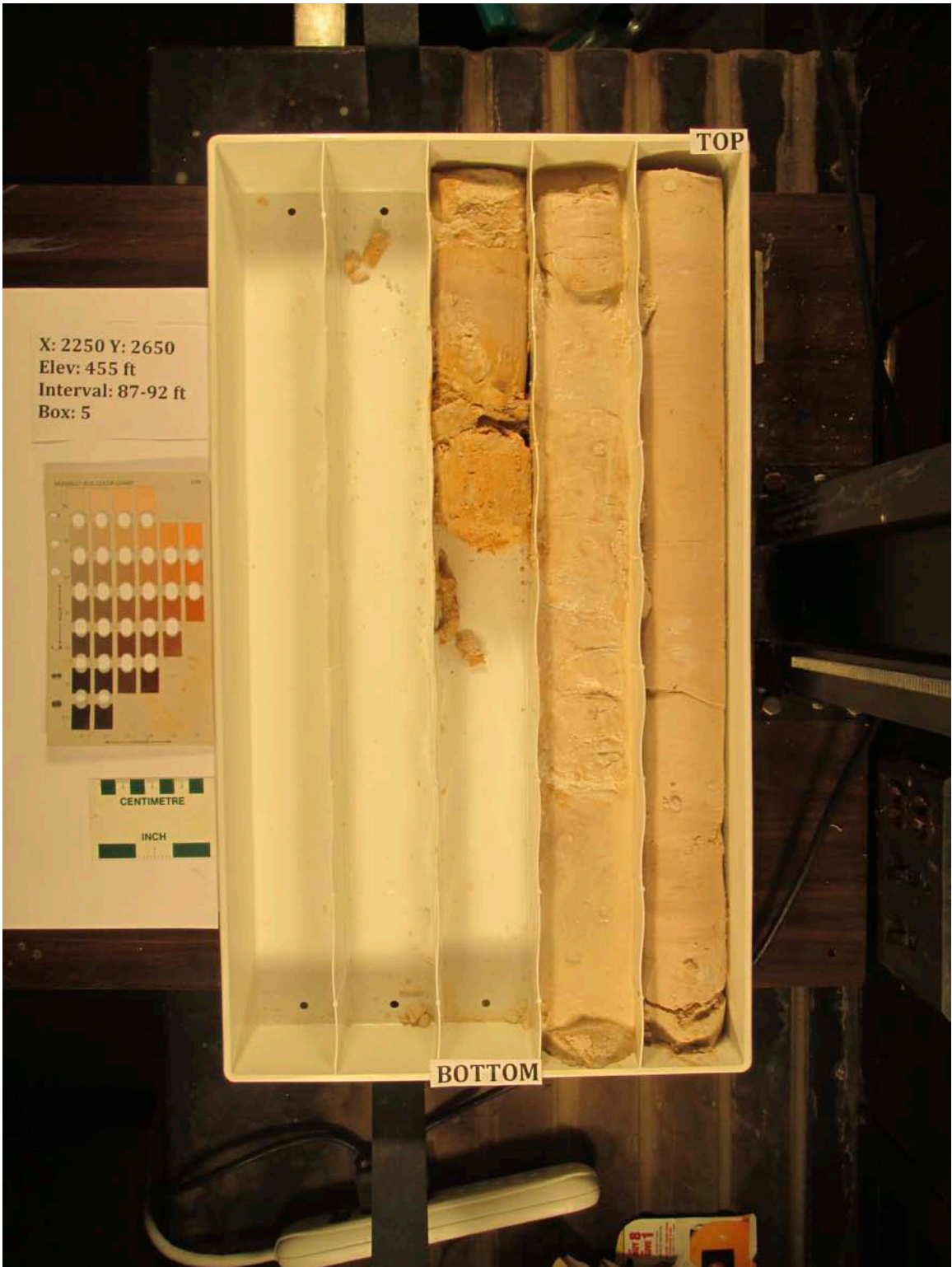


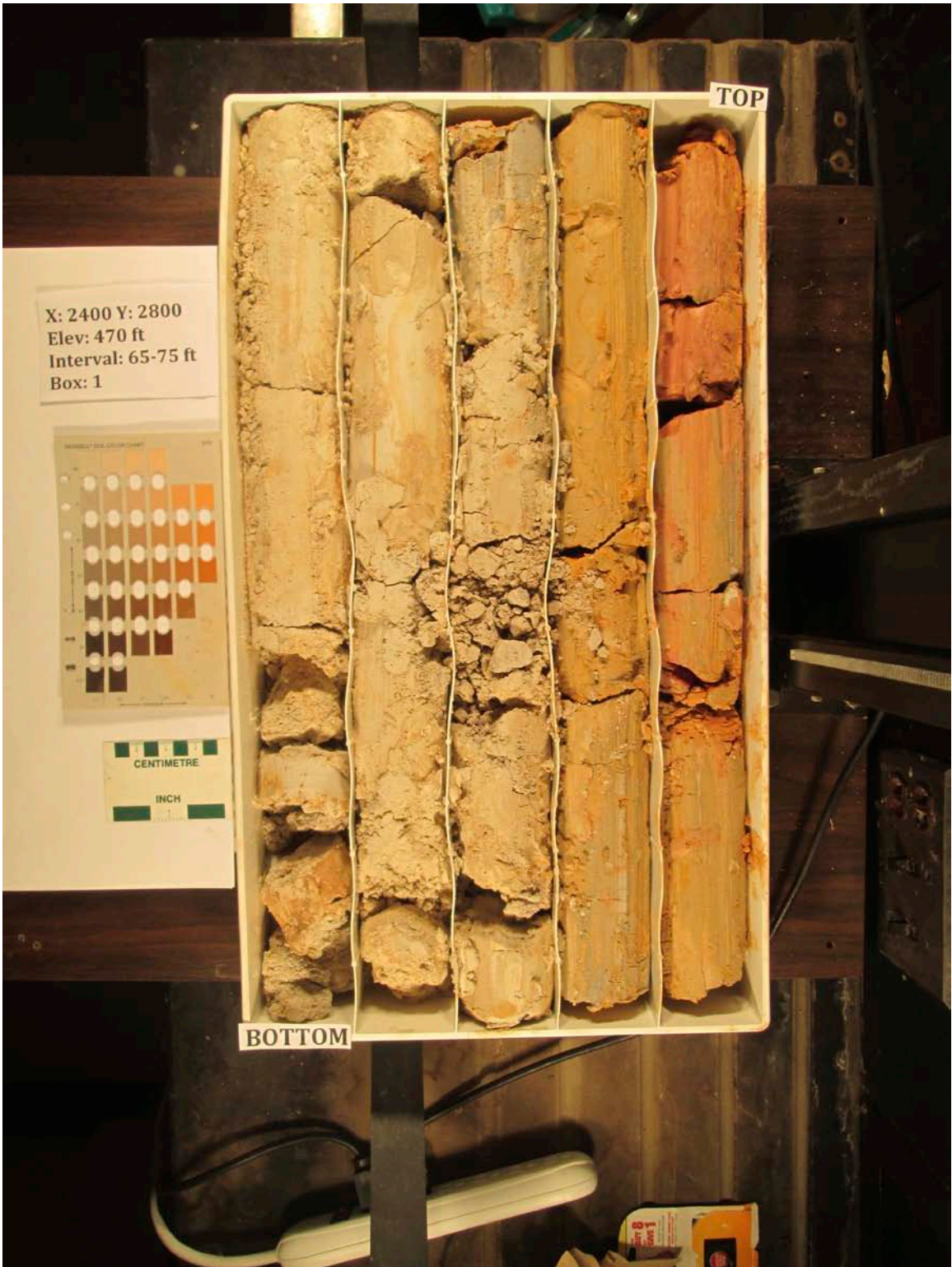
















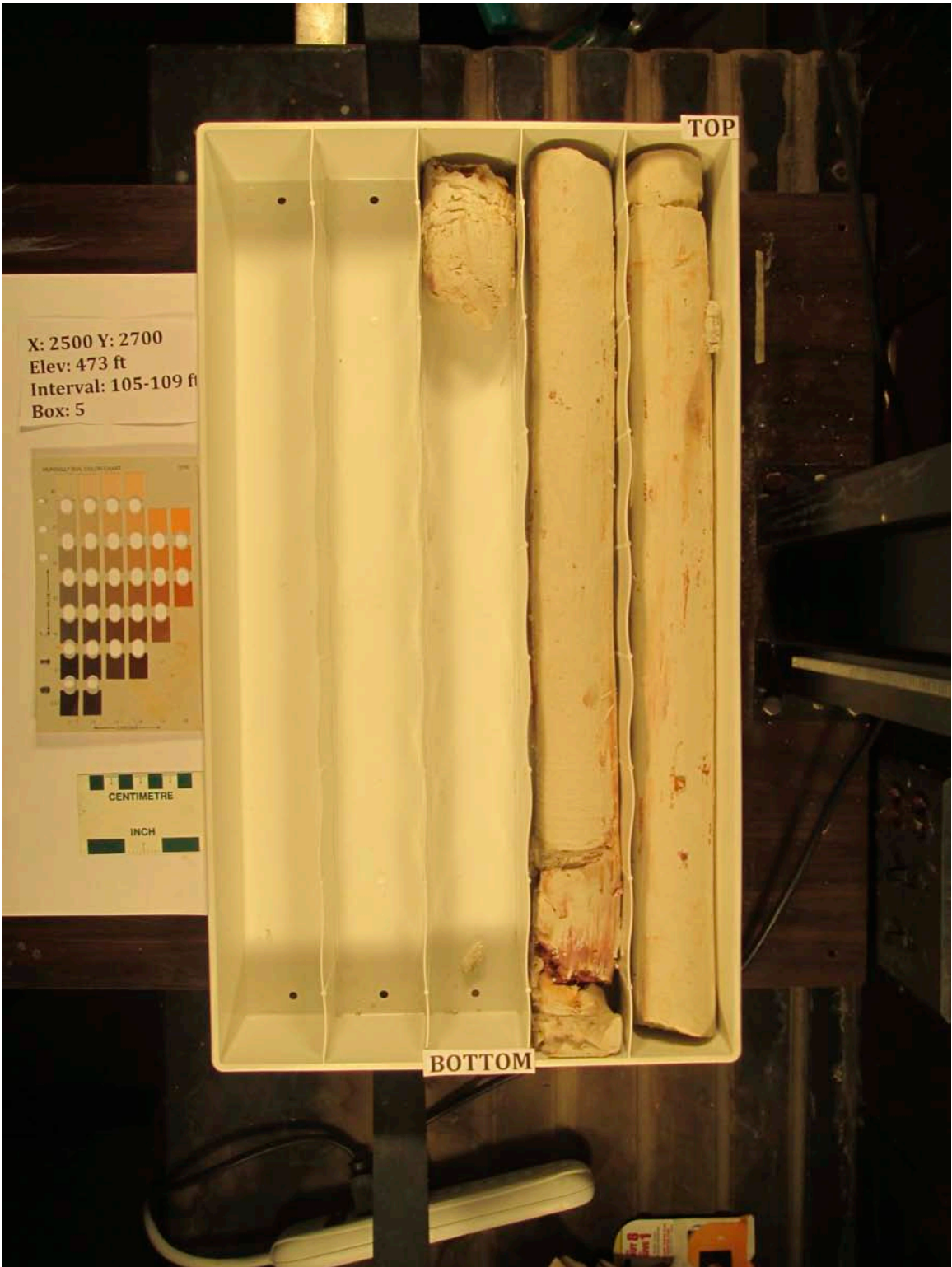








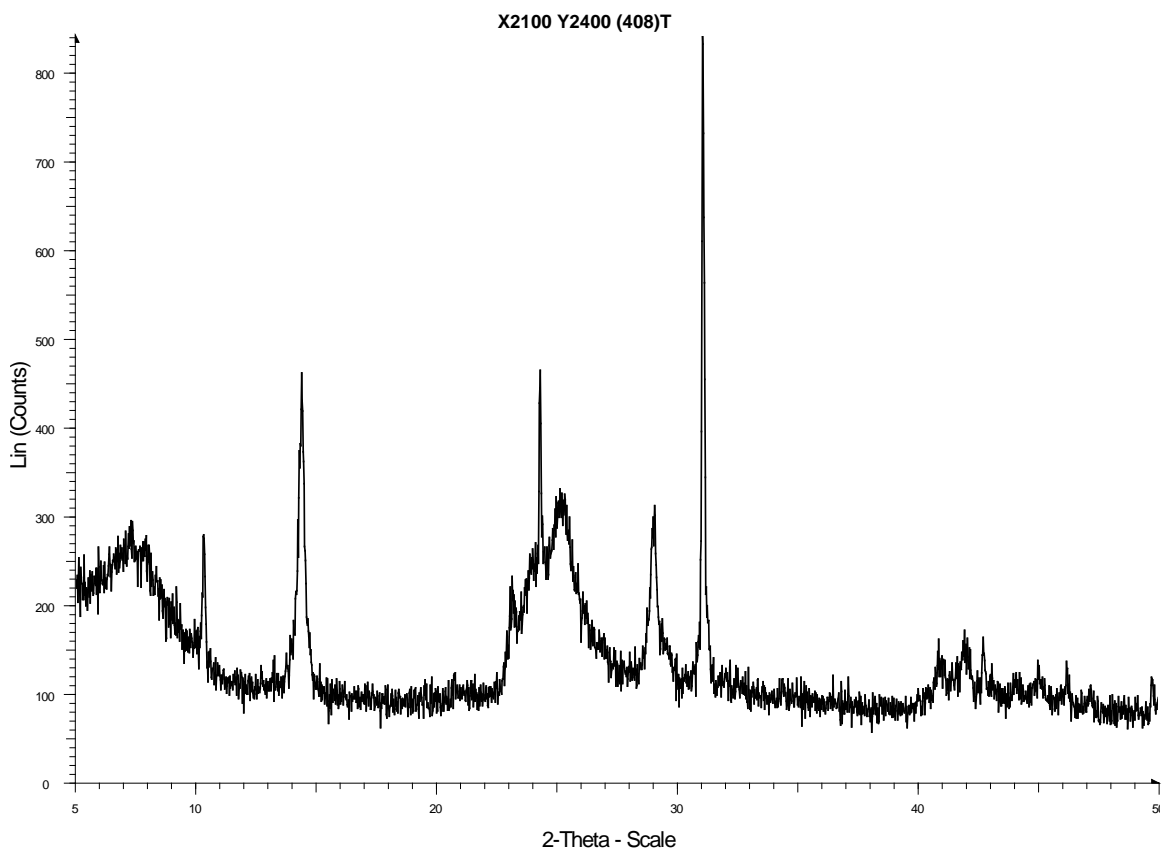
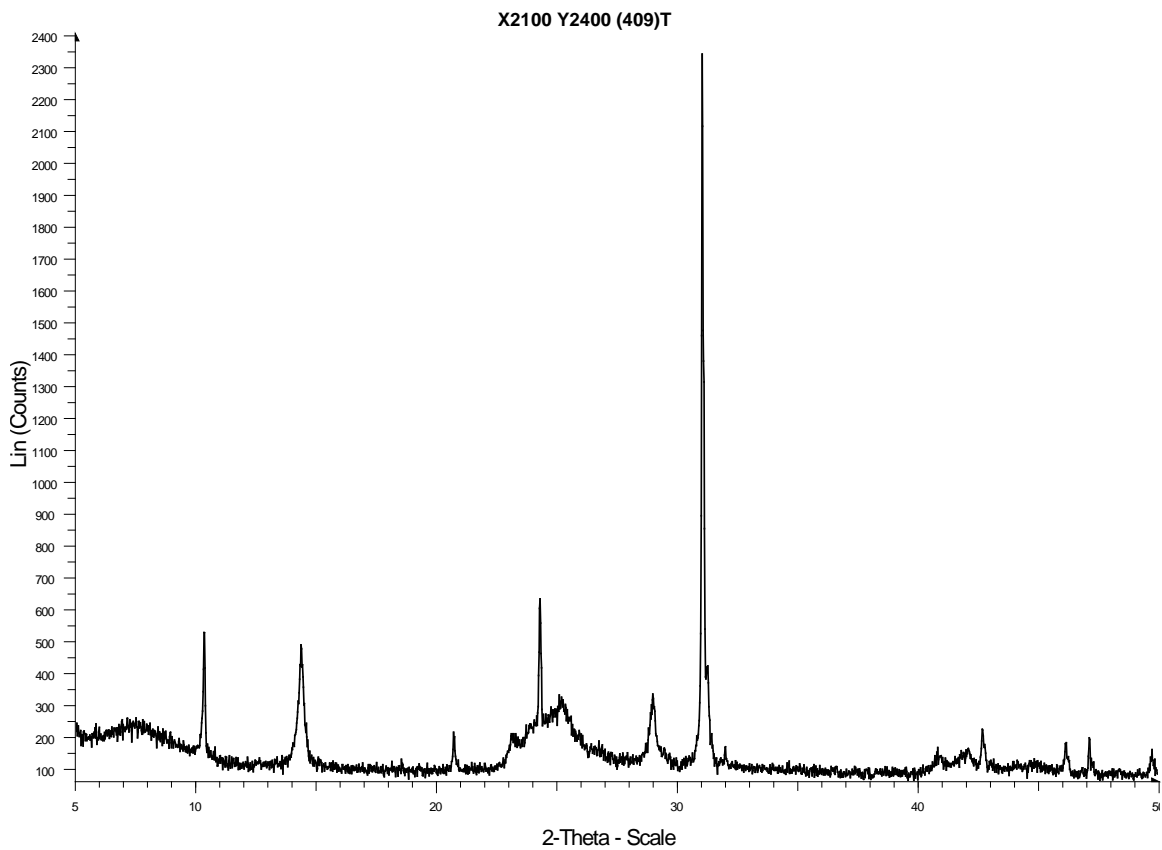


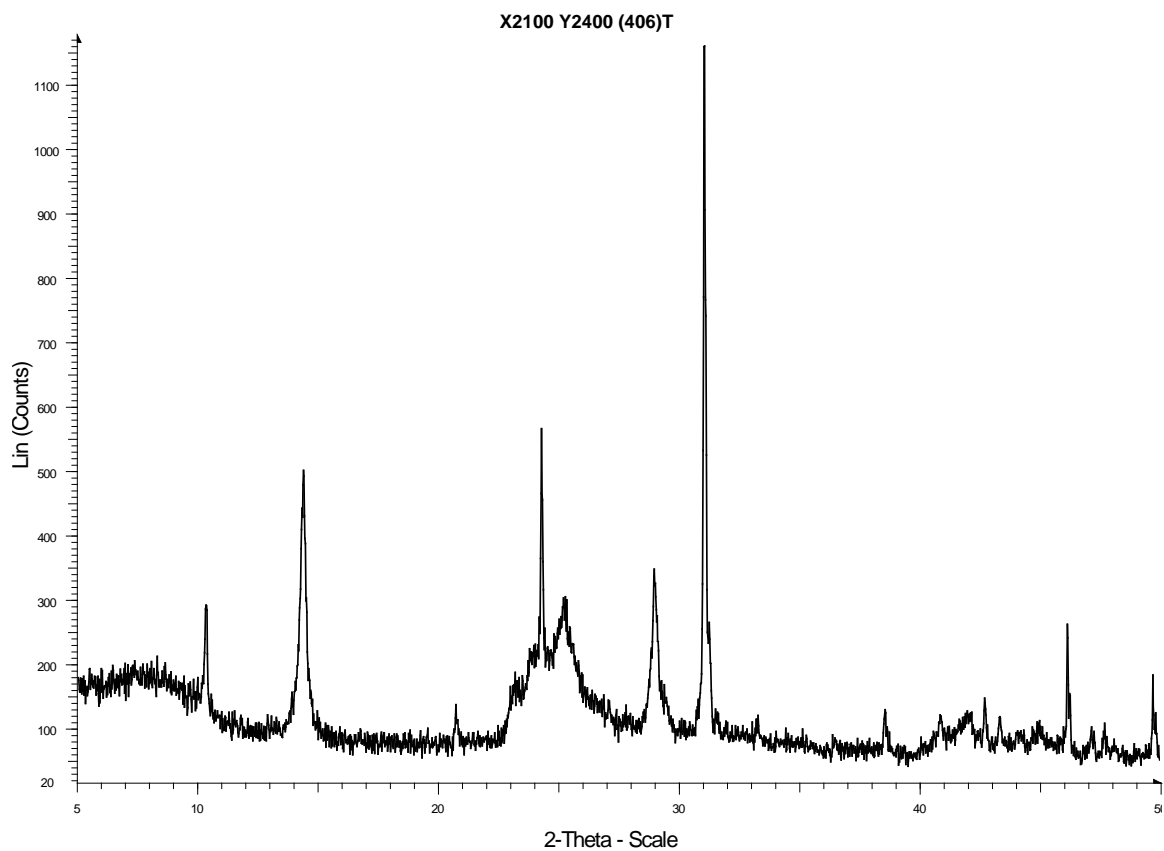
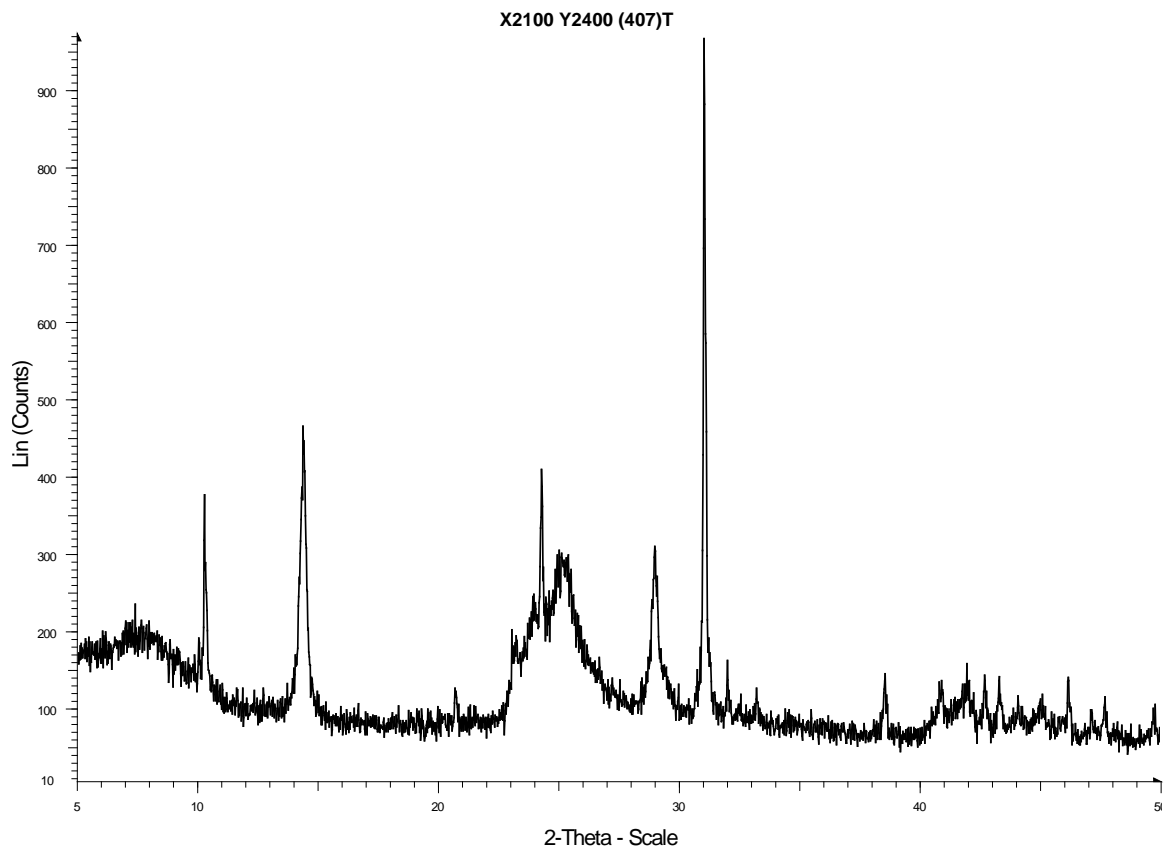


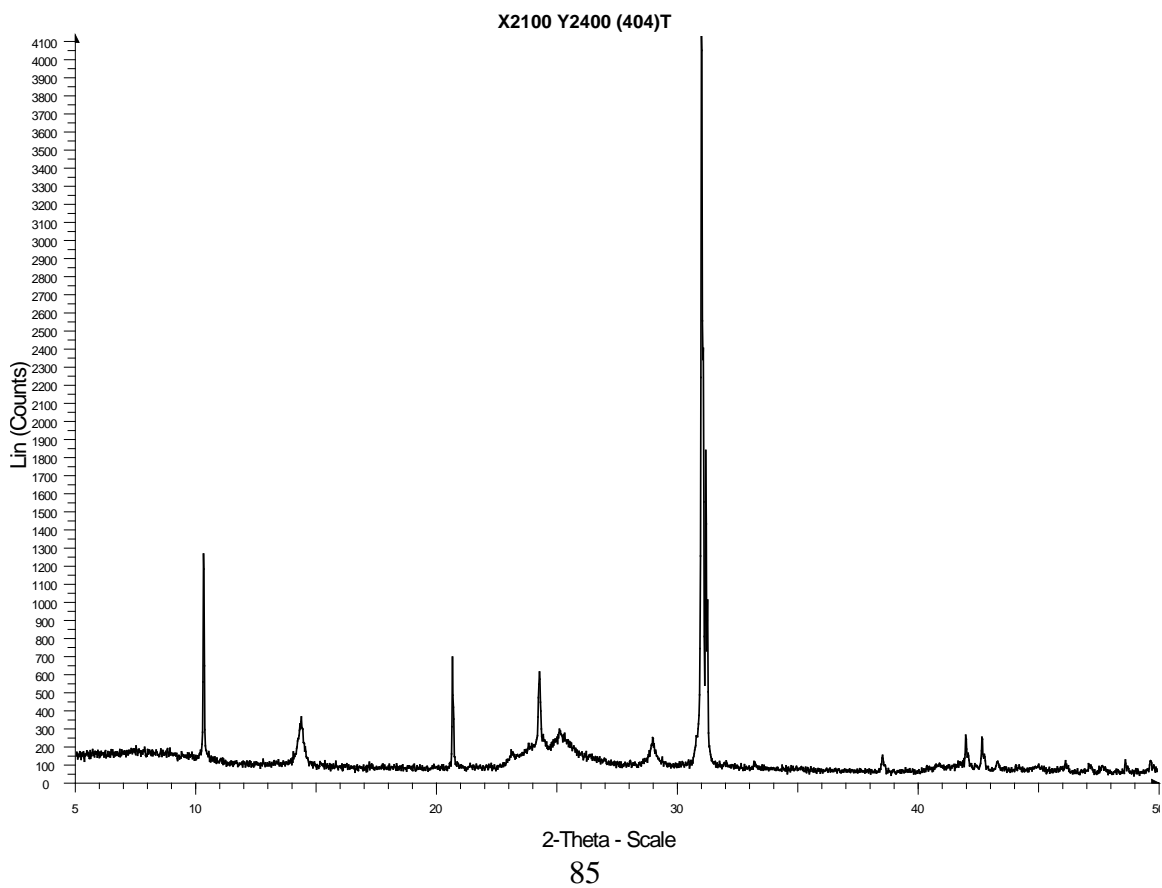
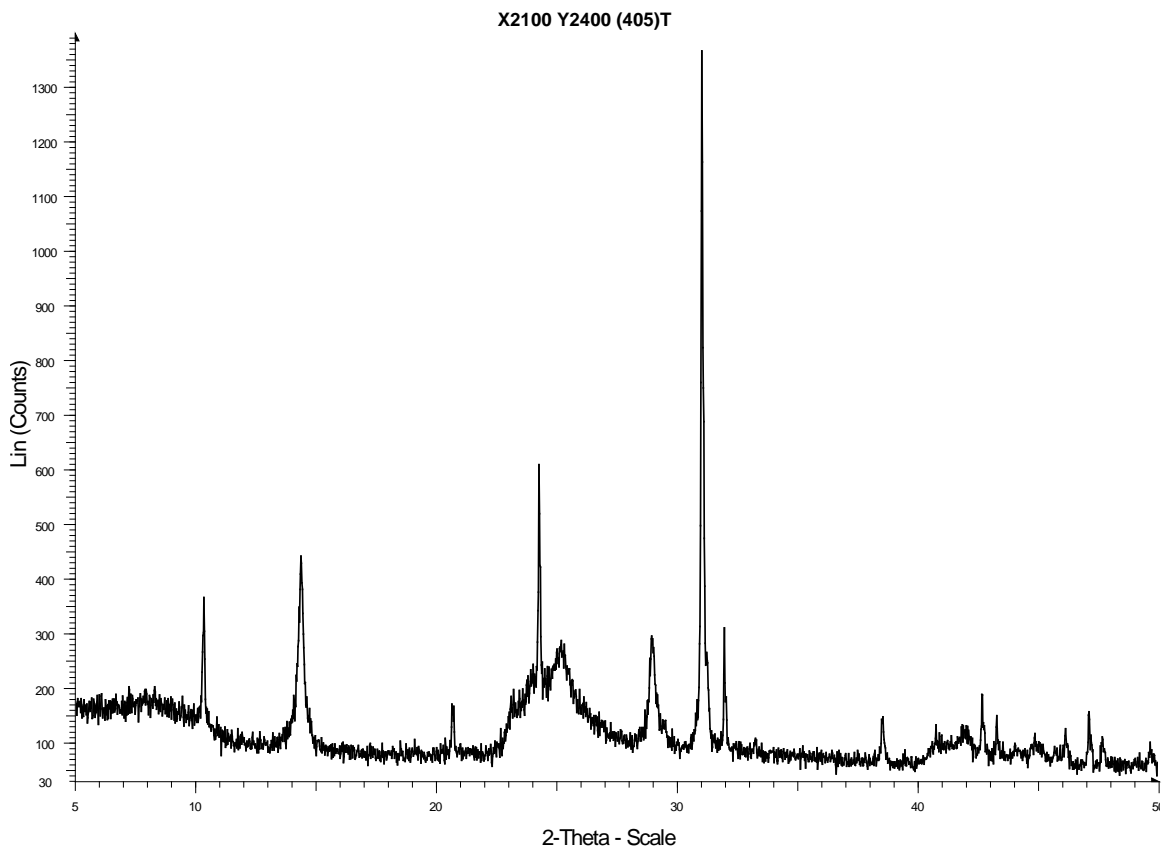
**APPENDIX B**  
**X-RAY DIFFRACTION PLOTS<sup>1</sup>**

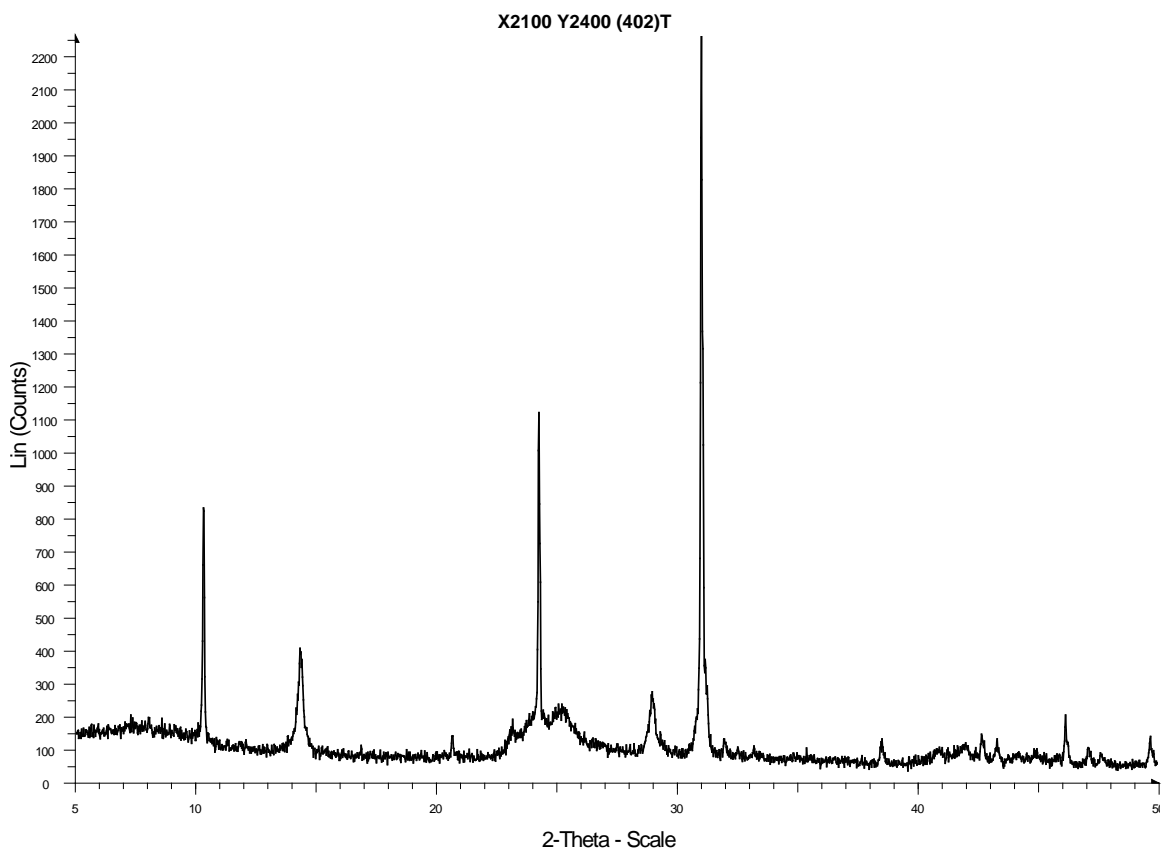
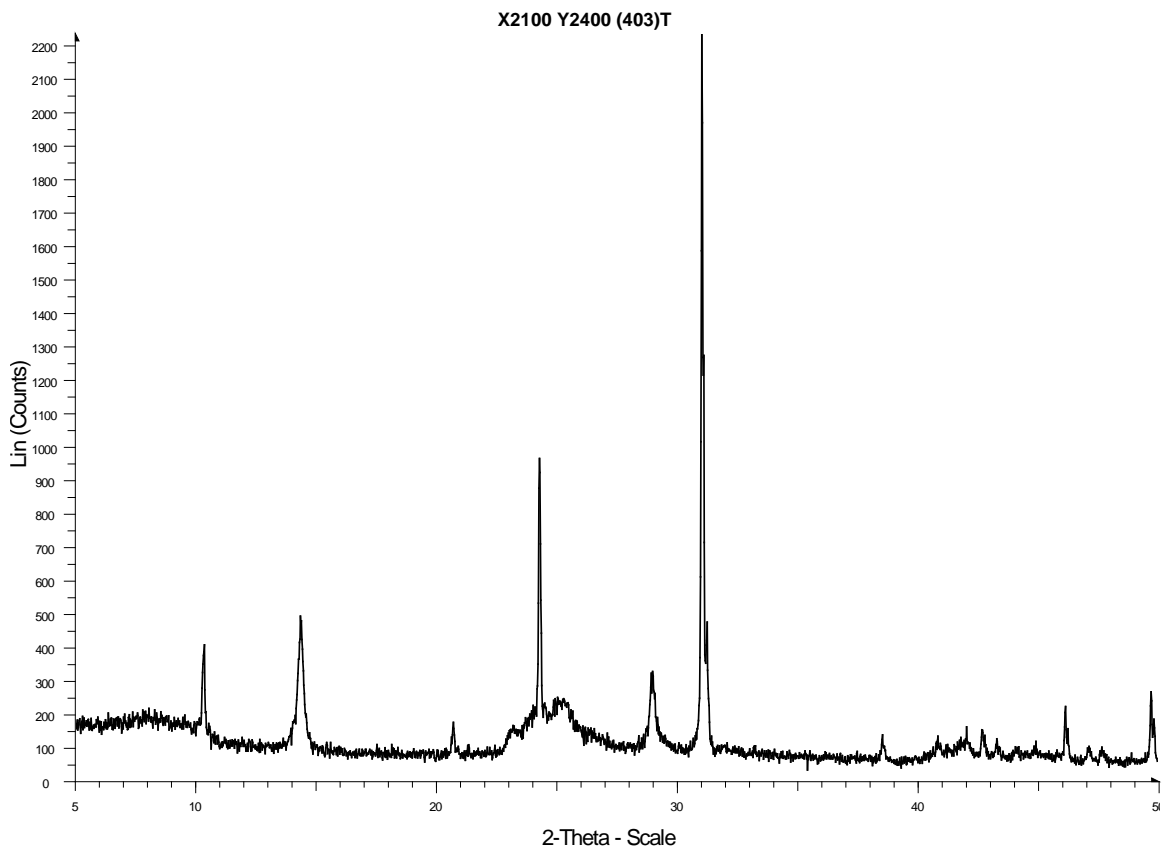
---

<sup>1</sup> All plots were collected under the following conditions: Start: 5.000° - End: 49.998° - Step: 0.020° - Step time: 15.4 s - Temp: 25° C (Room)

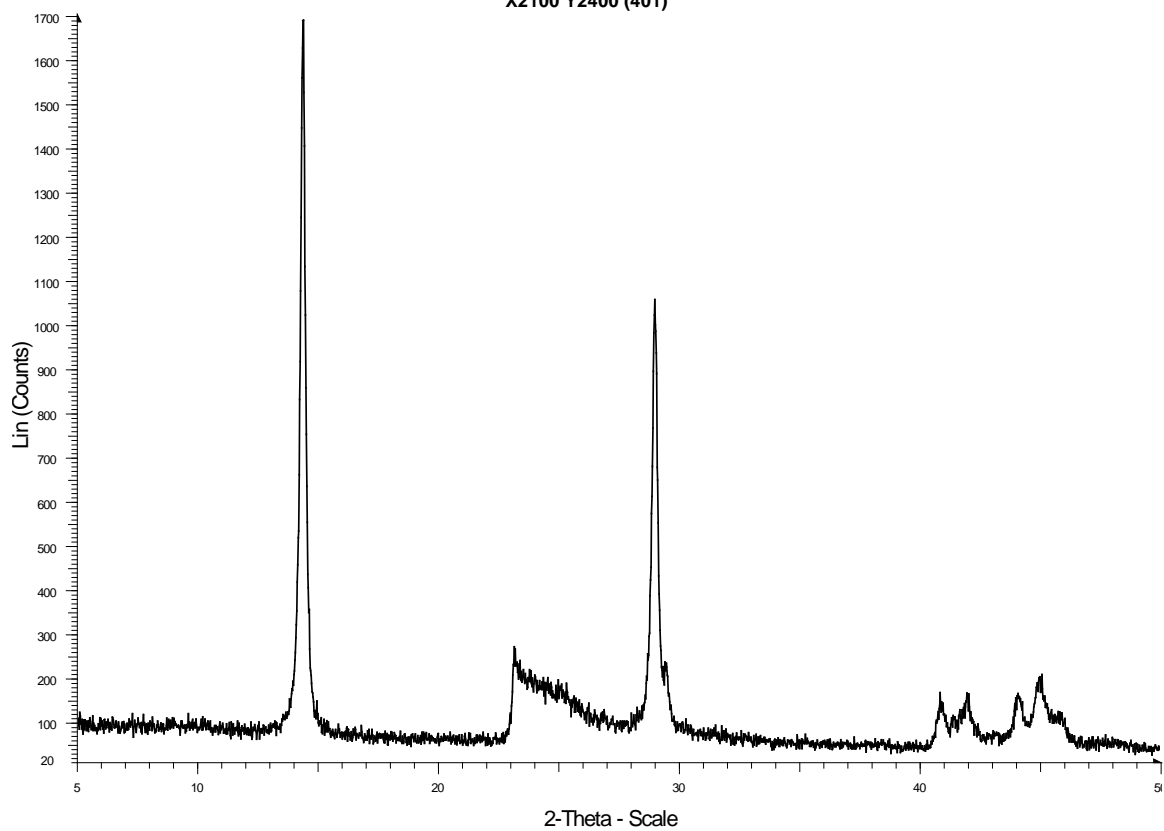




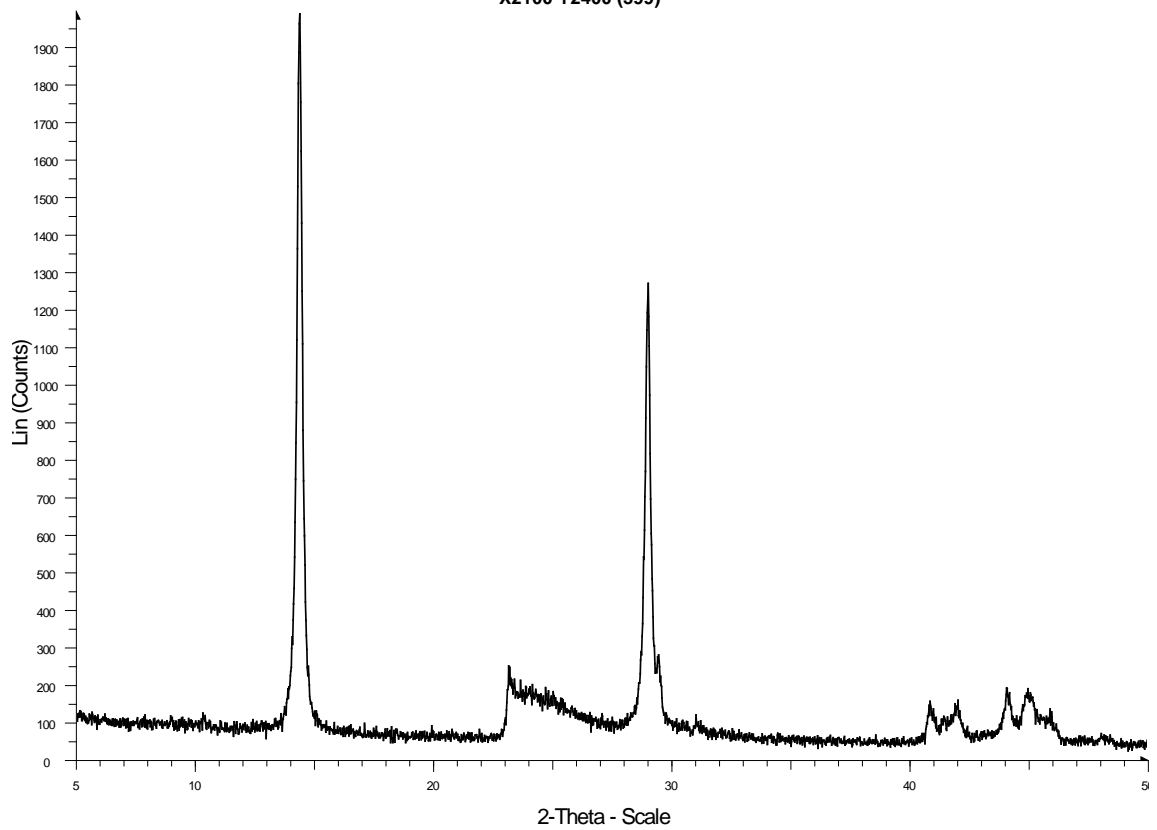




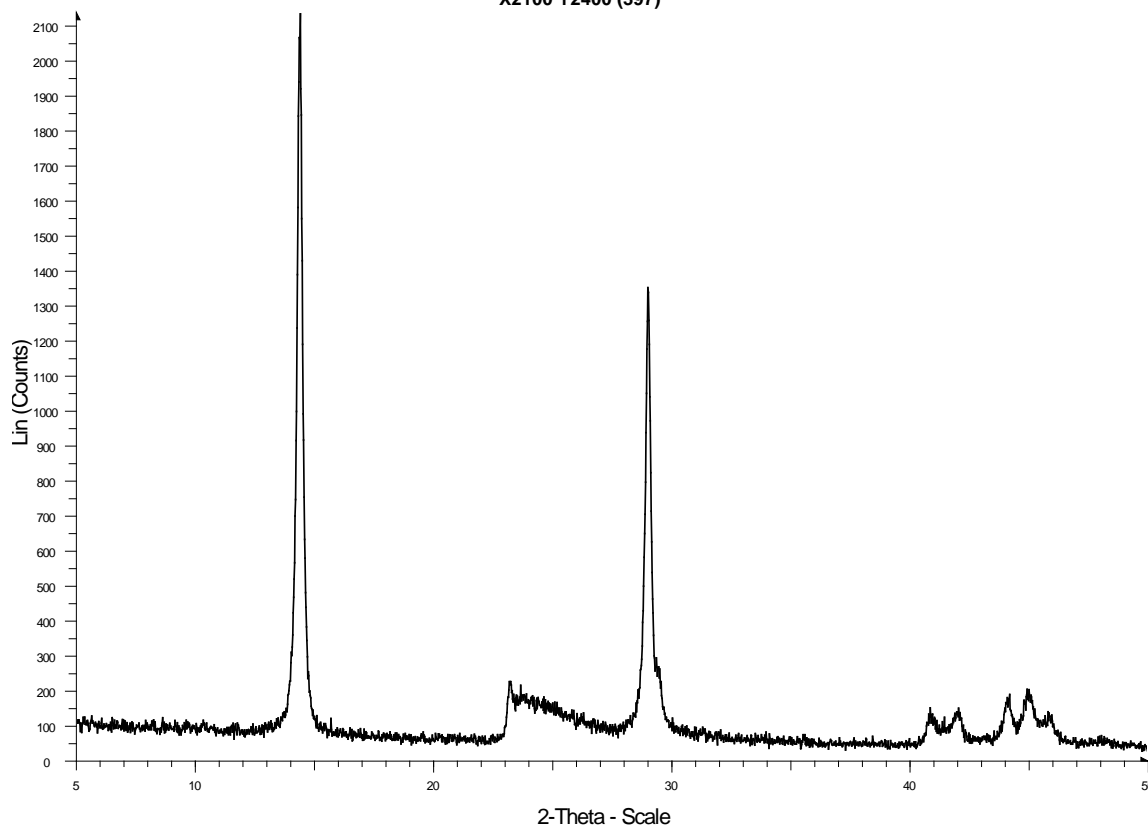
X2100 Y2400 (401)



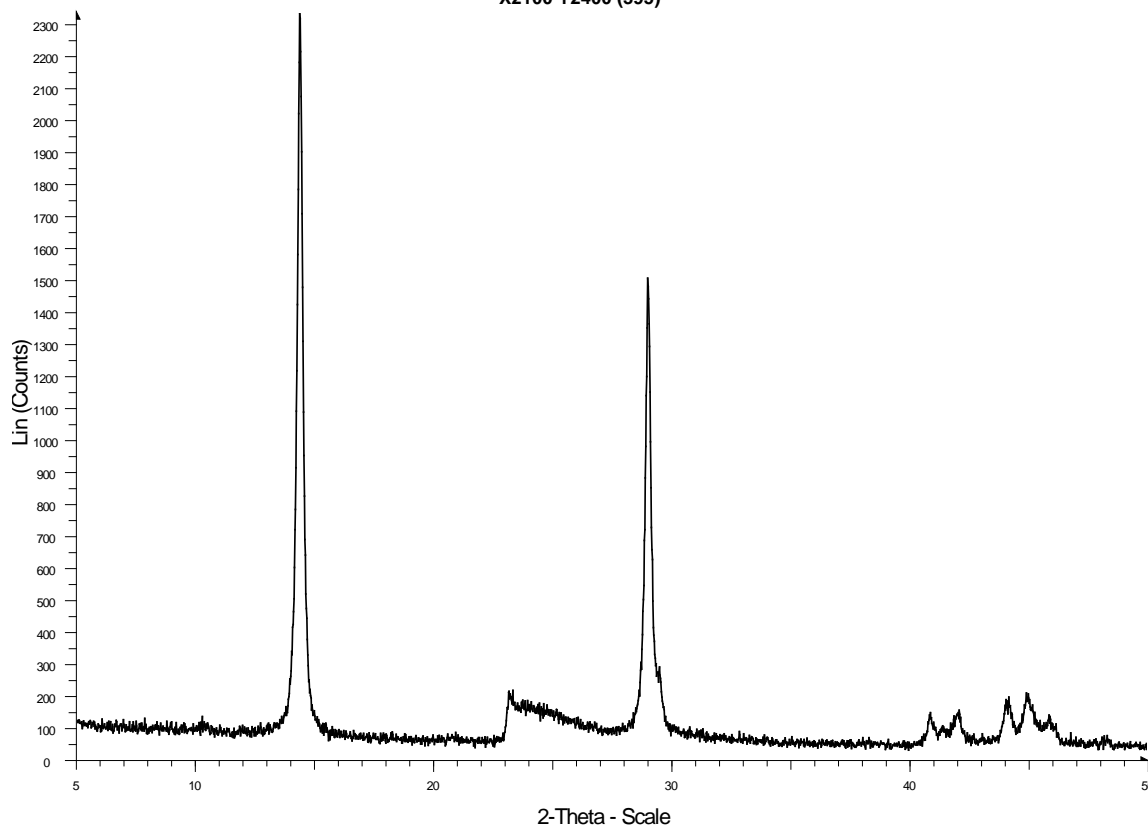
X2100 Y2400 (399)

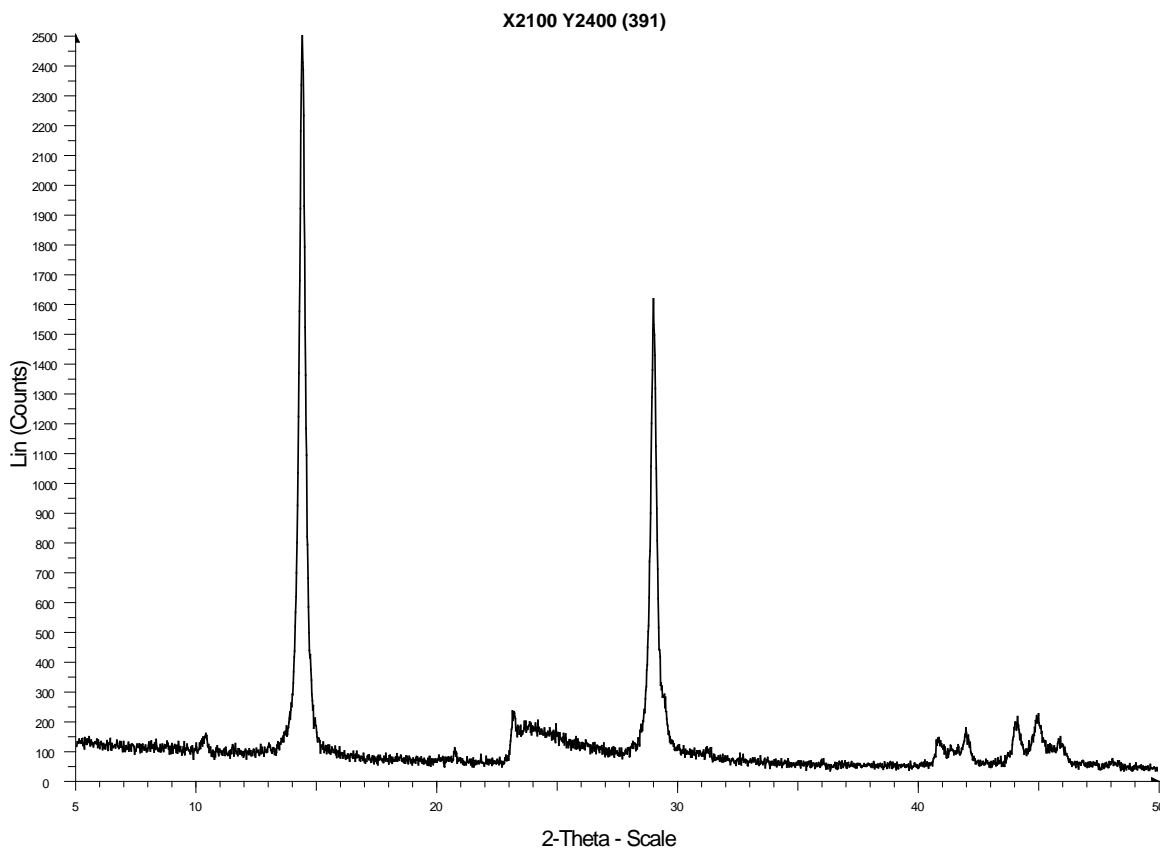
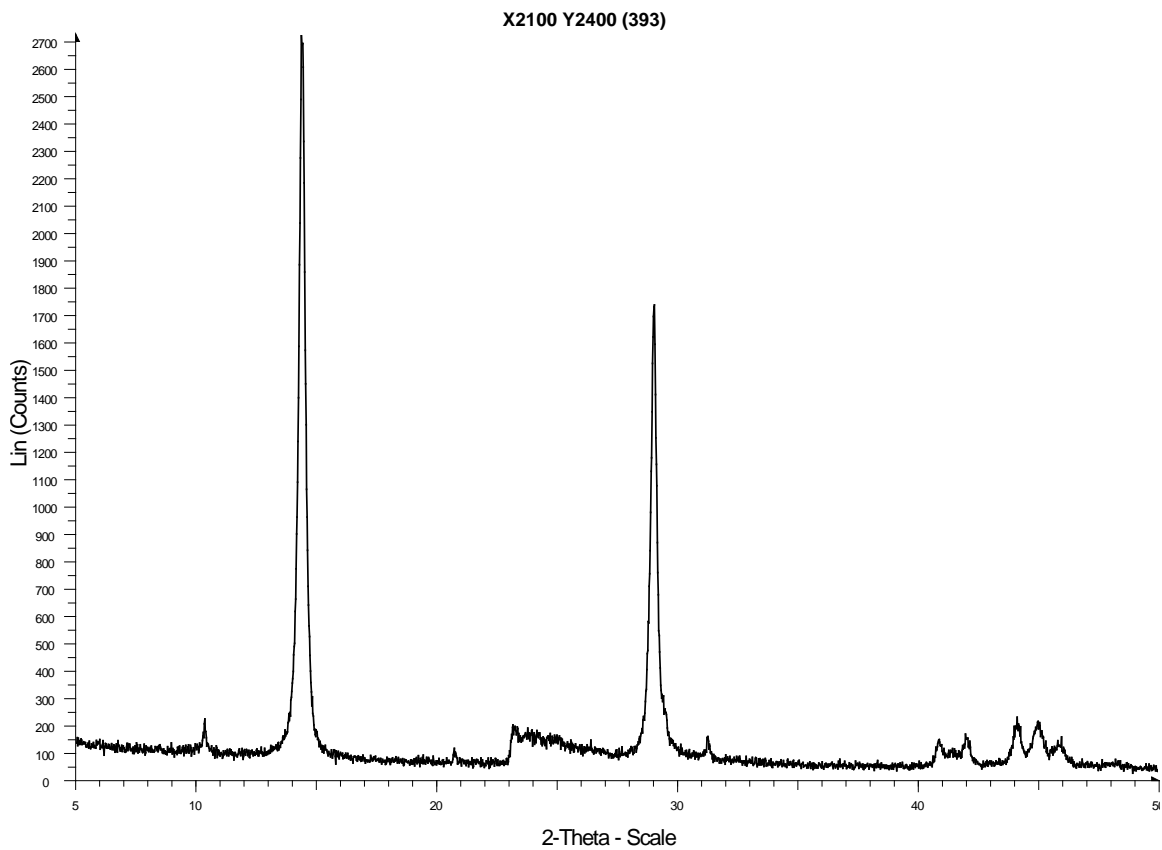


X2100 Y2400 (397)

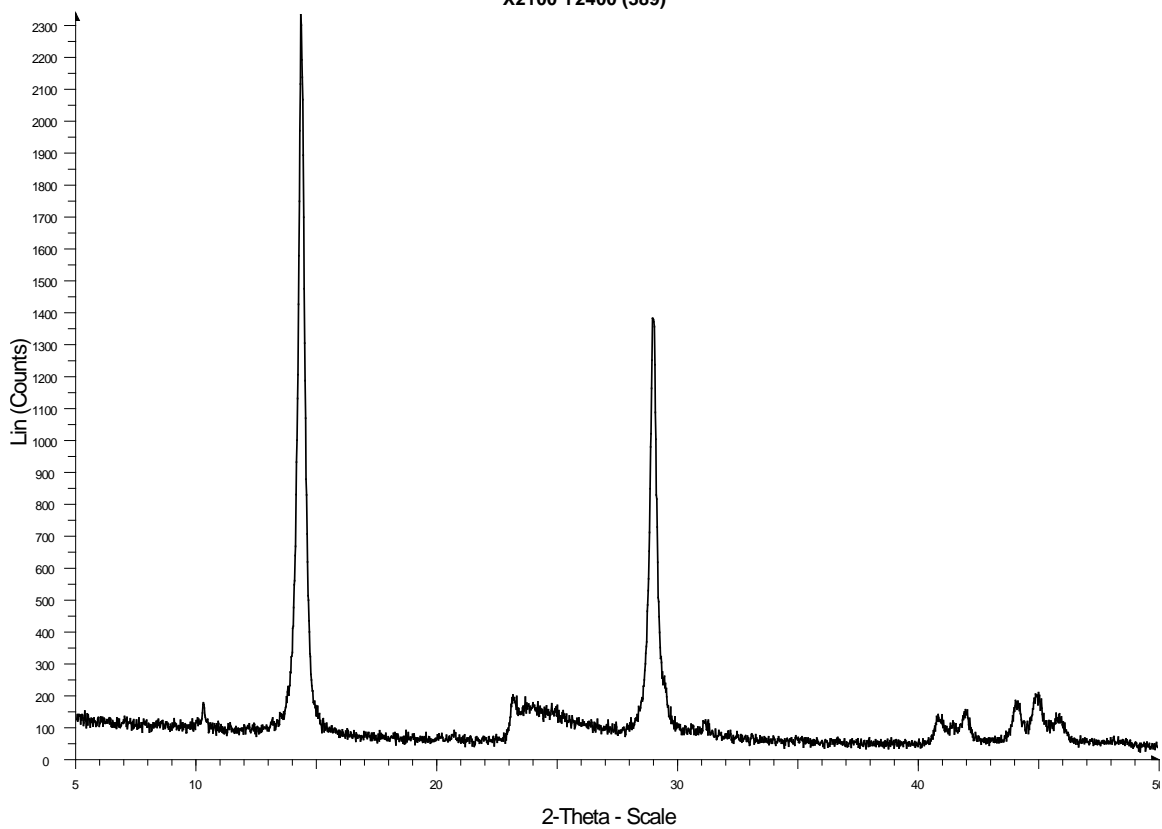


X2100 Y2400 (395)

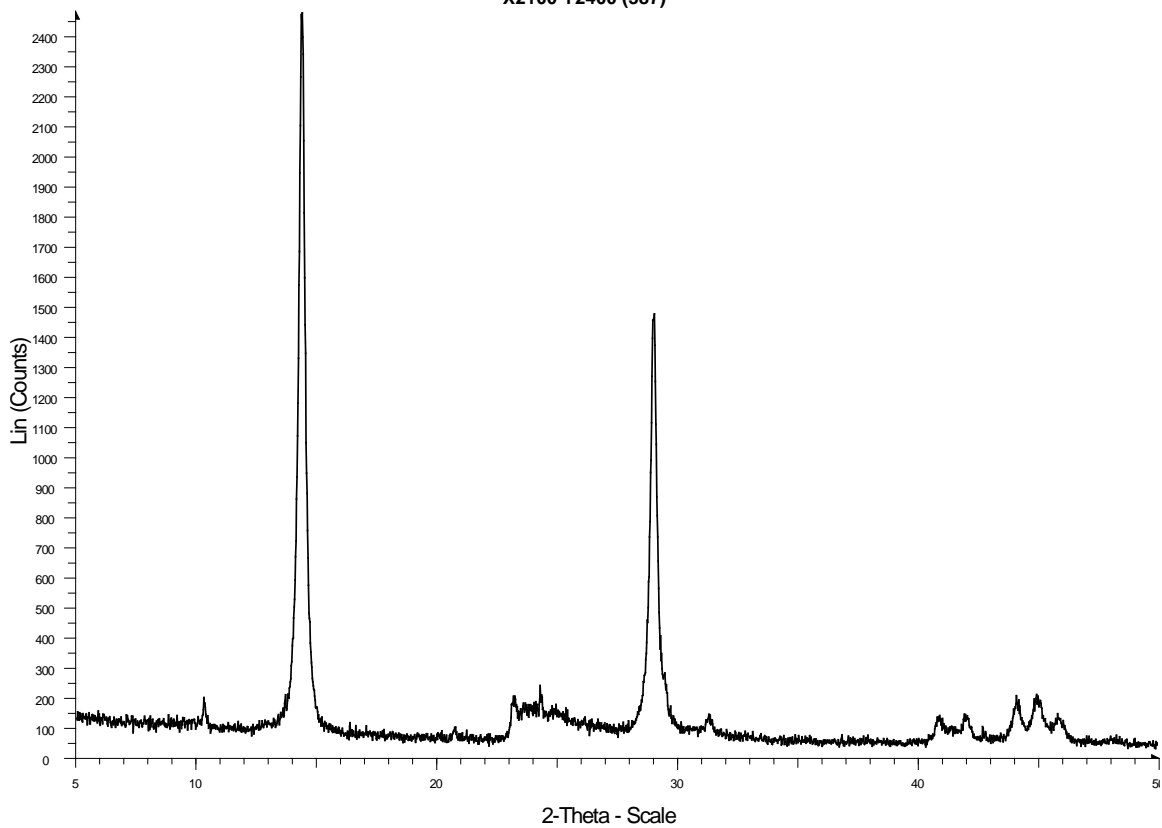


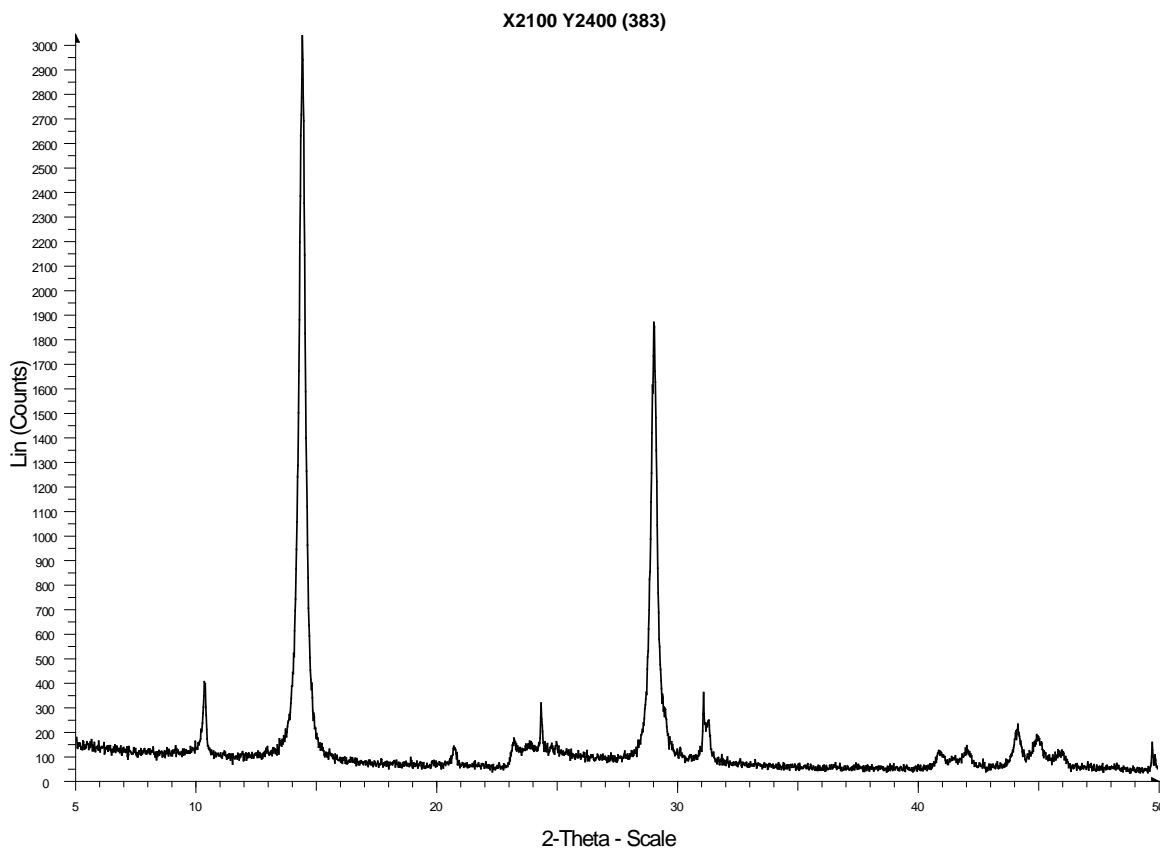
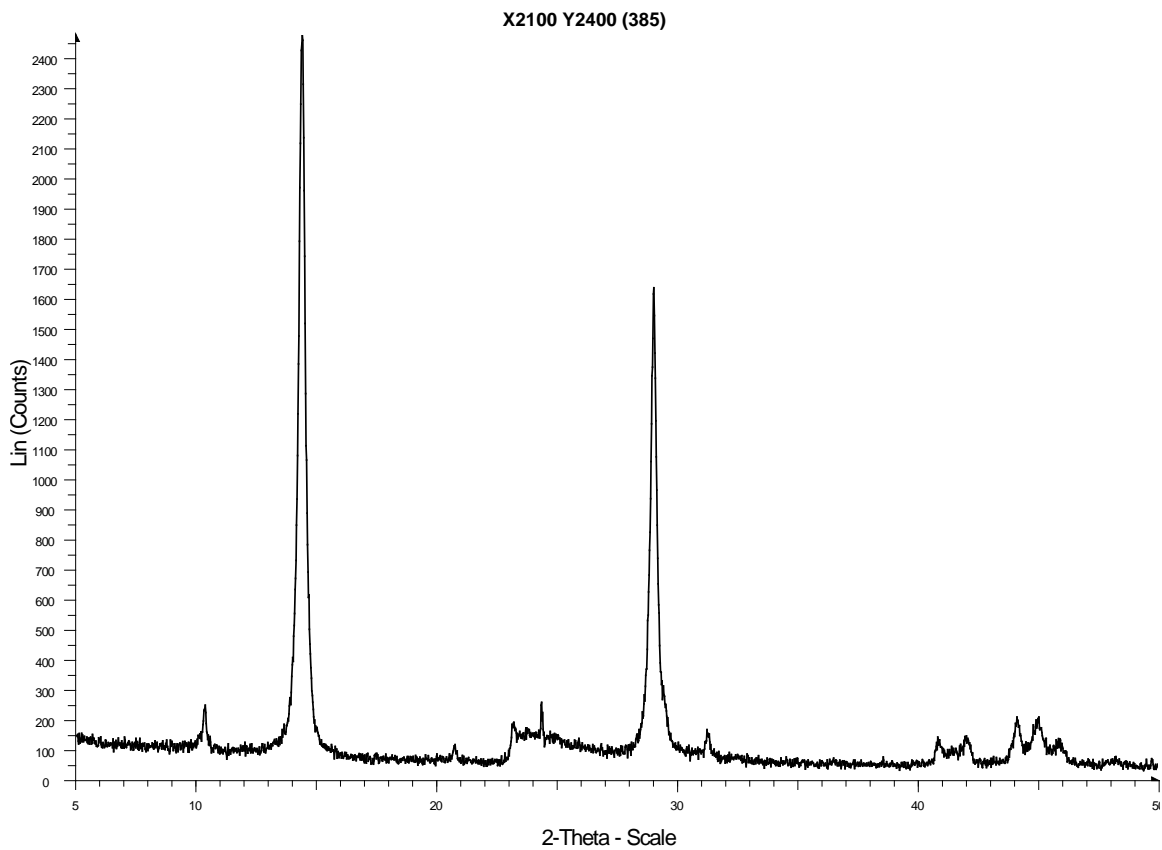


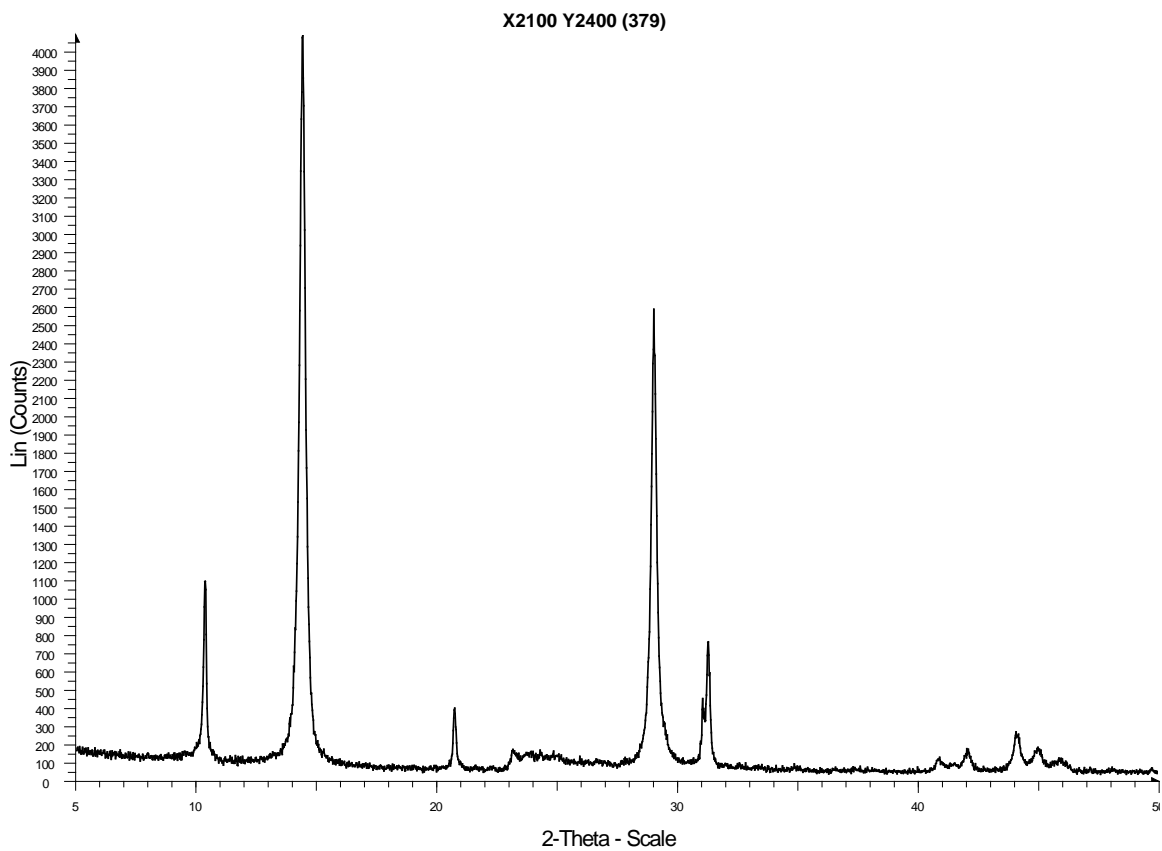
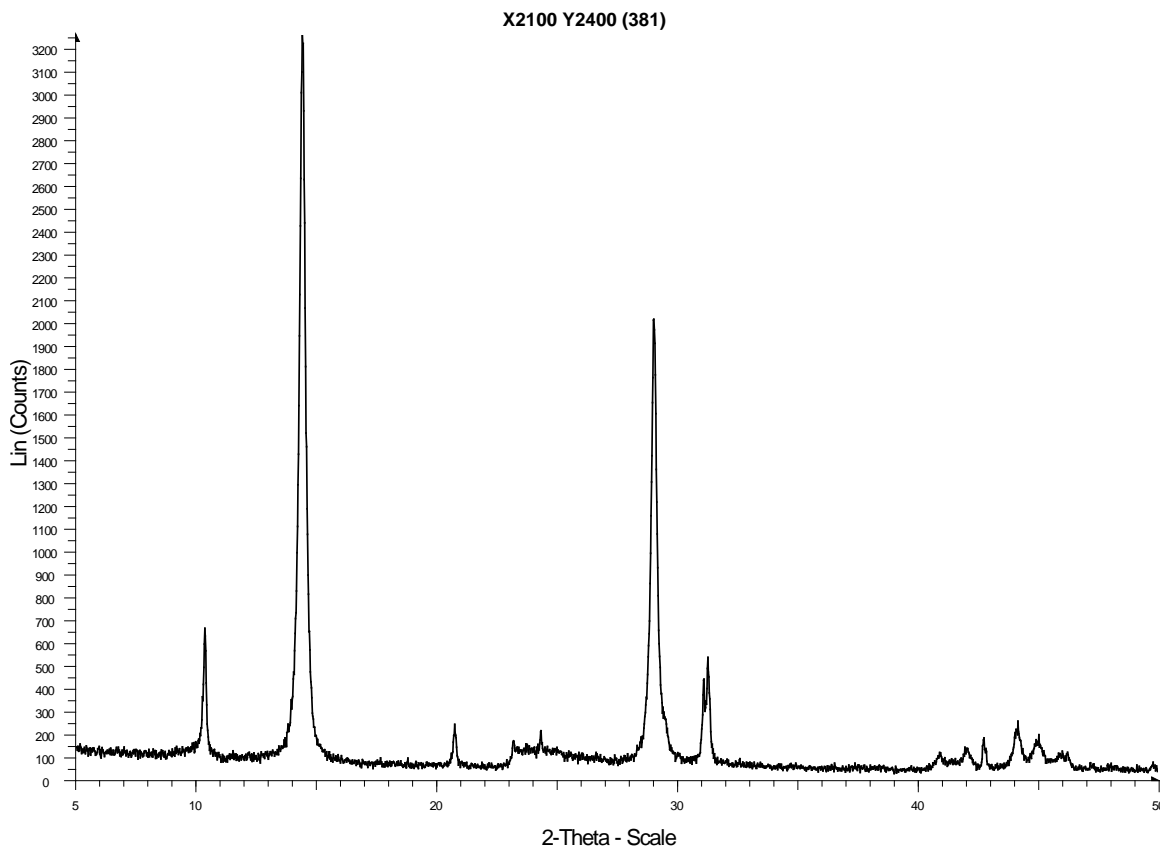
X2100 Y2400 (389)

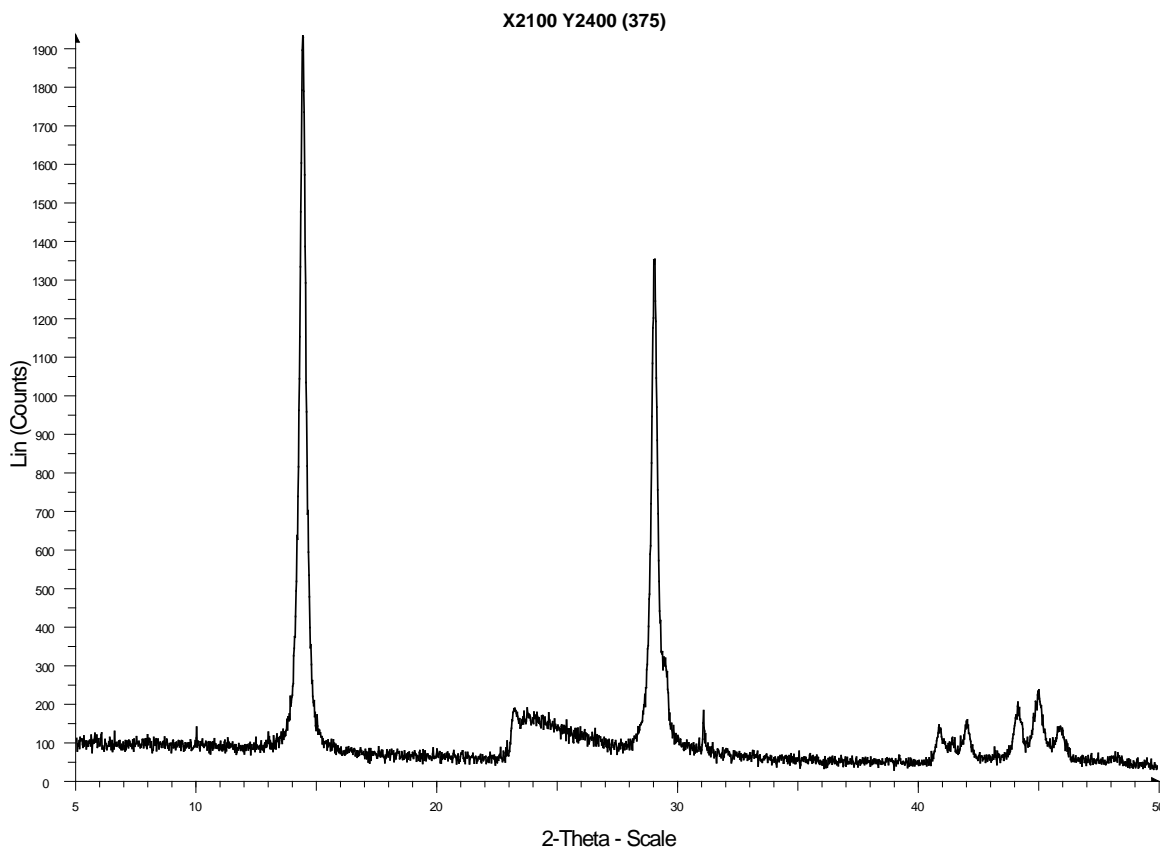
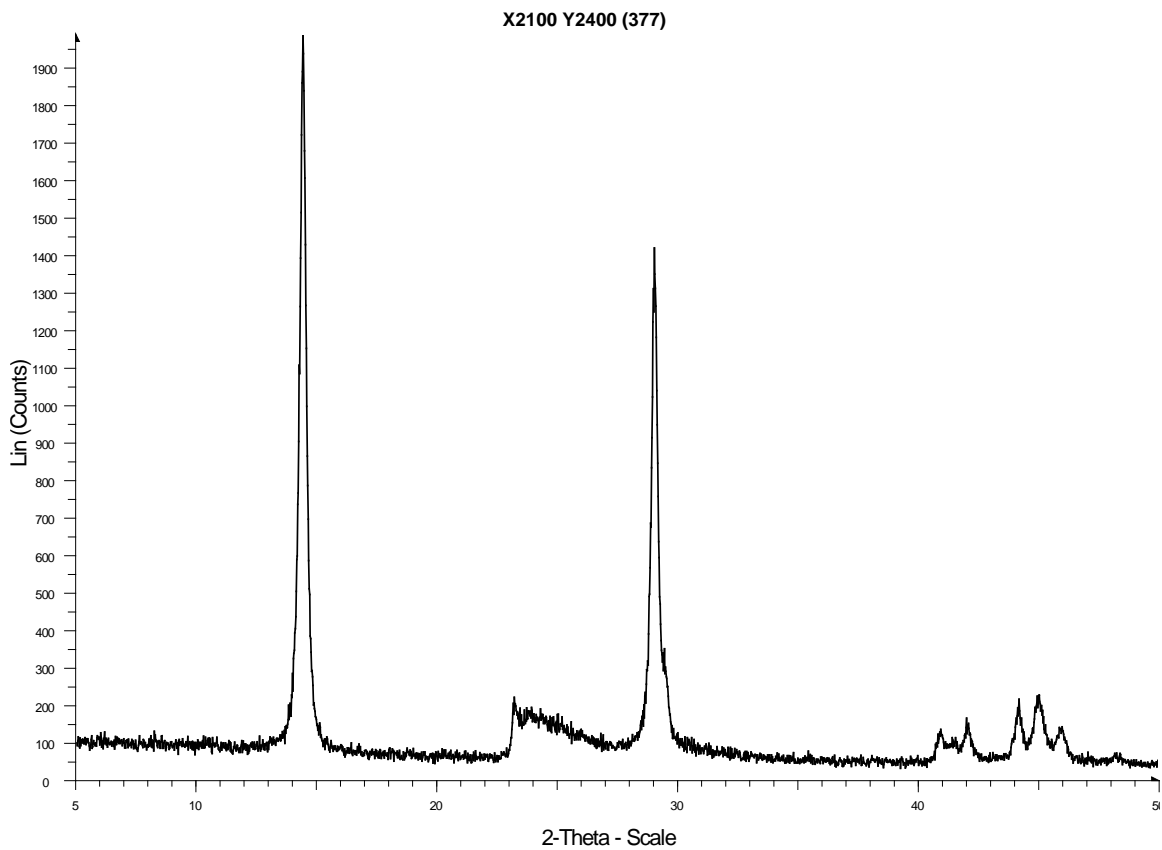


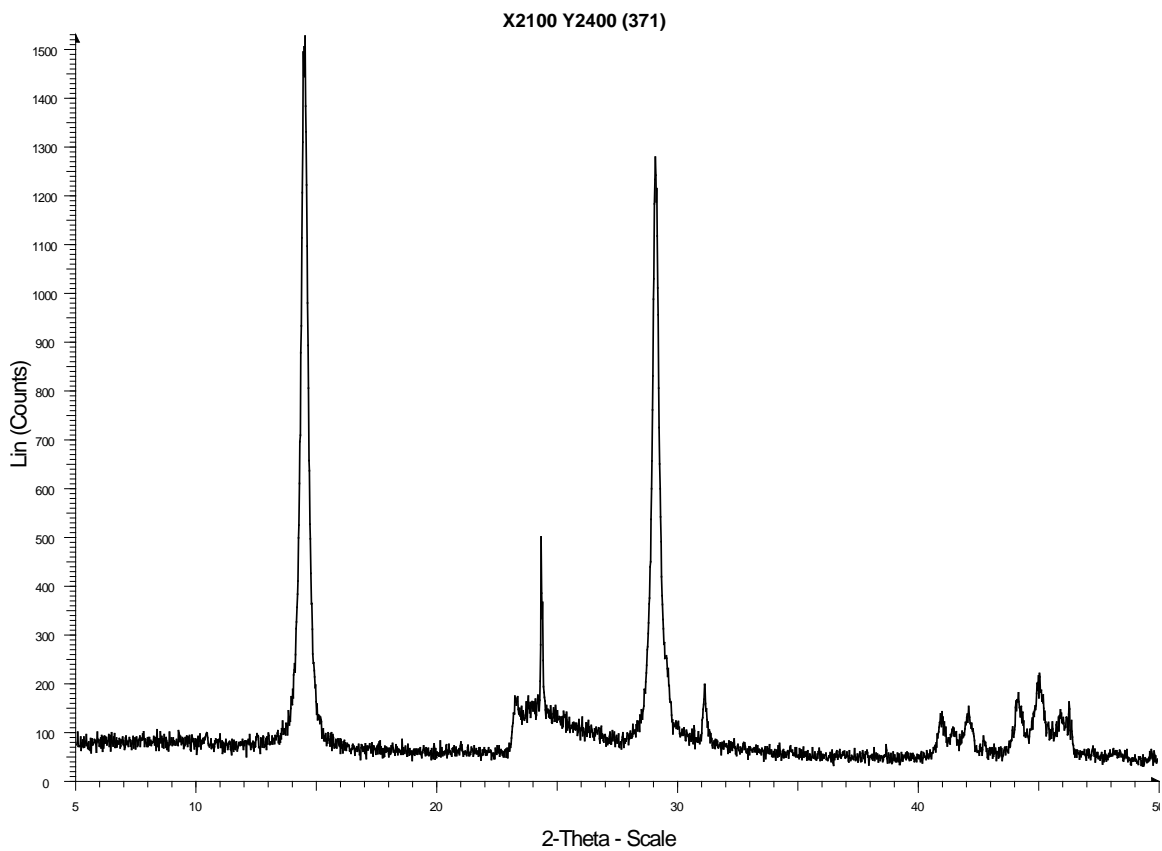
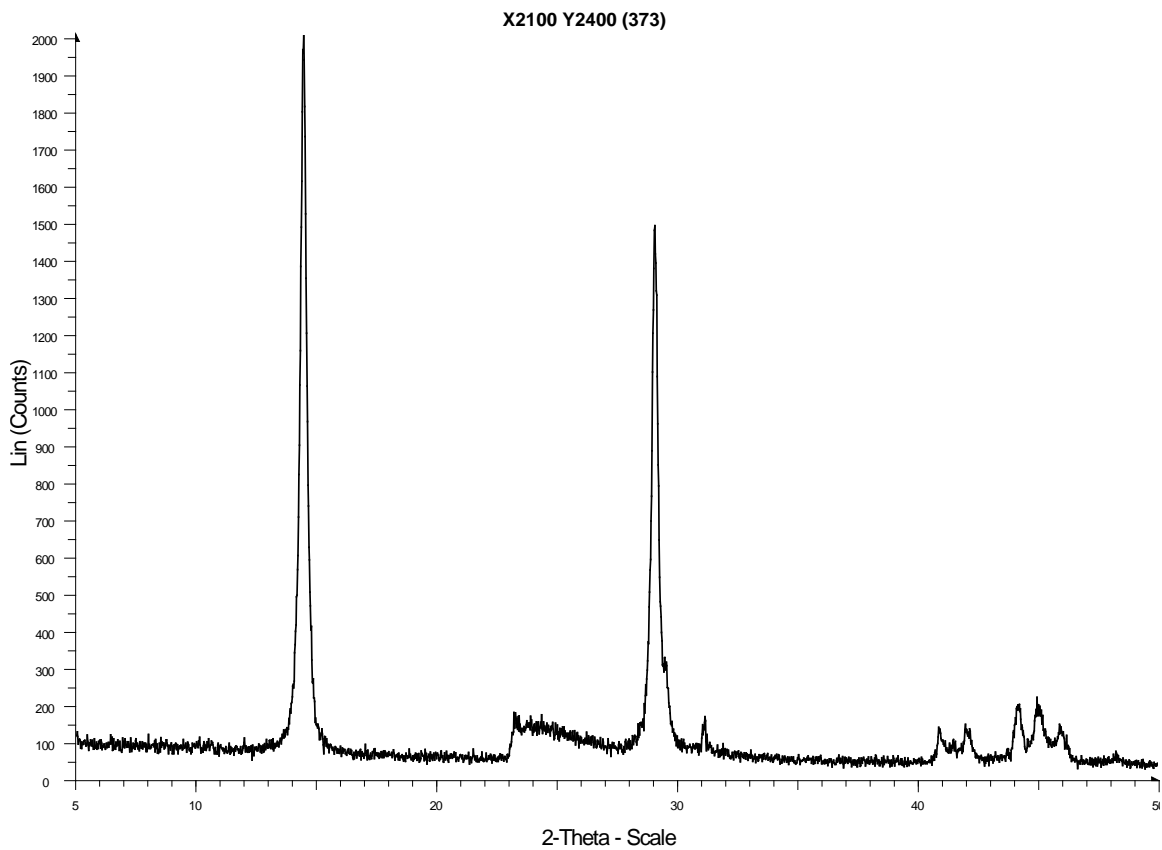
X2100 Y2400 (387)

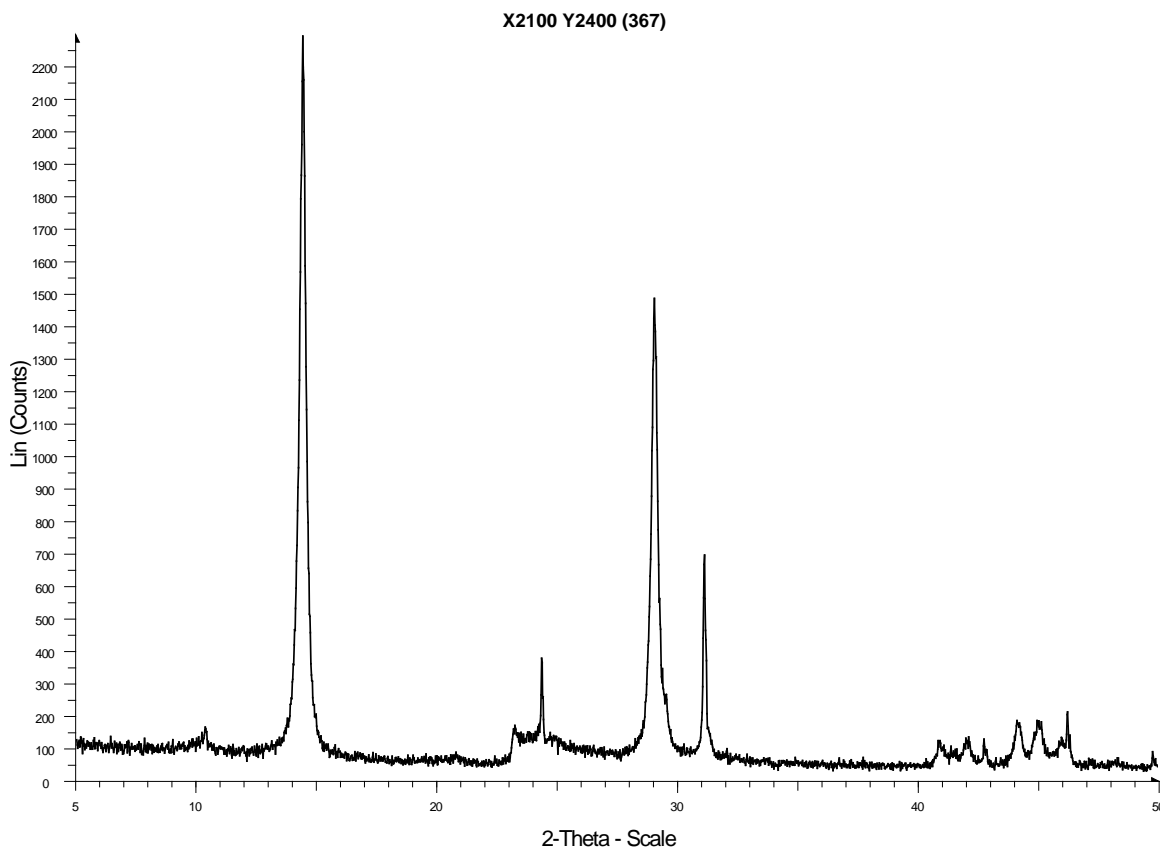
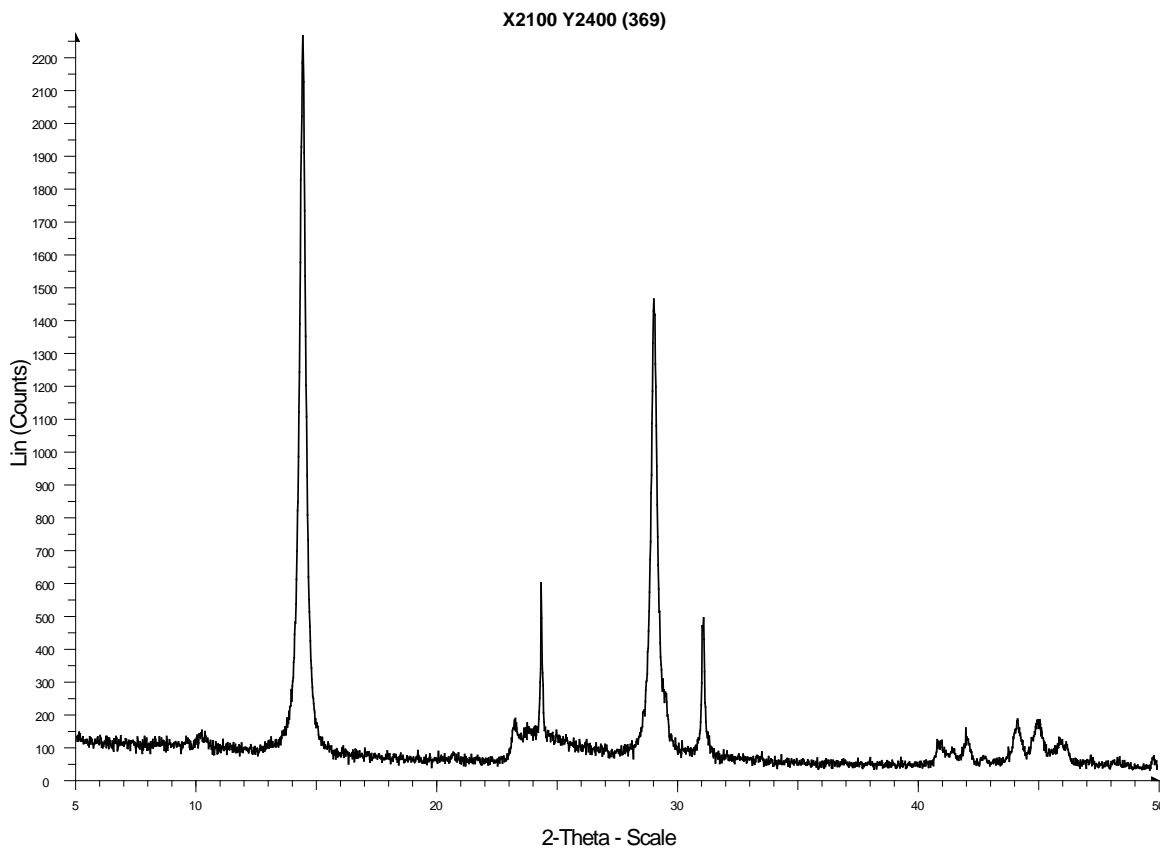


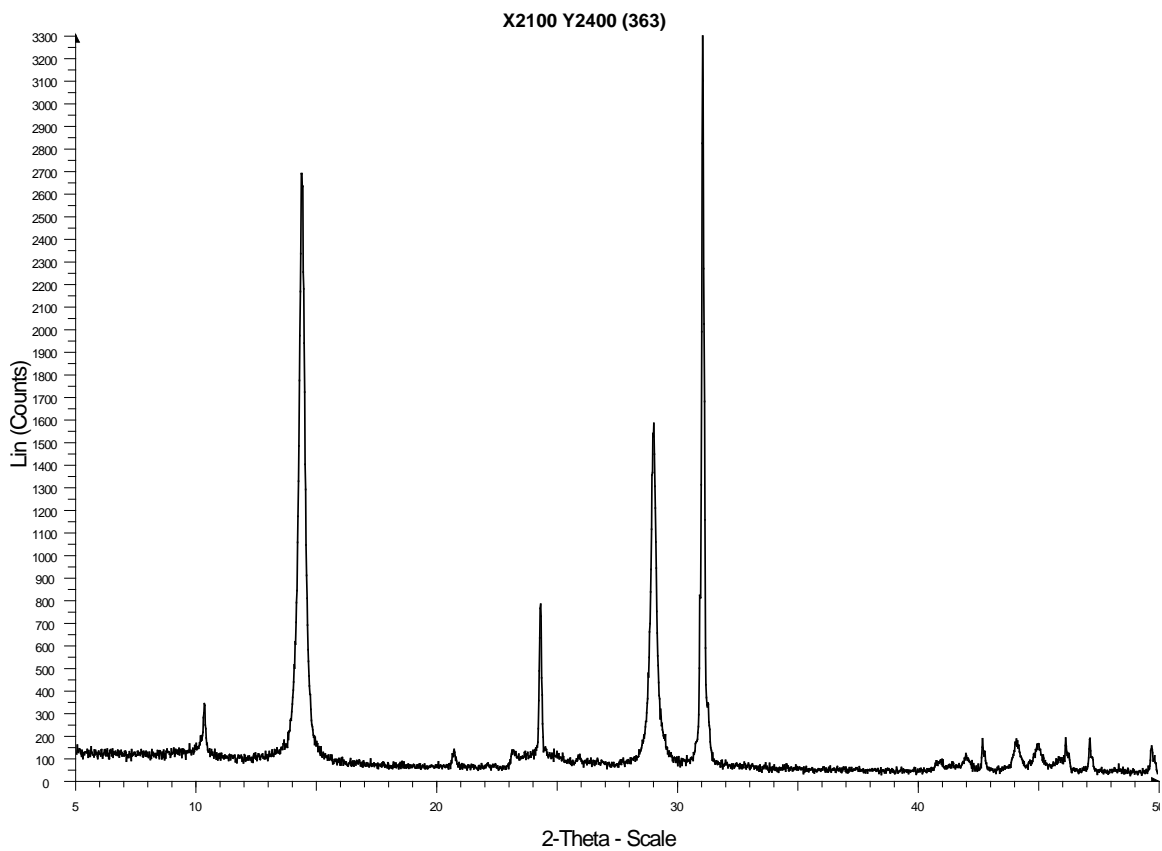
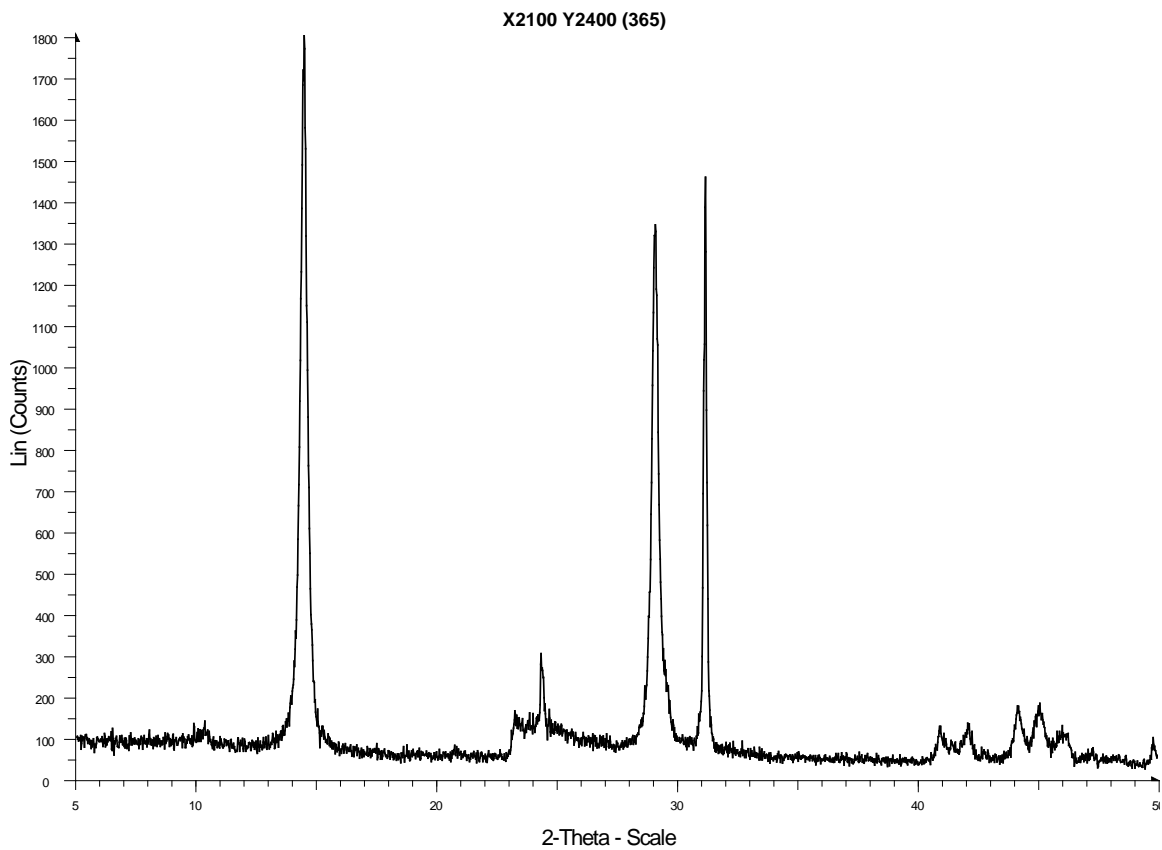


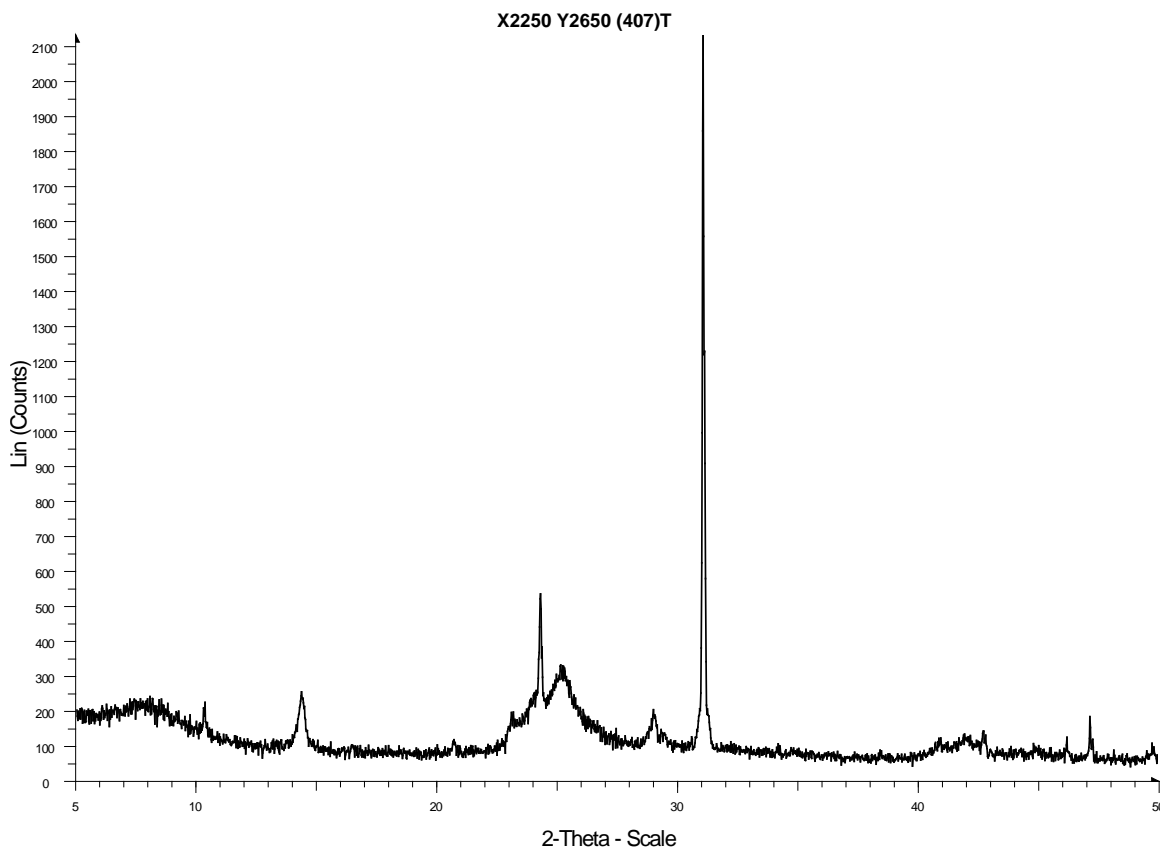
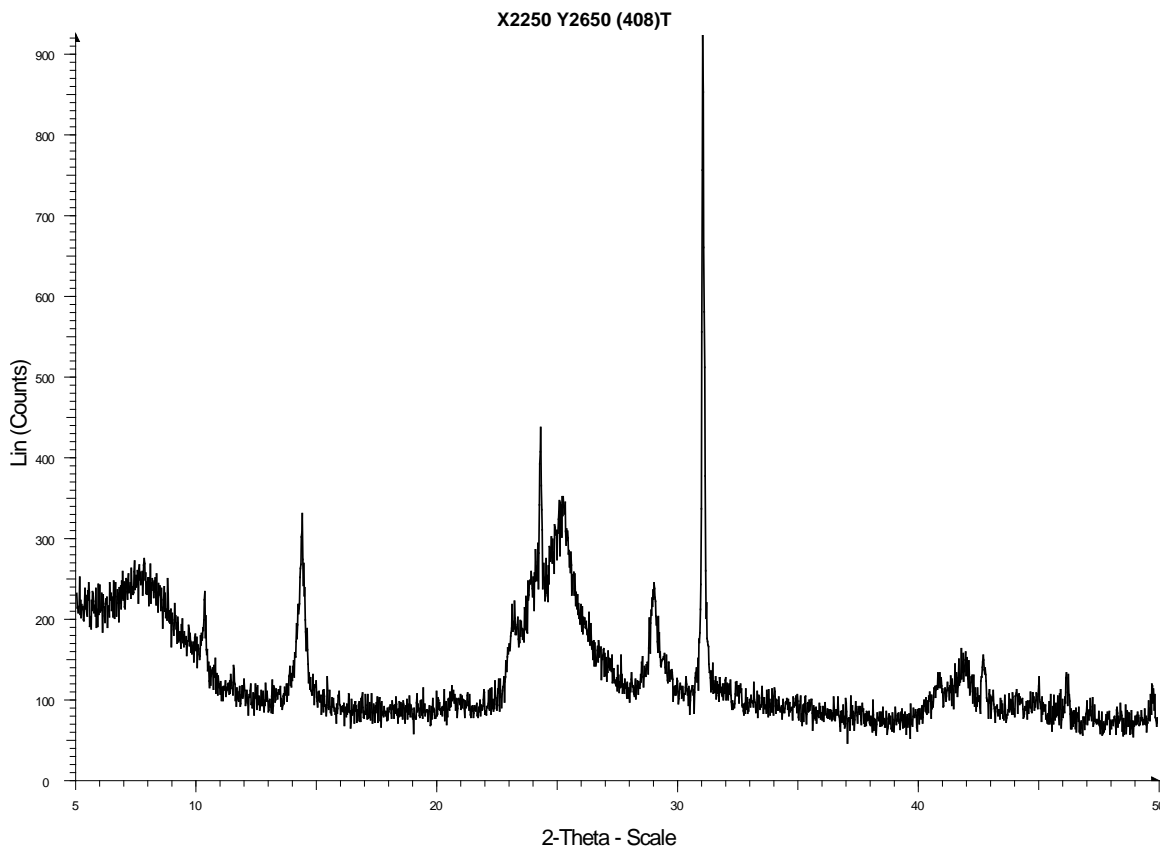


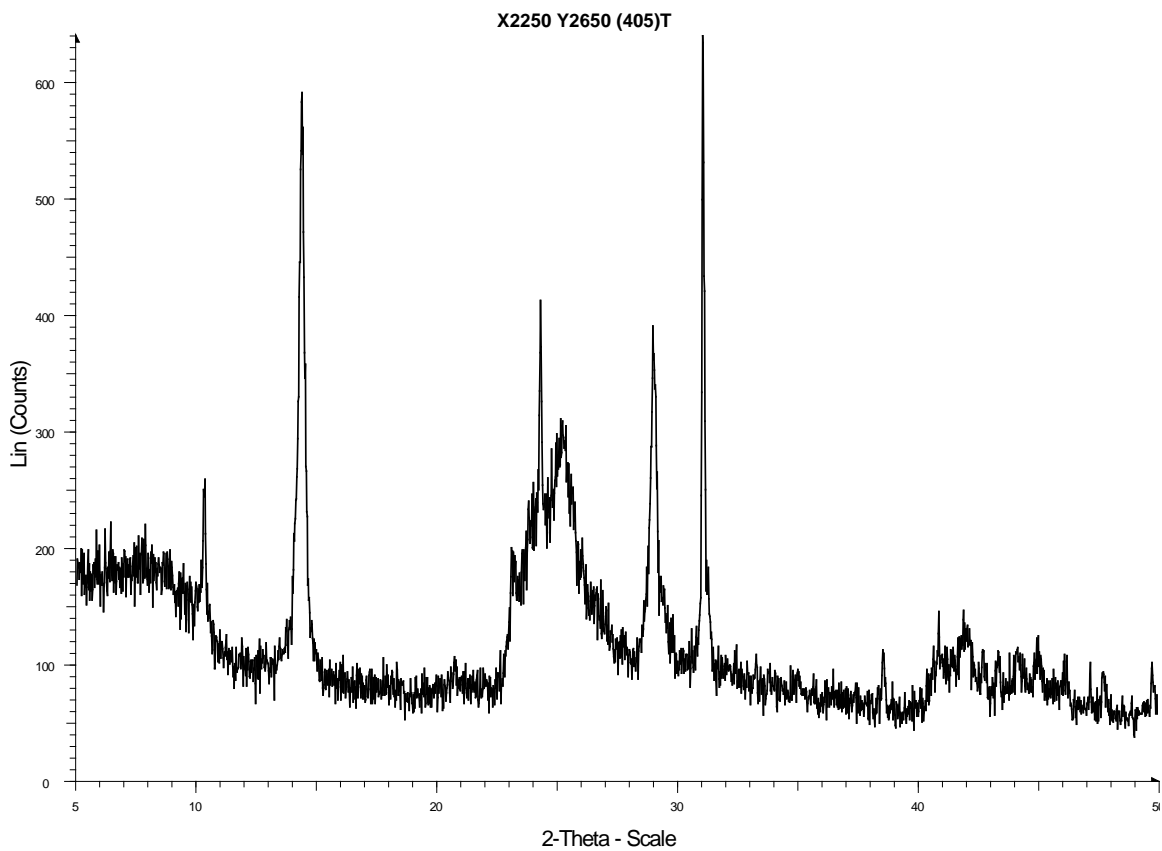
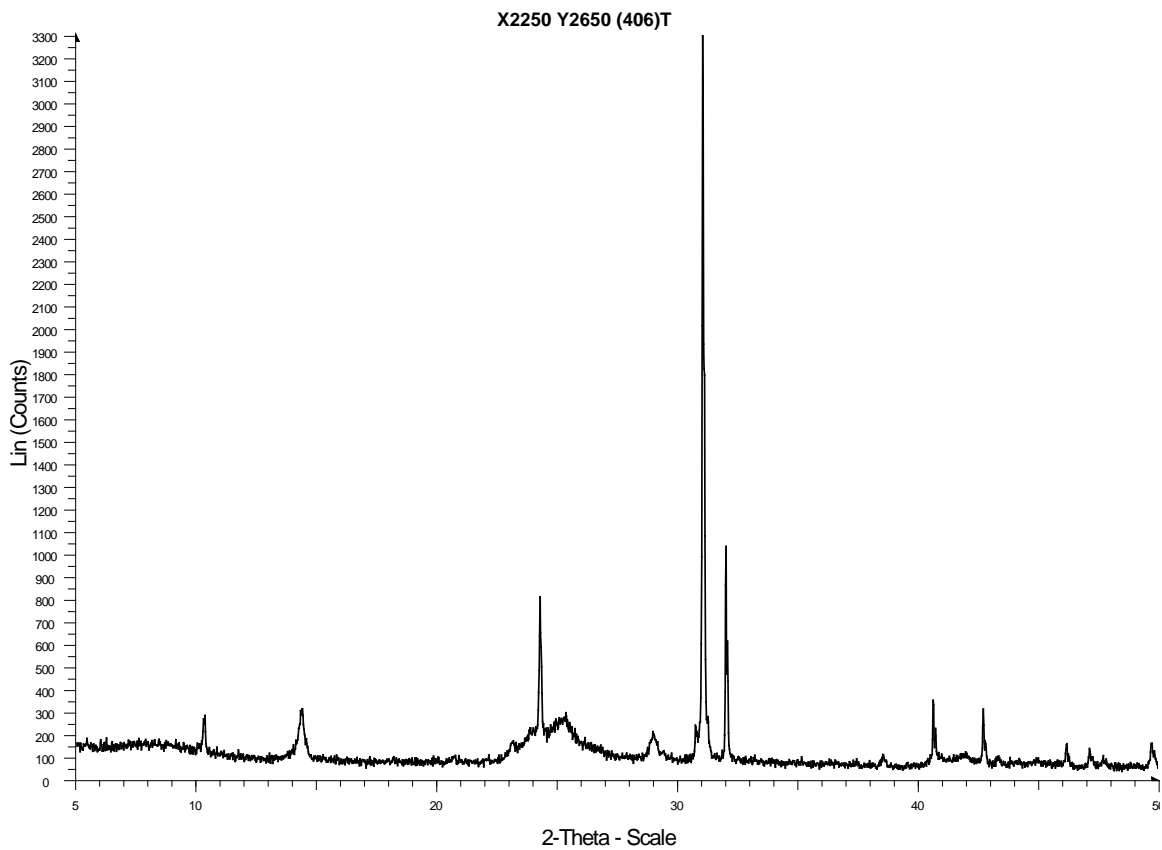


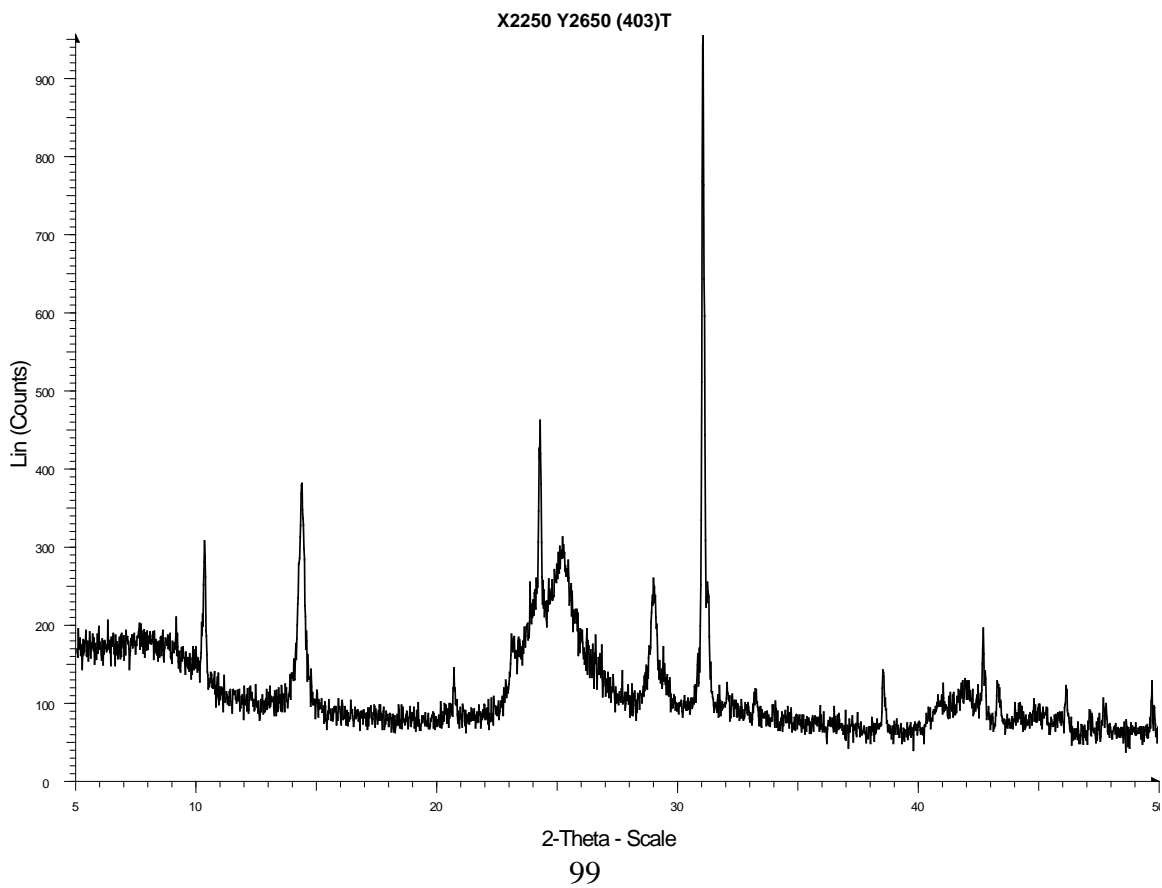
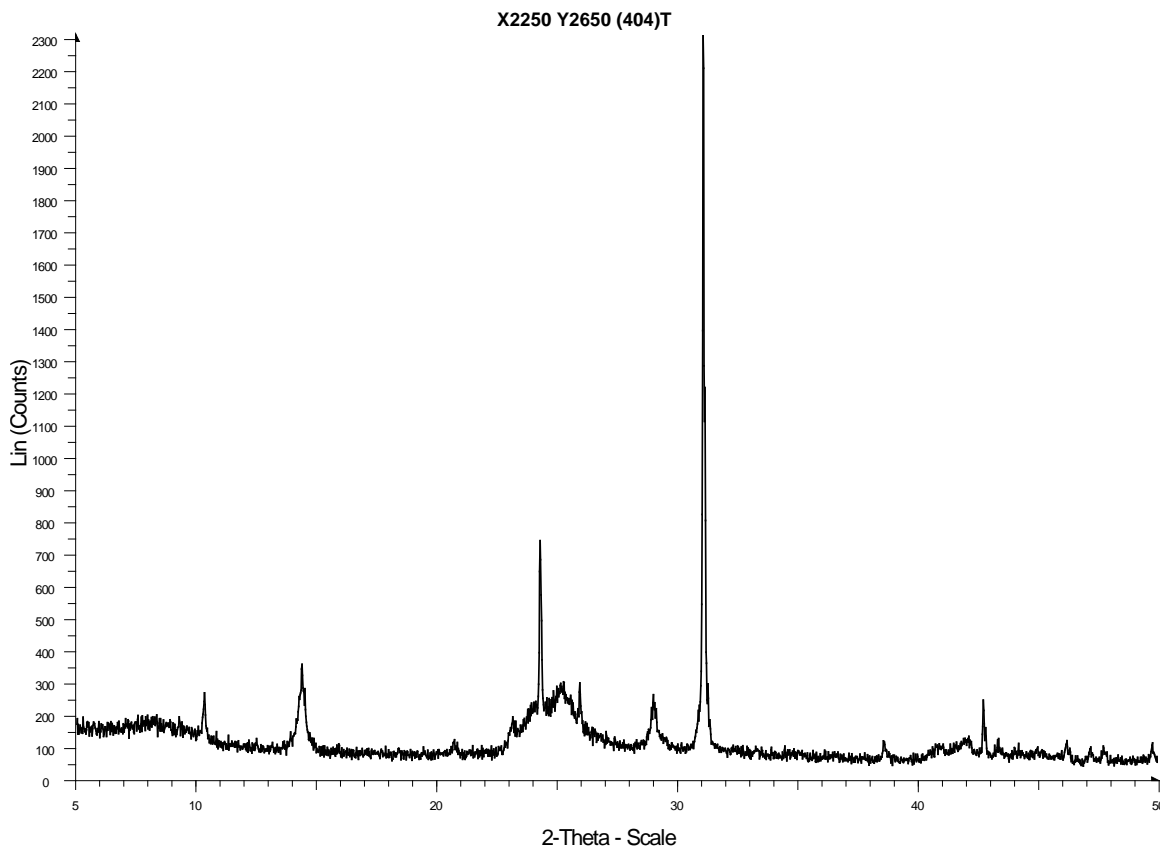


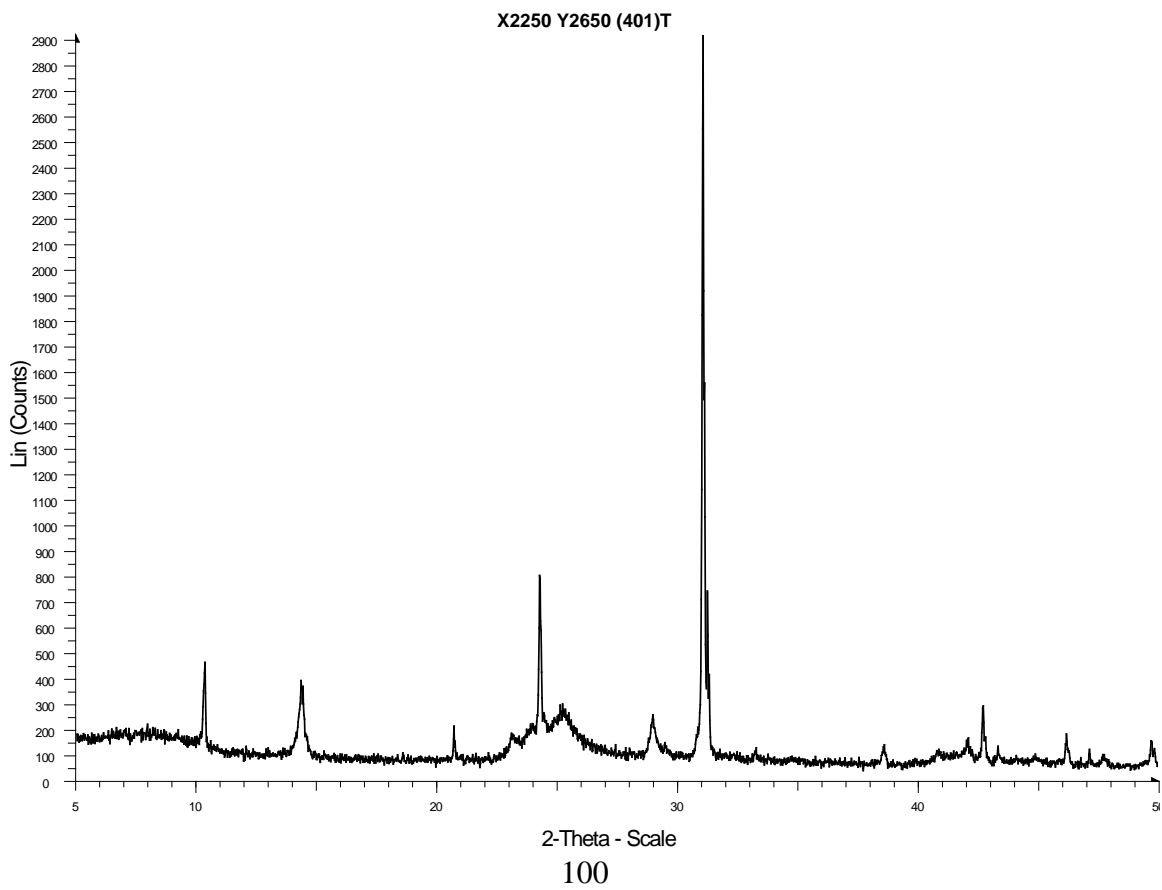
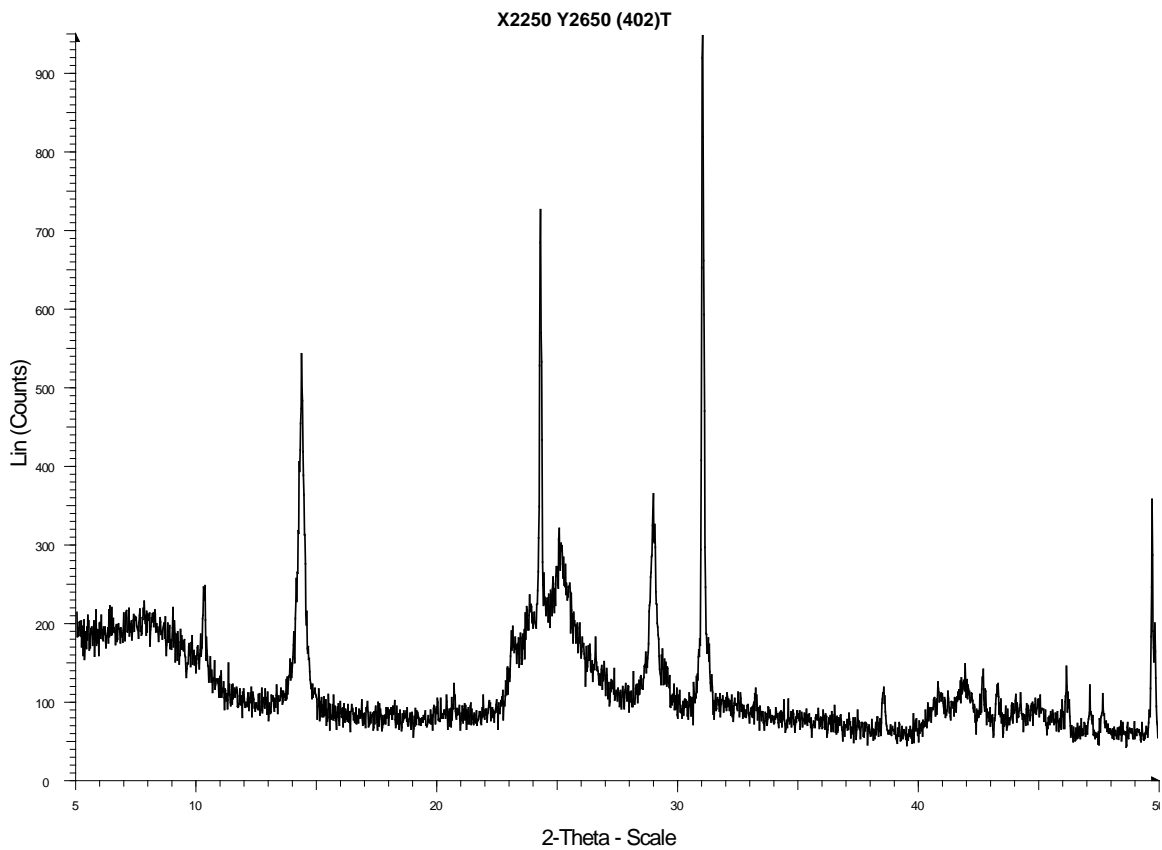


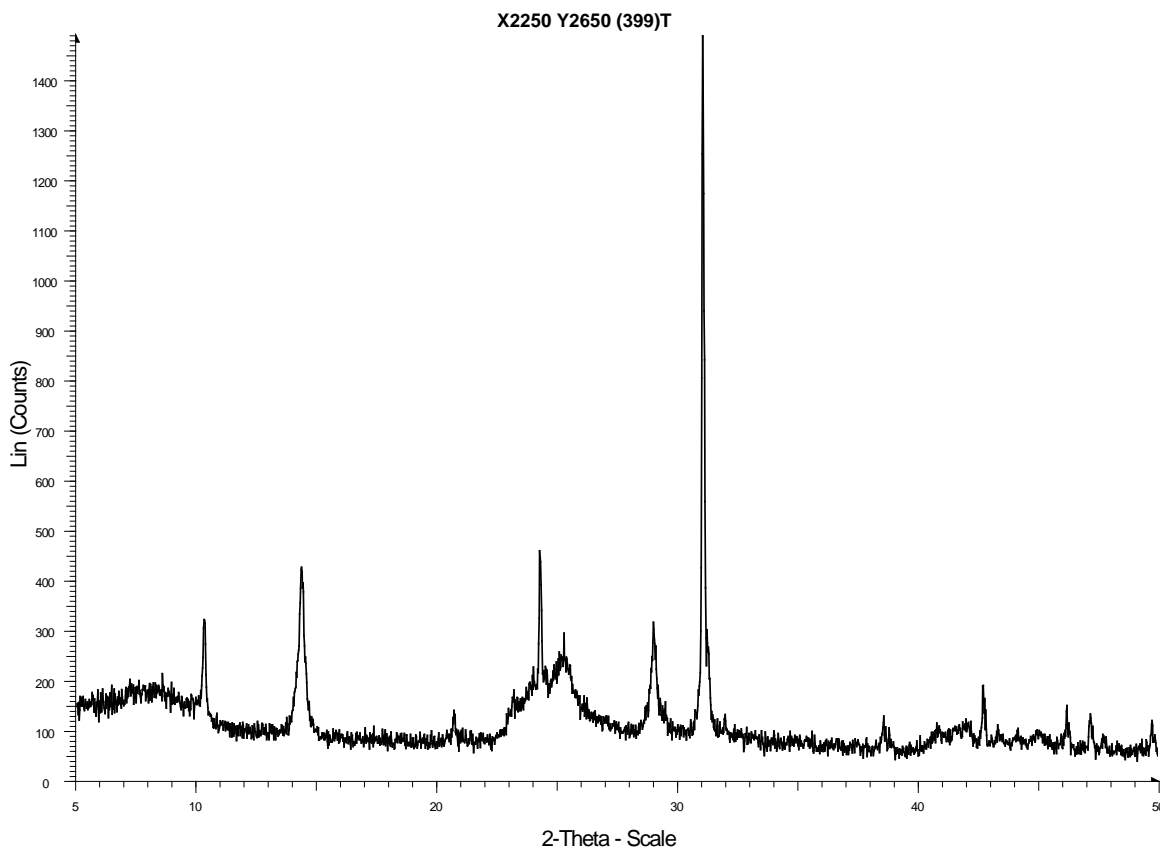
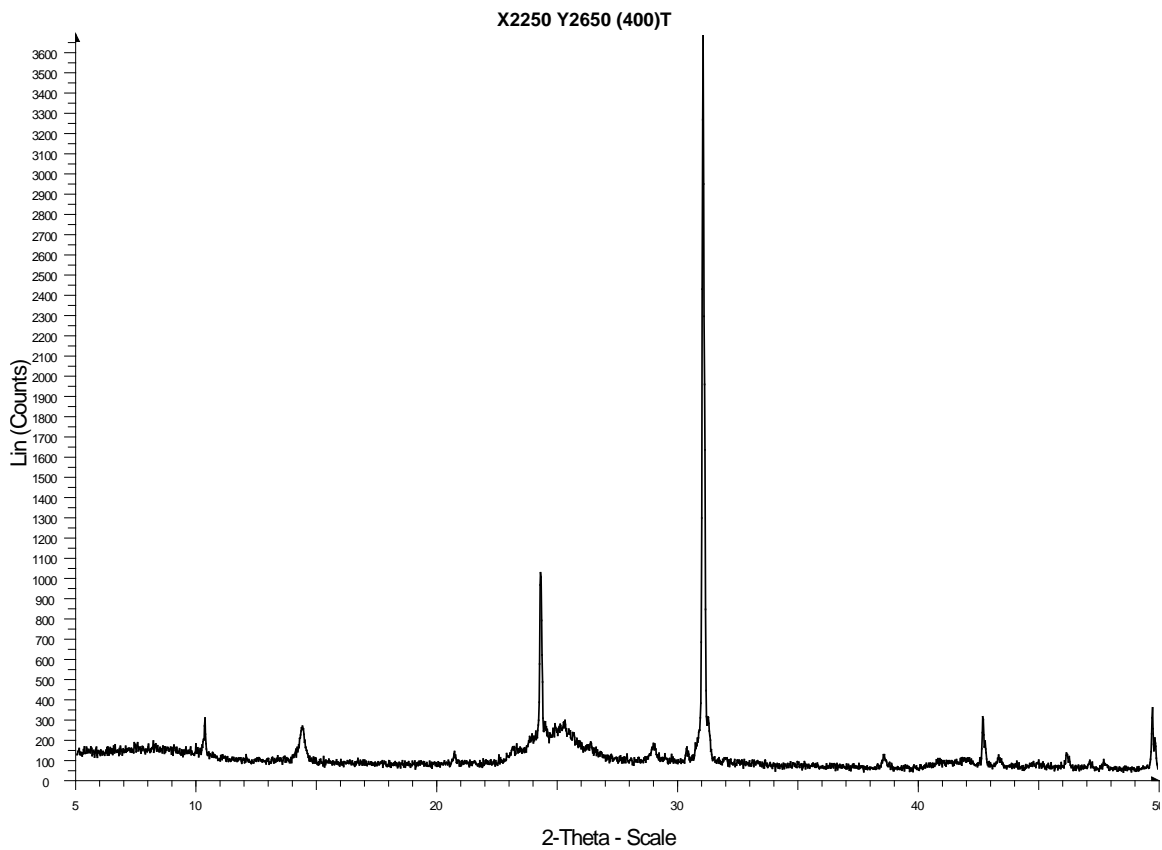




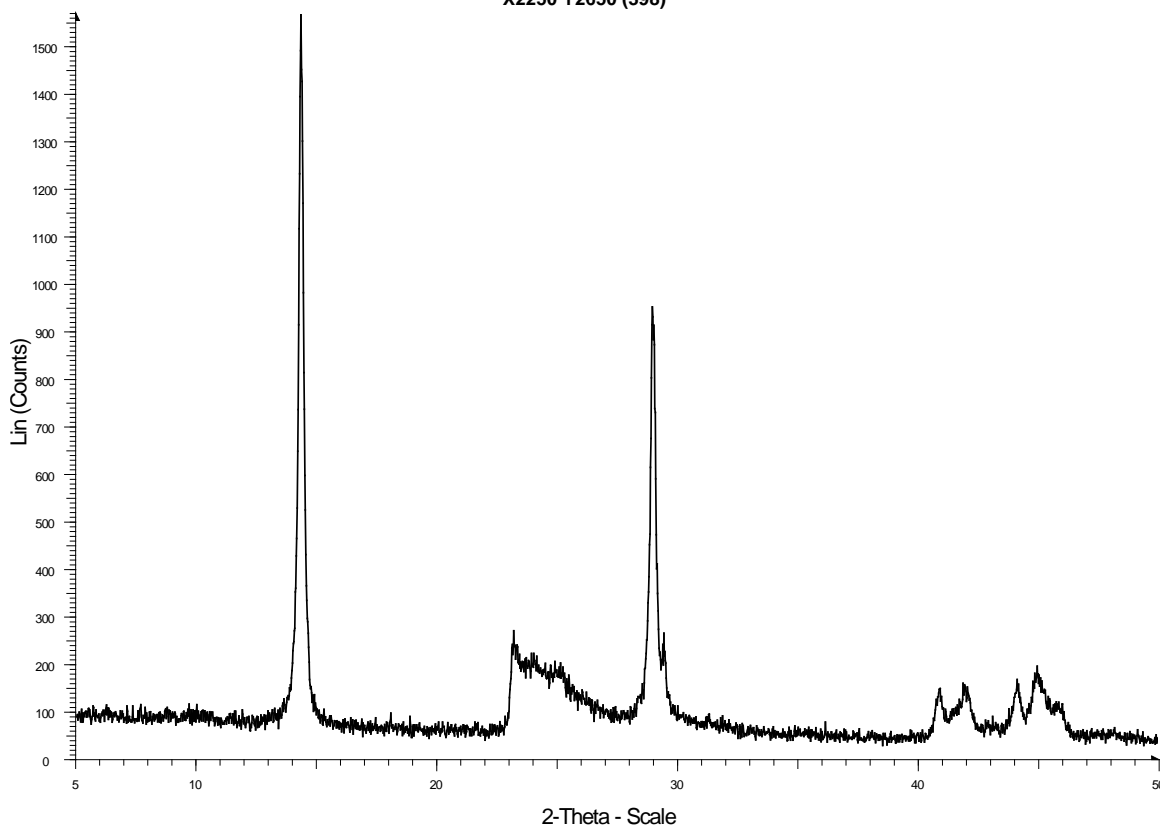




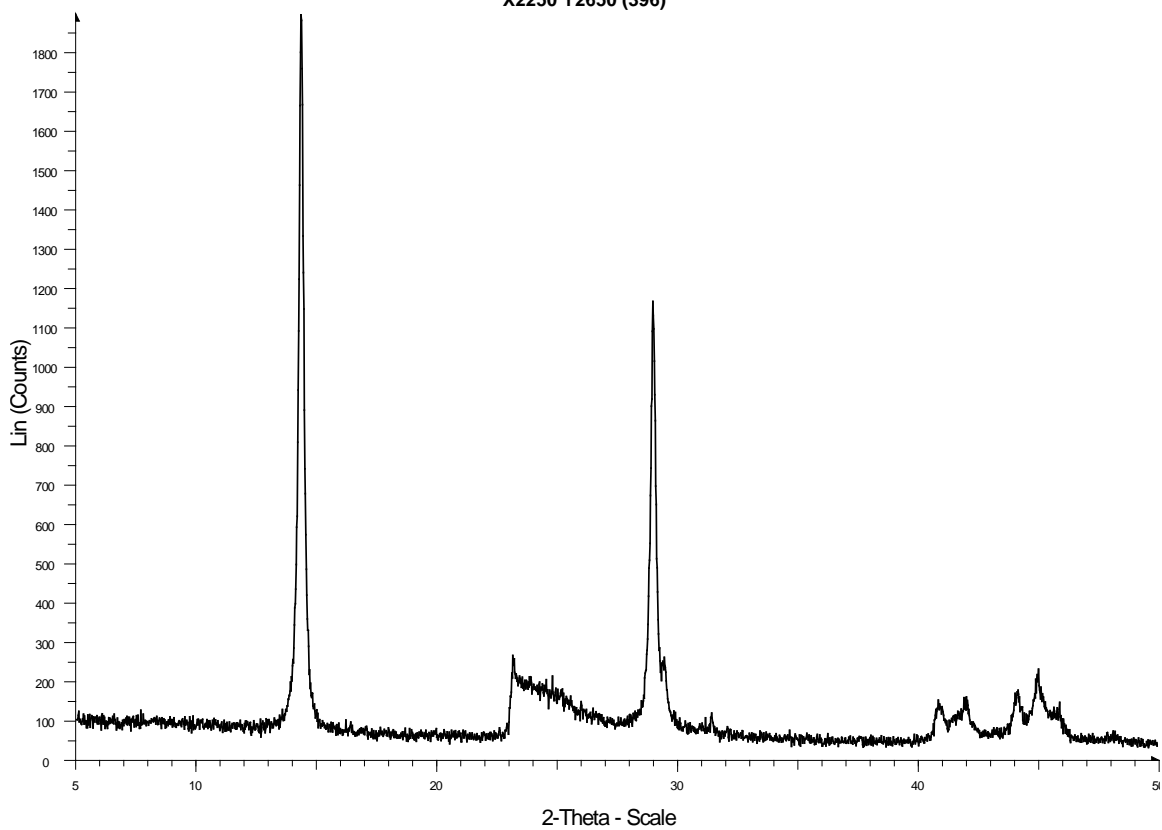


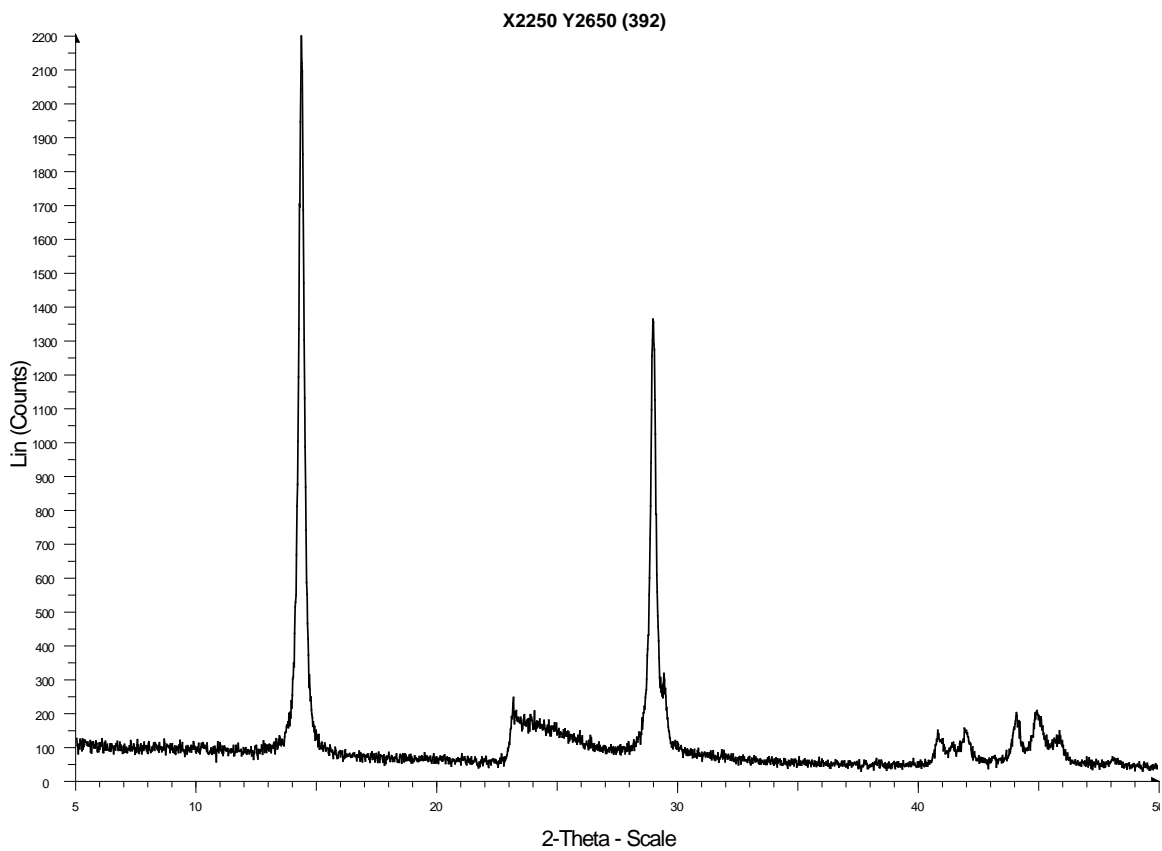
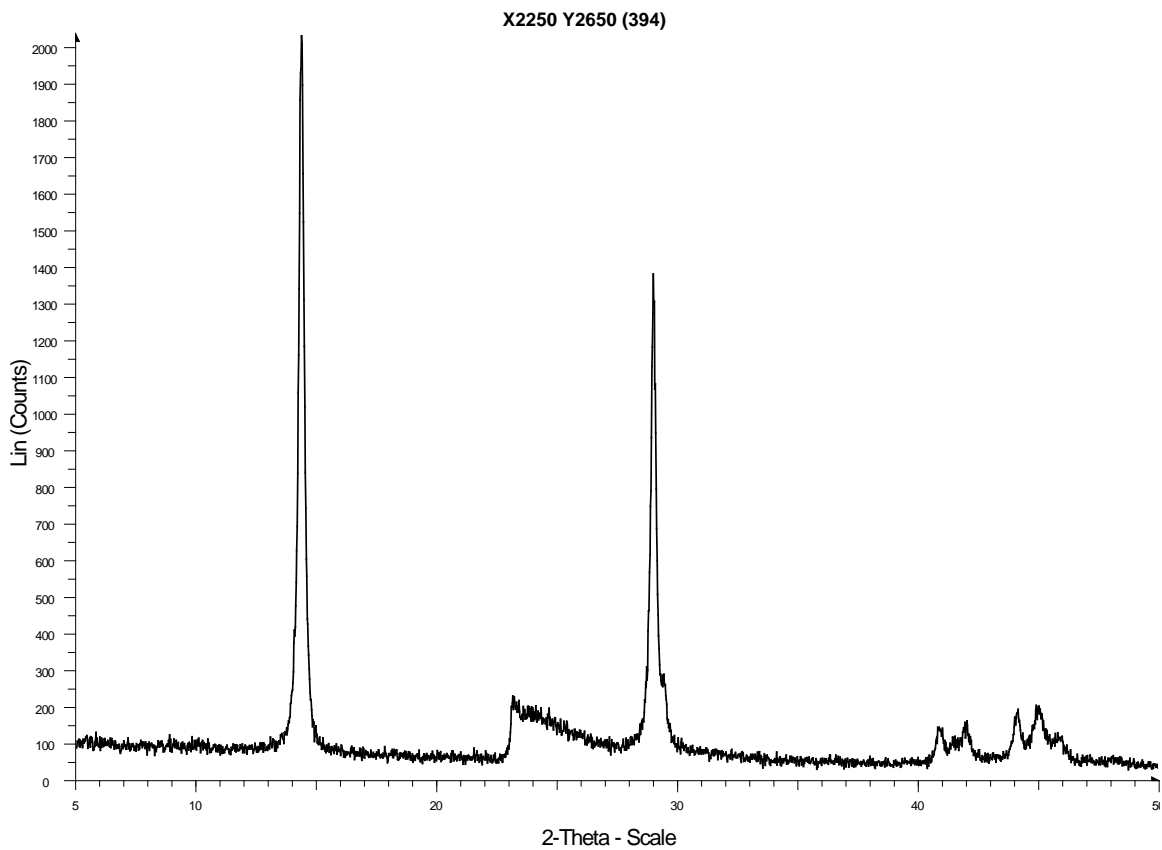


X2250 Y2650 (398)

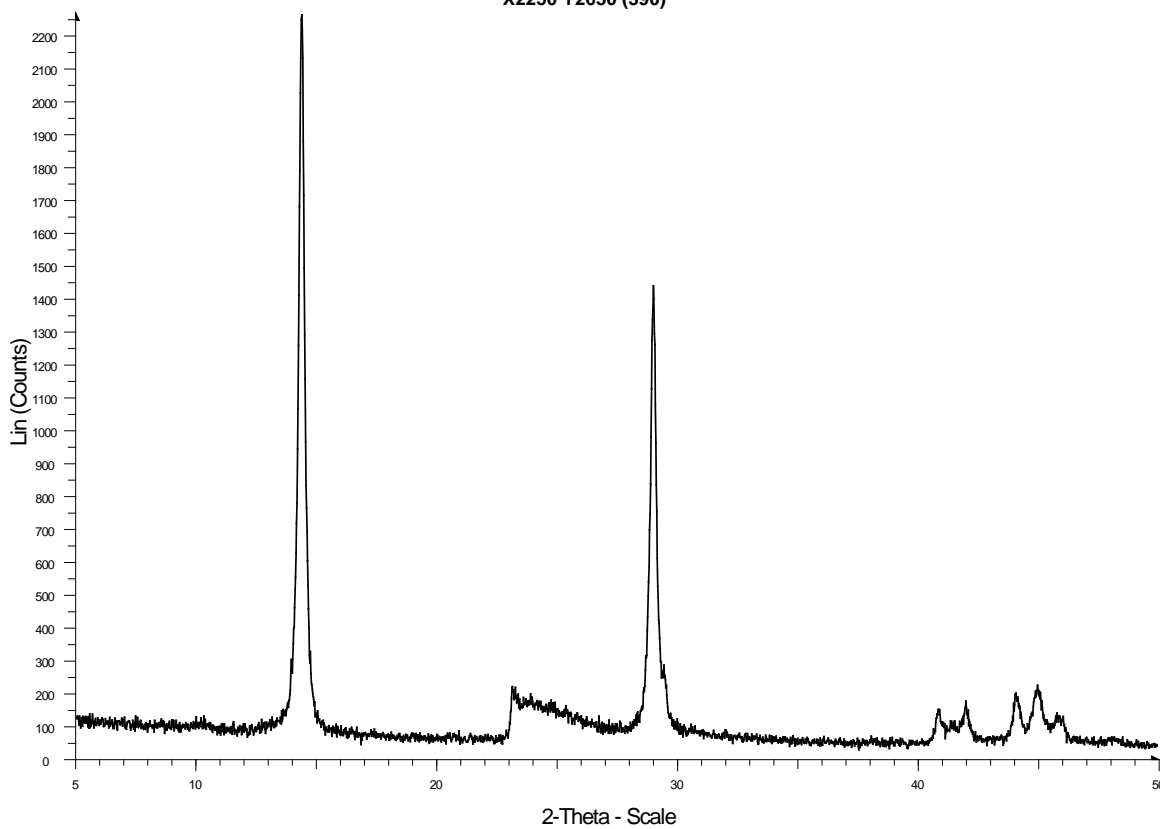


X2250 Y2650 (396)

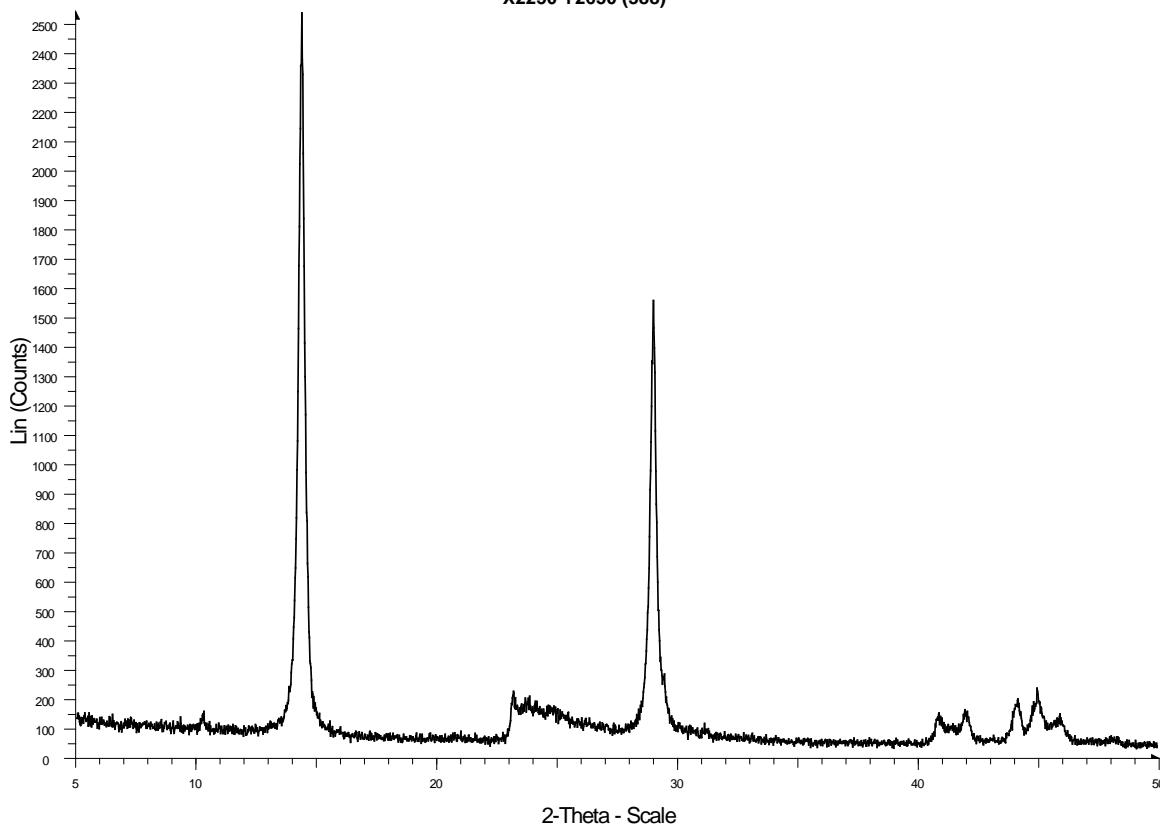


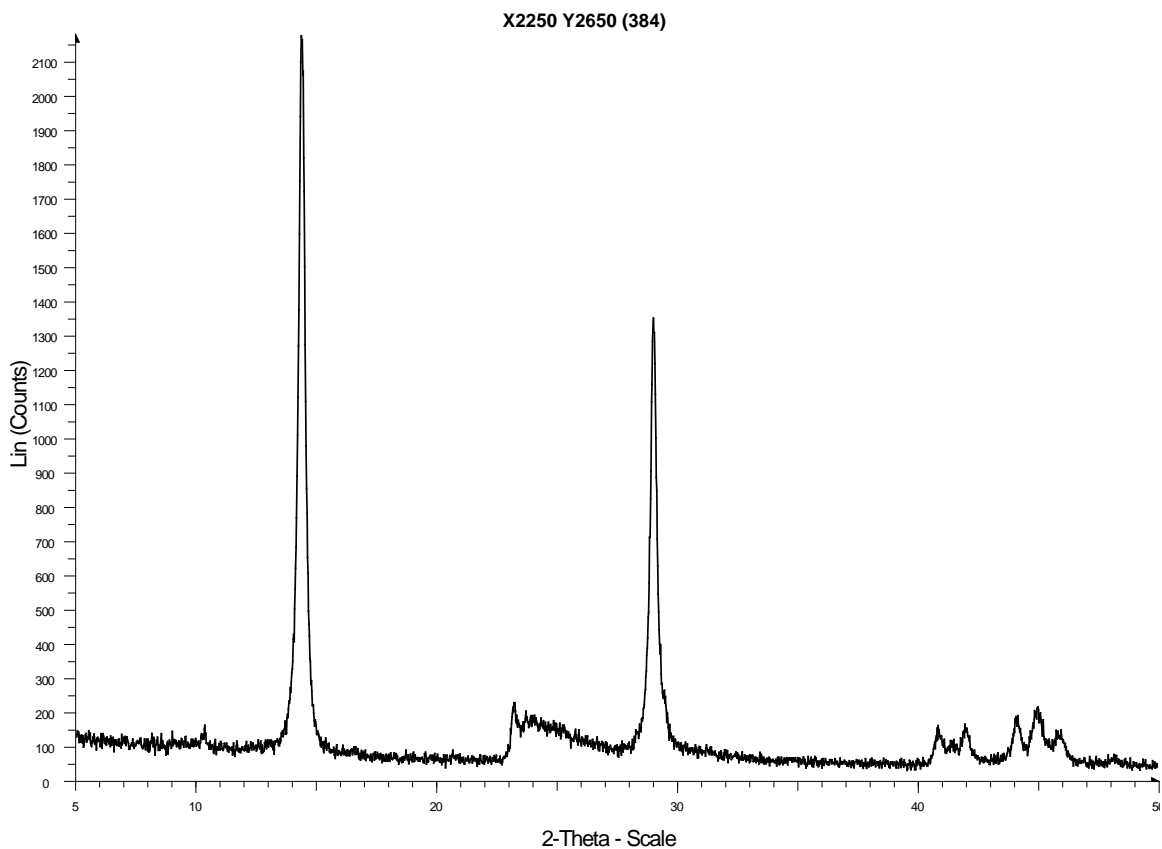
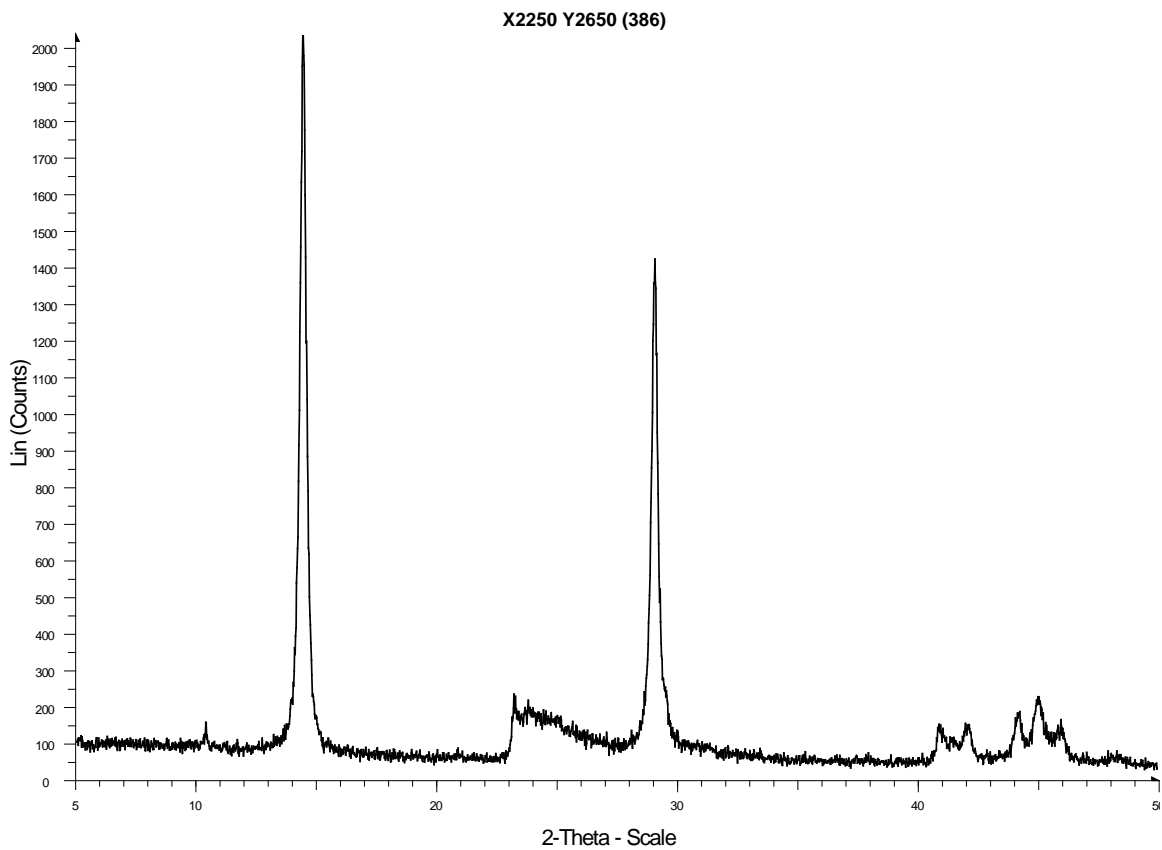


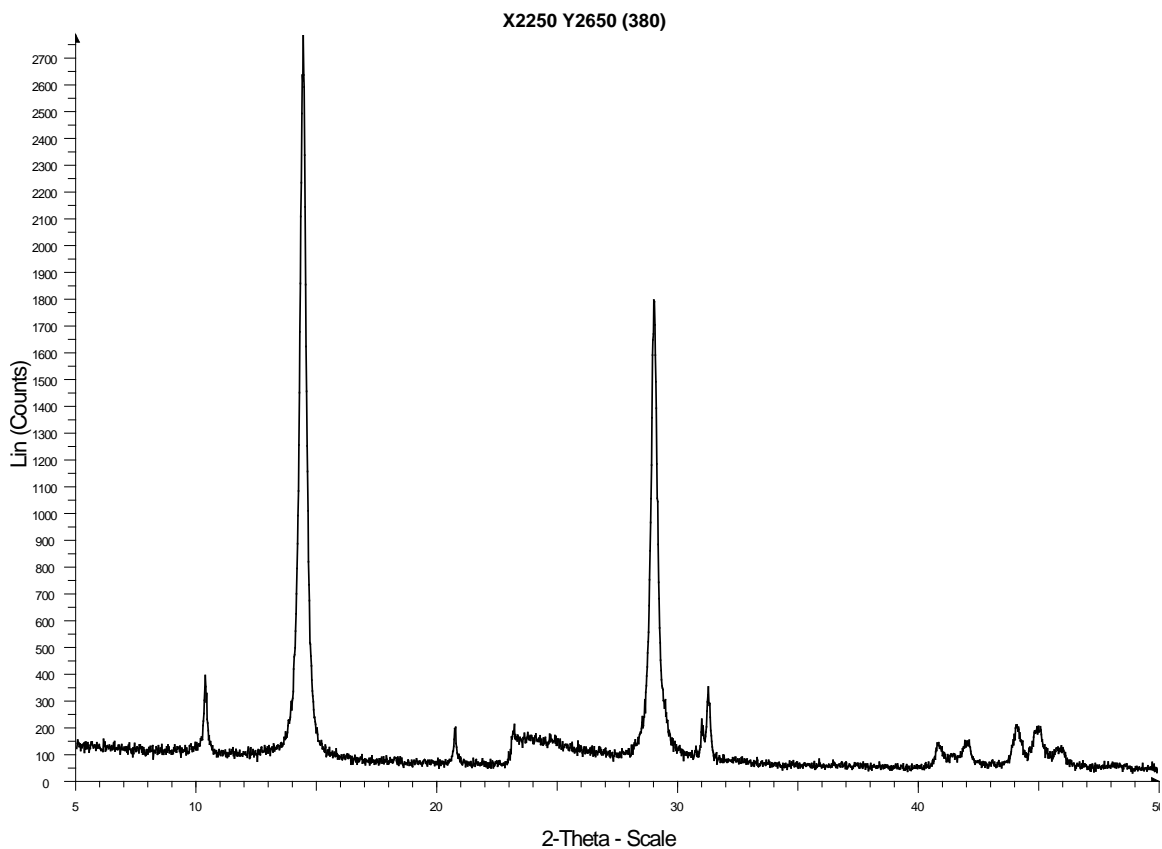
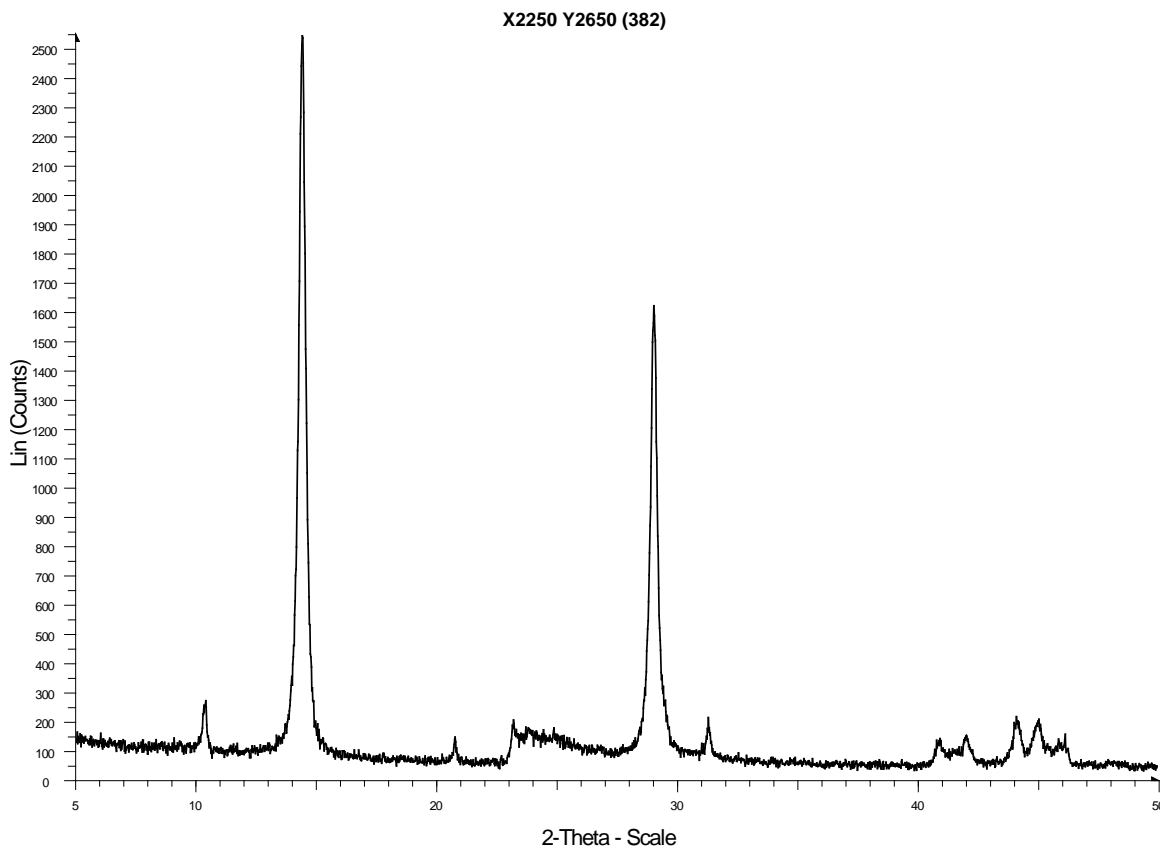
X2250 Y2650 (390)

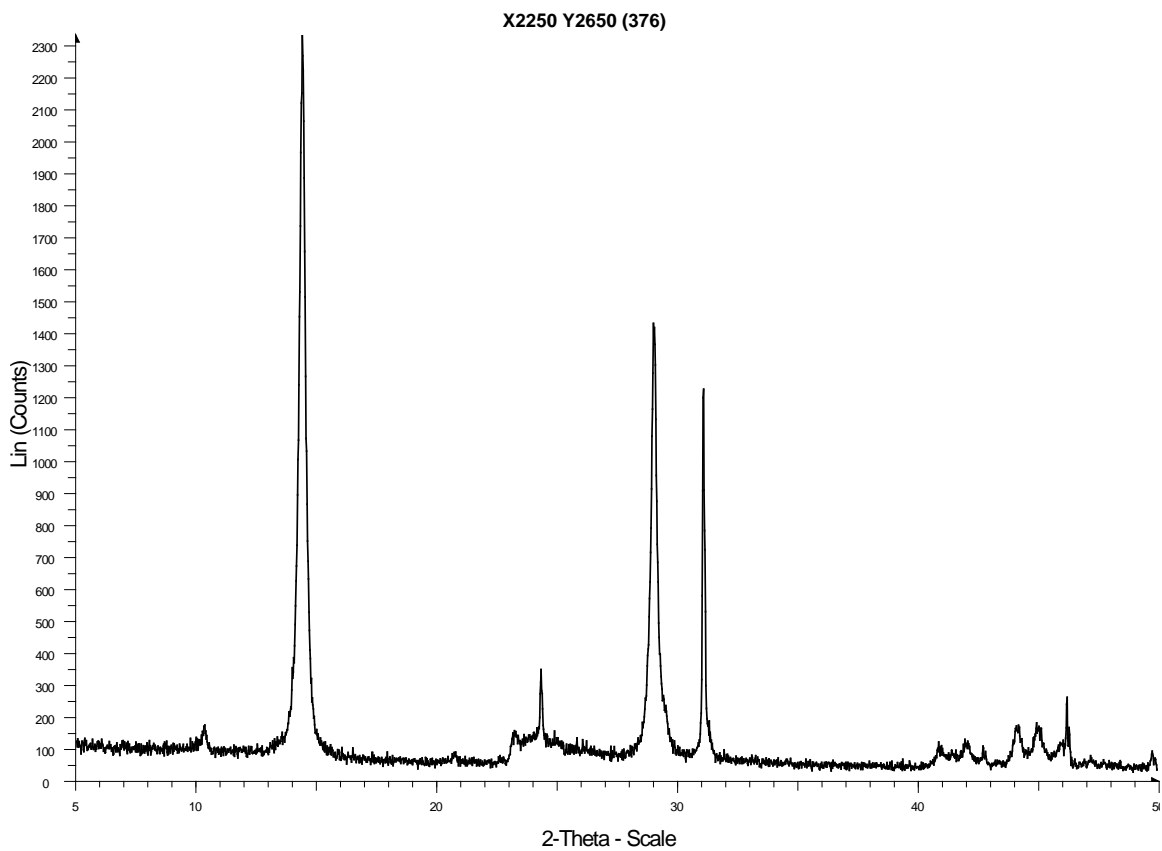
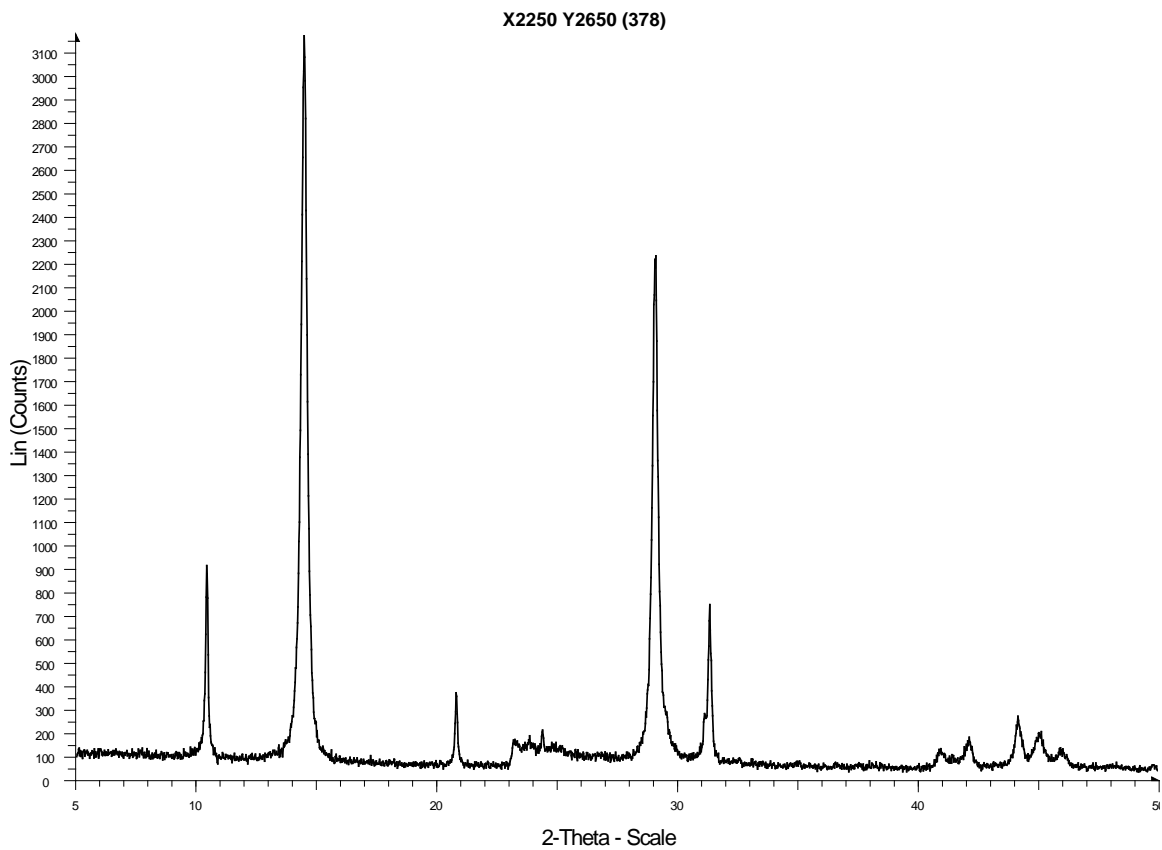


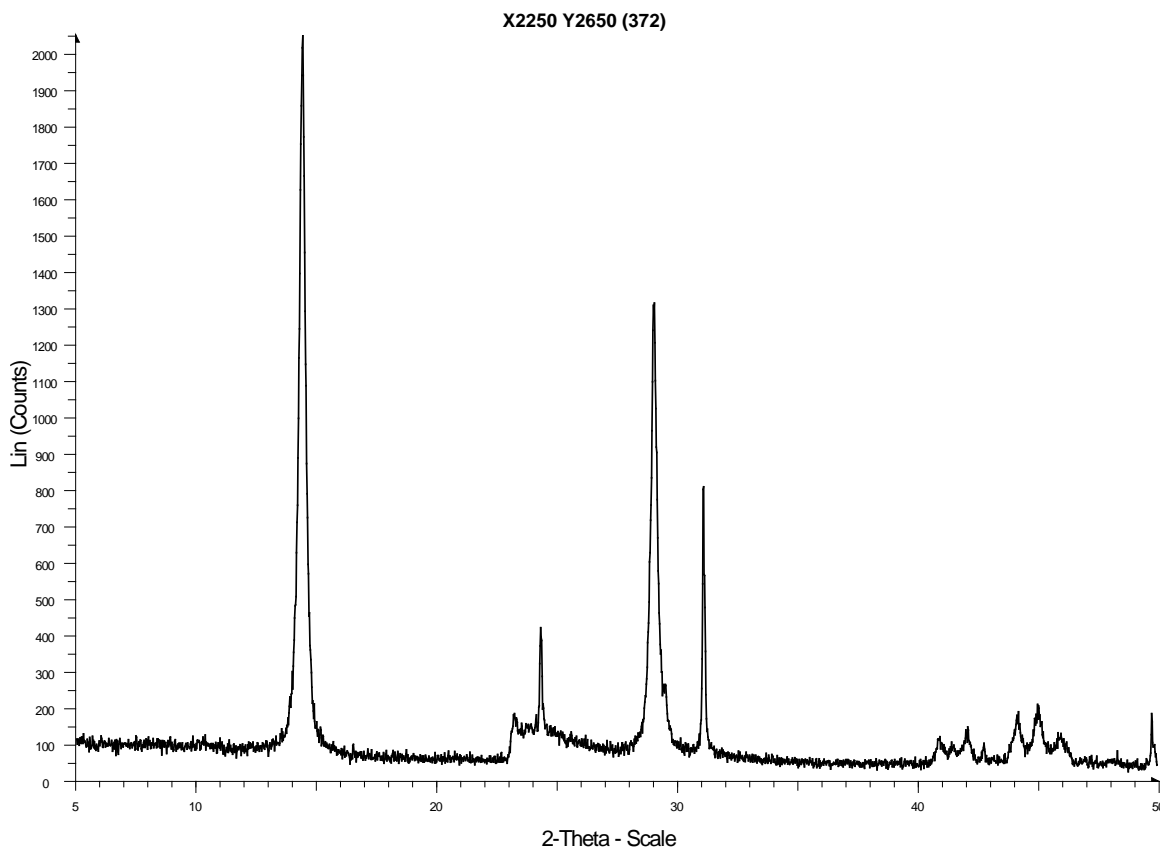
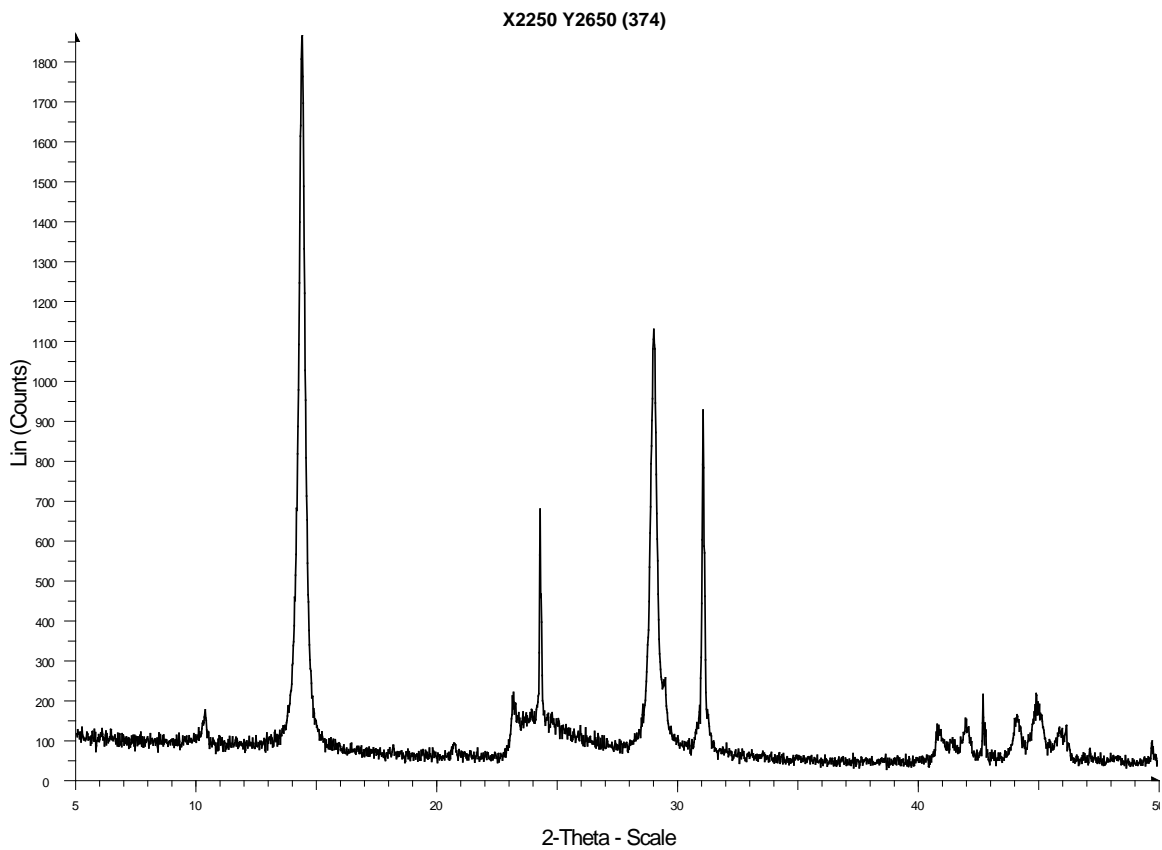
X2250 Y2650 (388)

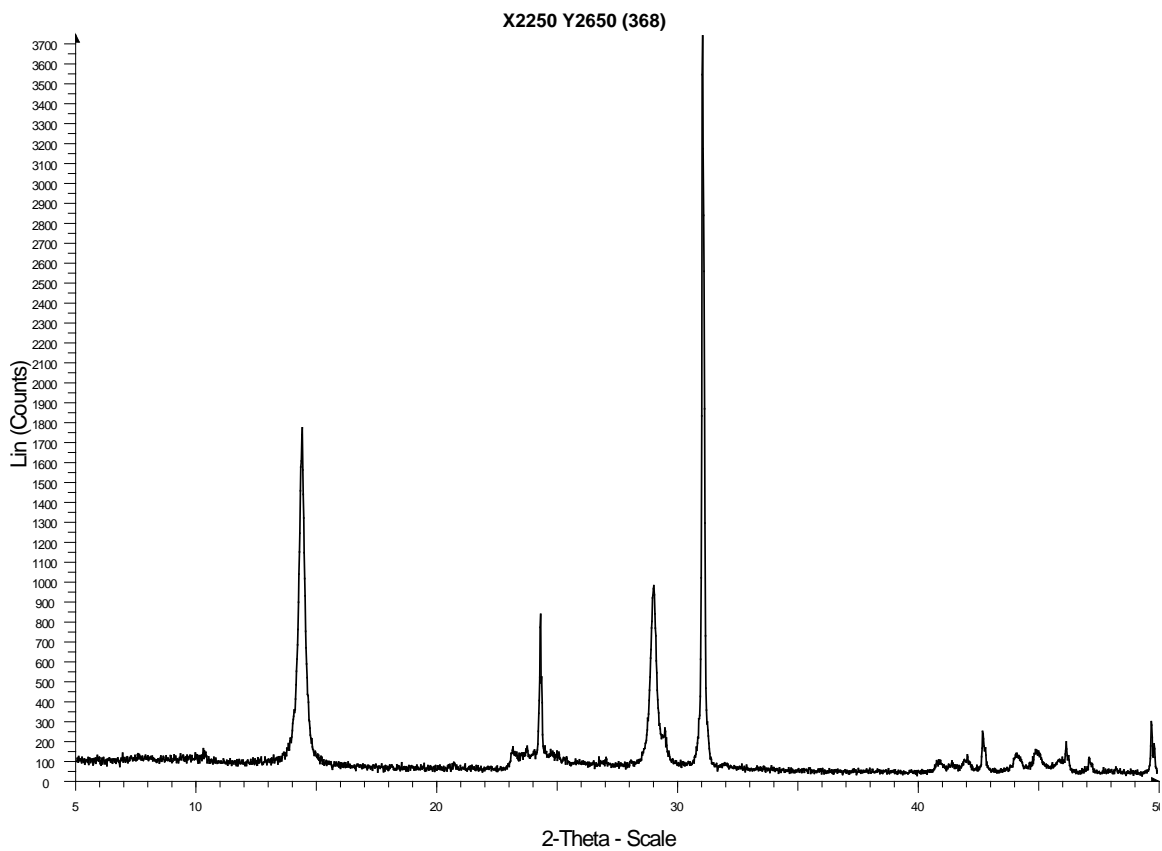
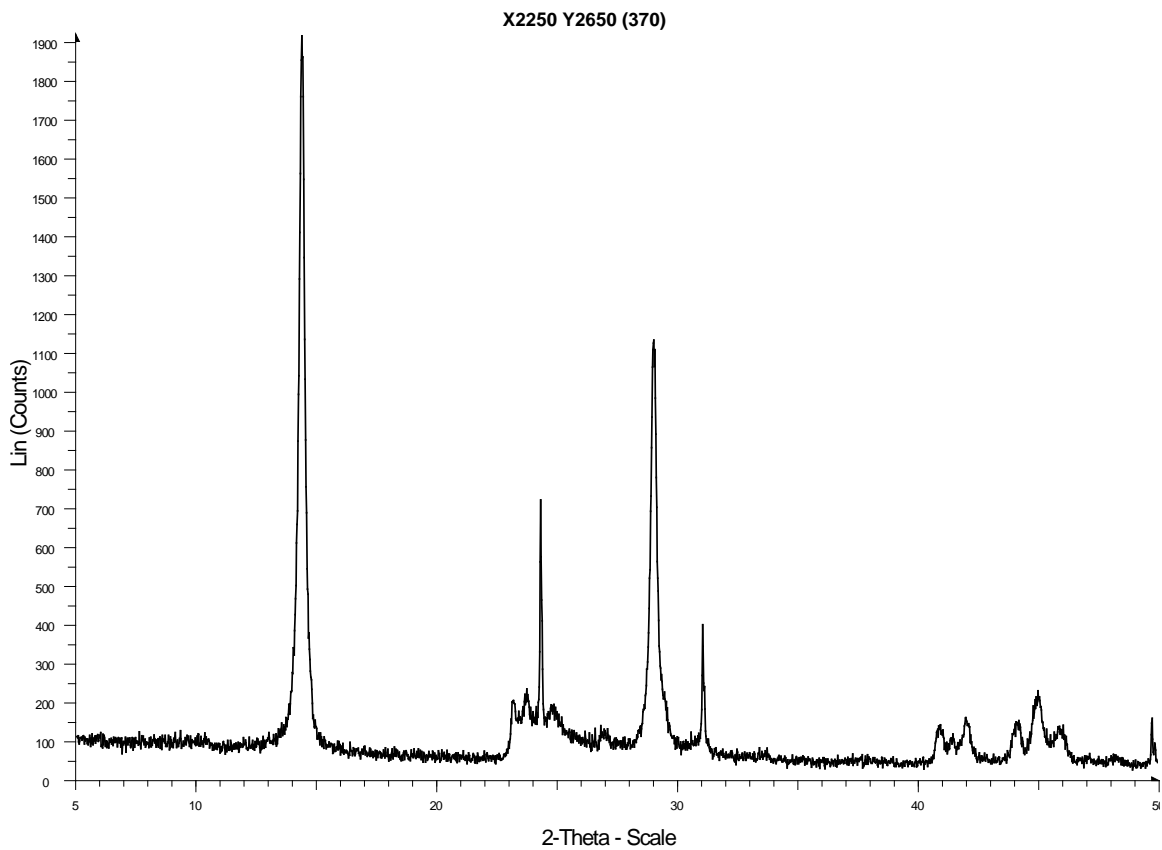


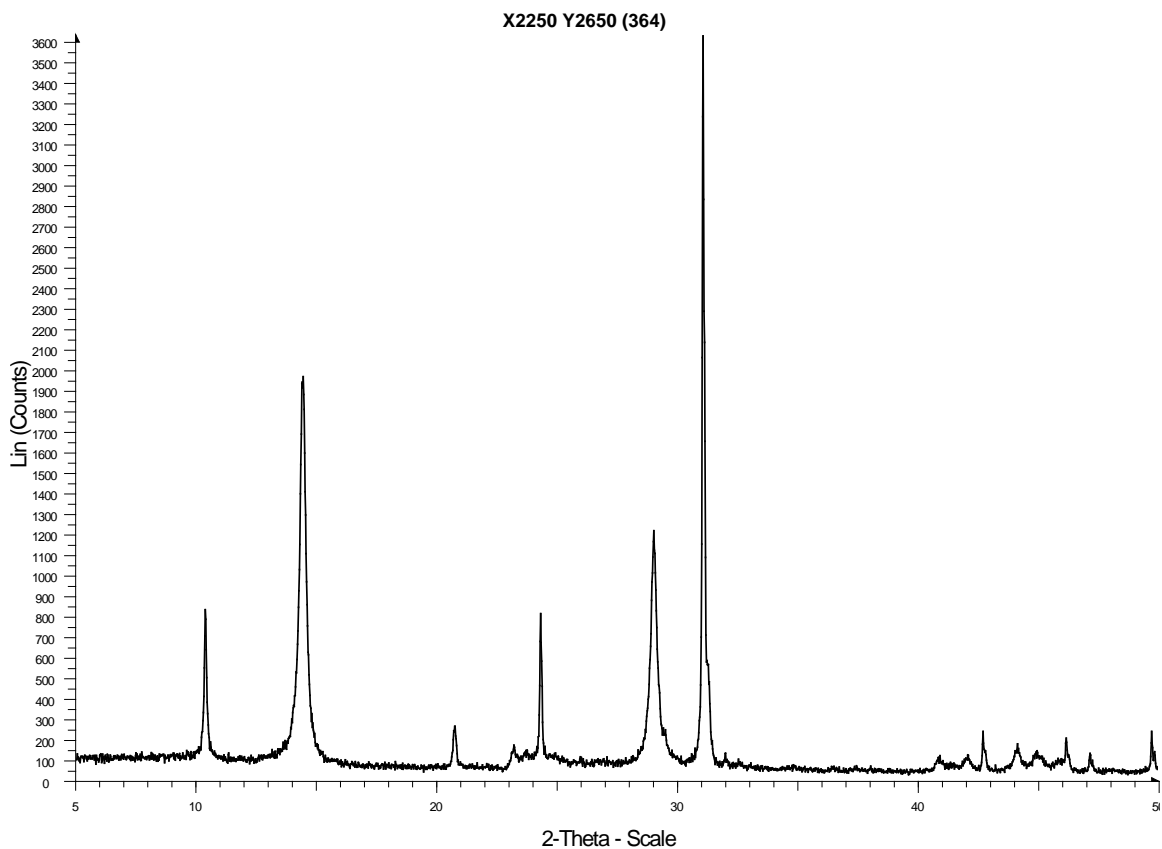
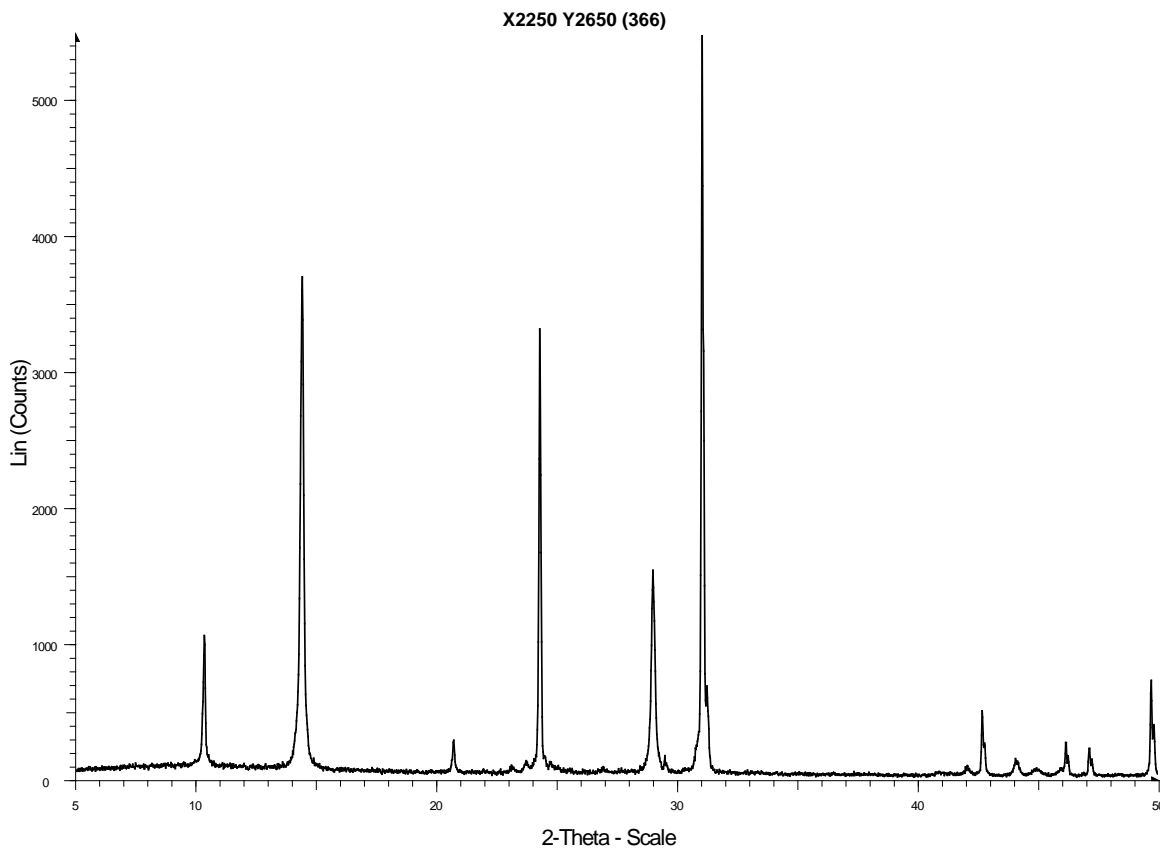


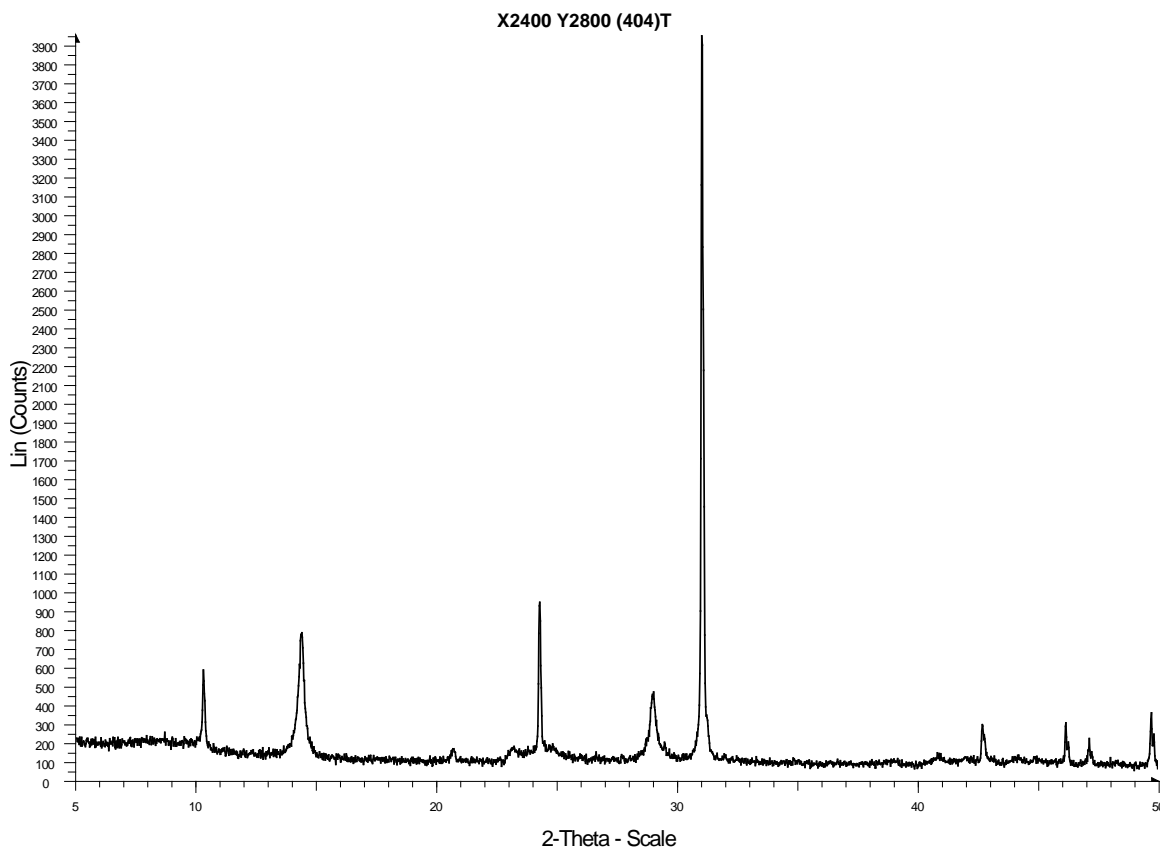
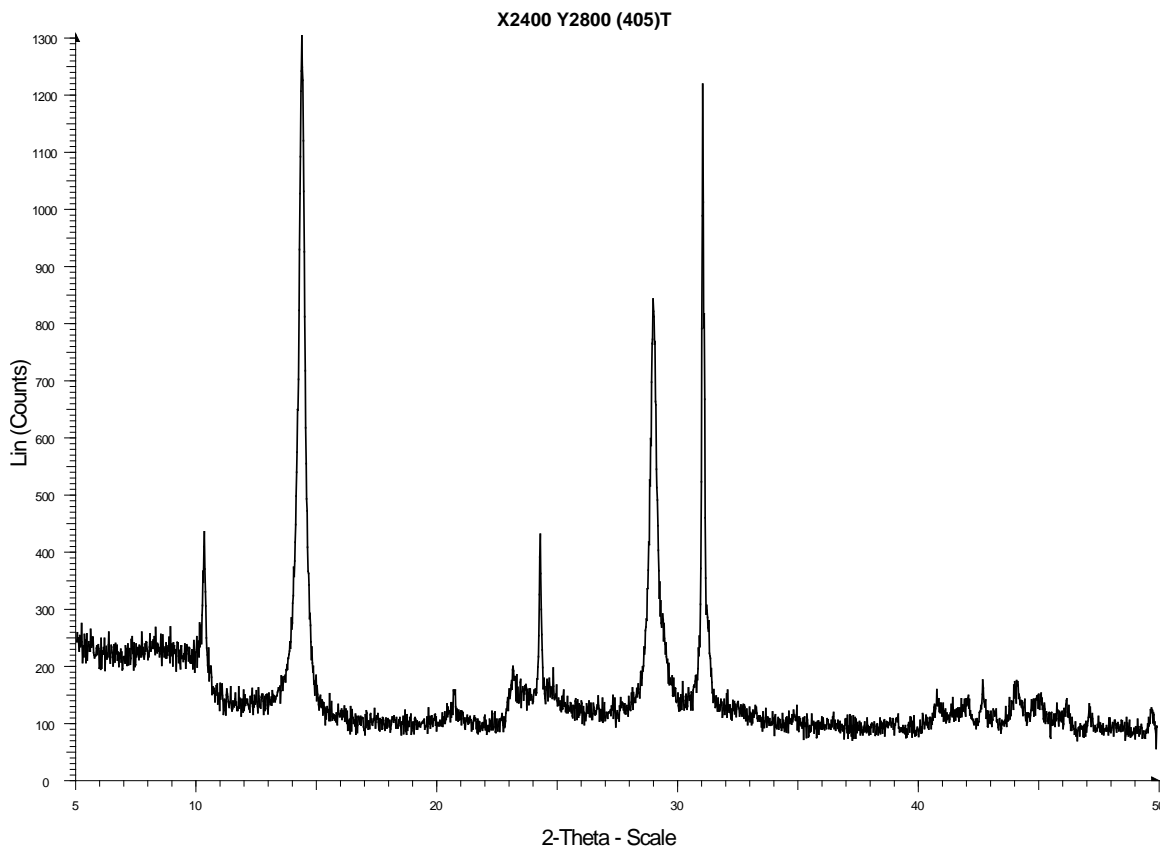


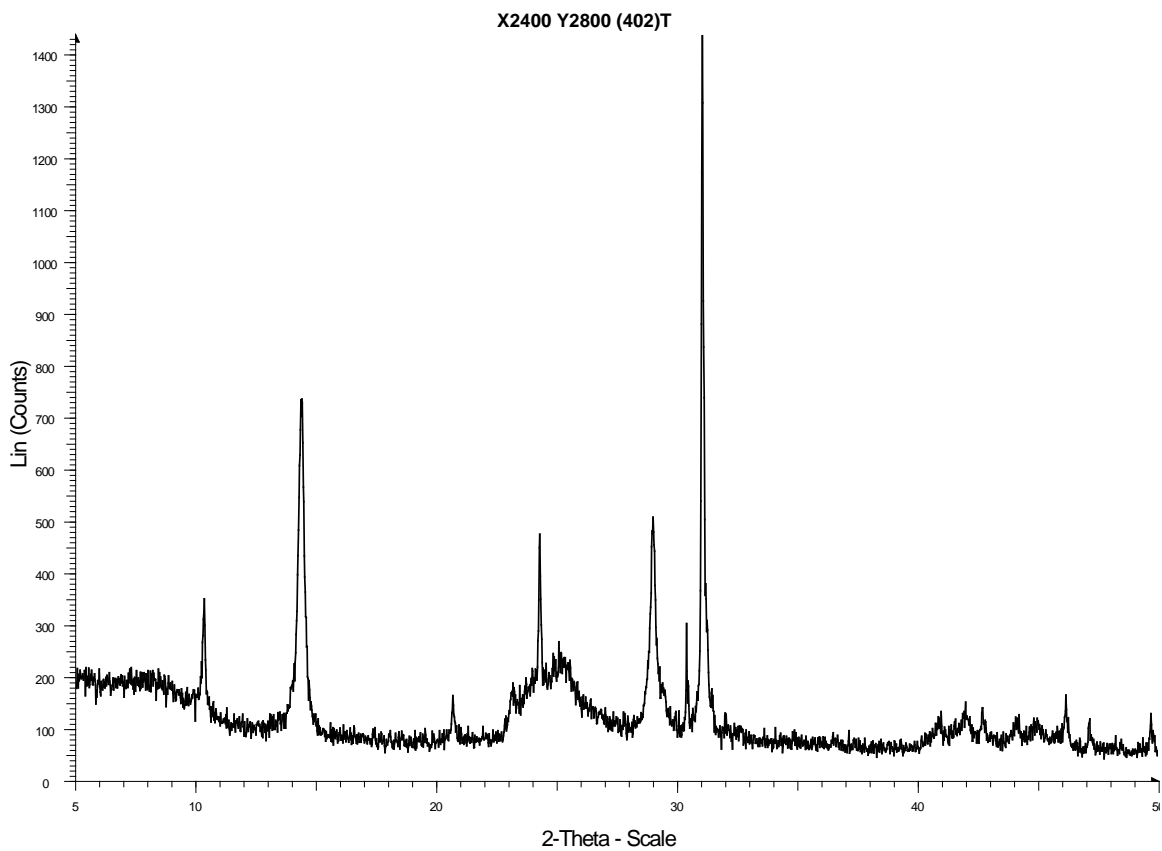
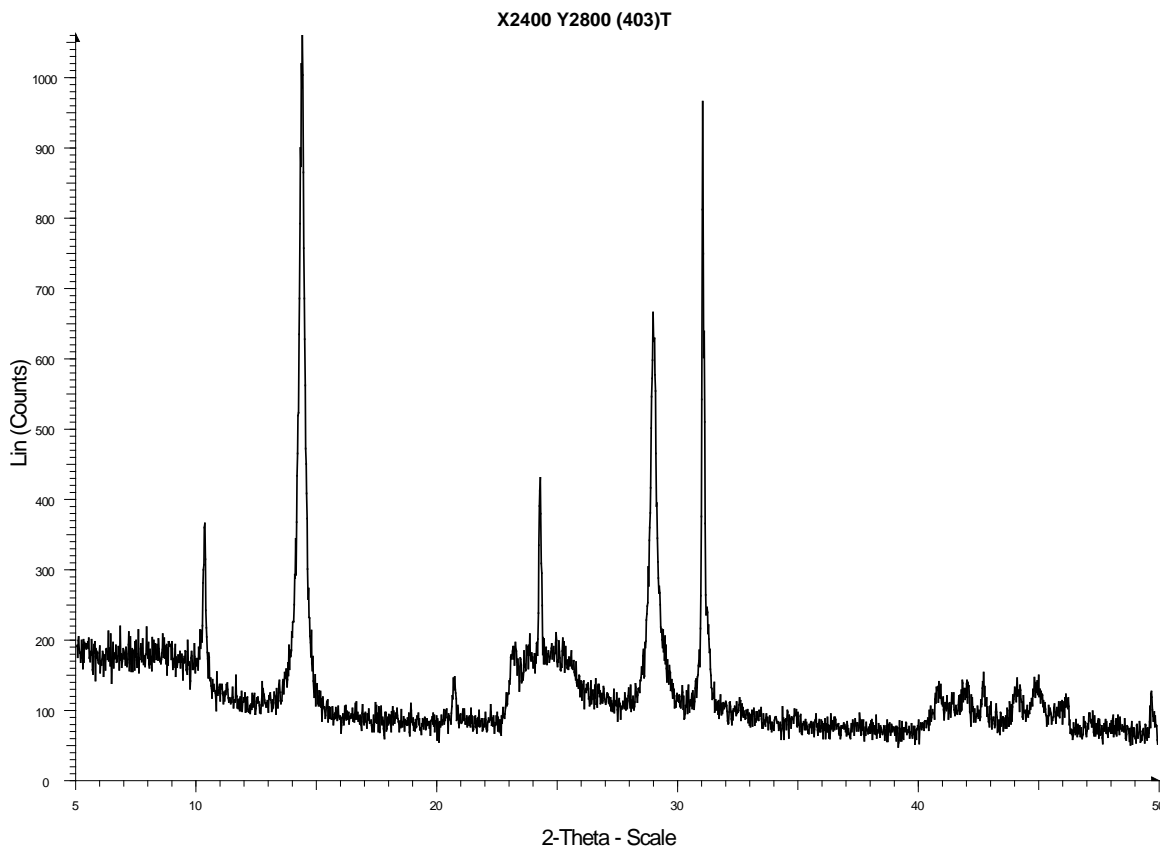


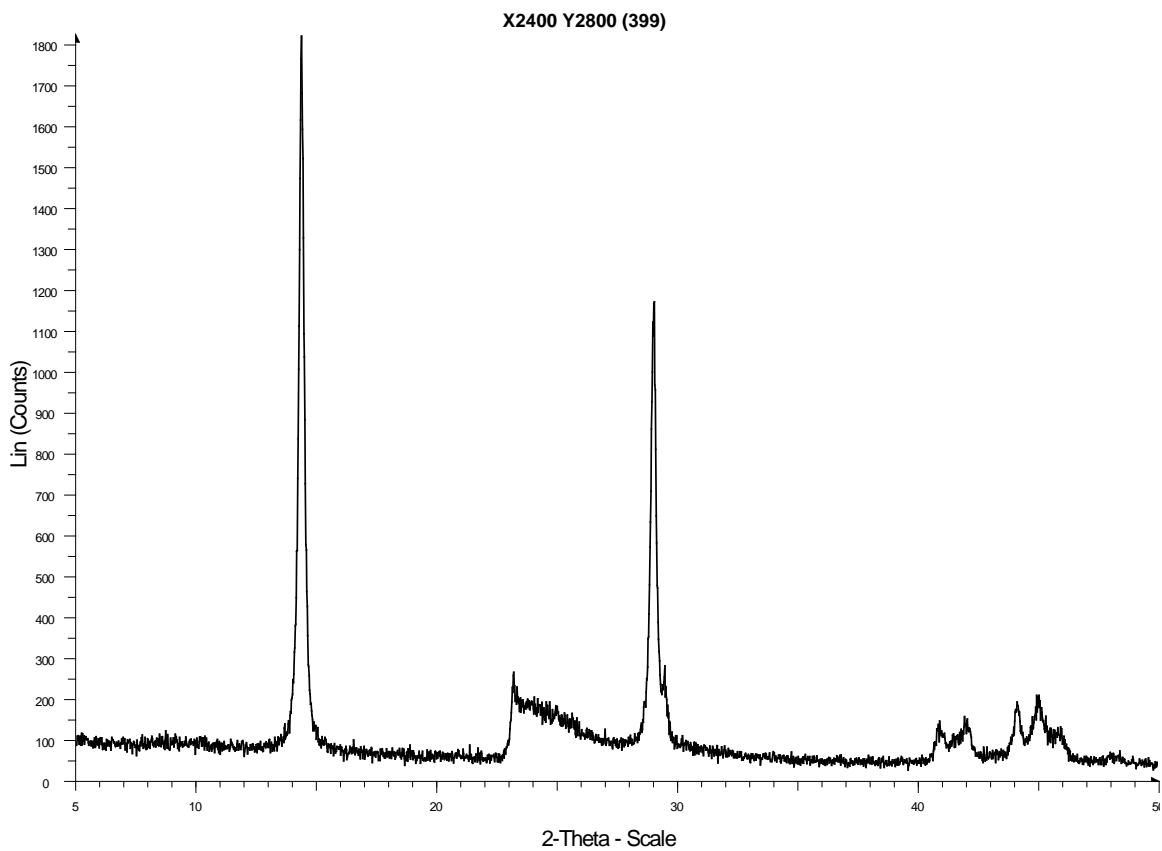
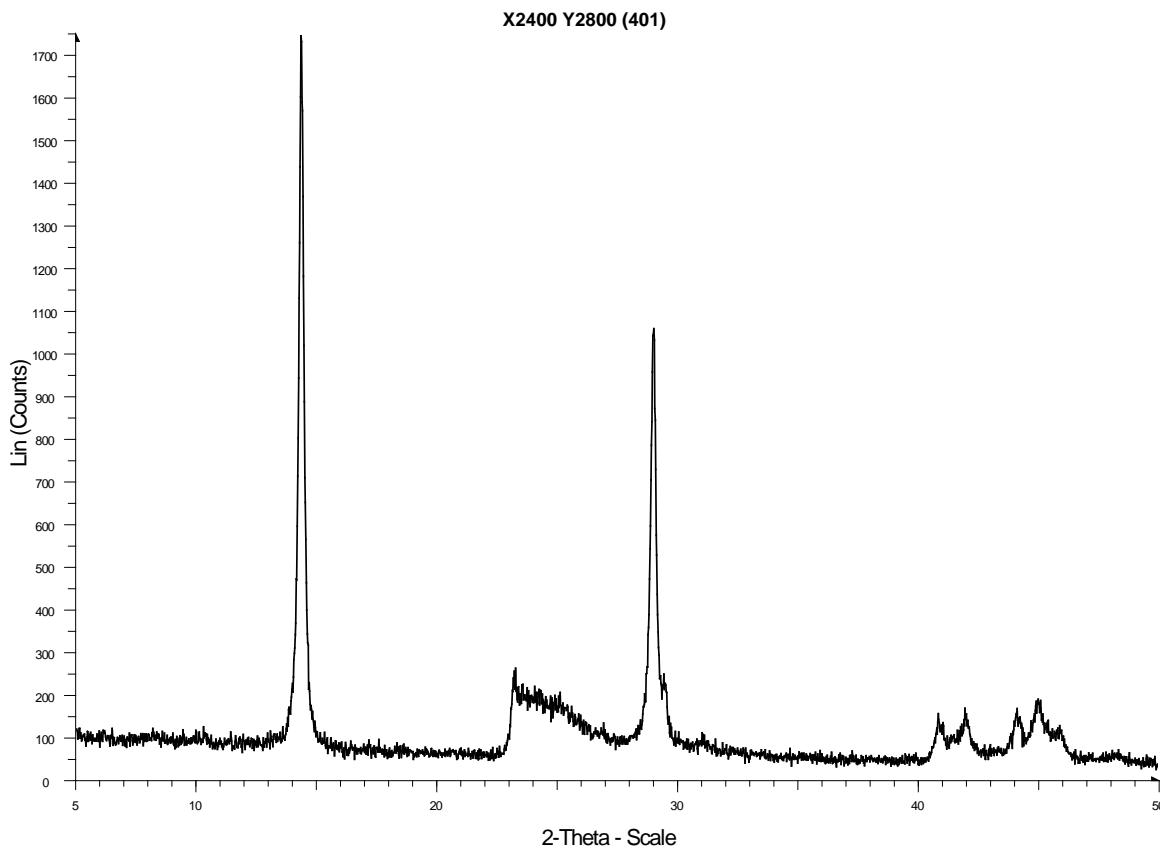


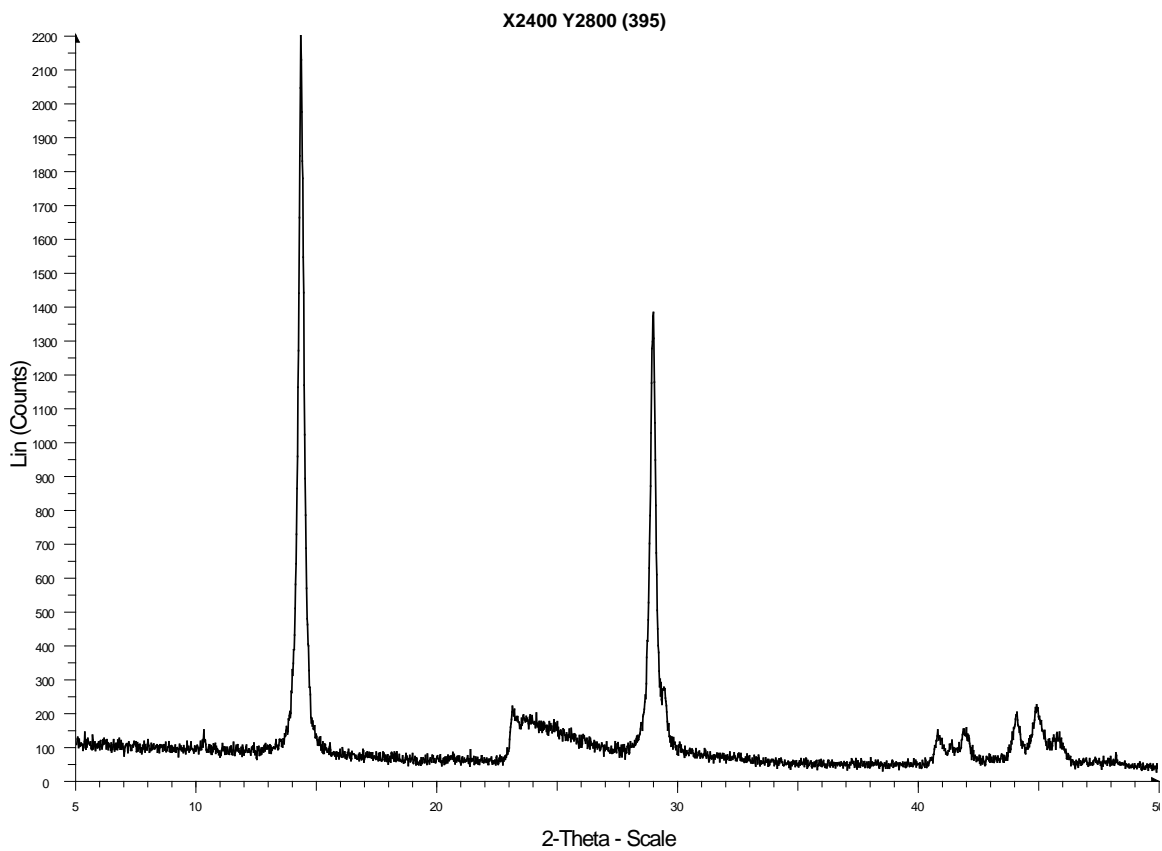
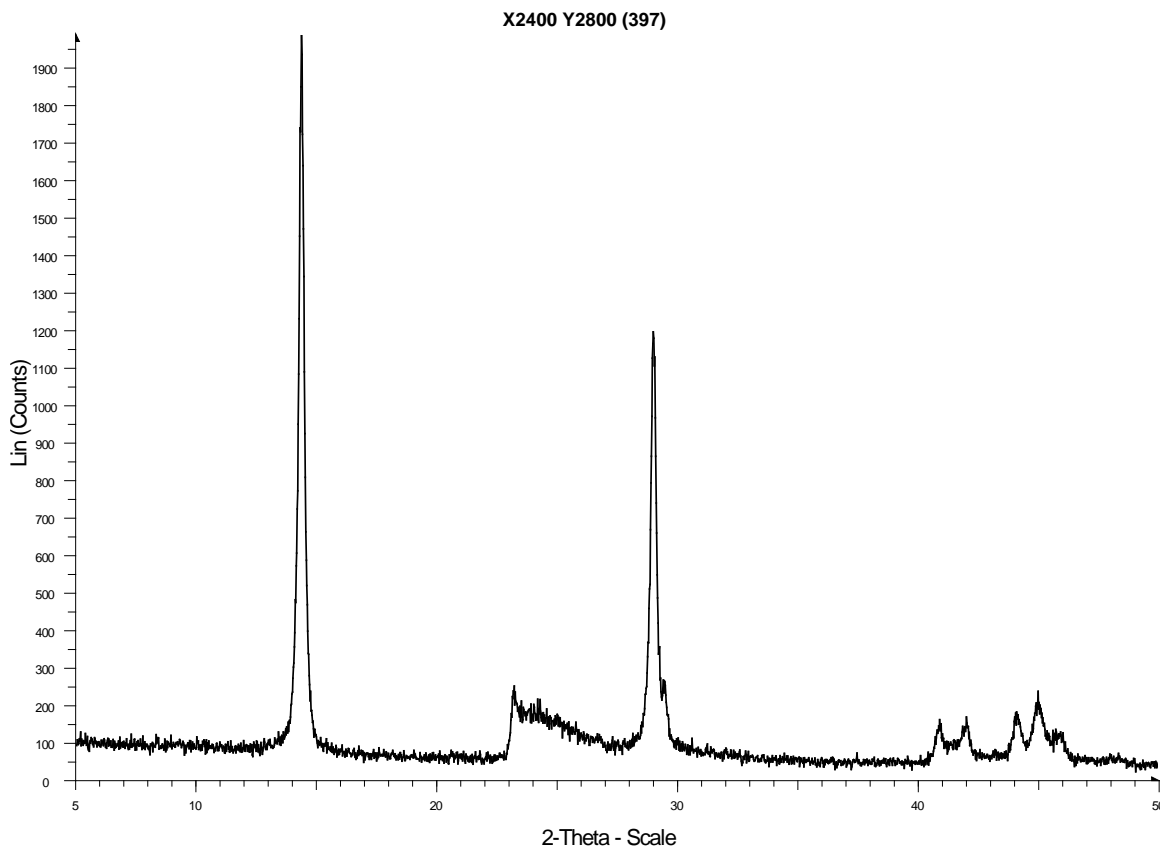


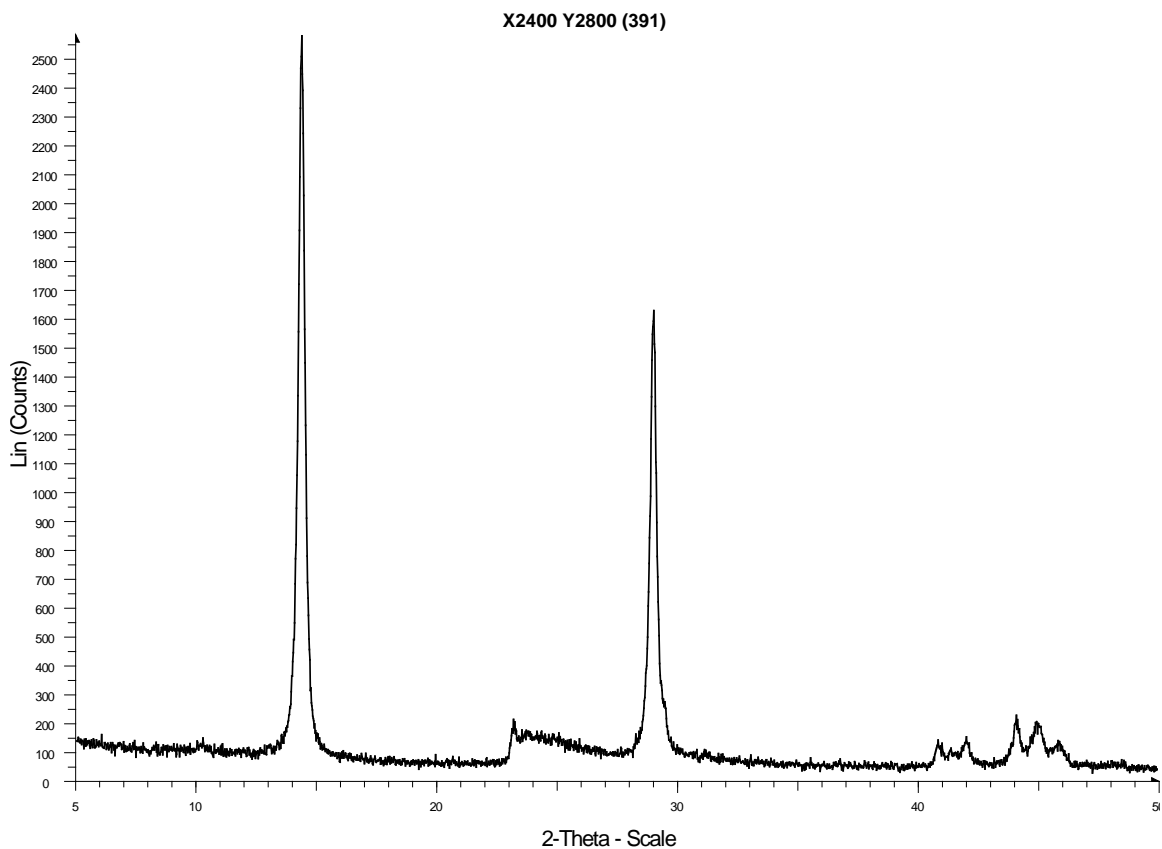
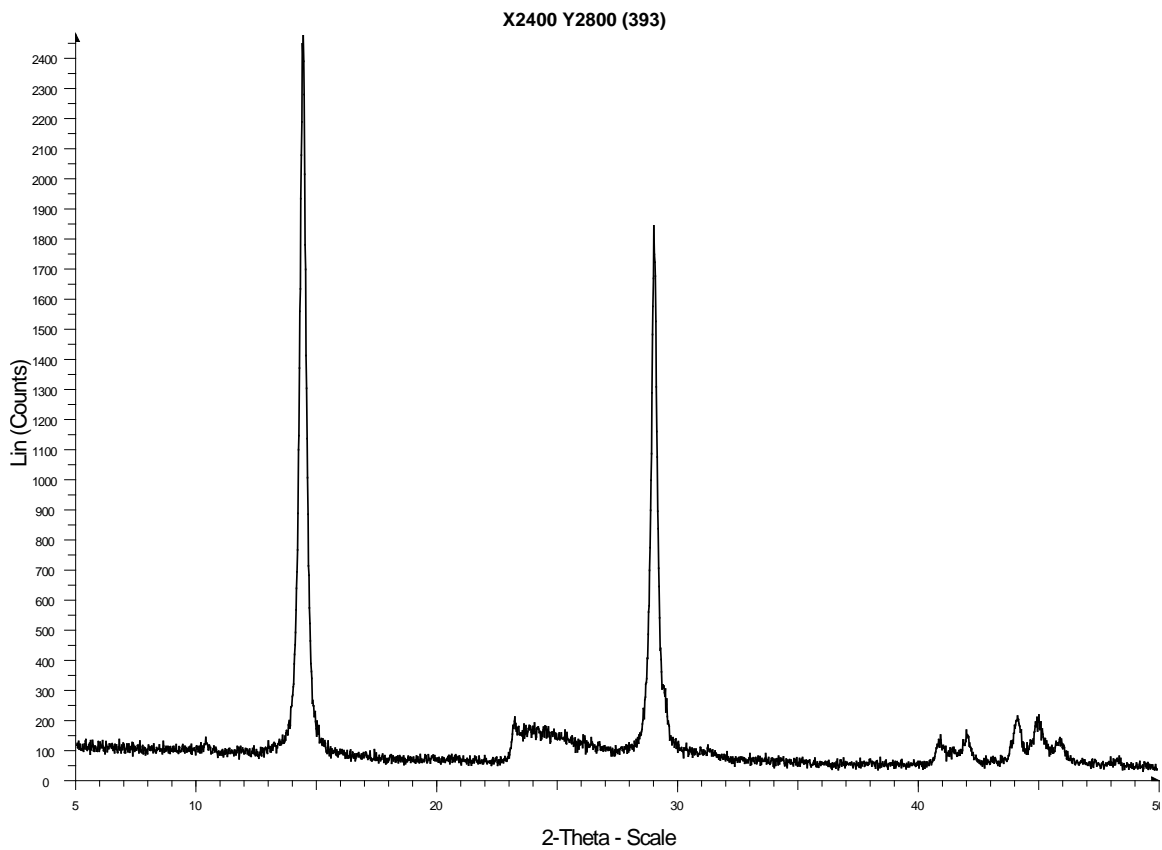


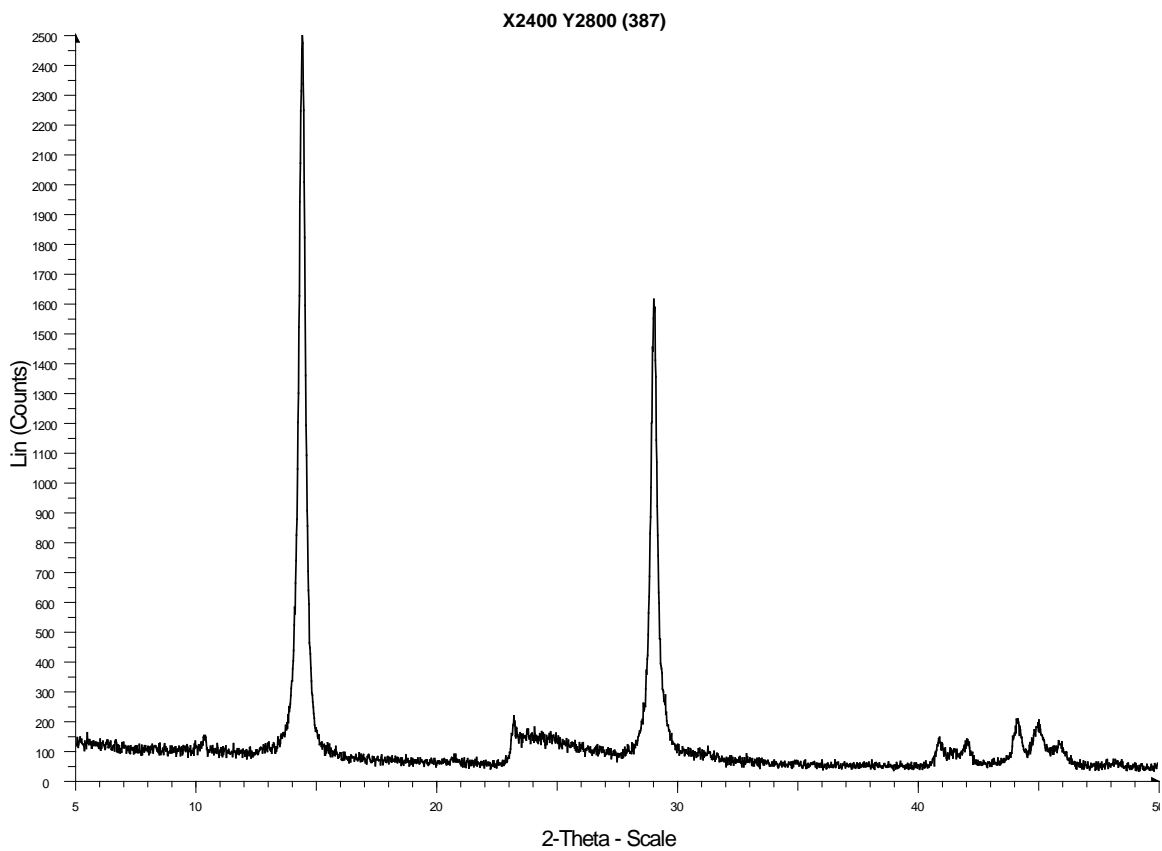
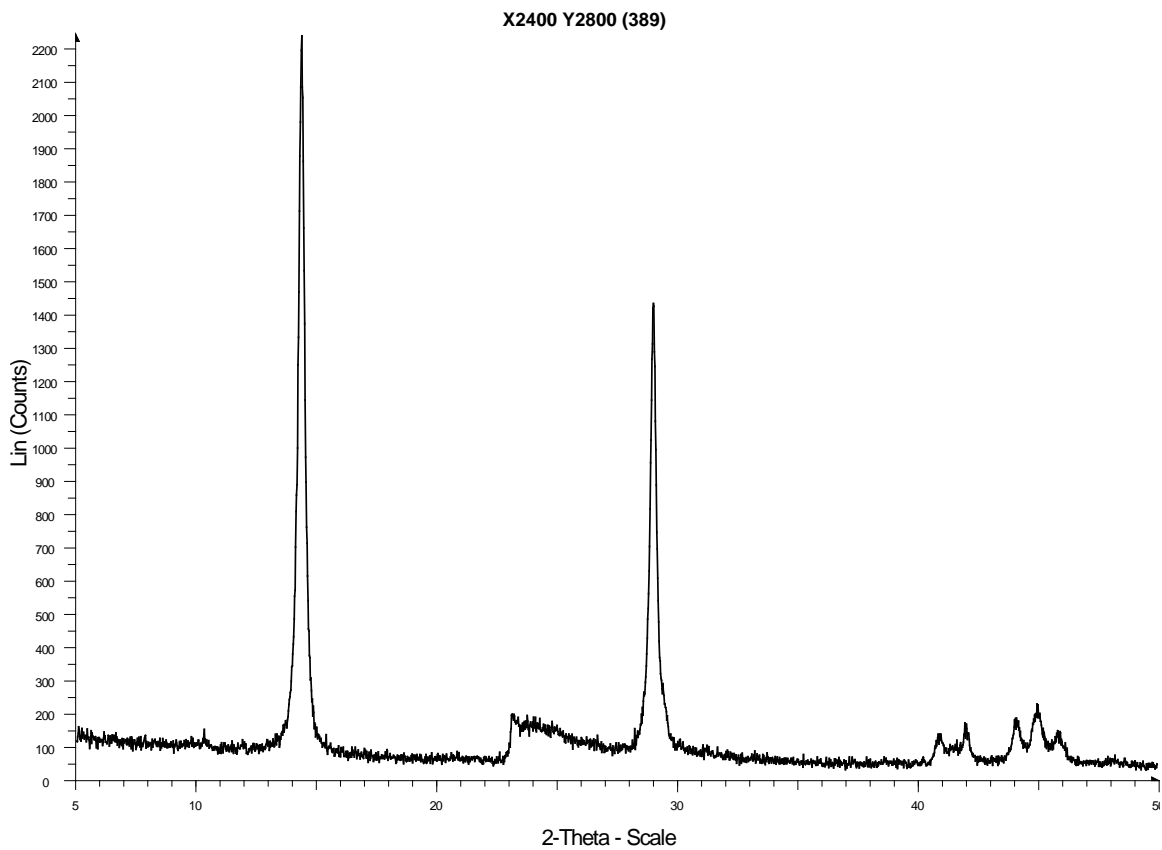


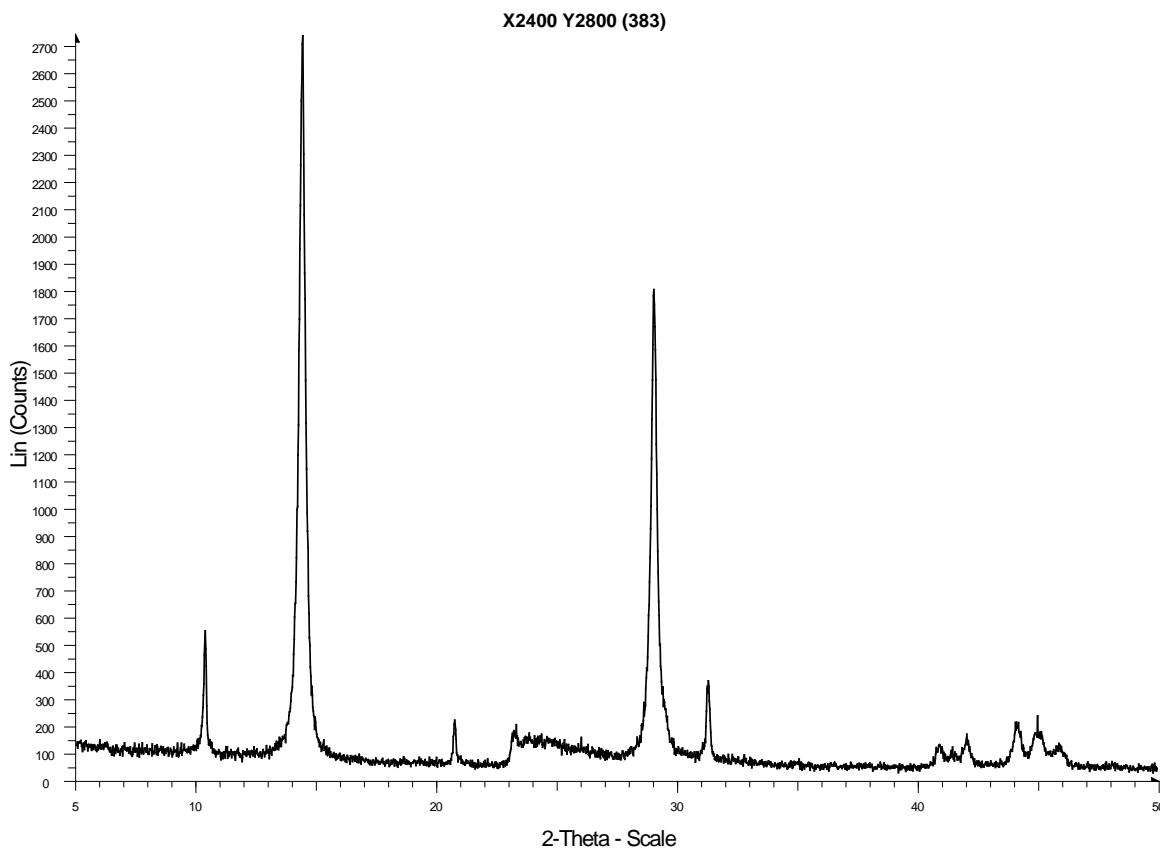
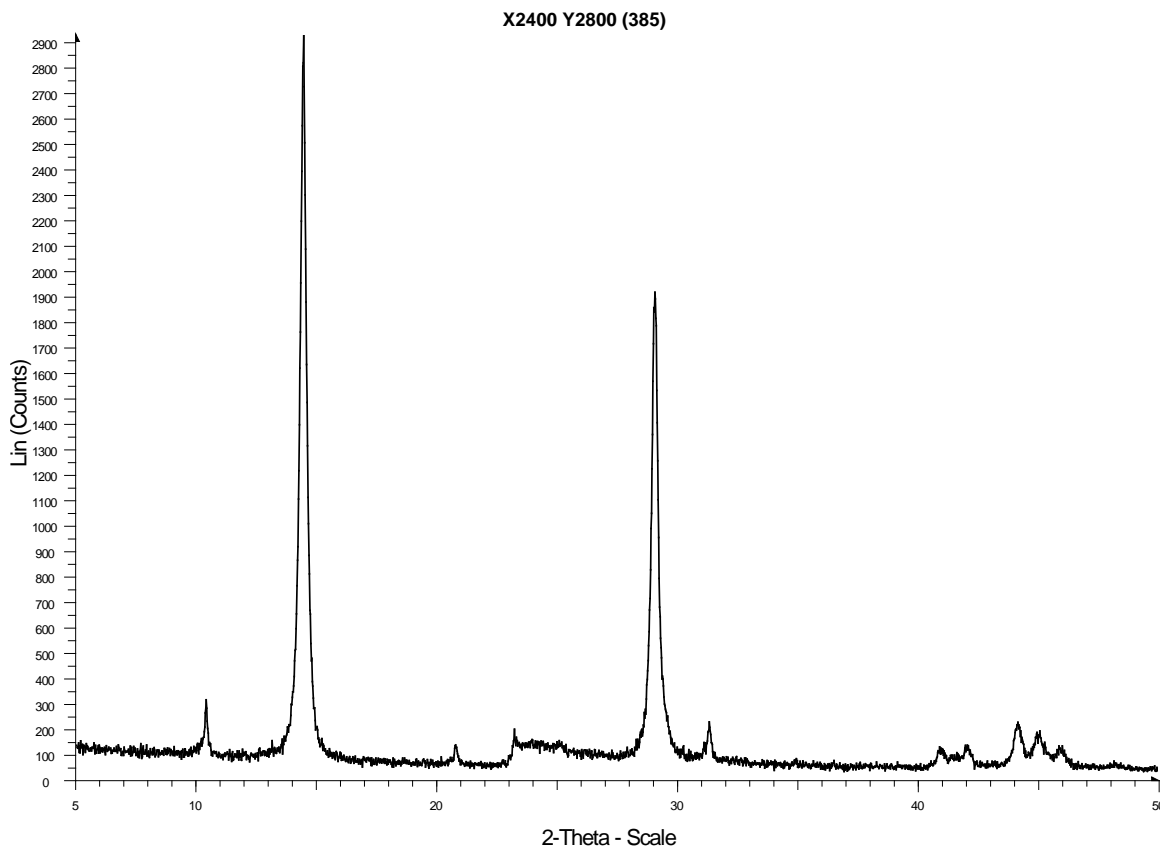


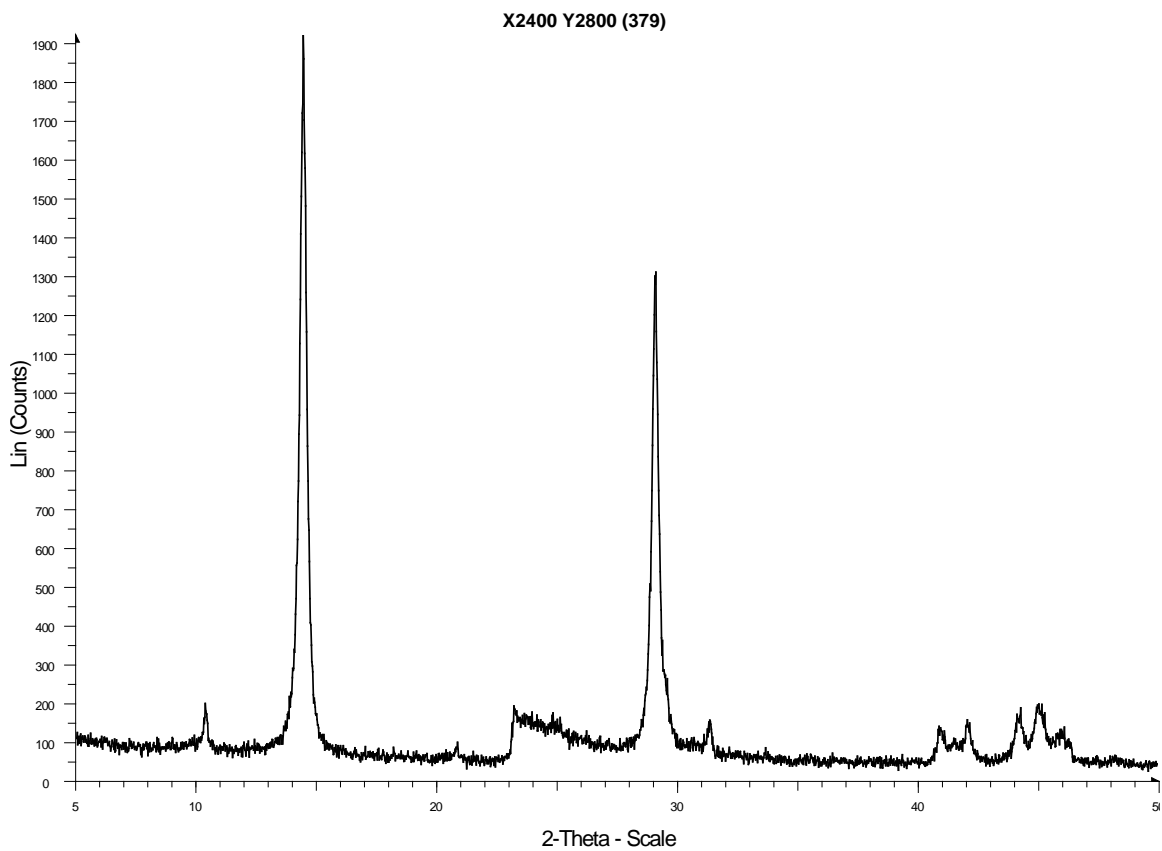
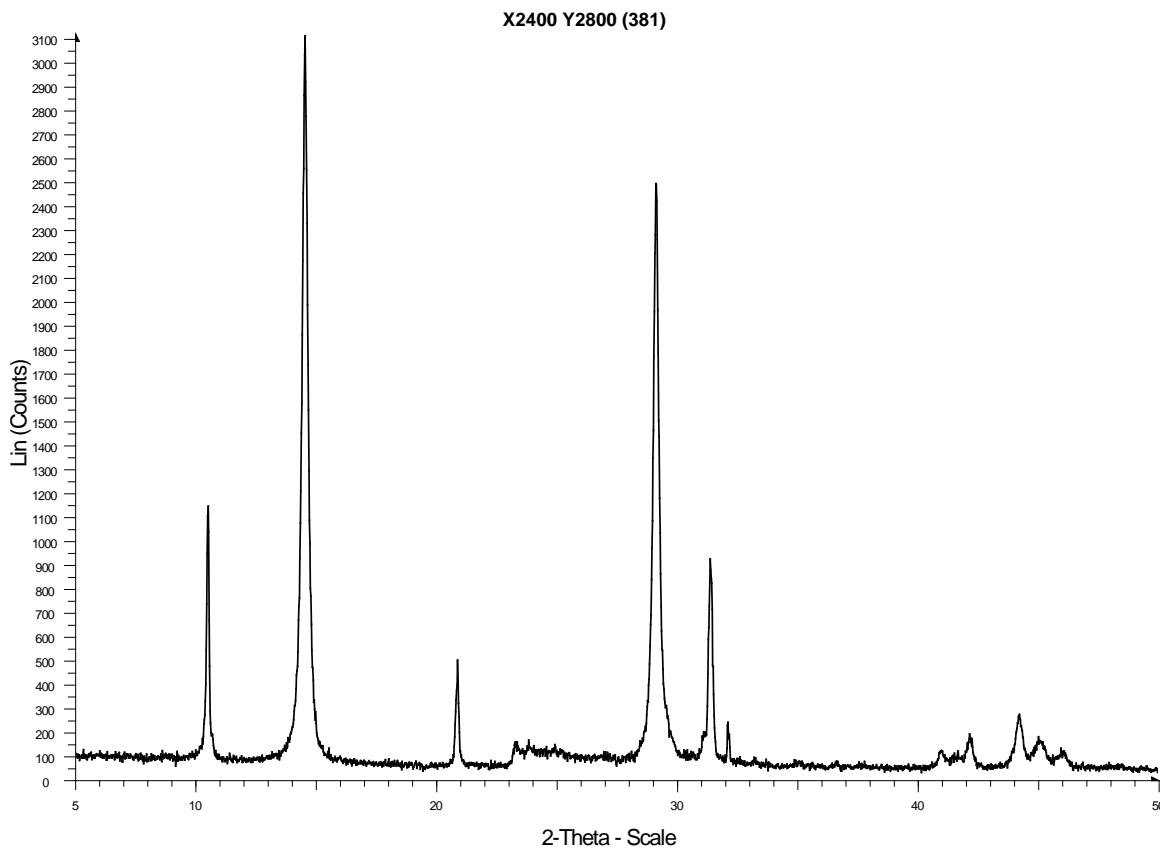


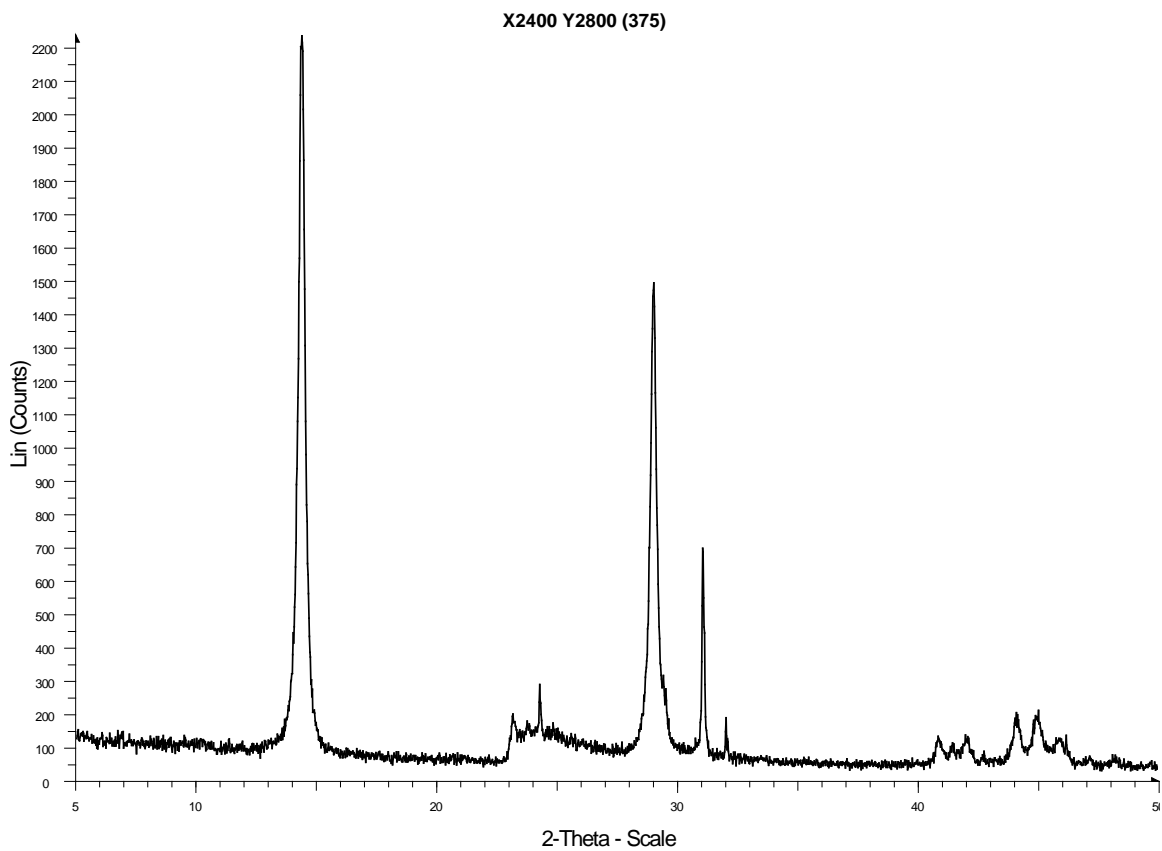
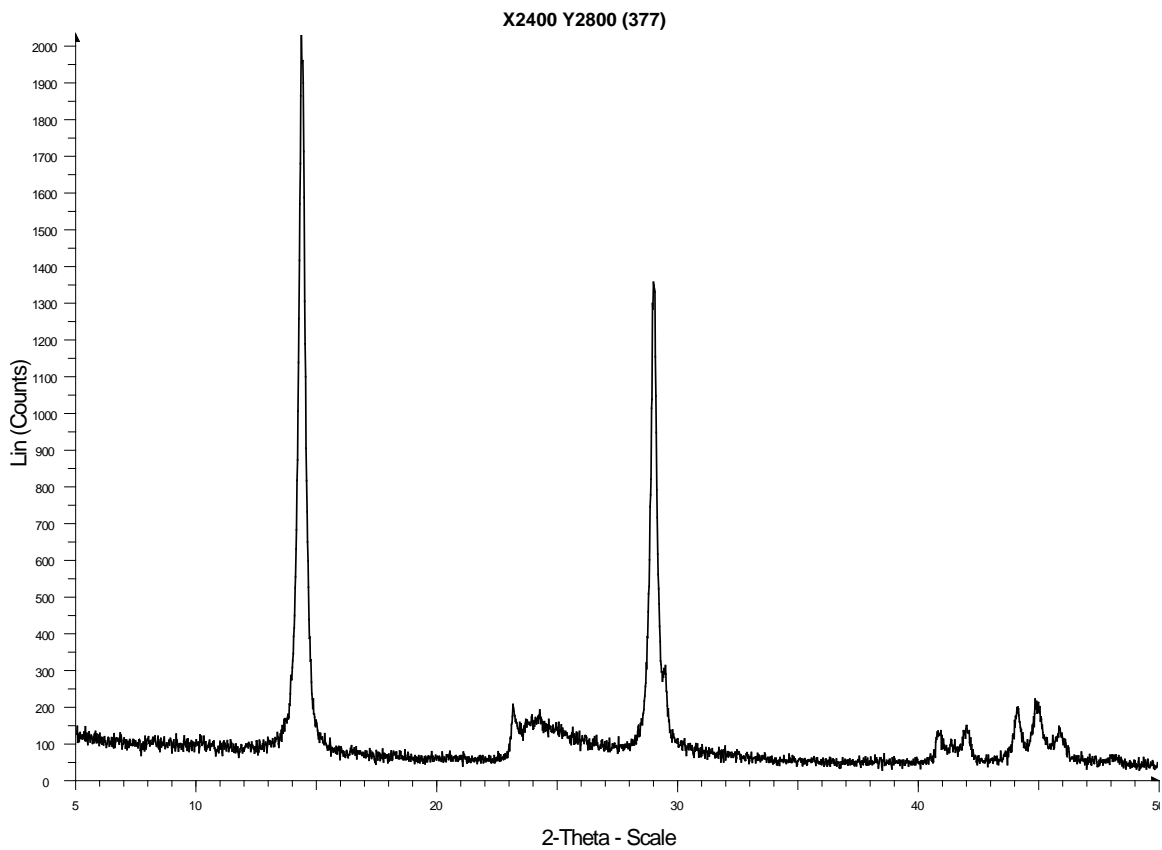




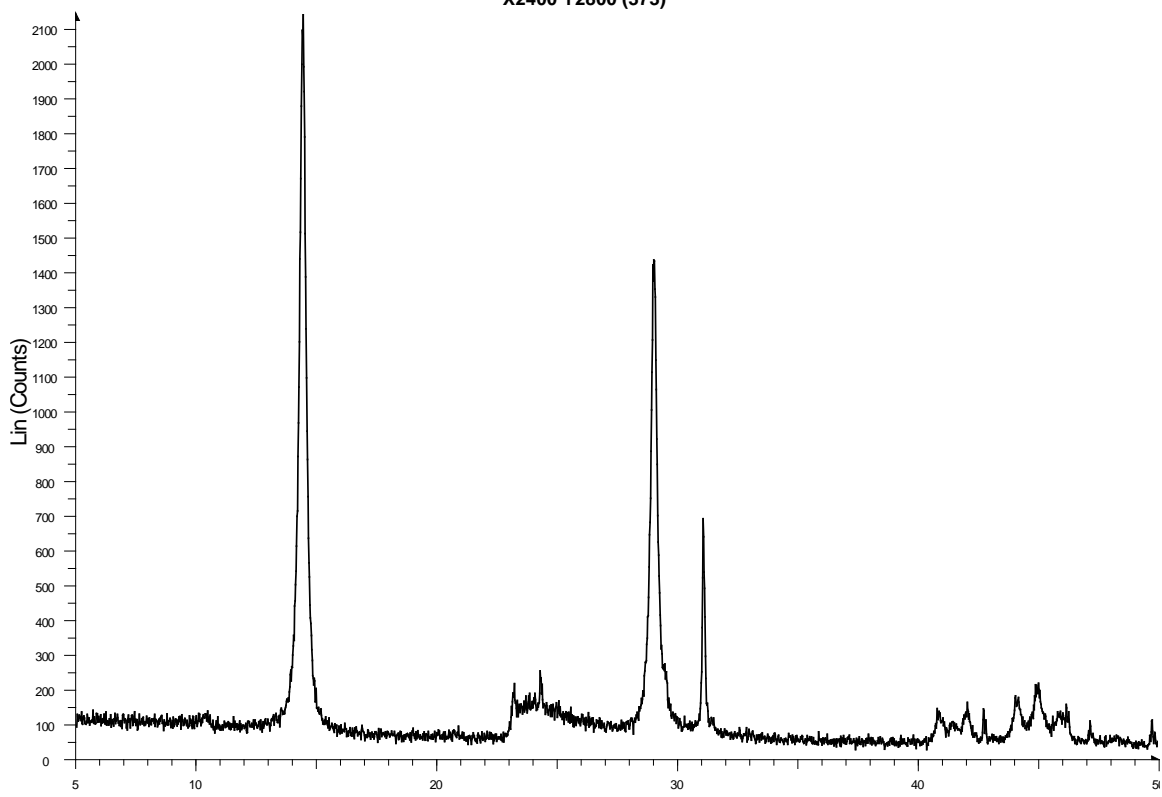






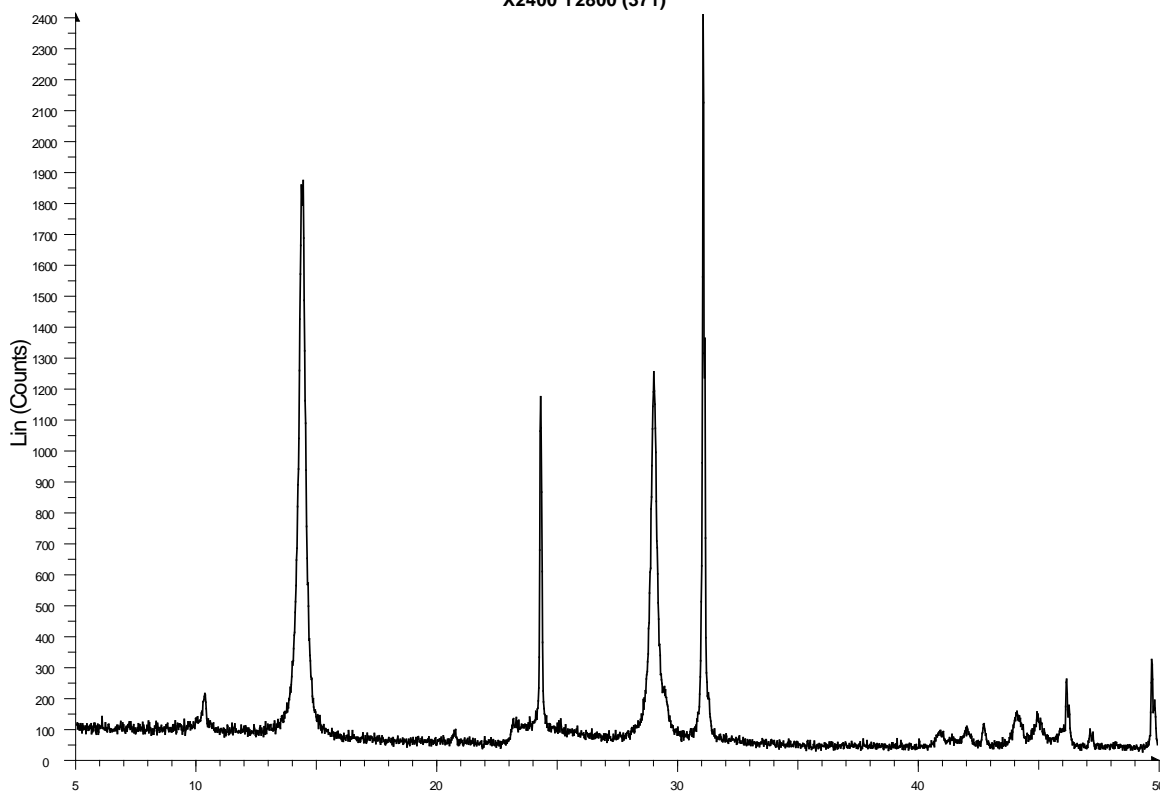


X2400 Y2800 (373)

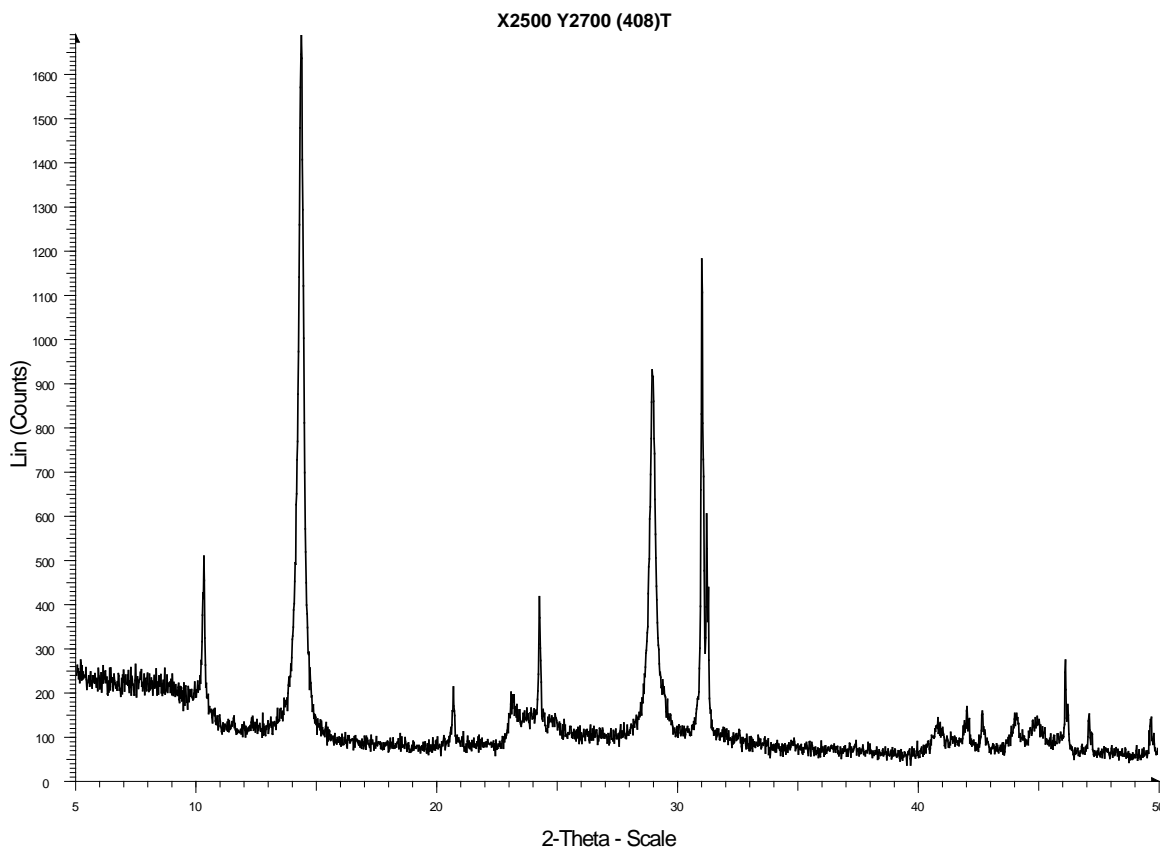
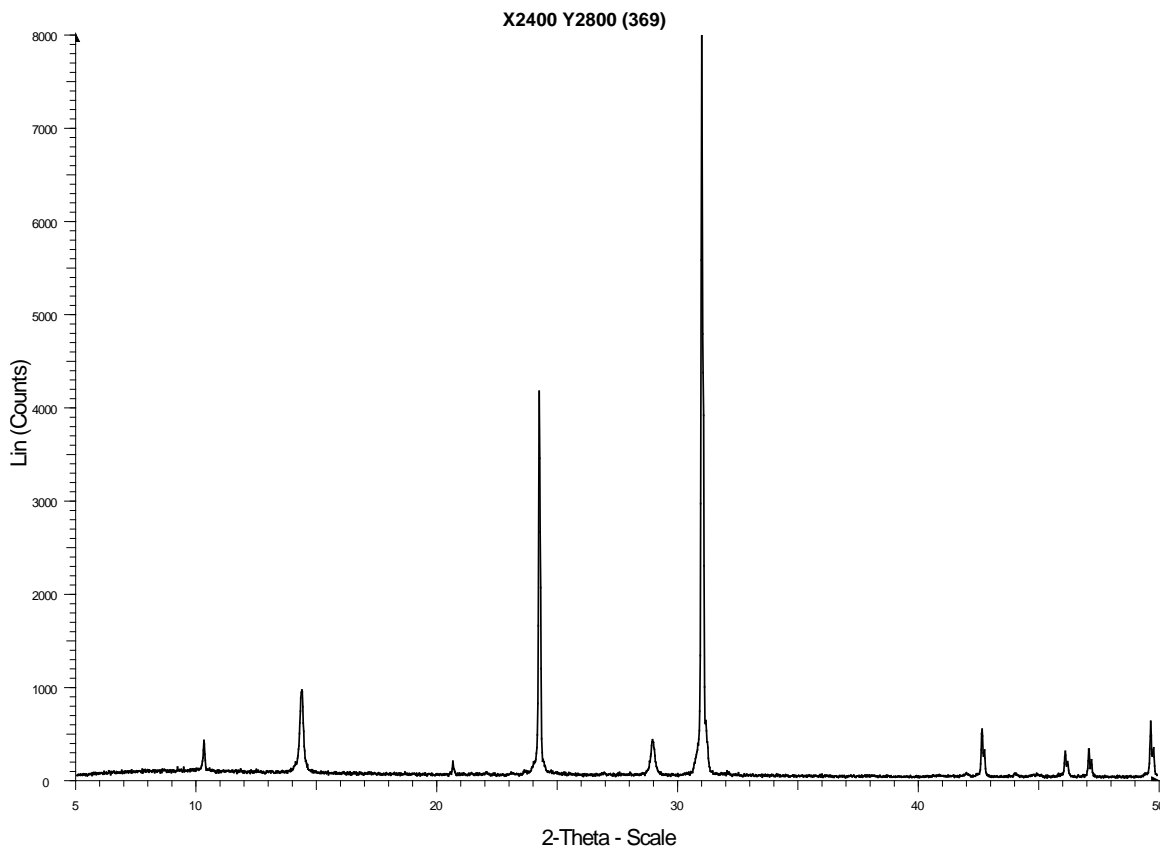


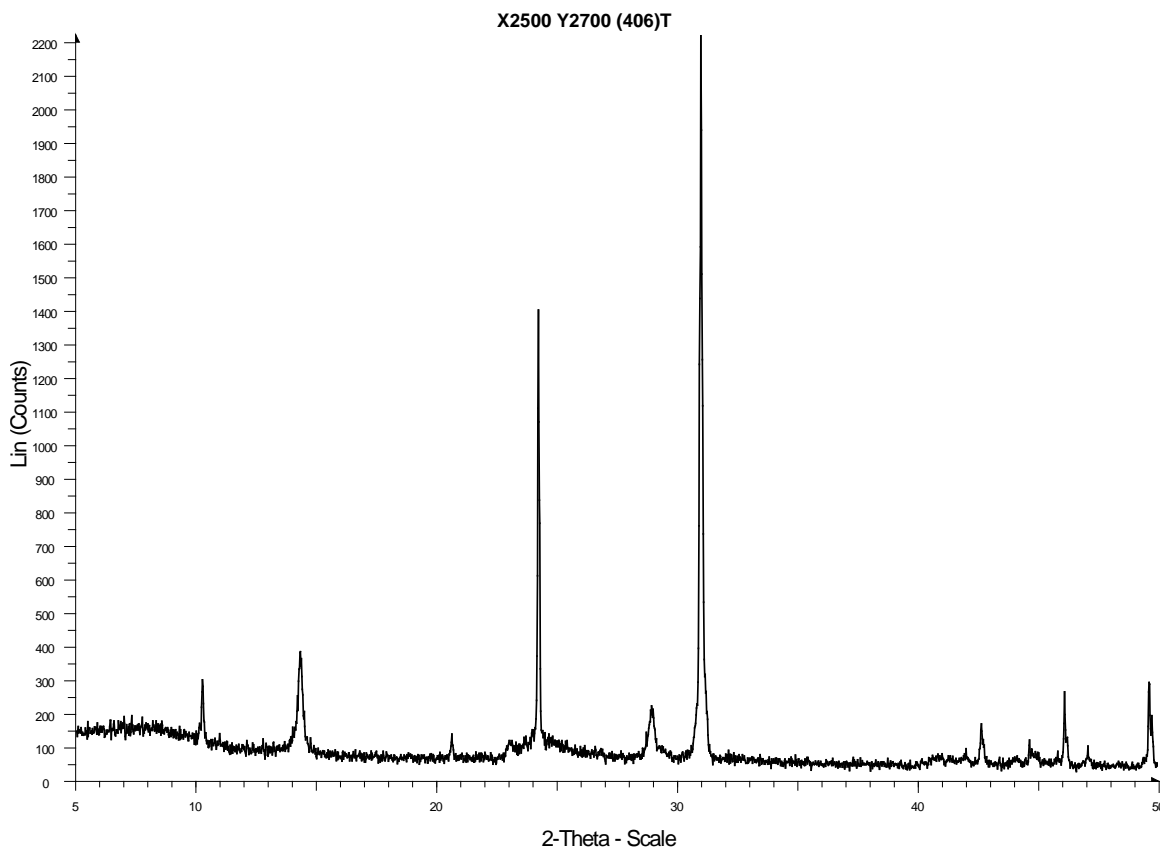
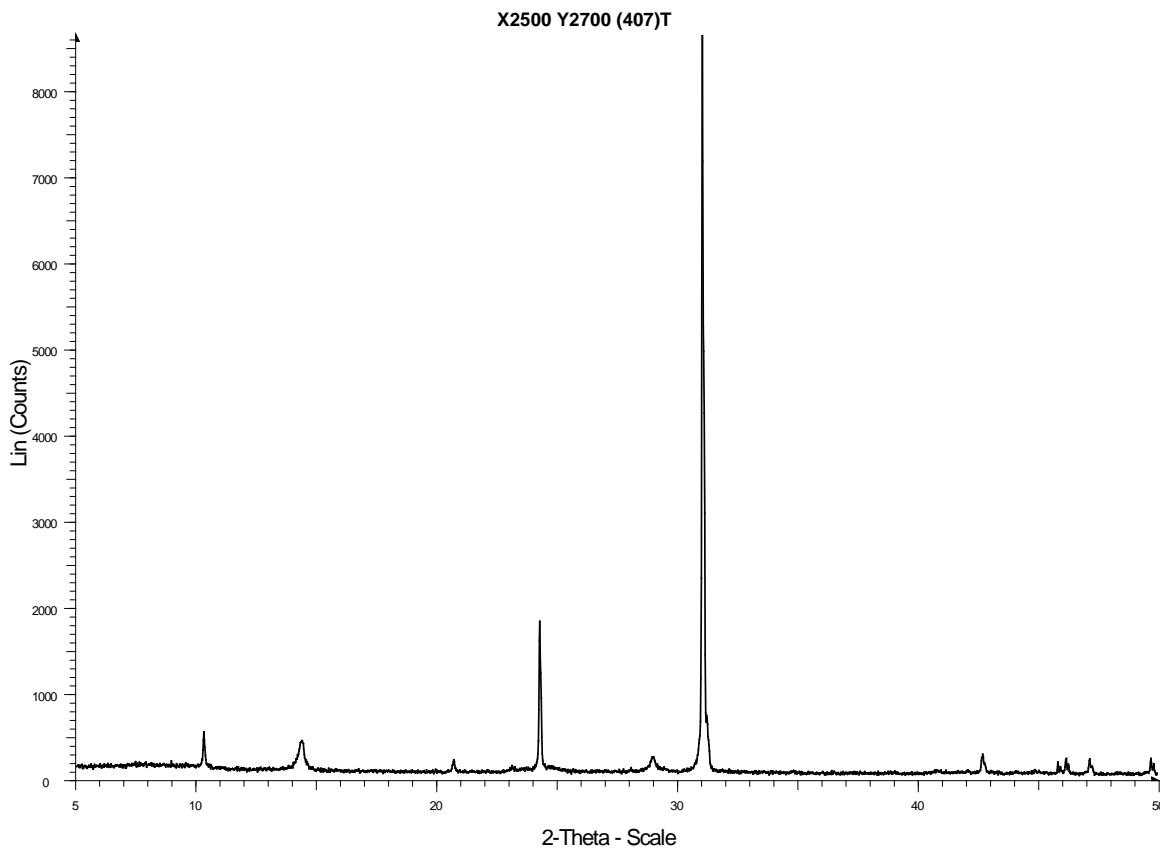
2-Theta - Scale

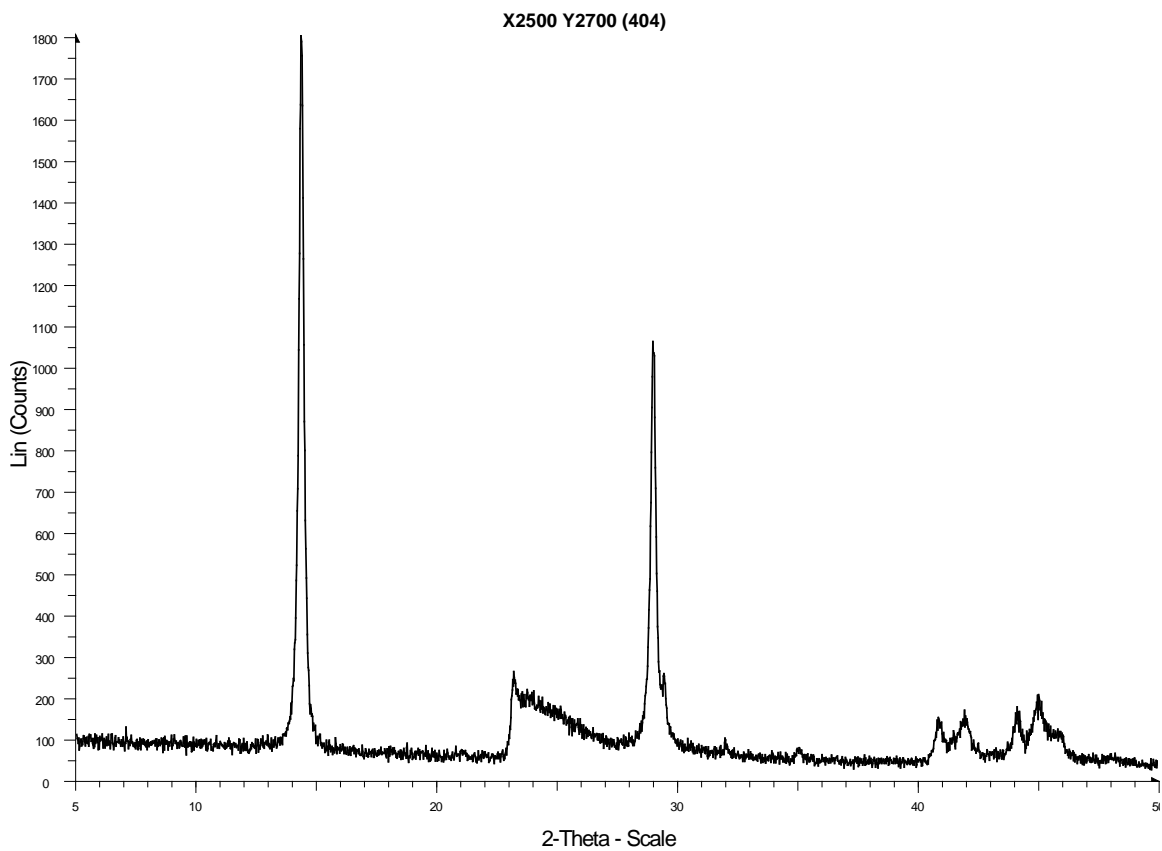
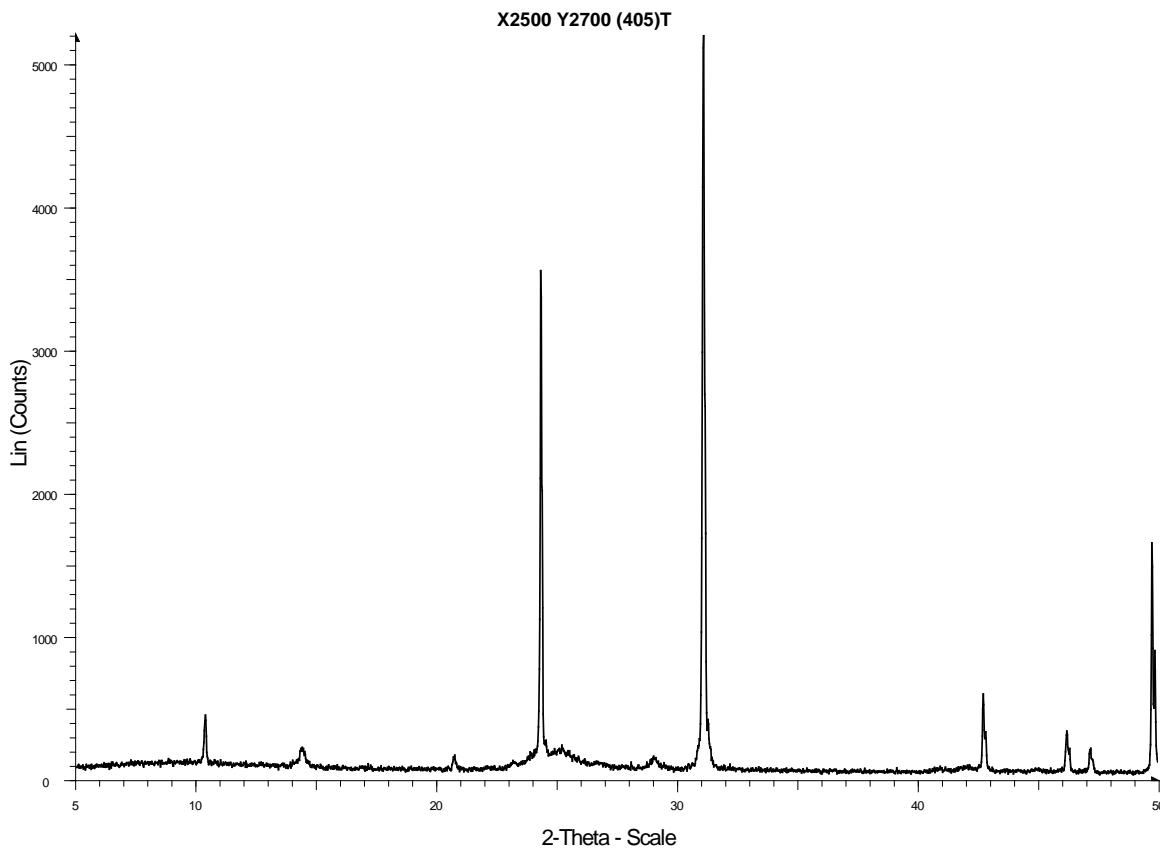
X2400 Y2800 (371)

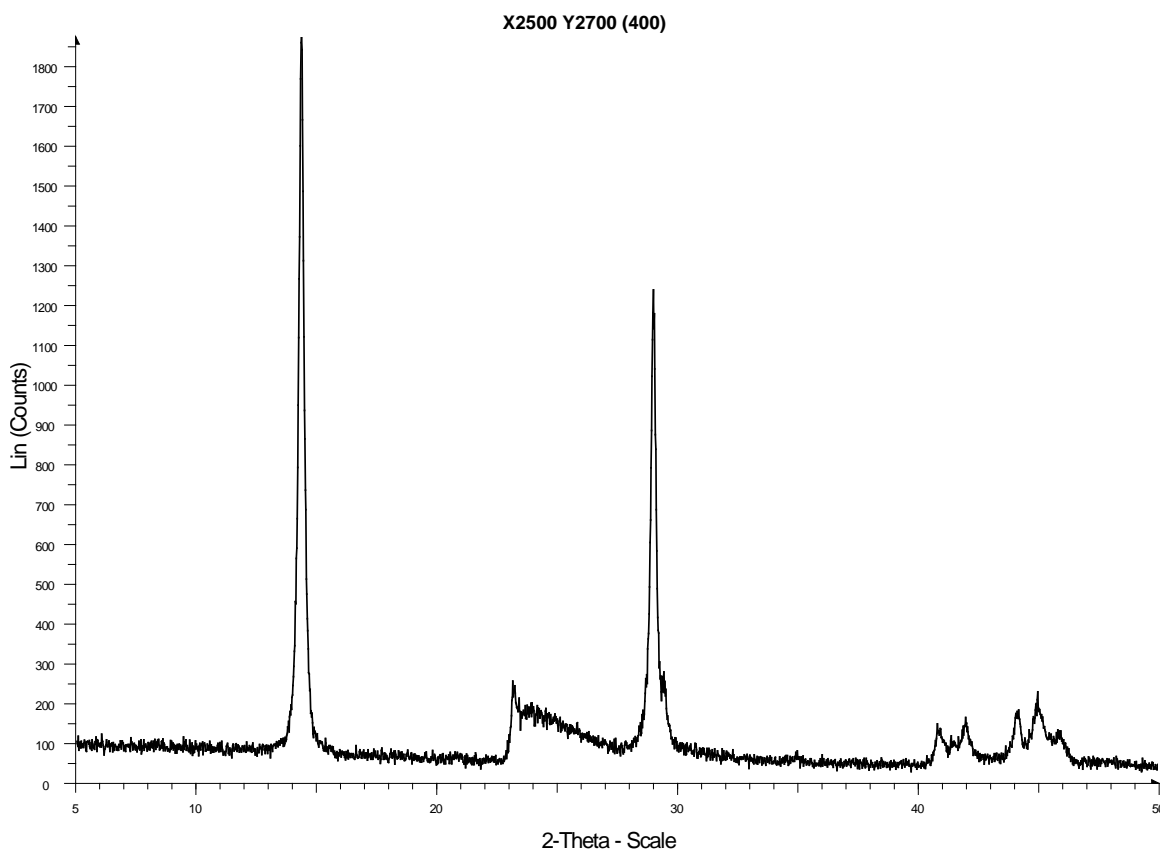
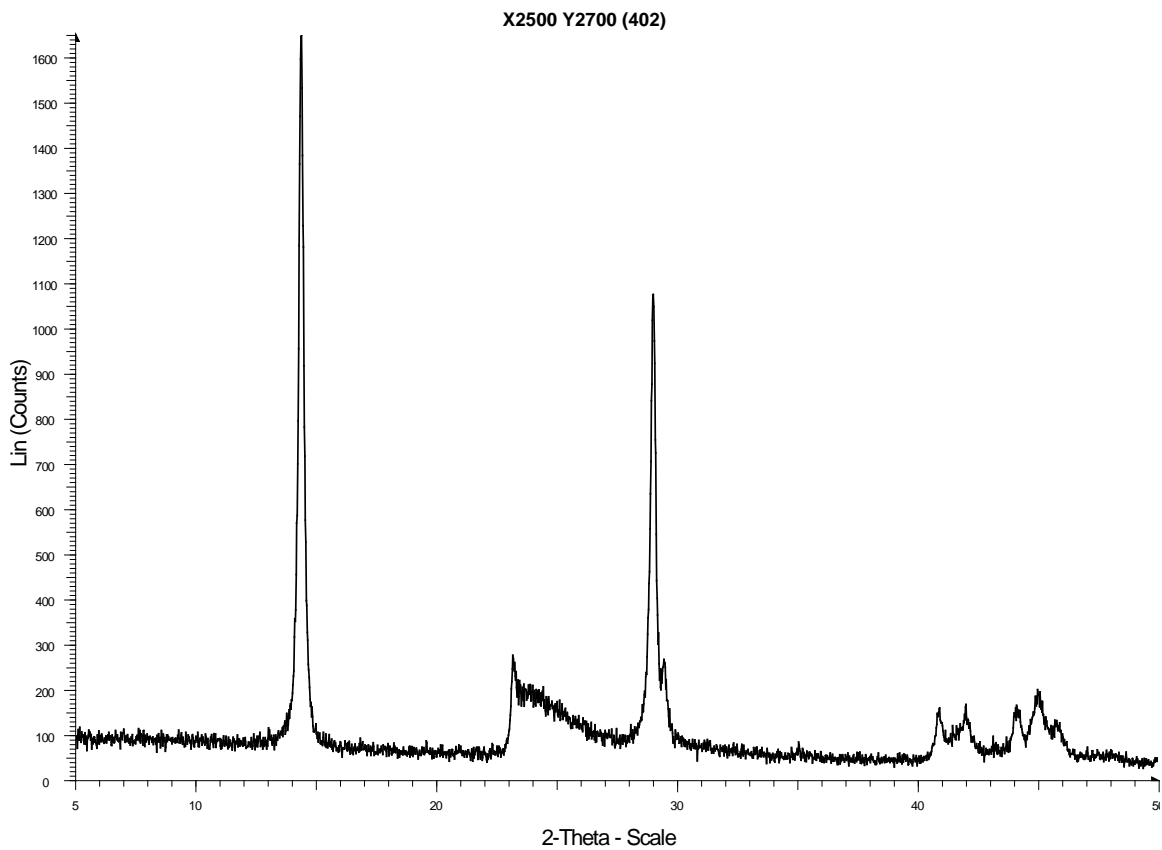


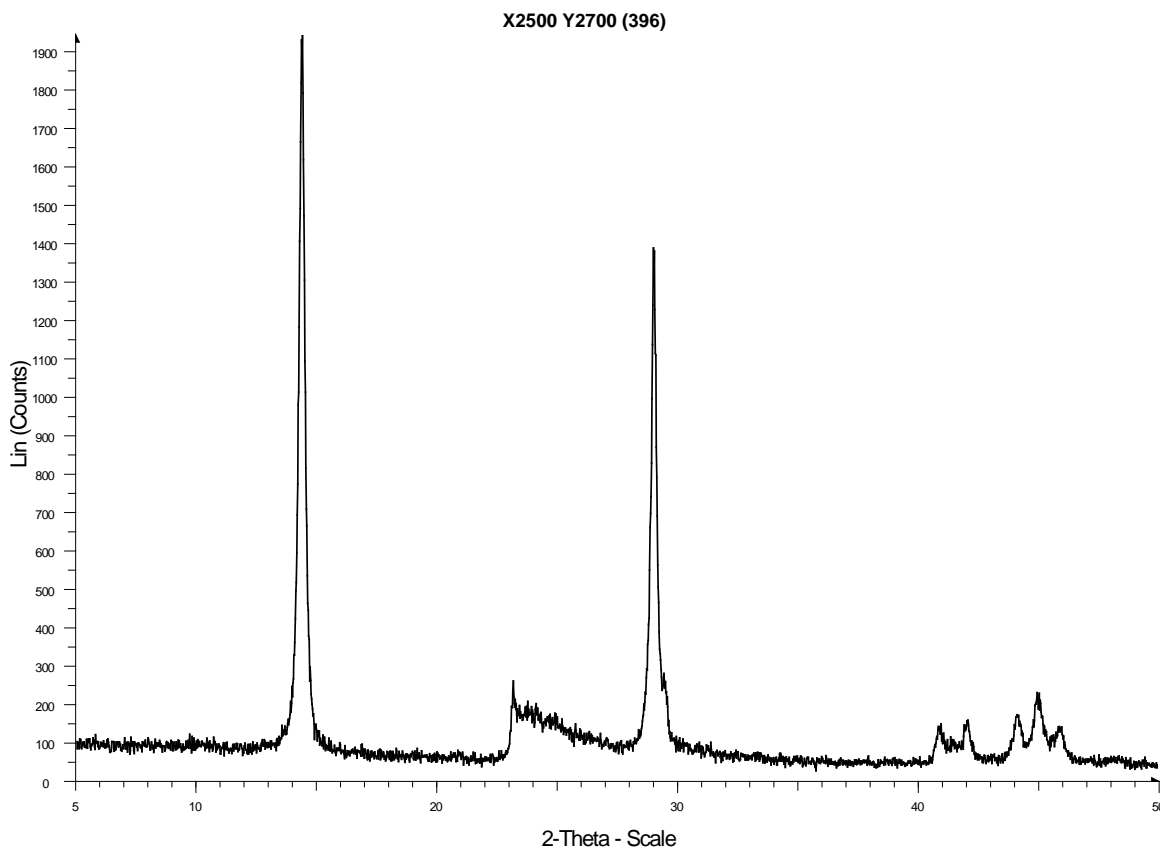
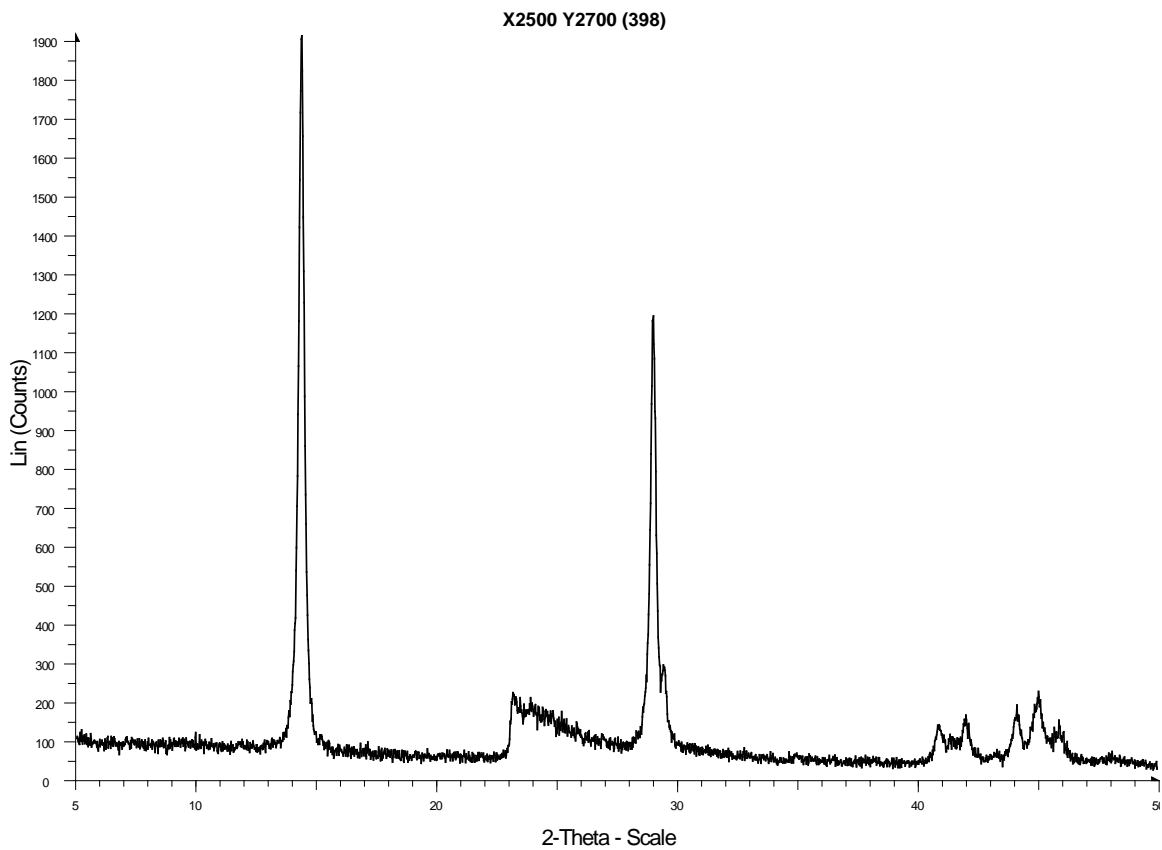
2-Theta - Scale



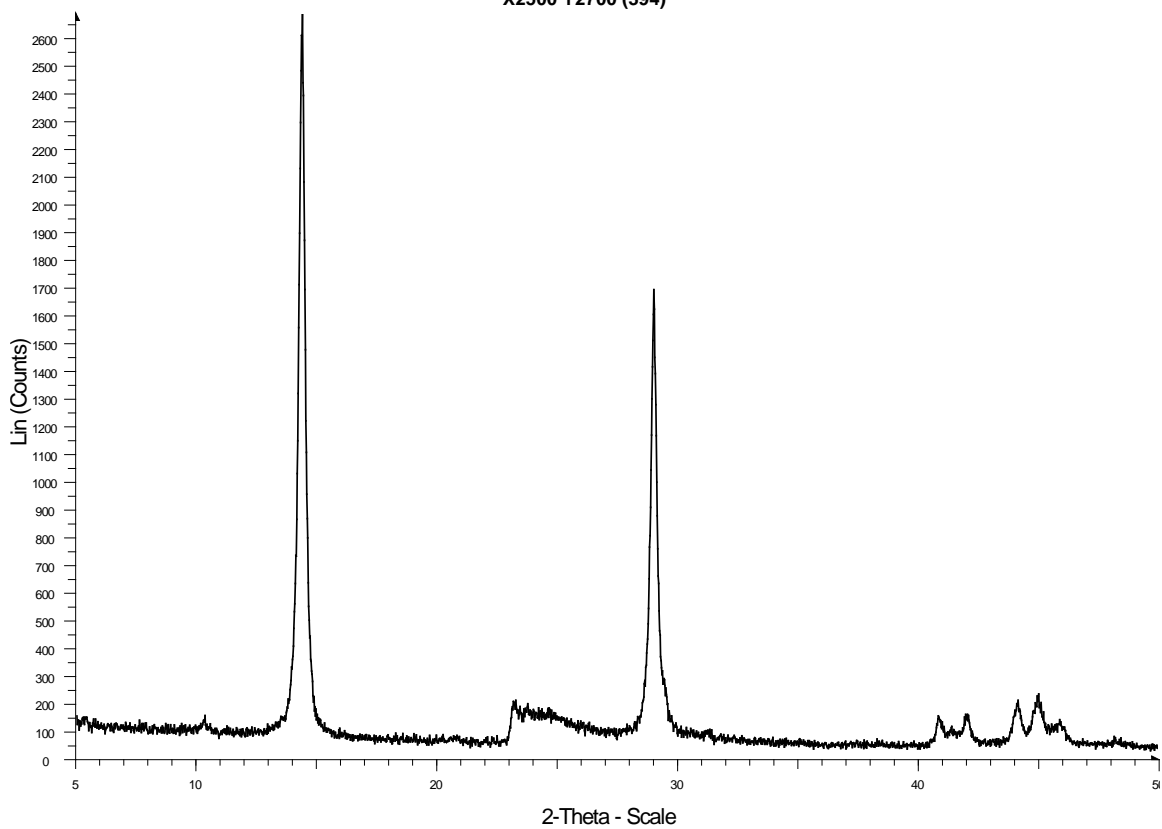




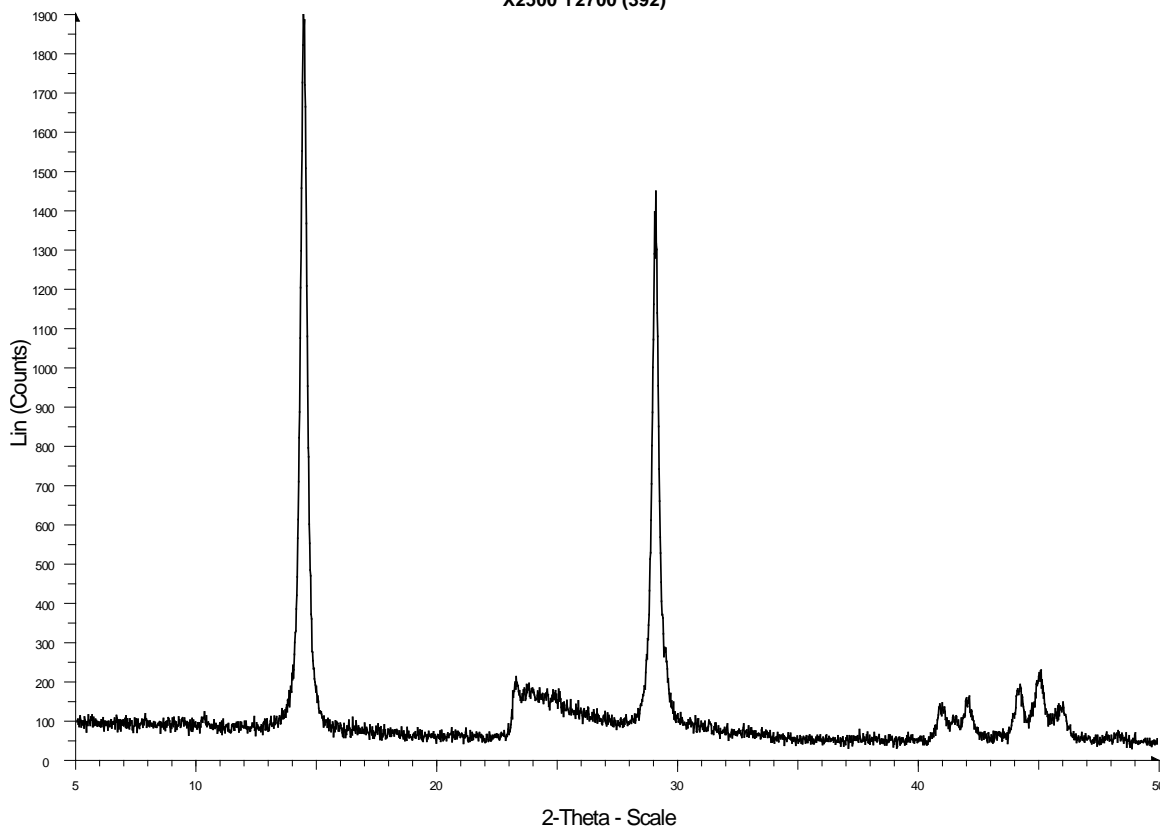




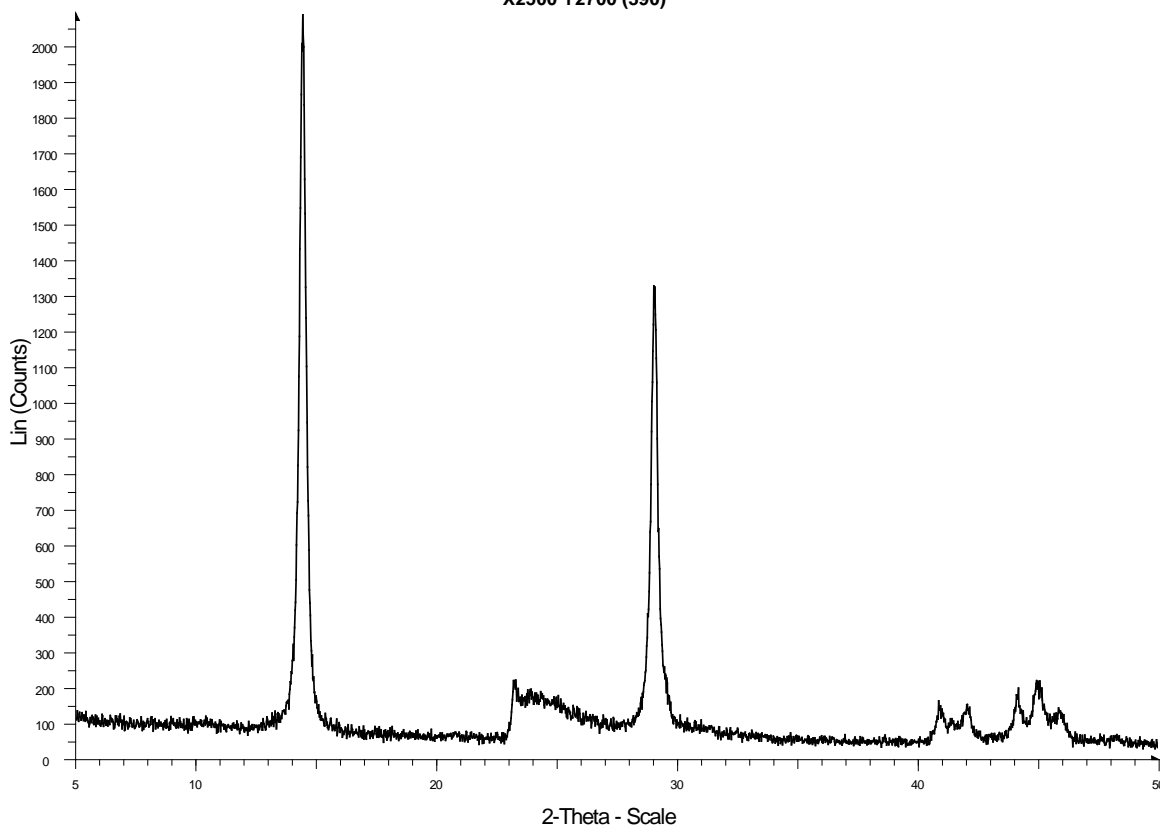
X2500 Y2700 (394)



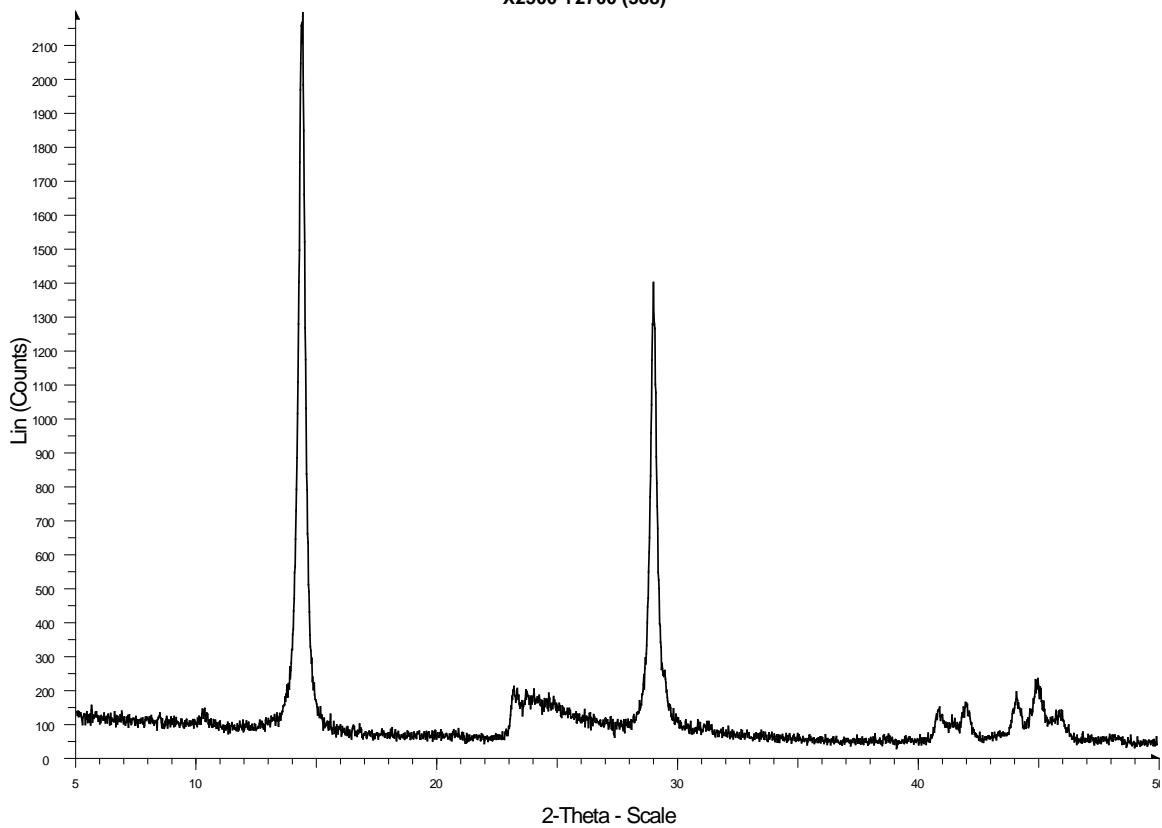
X2500 Y2700 (392)

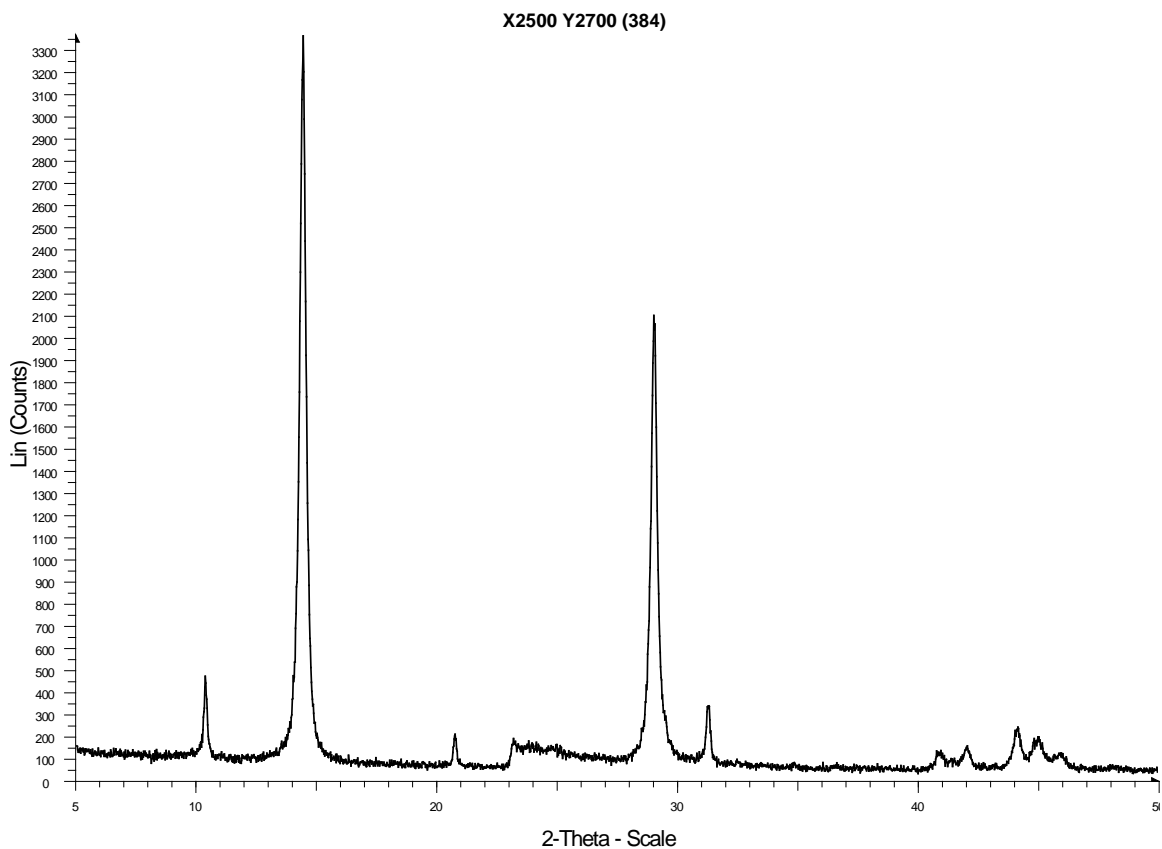
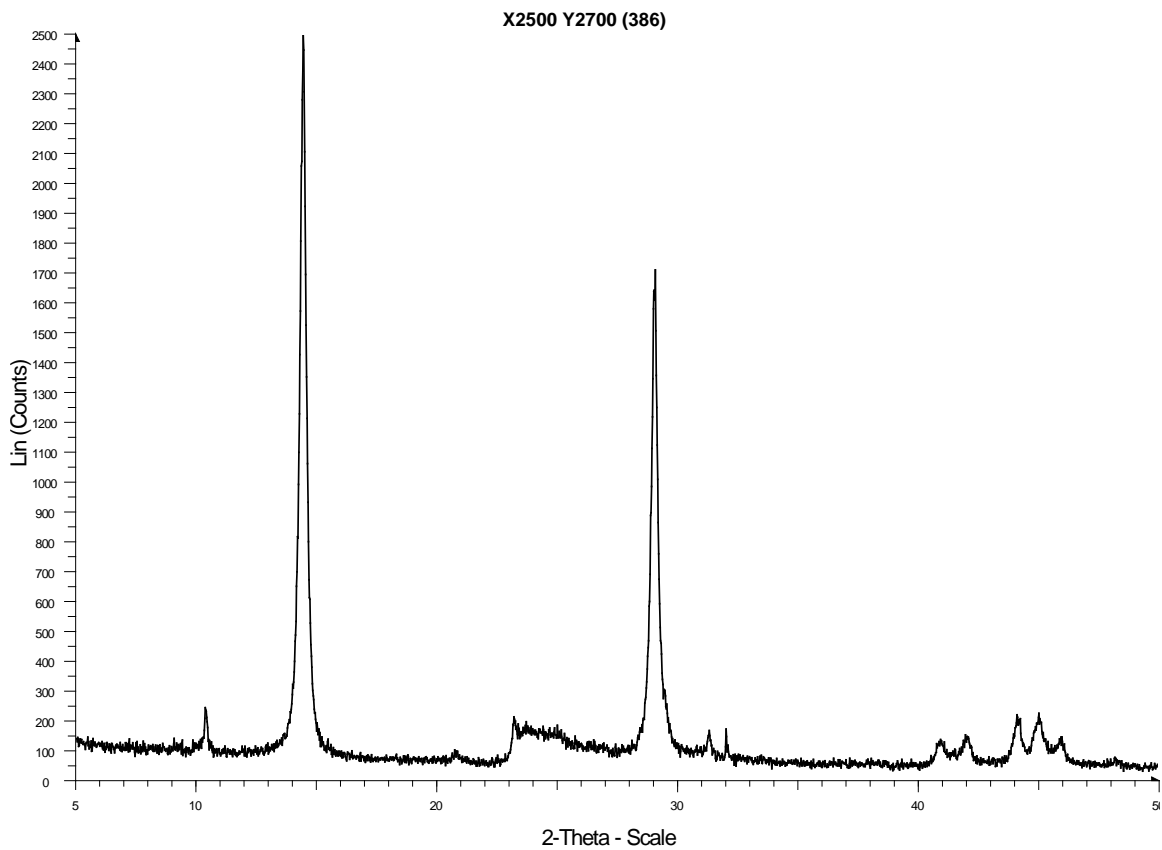


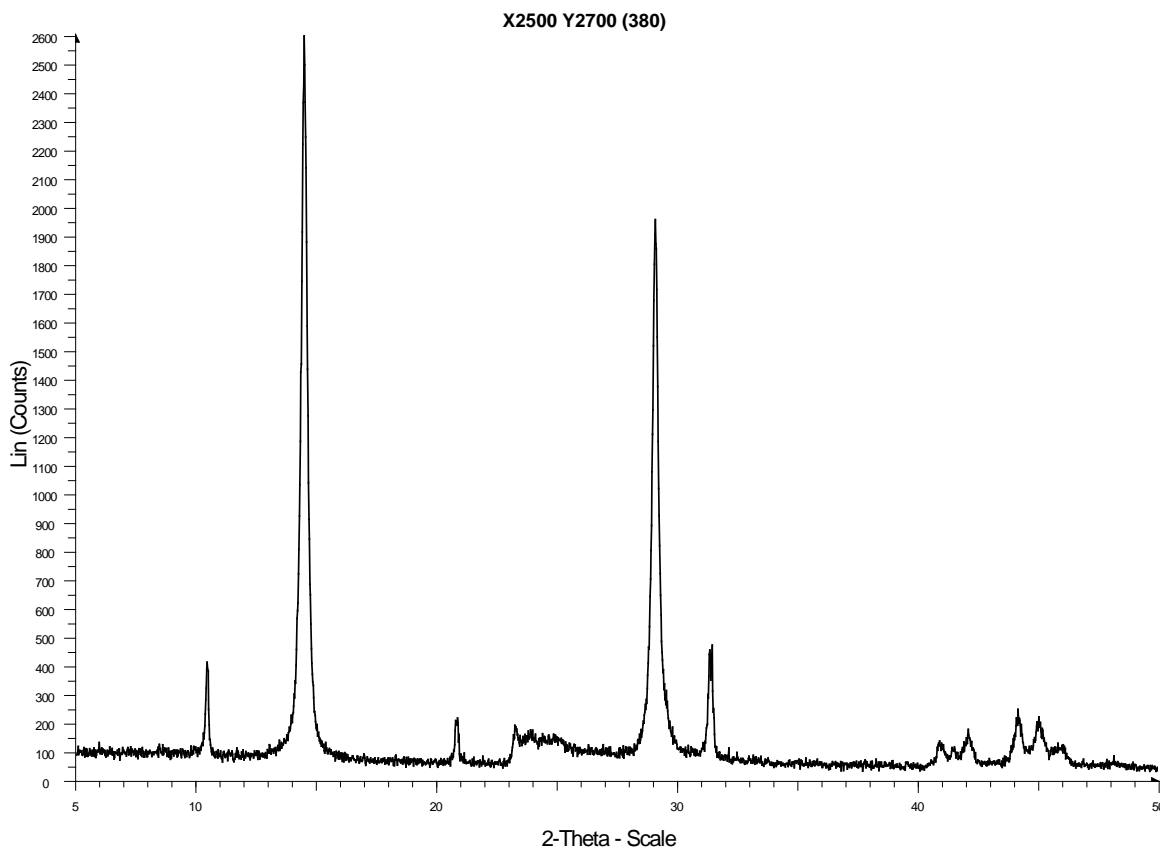
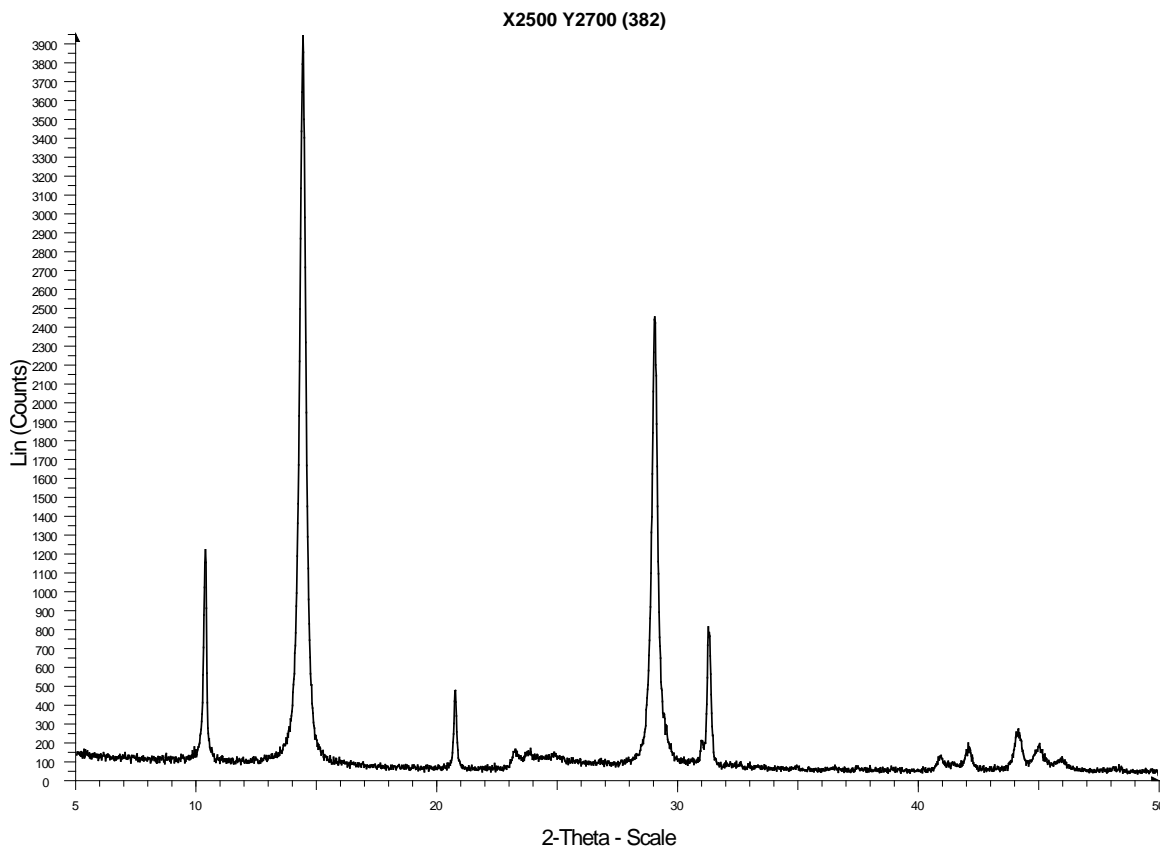
X2500 Y2700 (390)

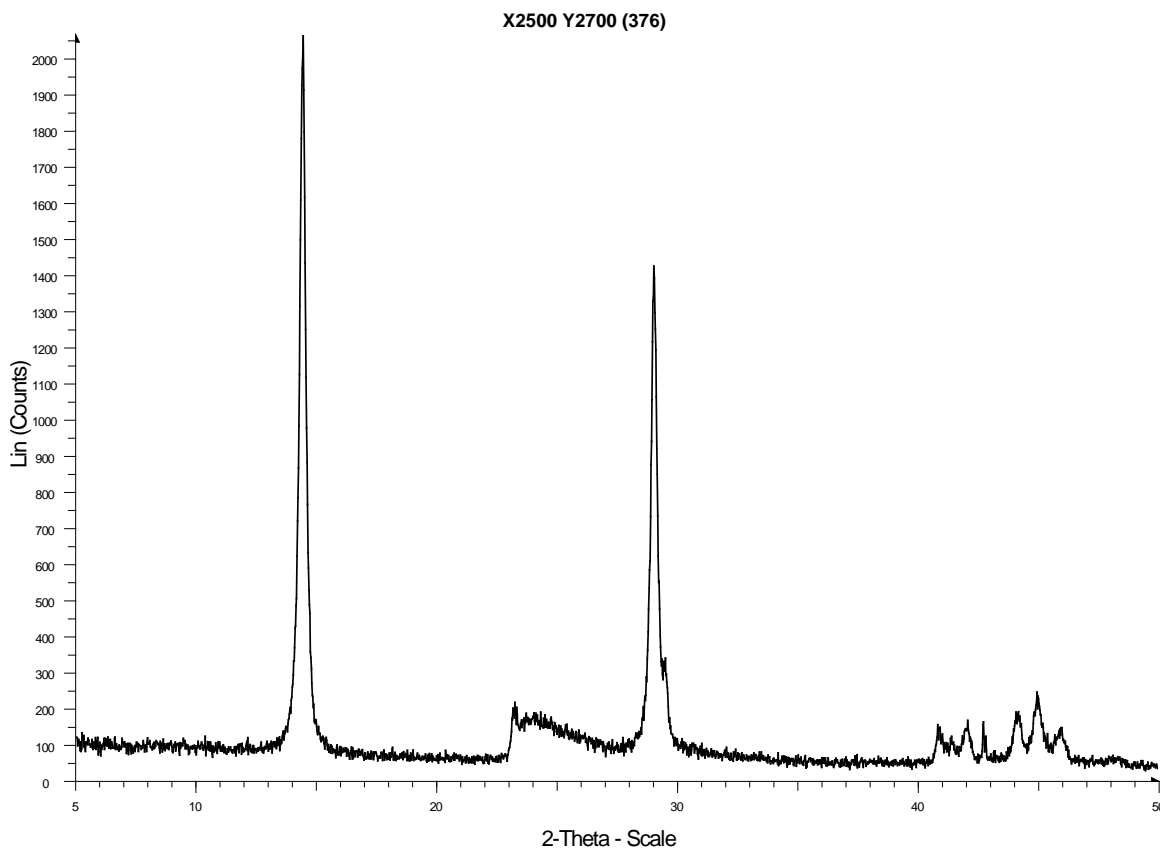
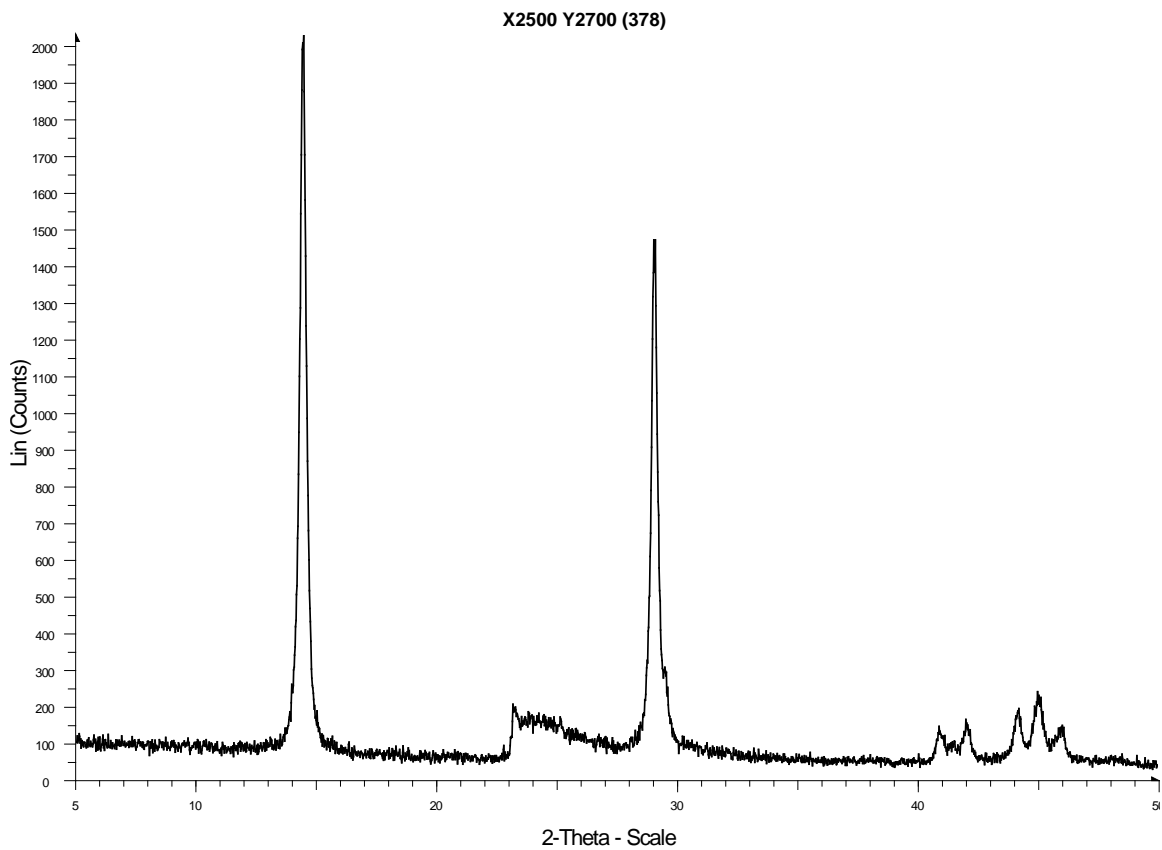


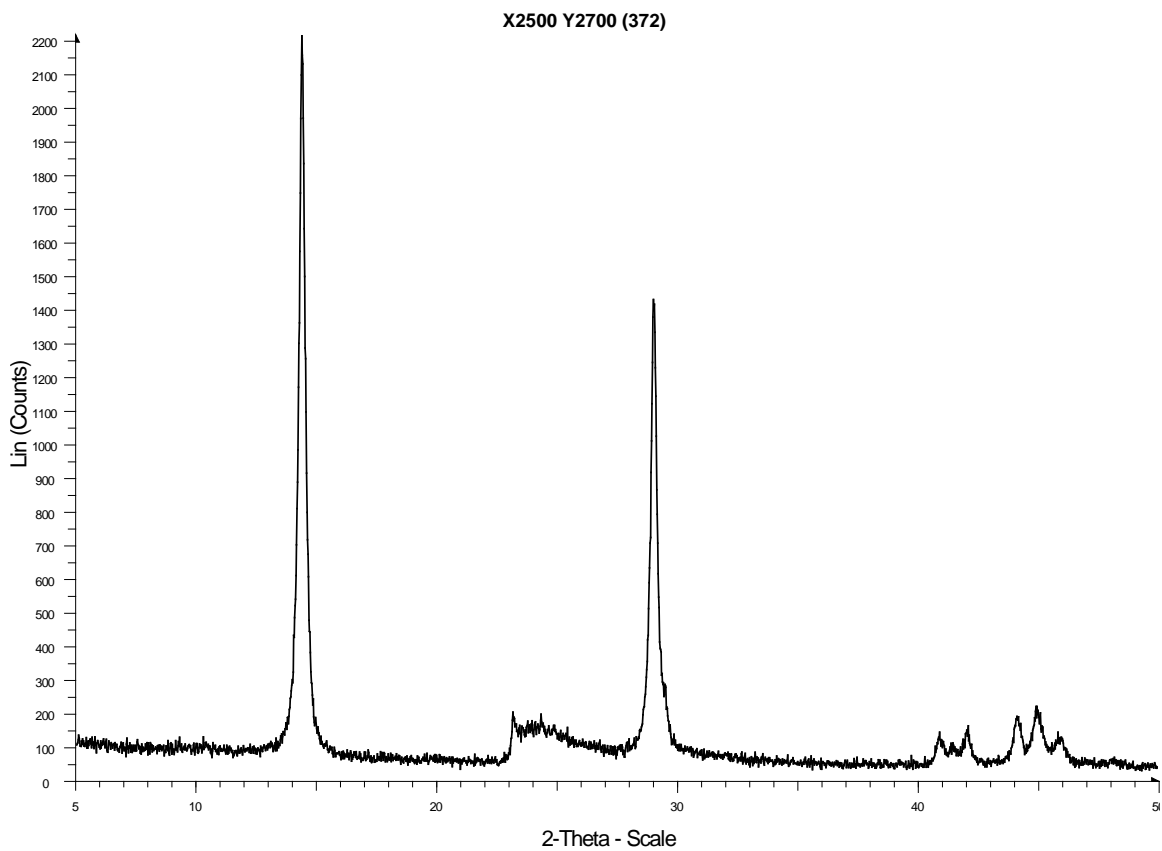
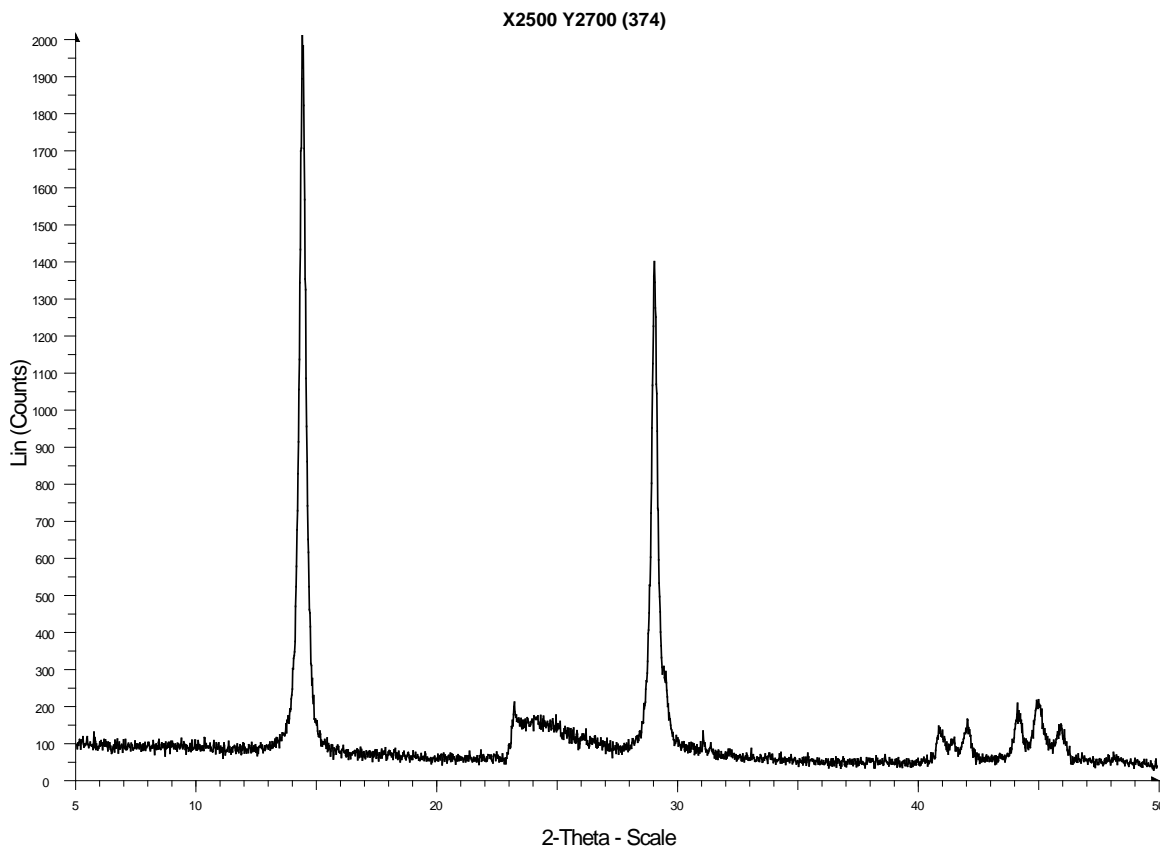
X2500 Y2700 (388)

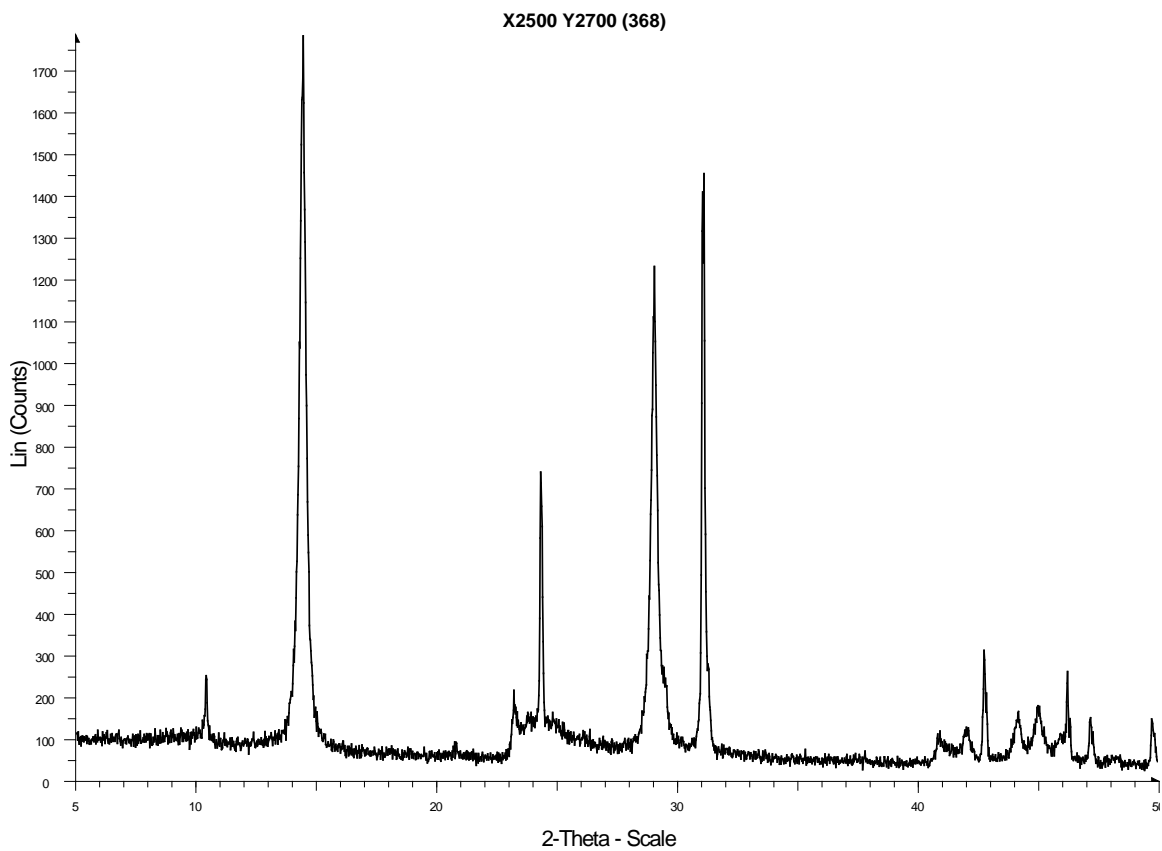
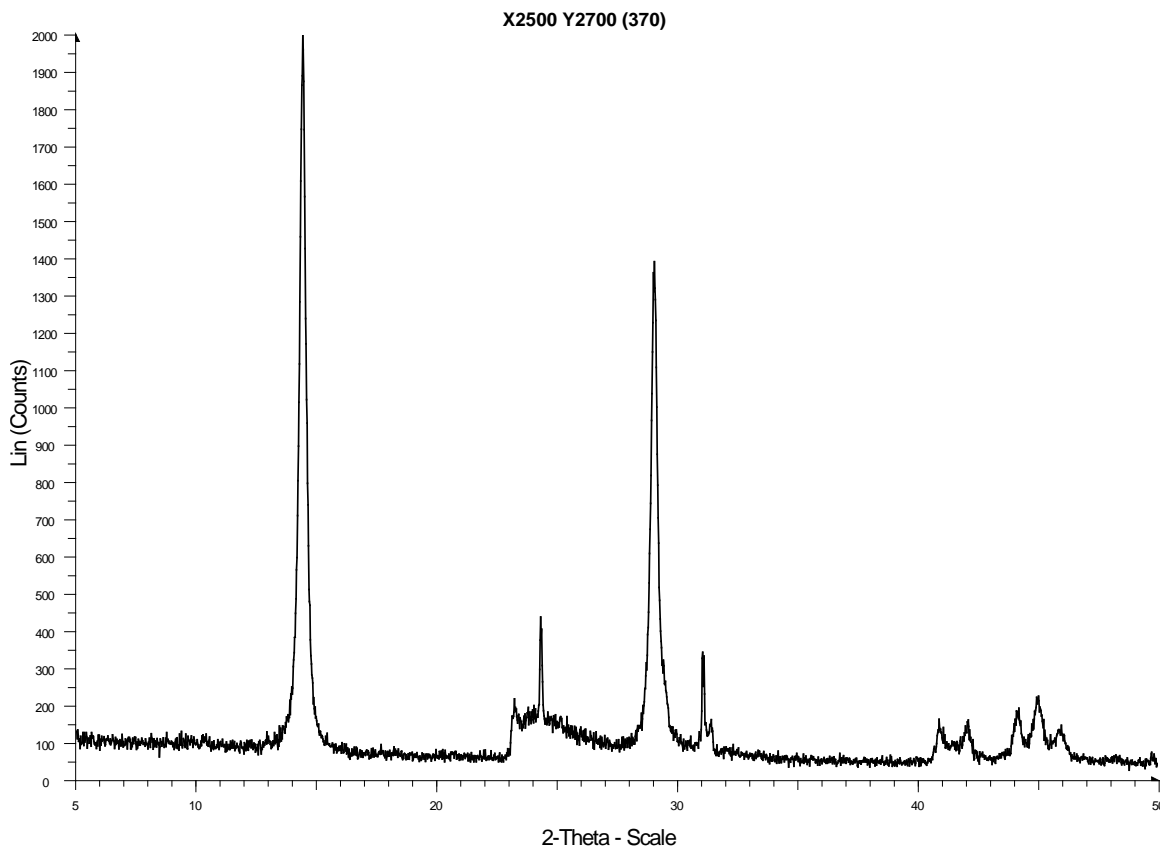


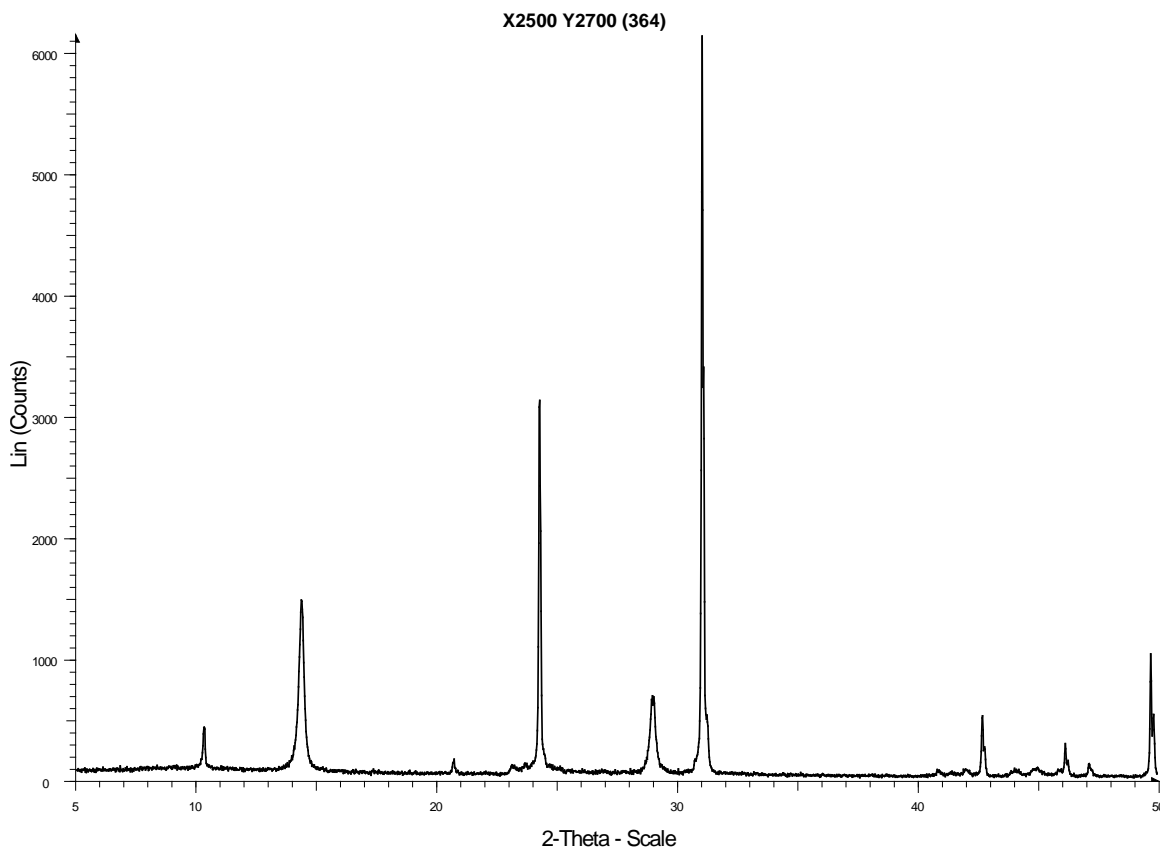
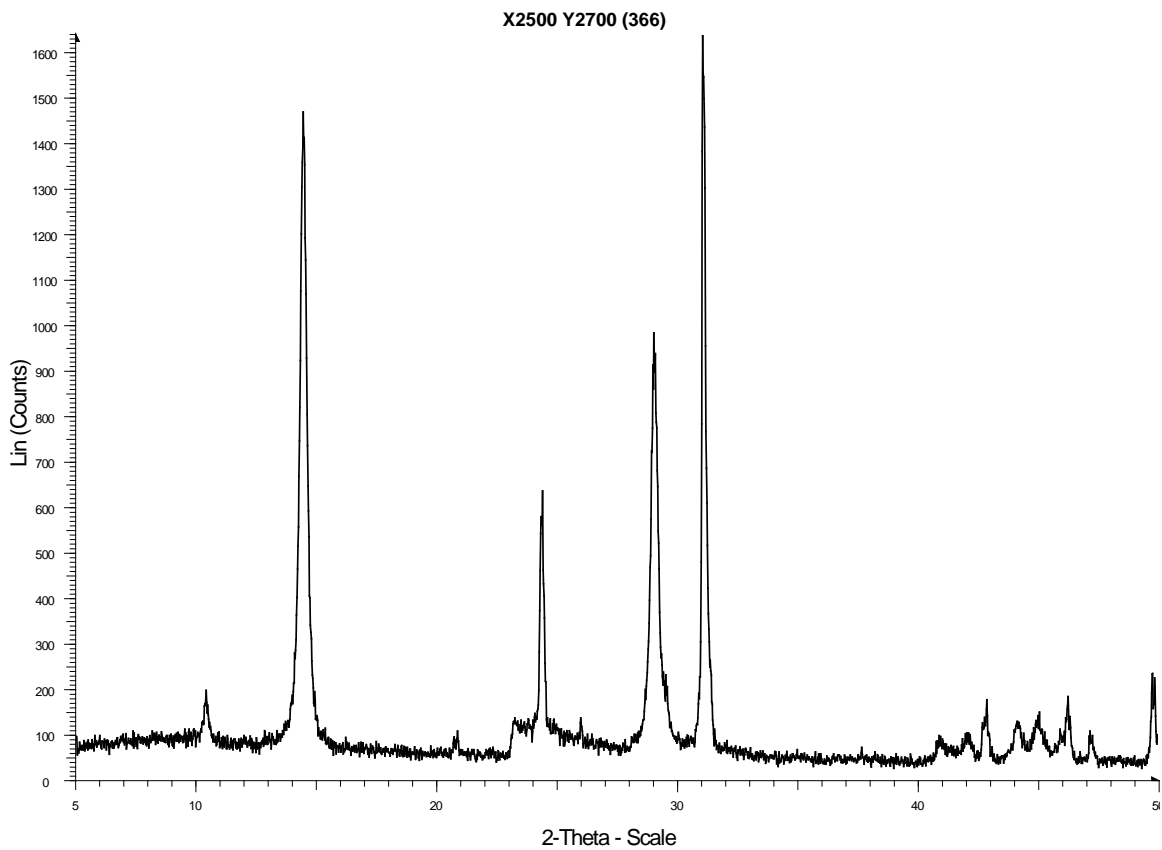












**APPENDIX C**  
**COMPLETE DATA TABLES**

TABLE APPENDIX C. ALL COLLECTED DATA

Sample ID	Formation	Elevation (feet)	Color	Texture	Sample (g)	V2O5 (mg)	$\mu\text{mol SO}_2$	$\delta^{34}\text{S}$	Error	$\delta^{34}\text{S}$ Corrected Value
X2100 Y2400 (409)	Twiggs	409	10 YR 6/8	Clay	2.00	52.02	31.3	-24.33	0.06	-8.91
X2100 Y2400 (407)	Twiggs	407	5 Y 4/1	Clay	2.00	52.67	331.9	-14.32	0.06	0.74
X2100 Y2400 (406)	Twiggs	406	5 Y 4/1	Clay	2.00	57.01	285.8	-18.09	0.04	-2.89
X2100 Y2400 (405)	Twiggs	405	5 Y 4/1	Clay	2.00	52.70	272.0	-19.32	0.05	-4.08
X2100 Y2400 (404)	Twiggs	404	5 Y 4/1	Clay	2.00	50.95	220.4	-19.99	0.04	-4.73
X2100 Y2400 (403)	Twiggs	403	5 Y 4/1	Clay	2.01	51.40	296.9	-16.45	0.05	-1.32
X2100 Y2400 (402)	Twiggs	402	5 Y 4/1	Clay	2.00	49.90	168.7	-23.60	0.05	-8.21
X2100 Y2400 (401)	Huber	401	5 Y 8/1	Clay	2.03	50.70	34.1	-11.34	0.07	3.61
X2100 Y2400 (399)	Huber	399	5 Y 8/1	Clay	2.00	51.70	24.9	-18.23	0.39	-3.03
X2100 Y2400 (395)	Huber	395	5 Y 8/1	Clay	2.02	51.20	19.4	-36.72	0.12	-20.84
X2100 Y2400 (393)	Huber	393	5 Y 8/1	Clay	2.01	52.90	8.3	-32.10	0.07	-16.39
X2100 Y2400 (391)	Huber	391	5 Y 8/1	Clay	2.00	49.50	6.5	-29.08	0.07	-13.49
X2100 Y2400 (389)	Huber	389	5 Y 8/1	Clay	2.00	50.40	21.2	-29.64	0.12	-14.03
X2100 Y2400 (385)	Huber	385	5 Y 8/1	Clay	1.00	50.30	7.4	-25.31	0.06	-9.85
X2100 Y2400 (383)	Huber	383	5 Y 7/1	Clay	2.01	51.90	16.6	-24.46	0.05	-9.04
X2100 Y2400 (381)	Huber	381	5 Y 8/1	Clay	1.99	50.00	11.1	-23.98	0.12	-8.57
X2100 Y2400 (379)	Huber	379	5 Y 7/1	Clay	2.00	49.90	17.5	-19.88	0.12	-4.62
X2100 Y2400 (377)	Huber	377	5 Y 8/1	Clay	2.00	50.50	17.5	-18.60	0.13	-3.39
X2100 Y2400 (375)	Huber	375	5 Y 8/1	Clay	2.00	50.40	12.0	-22.09	0.04	-6.75
X2100 Y2400 (373)	Huber	373	5 Y 8/1	Clay	2.00	57.24	18.4	-26.19	0.05	-10.70
X2100 Y2400 (371)	Huber	371	5 Y 8/1	Clay	2.01	50.50	11.1	-21.74	0.05	-6.41
X2100 Y2400 (369)	Huber	369	5 Y 8/1	Clay	2.01	56.90	10.1	-23.09	0.04	-7.72
X2100 Y2400 (367)	Huber	367	5 Y 8/1	Clay	2.00	50.10	12.0	-29.21	0.11	-13.61
X2100 Y2400 (365)	Huber	365	5 Y 8/1	Clay	2.00	56.70	7.4	-15.38	0.04	-0.29
X2100 Y2400 (363)	Huber	363	5 Y 7/1	Sandy Clay	2.00	54.30	14.8	-21.42	0.05	-6.11
X2500 Y2700 (408)	Twiggs	408	10 R 6/4	Sandy Clay	2.00	53.90	9.2	-20.87	0.05	-5.58
X2500 Y2700 (407)	Twiggs	407	5 R 6/4	V. Sandy Clay	2.01	50.20	7.4	-19.98	0.06	-4.72
X2500 Y2700 (406)	Twiggs	406	10 YR 6/8	V. Sandy Clay	2.00	50.26	14.8	-24.46	0.07	-9.04
X2500 Y2700 (404)	Huber	404	2.5 Y 8/2	Clay	2.00	51.90	96.8	-3.98	0.07	10.69
X2500 Y2700 (402)	Huber	402	2.5 Y 8/3	Clay	2.00	49.90	75.6	-3.03	0.08	11.61
X2500 Y2700 (400)	Huber	400	2.5 Y 8/3	Clay	2.01	53.70	72.8	-1.01	0.10	13.56
X2500 Y2700 (398)	Huber	398	5 Y 8/1	Clay	2.01	53.80	55.3	-13.70	0.06	1.33
X2500 Y2700 (396)	Huber	396	5 Y 8/1	Clay	2.01	49.60	24.9	-27.10	0.03	-11.58

X2500 Y2700 (394)	Huber	394	5 Y 8/1	Clay	2.00	51.40	12.9	-29.97	0.05	-14.34
X2500 Y2700 (392)	Huber	392	5 Y 8/1	Clay	2.00	54.70	18.4	-28.16	0.08	-12.60
X2500 Y2700 (390)	Huber	390	5 Y 8/1	Clay	2.00	50.40	21.2	-38.30	0.14	-22.37
X2500 Y2700 (388)	Huber	388	5 Y 8/1	Clay	2.00	50.75	154.9	-27.54	0.04	-17.00
X2500 Y2700 (386)	Huber	386	5 Y 8/1	Clay	2.00	54.70	44.3	-27.45	0.03	-11.92
X2500 Y2700 (384)	Huber	384	5 Y 8/1	Clay	2.04	55.40	26.7	-28.41	0.03	-12.84
X2500 Y2700 (382)	Huber	382	5 Y 7/1	Clay	2.00	50.65	79.3	-25.32	0.05	-9.86
X2500 Y2700 (380)	Huber	380	2.5 Y 8/2	Clay	2.01	57.90	15.7	-15.28	0.07	-0.19
X2500 Y2700 (378)	Huber	378	2.5 Y 8/2	Clay	2.02	55.20	6.5	-23.36	0.04	-7.98
X2500 Y2700 (376)	Huber	376	2.5 Y 8/2	Clay	2.00	52.30	9.2	-23.90	0.06	-8.49
X2500 Y2700 (374)	Huber	374	2.5 Y 8/2	Clay	2.00	57.62	10.1	-24.82	0.05	-0.39
X2500 Y2700 (372)	Huber	372	2.5 Y 8/2	Clay	2.01	50.30	7.4	-24.12	0.06	-8.71
X2500 Y2700 (370)	Huber	370	2.5 Y 8/2	Clay	2.01	49.60	22.1	-24.81	0.06	-9.37
X2500 Y2700 (366)	Huber	366	2.5 Y 8/2	Clay	2.00	51.10	7.4	-21.56	0.02	-6.24
X2500 Y2700 (364)	Huber	364	2.5 Y 8/2	Sandy Clay	2.00	52.82	5.5	-22.22	0.06	-6.88
X2250 Y2650 (408)	Twiggs	408	2.5 Y 6/3	Clay	1.00	50.72	14.8	-17.41	0.03	-2.24
X2250 Y2650 (407)	Twiggs	407	2.5 Y 6/3	Sandy Clay	2.00	52.00	11.1	-25.35	0.05	-9.90
X2250 Y2650 (406)	Twiggs	406	5 Y 4/1	Sandy Clay	2.00	54.14	237.9	-36.10	0.05	-20.25
X2250 Y2650 (405)	Twiggs	405	5 Y 4/1	Sandy Clay	2.00	49.70	49.8	-17.65	0.10	-2.47
X2250 Y2650 (404)	Twiggs	404	5 Y 4/1	Sandy Clay	2.00	54.70	265.5	-20.08	0.06	-4.81
X2250 Y2650 (403)	Twiggs	403	5 Y 4/1	Sandy Clay	1.00	51.10	147.0	-17.70	0.04	-2.04
X2250 Y2650 (402)	Twiggs	402	5 Y 4/1	Sandy Clay	1.00	52.46	134.6	-21.63	0.03	-6.30
X2250 Y2650 (401)	Twiggs	401	5 Y 4/1	Sandy Clay	2.00	52.95	272.9	-17.36	0.09	-2.19
X2250 Y2650 (400)	Twiggs	400	5 Y 4/1	Sandy Clay	2.00	59.00	243.4	-30.33	0.02	-14.69
X2250 Y2650 (399)	Twiggs	399	5 Y 4/1	Sandy Clay	2.00	52.60	291.4	-13.18	0.08	1.83
X2250 Y2650 (398)	Huber	398	5 Y 8/1	Clay	1.99	51.38	43.3	-13.93	0.03	1.11
X2250 Y2650 (396)	Huber	396	5 Y 8/1	Clay	2.00	50.40	26.7	-18.75	0.10	-3.54
X2250 Y2650 (394)	Huber	394	5 Y 8/2	Clay	2.00	49.70	20.3	-20.27	0.07	-4.99
X2250 Y2650 (392)	Huber	392	5 Y 8/2	Clay	2.00	50.30	10.1	-29.24	0.05	-13.64
X2250 Y2650 (390)	Huber	390	5 Y 8/2	Clay	2.00	52.50	23.1	-32.37	0.05	-16.65
X2250 Y2650 (388)	Huber	388	5 Y 8/2	Clay	2.00	52.20	21.2	-29.30	0.10	-13.70
X2250 Y2650 (386)	Huber	386	5 Y 8/2	Clay	2.00	53.10	21.2	-28.38	0.04	-12.81
X2250 Y2650 (384)	Huber	384	5 Y 8/2	Clay	2.00	53.27	23.1	-33.10	0.06	-17.36
X2250 Y2650 (382)	Huber	382	5 Y 8/1	Clay	2.00	51.00	30.4	-23.38	0.04	-7.99
X2250 Y2650 (380)	Huber	380	5 Y 8/1	Clay	2.00	54.41	30.4	-29.41	0.05	-13.80

X2250 Y2650 (378)	Huber	378	5 Y 8/1	Clay	2.00	55.35	15.7	-28.02	0.08	-12.46
X2250 Y2650 (376)	Huber	376	5 Y 8/1	Clay	2.00	50.67	44.3	-42.97	0.06	-26.87
X2250 Y2650 (374)	Huber	374	5 Y 8/1	Clay	2.00	51.20	12.9	-25.21	0.03	-9.76
X2250 Y2650 (372)	Huber	372	5 Y 8/2	Clay	2.00	51.48	12.9	-21.91	0.03	-6.58
X2250 Y2650 (370)	Huber	370	5 Y 8/2	Clay	2.00	52.56	11.1	-22.80	0.07	-7.43
X2250 Y2650 (368)	Huber	368	10 YR 7/2	Sandy Clay	2.00	55.90	11.1	-22.20	0.06	-6.86
X2250 Y2650 (364)	Huber	364	10 YR 7/2	Sandy Clay	2.00	53.10	12.9	-18.83	0.06	-3.61
X2400 Y2800 (405)	Twiggs	405	2.5 YR 5/6	Sandy Clay	2.00	52.85	23.1	-24.74	0.07	-9.30
X2400 Y2800 (404)	Twiggs	404	2.5 YR 5/6	Sandy Clay	2.01	50.50	15.7	-23.98	0.08	-8.57
X2400 Y2800 (403)	Twiggs	403	2.5 Y 6/6	Sandy Clay	2.00	52.24	32.3	-24.67	0.04	-9.24
X2400 Y2800 (402)	Twiggs	402	2.5 Y 6/6	Sandy Clay	1.00	51.40	7.4	-21.85	0.06	-6.52
X2400 Y2800 (401)	Huber	401	5 Y 7/1	Sandy Clay	2.00	53.50	45.2	-26.07	0.05	-10.58
X2400 Y2800 (399)	Huber	399	5 Y 8/1	Clay	2.00	50.61	47.0	-32.13	0.03	-16.42
X2400 Y2800 (397)	Huber	397	5 Y 8/1	Clay	2.00	52.50	22.1	-30.28	0.10	-14.64
X2400 Y2800 (395)	Huber	395	5 Y 8/2	Clay	2.00	50.10	21.2	-29.61	0.04	-13.99
X2400 Y2800 (393)	Huber	393	5 Y 8/1	Clay	2.01	60.20	16.6	-24.15	0.07	-8.74
X2400 Y2800 (391)	Huber	391	5 Y 8/1	Clay	2.03	51.70	11.1	-23.54	0.02	-8.15
X2400 Y2800 (389)	Huber	389	5 Y 8/1	Clay	2.00	51.55	18.4	-25.05	0.06	-9.61
X2400 Y2800 (387)	Huber	387	5 Y 8/1	Clay	2.01	52.40	20.3	-34.13	0.09	-18.35
X2400 Y2800 (385)	Huber	385	5 Y 8/1	Clay	2.00	51.70	18.4	-32.37	0.07	-16.65
X2400 Y2800 (383)	Huber	383	5 Y 8/1	Clay	2.00	49.60	204.7	-28.60	0.07	-13.02
X2400 Y2800 (381)	Huber	381	5 Y 8/1	Clay	2.00	49.20	16.6	-22.62	0.05	-7.26
X2400 Y2800 (377)	Huber	377	5 Y 8/2	Clay	2.01	49.50	8.3	-22.64	0.06	-7.28
X2400 Y2800 (375)	Huber	375	5 Y 8/2	Clay	2.00	51.59	8.3	-23.66	0.04	-8.27
X2400 Y2800 (373)	Huber	373	5 Y 8/2	Sandy Clay	2.00	50.60	8.3	-22.22	0.04	-6.87
X2400 Y2800 (371)	Huber	371	5 Y 8/2	Sandy Clay	2.00	53.71	9.2	-23.82	0.03	-8.41